Biopolymer Flocculant Systems and Their Chemically Modified Forms for Aqueous Phosphate and Kaolinite Removal

A Thesis Submitted to the

College of Graduate and Postdoctoral Studies

In Partial Fulfillment of the Requirements

For the Degree of Doctor of Philosophy

In the Department of Chemistry

University of Saskatchewan

Saskatoon

By

Henry Kwame Agbovi

Permission to Use

In presenting this thesis in partial fulfillment of the requirements for a Postgraduate degree from the University of Saskatchewan, I agree that the Libraries of this University may make it freely available for inspection. I further agree that permission for copying of this thesis in any manner, in whole or in part, for scholarly purposes may be granted by Dr. L. D. Wilson who supervised my thesis work or, in his absence, by the Head of the Department of Chemistry or the Dean of the College in which my thesis work was done. It is understood that any copying or publication or use of this thesis or part of it for financial gain shall not be allowed without my written permission. It is also understood that due recognition shall be given to me and to the University of Saskatchewan in any scholarly use which may be made of any material in my thesis. Requests for permission to copy or to make other use of material in this thesis in whole or part should be addressed to:

Head of the Department of Chemistry

University of Saskatchewan

110 Science Place

Saskatoon, Saskatchewan S7N 5C9 Canada

Dean

College of Graduate and Postdoctoral Studies

University of Saskatchewan

116 Thorvaldson Building, 110 Science Place

Saskatoon, Saskatchewan S7N 5C9 Canada

Acknowledgements

Foremost, to God be the glory for the great and wonderful things He has done. To Him, I owe infinitude of my heartfelt gratitude for His promise in the Bible, "*Being confident of this very thing, that He who has begun a good work in you will complete it until the day of Jesus Christ*" Philippians 1:6.

I would like to express my sincere heartfelt appreciation to my supervisor, Prof. Lee D. Wilson, for the continuous support of my entire period of study and research, his inspiration, patience, enthusiasm, immense knowledge, and considerable effort to explain things clearly and simply. Throughout the thesis-writing, he provided encouragement, sound advice, excellent teaching and lots of good ideas. This thesis would not have been possible without him. I am also thankful to my supervisory committee, Prof. Ingrid Pickering, Prof. Andrew P. Grosvenor and Prof. Jian Peng, for their sound advice, encouragement and constructive criticisms. I am also thankful to Prof. Scott Smith (Wilfrid Laurier University, Waterloo) for graciously accepting to be my external examiner.

My sincere thanks also go to Drs. Sammynaiken and J. Maley, and K. Thomas (Saskatchewan Structural Sciences Center (SSSC)) for their technical support. The Department of Chemistry is also acknowledged for given me the opportunity to do research and further my scientific career. I am equally thankful to the entire faculty, staff and students of the department for their invaluable supports. Special thanks also go to the Government of Saskatchewan through the Ministry of Agriculture (Agriculture Development Fund; ADF) for fully funding this research. I would like to especially thank the Saskatchewan Provincial Government for providing me with emergency financial aid during the lockdown due to the COVID-19 pandemic.

I am also thankful to my lab mates, Dr. Mohamed Mohamed, Dr. Abdalla Karoyo, Dr. Inimfon Udoetok, Dr. Leila Dehabadi, Dr. Asghar Dolatkhah, Chen Xue, Savi Bhalkaran, Michael Danquah, Mohammad Mahaninia, Bahareh Vafakish, Dexu Kong, and Mostafa Solgi, for their diverse academic and non-academic support throughout my study.

Special thank you to my parents, Rev. James Lawrence Agbovi and Mrs. Helena Obeng Agbovi for their love, encouragement, advice, spiritual and physical support. Lastly, and most importantly, I would like to thank my wife, Joana Agbovi and my children, Deborah Nhyirah Agbovi and Jacintha Nyamedo Agbovi for their equal involvement in this PhD study. Research would not have been possible without them.

Dedication

This thesis is dedicated to my wife, Joana Agbovi and my children, Deborah Nhyirah Agbovi and Jacintha Nyamedo Agbovi. To my parents, Rev. James Lawrence Agbovi and Mrs. Helena Obeng Agbovi and my siblings, Samuel, Eric, Linda, Esther, Rebecca and Alex.

I will forever remain grateful for your love, godly advice, encouragement and support.

TO GOD BE THE GLORY

Abstract

The fate and build-up of phosphate (P_i) nutrients in aquatic environments is an urgent environmental problem affecting global water security. At elevated levels, P_i causes eutrophication, leading to oxygen depletion. This thesis is aimed at the development, optimization and application of a sustainable biopolymer-based coagulation-flocculation (CF) system that has improved P_i and turbidity (T_i) removal performance over conventional CF systems. In Chapters 3 and 4, the removal efficacy of P_i from wastewater was investigated using variable combinations of coagulant and biopolymer-flocculant (chitosan and alginate) systems. The CF process was affected by several independent variables (CF factors). The optimization studies provided an empirical relationship between the P_i removal efficiency and these factors. The results demonstrated that the biopolymer-flocculants are more efficient in a ternary system in removing P_i from wastewater and the process is controlled by charge neutralization and polymer-bridging mechanisms. Chapters 5 and 6 are aimed at designing a high molecular weight amphoteric bioflocculant (CMC-CTA) for the co-removal efficacy of P_i and T_i in a binary system with $FeCl_3$. The effects of pH, settling time, coagulant and flocculant dosages were investigated through optimization studies, and the results showed that Fe(III)-CMC-CTA binary system was effective at acidic to neutral pH. Kinetics and equilibrium adsorption studies showed that the process was well described by kinetic pseudo-first-order and equilibrium Langmuir isotherm for uptake of P_i and T_i and the process was spontaneous and endothermic. Chapter 7 focused on the design of high molecular weight cationic chitosan-based flocculant (CTA-Chi-*g*-PAM). The functional properties of the flocculants were examined for the removal of P_i, and T_i, where the effects of several CF factors were tested in a single-component system. The experimental data were fitted by several kinetic (time-dependent) and adsorption (concentration dependent) models. Thermodynamic parameters revealed that the CF process was favored by entropy-driven electrostatic interactions and polymer bridging. Individual kaolinite-colloidal particles showed a higher aggregation rate due to Coulombic electrostatic and van der Waals attractive forces in the presence of CTA-Chi-*g*-PAM to form flocs. The studies reported herein provide a greater understanding of the structure-property relationship for biopolymer-based CF phenomena, and the findings will add to the design of bioflocculants with superior and tunable physicochemical properties.

Table of Contents

List of Tables

List of Figures

List of Schemes

Abbreviations and Symbols

Abbreviations

AFM……..... Atomic Force Microscopy

Alg……... Alginate

Al-OH…… Aluminol

ANOVA…….. Analysis of Variance

AR……. …… Analytical Reagent

AW…… Agricultural Wastewater

BBD…….…... Box-Behnken Design

CF……..… Coagulation-Flocculation

Chi…….. Chitosan

CMC ……..... Carboxymethyl Chitosan

CMC-CTA …….. Amphoteric Flocculant

COD……... Chemical Oxygen Demand

CP/TOSS……...Cross Polarization with Total Suppression of Spinning Sidebands

CPMAS ……..Cross Polarization Magic Angle Spinning

CTA ……... 3-chloro-2-hydroxypropyl trimethylammonium chloride

CTA-Chi-g-PAM……... Cationic Flocculant

DBPs ……..... Disinfection by-products

DD…….. Degree of Deacetylation

DLS……. Dynamic Light Scattering

DLVO……Dergagin Landau Verwey and Overbeek

DOE……... Design of Experiment

DRIFT ……...Diffuse Reflectance Infrared Fourier Transform

DS……. Degree of Substitution

DSC ……Differential Scanning Calorimetry

EDL ……. ……. Electrical Double Layer

E-E ……...… Edge-to-Edge Interaction

ESA ……... Electrokinetic Sonic Amplitude

F-E……. Face-to-Edge Interaction

F-F …… …… Face-to-Face Interaction

FTIR ……. Fourier Transform Infrared

HMW……... High molecular weight

IEP ……. …… Isoelectric point

MAE…… Mean Absolute Error

MW…… Municipal wastewater

NMR ……. Nuclear Magnetic Resonance

NOM ……... Natural Organic Matter

PAC-EPI-DMA ……. Polyaluminium chloride–epichlorohydrin-dimethylamine polyamine

PACl ……...Polyaluminium chloride

PAC-PDMDAAC……. Polyaluminium chloride–polydimethyldiallylammonium chloride

PAM……..Polyacrylamide

PASiC…… Polyaluminium-silicate-chloride

PFC-PDMDAAC……...Polyferric chloride–polydimethyldiallylammonium chloride

PFO …… Pseudo First Order

PFSiS…… Polyferric-silicate-sulfate

P_i ……. Orthophosphate / Phosphate

POME ……..… Palm Oil Mill Effluent

PSD …….. Particle Size Distribution

PSO …… Pseudo Second Order

pXRD …….. Powder X-ray Diffraction

PZC …… Point of Zero Charge

PZSiS…… ……... Poly-zinc-silicate-sulfate

RSM…… Response surface Methodology

SEE ……... Standard Error of Estimate

SEM …… Scanning Electron Microscopy

Si-OH……..…… …….. Silanol

SSE …….. Sum of Squares of Errors

SSE……... Sum of Squares of Errors

SSR……. Sum of squares due to Regression

SST……..... Total Sum of Squares

SW…….. Synthetic Wastewater

TGA ……Thermogravimetric Analysis

T_i ……Turbidity

TSS……...Total Suspended Solids

UOH……... Unrefined Oat Hull

ROH……... Refined oat Hull

UV-Vis ……..... Ultraviolet Visible

vdW……van der Waals

WHO ……World Health Organization

XAS……..X-ray absorption spectroscopy

xDLVO …… Hydrophobic Attractive Force

XPS…….. X-Ray Photoelectron Spectrometry

ζ-potential……... Zeta potential

Symbols

A_H …… Hamaker constant

c_e …… Equilibrium concentration

e …….. Charge of electron

F_{HD}……... Hydration force

g ……. …….. Gravitational constant

h…….. Planck's constant

h_o ……..... Minimum separation distance

I……. Molar ionic strength

k_1 ……..……Perikinetic rate coefficient

k_1 …….. Floc aggregation rate constant

k_2…… Floc breakage rate constant

k_B ……Boltzmann's constant

K_D ……... Equilibrium constant

K_f ……... Freundlich isotherm constant

K_{HD} ……... Hydration force constant

K_l …….. Langmuir equilibrium adsorption constant

K_s ……. Sips equilibrium constant

M_w …….. Molecular weight

n…….. Refractive index

$n_i(\infty)$ …….. Number per unit volume

n_T ……..... Total number of particles

ϕ ……..Volume fraction

q_e …… Equilibrium adsorption capacity

q_m ……. Maximum adsorption capacity

R ……..... Molar gas constant

R^2…….. Correlation coefficient

R_l ……... Separation factor

t_a ……... Aggregation time

V ……. Settling velocity

V_A…….. …. vdW attractive potential

V_R…… EDL repulsive potential

β …… Collision frequency

ΔG^o …… Change in Standard Gibbs Free Energy

ΔH^o……. Change in Standard Enthalpy

ΔS^o …….. Change in Standard Entropy

ε_0 ……. Permittivity of vacuum

ε_r …….. Relative permittivity

η……..Viscosity

κ……. …….. Debye constant

λ …….. Decay length

ρ…… Density

σ …… Collision efficiency

υ_e ……... Absorption frequency

χ …….. Polymer-solvent interaction parameter

ψ …… Electrostatic potential

CHAPTER 1

1. Introduction

1.1 Background

There are several contaminants in water bodies at elevated levels, such as phosphate and colloidal materials, that remain as a significant environmental concern to many countries around the world.[1] Municipal wastewater may contain about 10 mg/L to 20 mg/L of the total phosphorus in wastewater, with orthophosphate being the major species among the constituents.[2] To prevent the growth of algae in water bodies, many countries strictly regulate phosphorus levels to below 0.05 mg/L for surface water.[3] The presence of excess phosphorus in water bodies leads to eutrophication.[4–6] Phosphorus in water is usually present as a nutrient in the form of dissolved phosphate. In the removal of dissolved nutrients, it must first be converted into a solid phase followed by the removal of this phase from the bulk treated wastewater. Among the water treatment techniques (adsorption, coagulation-flocculation, precipitation, oxidation/reduction, membrane filtration, and evaporation), coagulation-flocculation (CF) has attracted much attention for primary and secondary water treatment due to its efficiency, simplicity, low cost and energy-efficient nature.[7,8] The process requires low energy inputs and material costs, especially if biopolymers can be substituted for synthetic polymers.[9] Conventional CF involves the addition of commercially available coagulants and/or flocculants such as alum or $FeCl_3$ to the wastewater to precipitate the contaminants. The precipitate formed is then removed by sedimentation and/or filtration. Despite the widespread use of CF systems, an understanding of their basic physicochemical properties in removing dissolved and suspended solids in wastewater is required to address water quality problems.[2] Coagulation-flocculation appears to be a simple process; however, the destabilization of the suspended particles (colloidal species) requires an understanding of colloidal stability.

The use of inorganic salts to precipitate contaminants has been utilized widely due to their cost-effectiveness and ready availability. However, these mineral salts pose several disadvantages, such as the use of large dosages, ineffectiveness at low water temperatures, pH-dependent (altering the pH of the water) performance, sludge production, and potential harm to human health (such as Alzheimer’s disease, Parkinson's disease, and multiple sclerosis due to aluminium).[10,11] The application of synthetic polymers, such as polyacrylamide, poly(diallyldimethyl) ammonium chloride and poly(styrene) derivatives, and biopolymers such as chitosan, alginate, cellulose, and

starch, as flocculants and/or coagulant aids for the removal of contaminants in wastewater, has been reported.[12] Synthetic and natural polymer flocculants have advantages over the use of inorganic salts that include greater purification efficiency, the ability to form large flocs with high density, high mechanical strength (resistance to shear stress), and favorable settling properties. Generally, polymers (synthetic or natural) possess useful properties over a wide pH range and yield reduced amounts of sludge without metal (aluminium) residuals whilst maintaining the alkalinity of water. However, synthetic polymers are non-biodegradable, relatively expensive and pose potential biological toxicity, which are major concerns for the environment as well as biological treatment plants.[13] The development of coagulant aid in conjunction with biopolymer flocculant (bioflocculant) systems, such as alginate, chitosan or cellulose, has several advantages: cost-efficiency, biodegradability, biocompatibility, non-toxic, with minimal production of pollutants and no side effects.[14] The application of bioflocculants seeks the benefits of a treatment with high production rate and biodegradable, innocuous waste production, whilst providing a solution to the challenges of its tendency for low flocculation activity and high cost.[13]

Even though native bioflocculants appear to be useful in water and wastewater treatment, they have reduced shelf life due to their biodegradability.[15] Also, individual polysaccharides have deficiencies in their application as bioflocculants. For instance, the low molecular weight, and poor solubility of chitosan limits its application as a bioflocculant over a wide pH range.[16] Additionally, alginate is an anionic polyelectrolyte, and hence it is not effective in the removal of negatively charged colloidal and dissolved substances in water and wastewater without further modification. Also, cellulose has poor water solubility and poor flocculation capacity.[17] Hence, it is important to chemically modify the structure and properties of these biopolymers with selected synthetic polymers to enhance their synergistic properties to effectively improve their flocculation performance.

1.2 Knowledge gaps

This thesis research is designed to bridge the following knowledge gaps based on the hypotheses that will be discussed in the subsequent section.

1. Understanding of the structure-activity relationship of biopolymers (e.g., chitosan and alginate) and their chemically modified forms for the removal of phosphate and colloidal materials in wastewater.

2. The effect of the structural properties and chemical composition of the biopolymer materials on the coagulation-flocculation mechanisms.

3. The effect of the structural properties and chemical composition of the biopolymer materials on the physicochemical characteristics of the flocs.

1.3 Objectives

The long-term goal of this thesis is aimed at the development, optimization and application of sustainable coagulation-flocculation systems that have improved water treatment performance toward oxyanion (mainly orthophosphate, P_i) and turbidity (kaolin colloidal dispersion, T_i) removal over conventional CF systems currently available. Additionally, this thesis is focused on strategies to develop single-component CF materials, with dual functional properties akin to that of conventional binary and ternary systems, from biopolymers with greater performance toward wastewater treatment and able to overcome the disadvantages accompanied with conventional CF systems (inorganic salt + synthetic polymer(s)). The overall objective of the thesis is further divided into three themes:

i. Flocculation efficacy of combined biopolymer-metal salt system towards dissolved phosphate removal in wastewater in single-component, binary, and ternary CF systems.

ii. Synthesis, characterization and flocculation properties of a high molecular weight chitosan-based amphoteric flocculant for P_i and T_i removal in single-component and binary systems.

iii. Synthesis, characterization and flocculation performance and floc properties of high molecular weight cationic chitosan-based flocculants in a single-component system.

Figure 1.1 represents a block scheme for the experimental design that will be followed to achieve the proposed hypotheses-driven objectives.

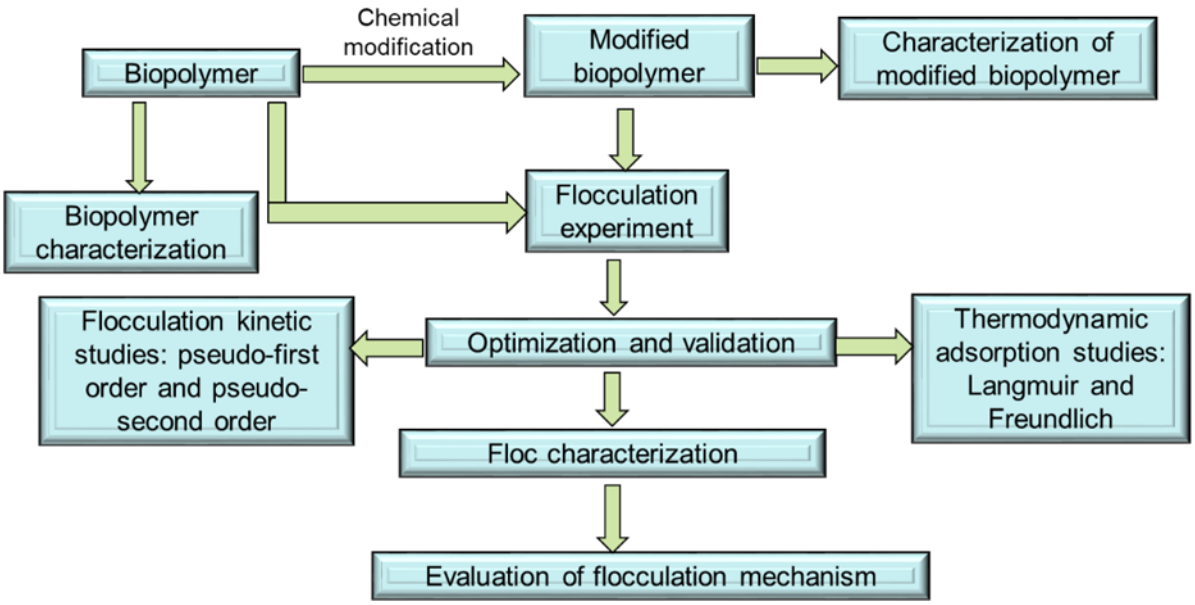

Figure 1.1: Proposed block scheme of the experimental design to achieve the proposed objectives.

1.4 Hypotheses

The following hypotheses will direct the experimental design to achieve the goals of this thesis research:

1. An increase in the molecular weight of the biopolymer flocculants will enhance their flocculation capacity. It has been postulated that higher molecular weight polymer flocculants have large surface area for adsorption of the suspended solid contaminants. Hence, to address this hypothesis, biopolymer materials such as chitosan will be modified via several synthetic routes to examine the effect of the increased polymer molecular weight on the flocculation efficiency.
2. External environmental conditions and molecular structural factors of the biopolymers can have a favorable effect on the flocculation performance of biopolymer materials. Therefore, this thesis will investigate the impact of the various external environmental factors (pH, temperature, flocculant dosage, dosage of the contaminant, stirring rates and settling time) and molecular structural factors (charge density and the degree of substitution of the functional groups) on the flocculation efficiency of flocculant systems.

3. Properties of the flocs such as size, surface morphology, stability, aggregation and breakage, and rapid settling can be improved via the utilization of bioflocculant systems over conventional inorganic coagulant and synthetic polymers. This will be addressed by chemical and physical characterization of the floc structure using different techniques. This will provide insights on how to manage the flocs and potentially providing alternatives to other possible applications of the flocs.
4. Additionally, the Box-Behnken experimental design (BBD) together with the response surface methodology (RSM) can provide an empirical relationship between the response function (degree of P_i and T_i removal) and the independent variables (external environmental factors) as well as provide optimized conditions for the CF process. To address this hypothesis, the BBD-RSM would be used to investigate and validate the CF process parameters affecting the removal of P_i and T_i in wastewater and to determine the optimal conditions maximizing the efficient removal of P_i and T_i.
5. The chemical composition and physical structure of the biopolymers can influence the type of flocculation mechanism that occurs. Therefore, it is proposed that the mechanism may involve polymer adsorption, polymer bridging, or charge neutralization or a combination of mechanisms. These mechanisms will be evaluated through a detailed investigation of the external environmental factors and molecular structural factors of the biopolymers towards the removal of P_i and T_i.
6. The CF process can be driven by kinetic (time-dependent) or thermodynamic effects at equilibrium. Evaluation of the flocculation kinetics, adsorption phenomena and thermodynamic parameters at equilibrium, and how the process parameters affect the system's efficiency will be investigated herein.

1.5 Thesis Organization

This thesis is focused on strategies to develop single-component CF materials, with dual functional properties akin to that of conventional binary and ternary systems, from biopolymers and their modified forms. The rest of the thesis is divided into seven chapters, starting from Chapter 2 through to Chapter 8. Chapter 2 is the literature review, Chapters 3 – 7 consist of formatted and edited published articles and manuscript in preparation, while chapter 8 consists of an integrated

discussion of manuscript chapters, concluding remarks and proposed future research work. The published articles and manuscript in preparation are outlined below:

1. **Agbovi**, H. K.; Wilson, L. D. *; Tabil, L. G. Biopolymer Flocculants and Oat Hull Biomass To Aid the Removal of Orthophosphate in Wastewater Treatment. *Ind. Eng. Chem. Res.* **2017**, *56* (1), 37–46. https://doi.org/10.1021/acs.iecr.6b04092. **(Chapter 3)**.

2. **Agbovi**, H. K.; Wilson, L. D. * Flocculation Optimization of Orthophosphate with $FeCl_3$ and Alginate Using the Box-Behnken Response Surface Methodology. *Ind. Eng. Chem. Res.* **2017**, *56* (12), 3145–3155. https://doi.org/10.1021/acs.iecr.6b04765 **(Chapter 4).**

3. **Agbovi**, H. K.; Wilson, L. D.* Design of Amphoteric Chitosan Flocculants for Phosphate and Turbidity Removal in Wastewater. *Carbohydr. Polym*. **2018**, *189*, 360–370. https://doi.org/10.1016/j.carbpol.2018.02.024. **(Chapter 5).**

4. **Agbovi**, H. K.; Wilson, L. D.* Optimization of Orthophosphate and Turbidity Removal Using an Amphoteric Chitosan-Based Flocculant–Ferric Chloride Coagulant System. *Environ. Chem*. **2019**, *16* (8), 599–612. https://doi.org/10.1071/EN19100 **(Chapter 6).**

5. **Agbovi**, H. K.; Wilson, L. D.* Flocculation performance of cationic chitosan-based flocculant for phosphate and turbidity remediation, *ACS Appl. Mater. Interfaces* **2020**. (To be submitted). **(Chapter 7).**

A summary of the research work and a description of the contributions of each author are presented at the beginning of each chapter. Besides, the justification for the completion of the general objectives of the Ph.D. thesis is also included. A summary of each chapter is given below.

Chapter 2 is the literature review and it discusses the various concepts used in the thesis. Firstly, the colloidal properties of clay (kaolinite) particles and interfacial chemistry of colloidal systems are highlighted, followed by interactive forces between colloidal particles. In addition, concerns for phosphate as wastewater pollutants are discussed. Moreover, the fundamentals of the CF process for wastewater treatment are presented, where CF kinetics, mechanisms and factors affecting the CF process are highlighted. In addition, polymer adsorption processes and thermodynamic concepts in CF are described. Herein, a description of adsorption studies and the various tools used for its evaluation, such as adsorption kinetic models (pseudo first and pseudo second order kinetic models) and adsorption isotherms models (Langmuir, Freundlich and Sips isotherm models) are also presented. The thermodynamic concepts that influence CF polymer flocculants materials such as hydrogen bonding, van der Waals forces, electrostatic interactions and hydrophobic interactions are also outlined. Finally, a literature survey of some conventional inorganic coagulants and biopolymer flocculants is discussed.

Chapter 3 reports on the removal of orthophosphate (P_i) by coagulation-flocculation with a variable combination of alum, biopolymers and biomass. The importance of this research was significant toward developing and understanding the flocculation properties of natural polymer and biomass materials for the removal of dissolved species such as phosphate. This project satisfies the first theme of the thesis research. The significance of this work relates to the overall objective of the thesis research because this research study demonstrated that the biopolymer flocculants are more efficient in a ternary system in removing phosphate in wastewater. The CF process depends on several factors, where the process is controlled by charge neutralization and polymer-bridging mechanisms, which supports hypotheses 2 and 5.

Chapter 4 focused on the demonstrated utility of native biopolymer flocculants combined with metal ion coagulant in a binary system for improved removal of phosphate. It relates to the overall objective of this thesis per the first theme. Herein, a CF optimization study was performed on $FeCl_3$-alginate binary system using the BBD-RSM for the removal of orthophosphate, P_i. The BBD-RSM was employed to provide an empirical relationship between the response function (P_i) and the independent variables (CF factors). The validity of the predicted response function was confirmed by experimental data, which showed comparable results. This study supports hypotheses 2, 4 and 6. Herein, the flocculation process followed electrostatic charge neutralization and ion-binding adsorption mechanisms.

An amphoteric chitosan-based flocculant material (CMC-CTA) was prepared and characterized using physicochemical methods related to flocculation properties in Chapter 5. The study reported in this chapter refers to the second theme of the thesis research. It also addresses the hypotheses 1, 2, and 3. The T_i and P_i removal properties of CMC-CTA were compared in the presence and absence of $FeCl_3$ coagulant. Herein, the increased molecular weight of the chitosan after the modification increased the flocculation efficiency. Also, several external conditions were observed to influence the flocculation properties of the flocculants. Additionally, the flocculation was well described by pseudo-first-order and pseudo-second-order kinetics for P_i and T_i removal, respectively. The CF process involved cooperative Coulombic electrostatic interactions between the biopolymer/Fe(III)/ P_i and/or kaolin colloidal species, along with the vital role of a polymer bridging mechanism.

Chapter 6 presents a continuation of Chapter 5, where an amphoteric chitosan-based flocculant material (CMC-CTA) was prepared and characterized using physicochemical methods related to

flocculation properties. This studies discusses the optimization of the factors affecting the CF process using BBD-RSM to obtain an optimal condition for efficient P_i and T_i removal using Fe(III)-CMC-CTA binary flocculant system. The study reported herein relates to the second theme of the thesis research. The second, fourth, fifth and sixth hypotheses are addressed in this chapter. An optimal condition was generated using the BBD-RSM for the removal of P_i and T_i, in which the experimental and predicted removal efficiencies were comparable. The flocculation process was observed to depend on entropy effects according to the thermodynamic properties of the process. The CF process is characterized by electrostatic charge neutralization, polymer bridging and polymer adsorption mechanisms.

Chapter 7 discusses the modification of chitosan to form a single-component cationic flocculant system for enhanced removal of P_i and T_i. It addresses the third theme, which focuses on synthesis, characterization and flocculation performance and floc properties of high molecular weight cationic chitosan-based flocculant in a single-component system. In addition, this study supported hypotheses 1, 2, 3 and 6. Herein, it was observed that modification of native chitosan improved its flocculation performance in a single-component system without the addition of metal ion coagulant. Also, external factors such as pH, temperature, settling time and flocculant dosage had a significant effect on the removal efficiency, where an optimum condition is required to obtain maximum removal. Moreover, the modified biopolymer improved the properties of the flocs. The flocculation process was observed to be driven by an entropy effect, following the thermodynamic studies. The T_i flocculation kinetics showed that the flocs formed at the optimal dosage had a greater rate of aggregation relative to breakage. In contrast, the P_i flocculation kinetics followed pseudo-second-order kinetics.

Lastly, Chapter 8 presents an integrated discussion of the manuscript chapters, conclusions drawn from the thesis, and proposed future work.

1.6 References

(1) Shannon, M. A.; Bohn, P. W.; Elimelech, M.; Georgiadis, J. G.; Marĩas, B. J.; Mayes, A. M. *Nature* **2008**, *452* (7185), 301.

(2) Rybicki, S. *Phosphorus Removal From Wastewater - A Literature Review*; 1997.

(3) Benyoucef, S.; Amrani, M. *Desalination* **2011**, *275* (1–3), 231.

(4) Powers, S. M.; Bruulsema, T. W.; Burt, T. P.; Chan, N. I.; Elser, J. J.; Haygarth, P. M.;

Howden, N. J. K.; Jarvie, H. P.; Lyu, Y.; Peterson, H. M.; Sharpley, A. N.; Shen, J.; Worrall, F.; Zhang, F. *Nat. Geosci.* **2016**, *9* (5), 353.

(5) Némery, J.; Garnier, J. *Nat. Geosci.* **2016**, *9* (5), 343.

(6) Smith, V. H.; Schindler, D. W. *Trends Ecol. Evol.* **2009**, *24* (4), 201.

(7) Teh, C. Y.; Budiman, P. M.; Shak, K. P. Y.; Wu, T. Y. *Ind. Eng. Chem. Res.* **2016**, *55* (16), 4363.

(8) Iwuozor, K. O. *Adv. J. Chem. A* **2019**, *2* (2), 105.

(9) Quinlan, P. J.; Tanvir, A.; Tam, K. C. *Carbohydr. Polym.* **2015**, *133*, 80.

(10) Wei, H.; Gao, B.; Ren, J.; Li, A.; Yang, H. *Water Res.* **2018**, *143* (2015), 608.

(11) Zhang, L.; Zeng, Y.; Cheng, Z. *J. Mol. Liq.* **2016**, *214*, 175.

(12) Mohammed, S. A. M.; Shanshool, H. A. *Iraqi J. Chem. Pet. Eng.* **2009**, *10* (2), 35.

(13) Renault, F.; Sancey, B.; Badot, P. M.; Crini, G. *Eur. Polym. J.* **2009**, *45* (5), 1337.

(14) Sharma, B. R.; Dhuldhoya, N. C.; Merchant, U. C. *J. Polym. Environ.* **2006**, *14*, 195.

(15) Lee, C. S.; Robinson, J.; Chong, M. F. *Process Saf. Environ. Prot.* **2014**, *92* (6), 489.

(16) Rojas-Reyna, R.; Schwarz, S.; Heinrich, G.; Petzold, G.; Schutze, S.; Bohrisch, J. *Carbohydr. Polym.* **2010**, *81* (2), 317.

(17) Cai, T.; Li, H.; Yang, R.; Wang, Y.; Li, R.; Yang, H.; Li, A.; Cheng, R. *Cellulose* **2015**, *22* (2), 1439.

CHAPTER 2

2 Literature review

2.1 Clay particles as colloids

2.1.1 Colloidal suspensions

In solid-liquid colloidal suspensions, the solid particles in the liquid phase are stable phases that exhibit little or no tendency to aggregate and separate from the water-phase.[1] Destabilization of colloidal suspension is necessary to ensure the separation of chemical precipitates from aqueous media. In solid-liquid colloidal suspensions, the collision between the solid particles occurs via Brownian motion. Colloidal particles have a large surface-to-volume ratio, and due to their negative or positive surface charge, they can remain as stable dispersion over a long period. Hence, they are less responsive to gravitational forces relative to surface phenomena. Due to the electrical charges of colloidal particles with their surroundings, they form suspensions, which are stable over time. Such suspensions include foams, emulsions, aerosols, gels, liquid, solids and gases. The behavior of colloidal particles in an aqueous medium is controlled by electrokinetic charge for hydrophobic colloidal systems. Each particle is negatively charged and remains stable due to electrostatic repulsion owing to the presence of electrical double layer (EDL) effects. For hydrophilic colloids with positive surface charge, these charges are mainly attributed to the presence of polar groups such as amine or carboxylic acid groups.[2] Equilibrium between two opposing forces, van der Waals (vdW) attractive and electrostatic repulsive forces determine the stability of colloid dispersions. However, due to the size of colloidal particles (0.01-1.0 μm), the repulsive forces between the particles are stronger than the attractive forces; hence, they tend to remain discrete and stably dispersed in the suspension. This occurs because there is a difference in the potential of the solvent medium and the surface of the electrostatically charged particles. The difference in potential between the solution and shear plane is known as the zeta (ζ) potential. Colloidal particles undergo agglomeration via vdW attractive forces when the ζ-potential is near zero, where they tend to be destabilized. On the other hand, colloidal stabilization occurs when the ζ-potential value is greater (negative or positive) through electrostatic repulsive forces. These phenomena of colloidal systems were initially described by the DLVO theory, named after Dergagin and Landau and Verwey and Overbeek.[3] Destabilization of the colloidal particles can be achieved through charge neutralization, electric double layer compression, colloidal entrapment, and interparticle bridging.[4] The most effective way to destabilize colloidal dispersions is to

aggregate the fine and discrete particles via coagulation-flocculation, where cationic mineral salts are added to neutralize the negative charges of the colloidal particles.[5] Clay particles are small in size due to their plate-like morphology, random isomorphic impurities and slow crystal growth rate during formation.[6] Due to their fine size and negative surface charge, they are among the most widely employed colloidal systems. The colloidal behavior of suspended clay particles is due to the physicochemical and interfacial characteristics of the minerals. Kaolin is the clay mineral often found in many industrial processes such as mining, painting, ceramics, pharmaceuticals and dye industries.[7] Hence, it is essential to understand the interaction between these colloidal particles to ensure better stability and develop appropriate approaches to destabilize them using coagulation-flocculation process.

2.1.2 Properties of kaolin

Kaolin is a white and soft powder consisting of fine-grained plate-like particles. It has suitable applications such as paper making, coating, pigment in paints, ceramic raw materials, functional fillers, extender, cosmetics, food additives and adhesives, due to its physicochemical properties.[7] Kaolin is mainly composed of SiO_2 and Al_2O_3 and has 1:1 hydrated aluminosilicate structure ($Al_2Si_2O_5(OH)_4$) with a chemical composition consisting of stacked pairs of tetrahedral silica sheets and octahedral alumina sheets, as shown in Figure 2.1.[8,9] This clay mineral has two different basal faces, an inert tetrahedral siloxane structure and octahedral gibbsite structure ($Al(OH)_6$) terminating in OH^-.[10] The layer edges end in both OH^- and O^{2-} anion groups. The two faces are connected by covalent (shared atoms), and hydrogen bonds (between silica-oxygen and aluminium-hydroxyl groups). Above pH 2, dispersed kaolin particles have a net negative charged surface due to accumulated amounts of minor isomorphous substitutions, broken bonds, crystal defects, structural disorder and surface protonation or deprotonation. Studies have shown that isomorphic substitution accounts for a small percentage of the overall charge of the kaolin colloidal particles.[8,10] Theoretically, both basal faces are electrically neutral, where the majority of the negative charge of kaolin particles takes place at the edge termination sites. At the particle edge, there is an exposure of aluminol (Al-OH) and silanol (Si-OH) groups due to the breaking of the silica tetrahedral and alumina octahedral bonds. Also, variable ionization (hydrolysis) of the hydroxyl groups leads to charge formation, and the nature of the charge is dependent mainly on the pore fluid environment such as pH and ionic strength.[11] The diameter, thickness and density of kaolin are 0.2-10 μm, 0.7 nm and 2.6 g/cm^3, respectively.[12]

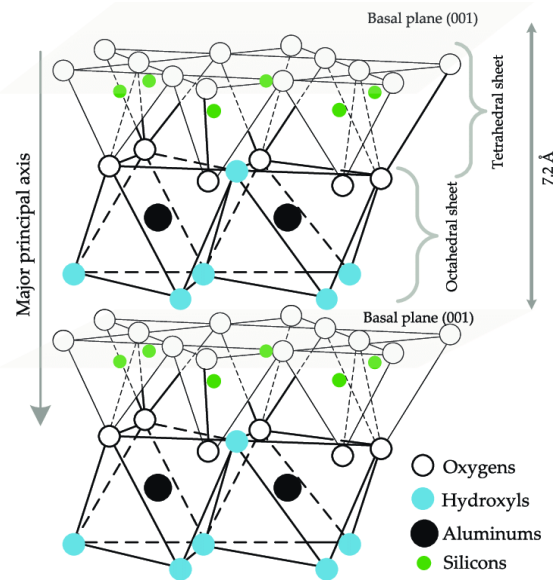

Figure 1.2: Lattice structure of kaolin. (obtained with permission from reference[12]).

2.1.3 Colloidal properties of kaolin

Kaolin has complex surface chemistry due to the heterogeneity of the charged surface site. It has two different surface sites, namely, basal and edge faces, which are arranged parallel and perpendicular, respectively, to the direction of the tetrahedral sheets.[13,14] The surface chemistry of the two faces are quite different, which results in anisometric charge distribution and aggregate structures which are influenced by pH. Many different particle arrangements can result from the interaction between face and edge sites from two or more particles. For kaolin particles, there are four major particle interactions or associations, which are face-to-face (F-F), edge-to-edge (E-E), face-to-edge (F-E) associations and dispersion.[15] F-E association is caused by Coulombic electrostatic attraction between negatively and positively charged faces and edges, while vdW attractive forces between the same charged faces lead to F-F and E-E interactions. Dispersion interaction occurs between similar faces due to EDL repulsion.[13] In the dispersed form, there is no interaction faces to form aggregates because the EDL of the particles is large, i.e., high repulsive forces between the particles, leading to the formation of stable colloidal dispersion. E-E and F-F aggregation result in large sludge volume with poor packing density (lower density), while F-E association produces flocs with large size and higher density.[13,14,16,17] The aspect ratio of kaolin clay particles is quite high, where the face sites exceed the edge sites by a factor of 5-10, but sufficient edge area is available for E-F association to occur when the edge is positive. During

association of colloidal particles, the pore fluid pH and ionic strength play key roles in the process.[14,15] E-F association dominates at low pH (pH <7.2) and low ionic strength because of Coulombic attraction between negatively charged faces and positively charged edge sites. At high ionic strength, F-F and E-E aggregation occur due to weak double layer repulsive forces. At high pH and low ionic strength, the edges and faces are both negatively charged, and the kaolin particles are dispersed in an aqueous medium due to increased EDL thickness. Other non-covalent interactions are also present between polymers and kaolin particles. These forces include vdW Coulombic electrostatic (attractive/repulsive) interaction, polar (or Lewis acid-base) and Brownian motion interactions.[18]

2.2 Interfacial chemistry

2.2.1 Surface charge

Gravitational sedimentation of colloidal suspensions is problematic due to the stability of the finely dispersed particles. When colloidal particles interact with an aqueous electrolyte, they may acquire surface charge through several means, such as ionization, specific ion adsorption, isomorphous substitution or ion dissolution.[19] When ions of opposite charge are unevenly dissociated from the surface of sparingly soluble substances, this leads to differential ion dissolution.[20] The process of ionization occurs via adsorption-desorption equilibrium between the surface potential and potential of the aqueous medium to determine H^+ and OH^- ions, and the process is pH-dependent. At alkaline conditions (pH >7), the colloidal surface undergoes deprotonation and becomes negatively charged, but the surface is positively charged at acidic conditions due to protonation at the surface. The isoelectric point (IEP) or point of zero charge (PZC) is the pH at which the surface is electrically neutral. When electrostatically driven surface adsorption of ionic species occurs, it results in charging of the surface, the process is known as specific ion adsorption and it occurs in the Stern layer of the EDL. Isomorphous substitution occurs mostly in clays when an ion of similar size but lower valency replaces another ion in a crystal structure, which then causes a negative charge surface.[21] In kaolin colloidal particles, the different crystal faces, such as basal faces and edges lead to heterogeneous charge distribution. The basal faces have a negative charged surface at all pH conditions, and the edges could have positively or negatively charged surfaces depending on the pH.[22] The negative charge of the basal face is due to isomorphous substitution in the kaolin sheets, which resides at the hydrophobic basal faces, with the hydrophilic basal faces covered with strongly associated water molecules.[20] At pH below and

above the PZC of the surface groups of the kaolin, the silanol and aluminol groups undergo protonation and deprotonation, respectively, to become positively or negatively charged at the edges. Since the basal faces carry negative charges, they may be repelled from or attracted to the edges at pH values above and below the PZC of the edges, respectively. The PZC has been reported to range from pH 5-7, which is a balance between the low IEP of the silanol groups (pH 2-3) and high IEP of the aluminol groups (8-9).[23]

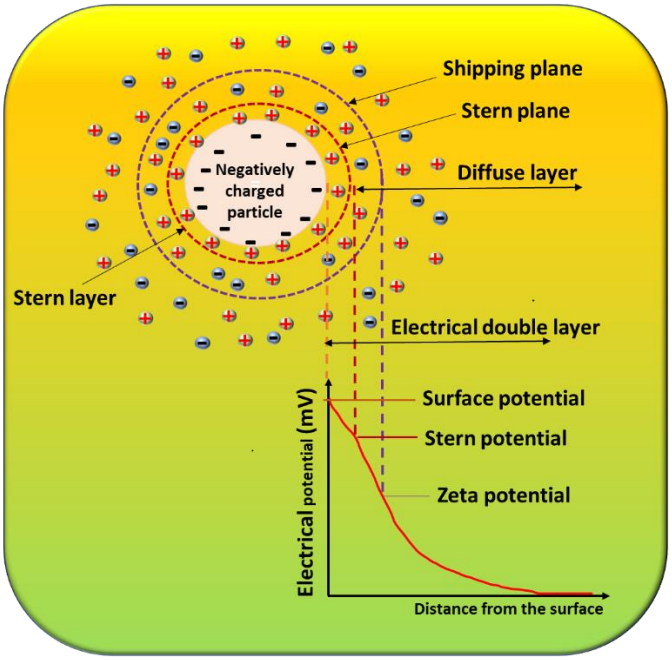

Figure 1.3: Schematic illustration of the electric double layer. (Adapted with permission from refences[4]).

2.2.2 The electric double layer (EDL)

Colloidal particles develop an electrical surface charge at their surface when in contact with an electrolyte solution. Hence, the electrostatic attraction takes place between dispersed colloidal particles and oppositely charged ions, or counterions in aqueous solution. Some counterions are adsorbed specifically to the surface to balance the negative surface charges, while most are distributed into a diffused double layer, as shown in Figure 2.2.[4] The ions specifically adsorbed at the surface are held together by vdW and electrostatic forces and they form the Stern layer. The counterions on the surface will attract their oppositely charged ions (co-ions of the primary

charge), to form the diffused layer, which is defined as a loosely associated cloud of ions distributed according to electrostatic forces, random Brownian motions, thermal agitation and their hydration volume.[24] When the colloidal particles are in motion, only a fraction of the diffused layer will move along with the Stern layer, but shearing at the plane. The potential at this surface shearing is called the ζ-potential, which is a measure of the surface charge of colloidal dispersions. The zeta potential of colloidal dispersions in wastewater ranges from -5 mV to -40 mV, due to the presence of its negative charged groups on the surface.[25] The Stern layer and the diffused layer constitute the electric double layer, and its formulation ensures electroneutrality, and hence the stability of the overall colloidal system. The thickness of the double layer is designated by the reciprocal Debye constant, also known as the Debye length. The Debye constant (κ) is given as the ratio of the Coulomb force to thermal energy according to equation (2.1).[26]

$$\kappa = \left\{ \frac{e^2 \sum n_i(\infty) z_i^{\,2}}{\varepsilon_r \varepsilon_o k_B T} \right\}^{1/2} \tag{2.1}$$

Here, e is the charge of an electron, $n_i(\infty)$ is the number per unit volume of electrolyte ions (i) with valence z_i in the bulk solution distant from the surface, k_B is the Boltzmann's constant (1.38×10^{-23} J/K), T is the absolute temperature, ε_0 is the permittivity of vacuum and ε_r is the relative permittivity (or the dielectric constant) of the solution. Based on the Gouy-Chapman model[27,28] of the electrical double layer where the solvent is seen as a structureless continuum, and ions as point charges, the electrostatic potential (ψ) around a surface in an electrolyte solution is given as

$$\varepsilon_r \varepsilon_o \nabla^2 \psi = -e \sum z_i n_i(\infty) \exp\left\{ \frac{-e z_i \psi}{k_B T} \right\} \tag{2.2}$$

Equation (2.2) is also known as the non-linear Poisson-Boltzman equation, which is a combination of Boltzman equation, the Poisson equation and volume density of charge when the solution permittivity is constant, given in equations (2.3-2.5), respectively.[29] Here, ρ is the density, ψ is the electrostatic potential. Even though equation (2.2) is useful in calculating the electrostatic potential, it has certain limitations and boundary conditions applied to it, which limits its application. Details of these limitations and boundary conditions have been discussed elsewhere.[24]

$$n_i = n_i(\infty) \exp\left\{ \frac{-e z_i \psi}{k_B T} \right\} \tag{2.3}$$

$$\nabla^2 = \frac{\rho}{\varepsilon_r \varepsilon_o} \tag{2.4}$$

$$\rho = \sum e z_i n_i \tag{2.5}$$

2.2.3 Electrokinetic zeta (ζ) potential

Colloidal dispersion with a compactly packed Stern layer around it will be generally neutral; however, counterions are attracted to the surface, and co-ions are repelled from the surface toward the bulk solution. Hence, there will be non-uniform ionic distribution around the surface, resulting in a potential difference within the EDL.[24,30] The surface potential is the potential at the particle surface, which changes into Stern potential in the Stern layer and eventually becomes zero in the far-out bulk solution according to Figure 2.2. In the Stern double layer model, ions are considered to have finite size instead of point charges.[31] The Stern layer is considered as the distance between the surface and the Stern plane, which is an inner boundary equivalent to the radius of one hydrated ion, while the diffused layer is seen as a mobile layer found behind the Stern layer. The distance between the Stern layer and the diffused layer has a boundary called the shear plane and the corresponding potential is known as the zeta potential (ζ-potential).[31] Measurement of the ζ-potential of colloidal dispersions provides an important tool to understand the nature of the surface charge and interaction between particles within the colloidal system. For a colloidal system, when the zeta potential is low, ($10 < \zeta > -10$ mV), the particles aggregate due to attractive vdW forces which bring about the destabilization of the colloidal dispersion to enable rapid sedimentation of the fine particles. However, there are repulsive forces between the colloidal particle when the ζ-potential is high ($\zeta = \pm 50$ mV) due to the overlapping of the electrical double layers, which enhances their stability and remain dispersed in the aqueous medium.[32]

Zeta potential may be determined experimentally via electrokinetic measurement such as electrophoresis or electroacoustics.[33] Electrophoretic technique involves the passage of light through the colloidal suspension. It requires the use of dilute suspension (< 0.02 wt% solid) in order to avoid significant attenuation of the light intensity. The electroacoustic technique is based on the principle that the application of an alternating electric field to a charged colloidal suspension will generate a series of sound waves and this phenomenon is known as electrokinetic sonic amplitude (ESA) effect.[34] The difference in the density of the colloidal particles and the fluid is

required to enable the two phases, not moving as a single phase. Details regarding the theory, technique and shortcomings associated with this technique and their relationship to zeta potential and size measurement are described further elsewhere.[35,36] The zeta potential values of colloidal suspension are determined via electrokinetic measurements using instruments such as zetasizer, zetaphore meter and zeta.[25]

2.2.4 Point of zero charge (PZC) and isoelectric point (IEP)

The point of zero charge is another important parameter of particles with an EDL. It is defined as the pH at which the net surface charge of colloidal particles is zero due to effect of potential determining ions.[37] PZC and IEP are used interchangeably and they are the same when there is no adsorption of other ions except potential determining H^+ or OH^- ions at the surface of the colloidal material.[38] However when other specific ion adsorption occurs, the PZC and IEP generally have different values. PZC is generally determined by pH values and different particles have different PZC values in different solutions. The PZC is essential in coagulation-flocculation system because it has a significant impact on adsorption of ions in solution, especially that of counterions. The particle ζ-potential is 0 mV at the pH of the PZC. However, at pH values beyond and below that of the PZC, the ζ-potential of the particles begins to reverse, and the surface properties behave in an opposite fashion. These changes in the zeta potential or the surface charges result in changes in the corresponding electrostatic double layer force; hence, a variation in the interaction between particles.[38–40] For instance, at pH lower than the PZC, the surface charge of the particles becomes positively charged due to protonation at the surface. However, at pH above the PZC, there is deprotonation on the surface; hence, the particle surface is negatively charged. PZC is employed in this study as a complementary method to the measurement of the ζ-potential, in observing the surface charge of the flocculants and the colloidal particles to understand the effect of the electrostatic double layer in the coagulation-flocculation process for colloidal particles and dissolved phosphate.

2.3 Interactive forces between colloidal particles

2.3.1 DLVO theory of colloidal particles

The stability of colloidal particles is mostly determined by the interaction of the various attractive and repulsive forces between the particles, which was independently described by Dergagin and Landau and Verwey and Overbeek in the DLVO theory.[4] DLVO theory is a known

established framework that considers the total interaction energy between any two particles as a function of particle separation distance and helps to predict whether or not a particular colloidal suspension will be stable. According to this theory, the total energy (V_T) of interaction between two particles is expressed as the summation of the vdW attractive (V_A) and EDL repulsive (V_R) forces, as given in equation (2.6).

$$V_T = V_A + V_R \tag{2.6}$$

The vdW attractive force arises from three types of electrical interactions, which are the Keesom (orientation) interaction between two randomly arranged dipoles, the Debye (induction) interaction between a randomly oriented dipole and induced dipole; and London (dispersion) interaction between a fluctuating dipole and an induced dipole.[41,42] The vdW force is effective over a short range of distance (<10 nm) and decays rapidly as the interaction distance increases owing to electromagnetic radiation. vdW energies are independent of solution pH and ionic strength and are strongly affected by the refractive index difference between the solvent and the colloidal particles. The repulsive component of the DLVO theory is attributed to the systematic interactions of the overlapping electrical double layers at the surface of the colloidal particles as they meet each other in an aqueous medium.[42,43] Solution conditions such as pH and ionic strength and presence of charged species are known to affect the range and magnitude of the EDL drastically.[11] According to the DLVO theory, there is no additional repulsive interaction resulting from hydration forces since it is assumed that the dispersed particles are not hydrated.

The vdW force between two particles depends on the geometry of the two particles and the Hamaker constants of the system. The vdW expression for two spherical particles of radii r_1 and r_2 and a shortest-center distance (h_o) is given as[25]

$$V_A = -\frac{A_H}{6}\left\{\frac{2r_1r_2}{h_o^2-(r_1+r_2)^2}+\frac{2r_1r_2}{h_o^2-(r_1-r_2)^2}+\ln\frac{h_o^2-(r_1+r_2)^2}{h_o^2-(r_1-r_2)^2}\right\} \tag{2.7}$$

For an interacting system where $r >> h$, equation (2.7) can be asymptotically reduced to

$$V_A = -\frac{A_H}{6}\frac{2r_1r_2}{r_1+r_2} \tag{2.8}$$

Here, h_o is the distance between the centers of the respective diameter of the two spherical particles approaching each other, whereas, r_1 and r_2 are half the diameter of particles 1 and 2, respectively. A_H (in J) is known as the Hamaker constant. The estimated A_H value of kaolin is 10 – 70 $\times 10^{-20}$ J

from colloidal measurements. At larger distances, a retardation factor is needed to account for the finite velocity of the propagation of electromagnetic radiation between dipoles, which leads to a rigorous rapid decay of the strength of the vdW attraction than described in equation (2.7). An analytical estimate for the magnitude of A_H can be calculated from equation (2.9).[44]

$$A_H = \frac{3}{4}k_B T\left(\frac{D_1 - D_3}{D_1 + D_3}\right)\left(\frac{D_2 - D_3}{D_2 + D_3}\right) + \frac{3}{8\sqrt{2}}h\upsilon_e \frac{\left(n_1^2 - n_3^2\right)\left(n_2^2 - n_3^2\right)}{\left(n_1^2 + n_3^2\right)^{1/2}\left(n_2^2 + n_3^2\right)^{1/2}\left[\left(n_1^2 + n_3^2\right)^{1/2} + \left(n_2^2 + n_3^2\right)^{1/2}\right]} \tag{2.9}$$

Here, D and n are the dielectric constant and refractive index of the macroscopic phases (1) and (2), and the aqueous medium, (3), respectively, h is the Planck's constant and υ_e is the major absorption frequency. Using the equation (2.9), the A_H value of kaolin at 25 ^oC has been reported to be 1.53×10^{-20} J, which is comparable to an experimental value of 2.2×10^{-20} J.[44]

For two spherical particles of equal radius, the electrostatic repulsive potential is as follows:[24,44]

$$V_R = 32\pi_\varepsilon r\varepsilon_o\left(\frac{k_B T}{ze}\right)^2 \gamma^2 \exp\left(-\kappa h_\circ\right) \tag{2.10}$$

Here, z is the ionic concentration in the medium, e is the electronic charge; γ is a function of dimensionless surface potential, h_o is the distance between the particles. As the diameter of the particles increases, their radii also increases, which subsequently leads to greater repulsive energy between the two spherical particles. The important parameter that describes the double layer is the zeta potential (ζ) and the Debye-Hückel constant (κ).[45] The Debye length (κ^{-1}) can be calculated from the above equation by considering the outer part of the double layer to be essential using equation (2.11)[46]

$$\kappa = \left(\frac{2000F^2}{\varepsilon DRT}\right)^{1/2}\sqrt{I} \tag{2.11}$$

Here, F is the Faraday constant (96486 C/mol), R is the gas constant (8.321 J/Kmol), and I is the molar ionic strength, which can be calculated from equation (2.12), where c_i is the molar concentration.

$$I = \frac{1}{2}\sum z_i^2 c_i^2 \tag{2.12}$$

According to equation (2.12), the repulsive interaction decreases exponentially as the particle separation increases, and the range of repulsion is remarkably reduced with counterion valence and electrolyte solution concentration, due to the ionic strength dependence on Debye constant (κ).

The DLVO theory involves the estimation of attraction energy (vdW) and repulsive energy (overlapping EDL) as a function of the distance between the particles, as shown in Figure 2.3. It predicts that the agglomeration of colloidal particles depends on the extent of the EDL compression, which is strongly influenced by the solution pH and the concentration and the valence of the counterions.[47] In Figure 2.3, repulsion forces dominate at larger distances up to 100 nm, while at shorter distances (<10 nm), vdW attractive force dominates, depending on their magnitude. The combination of the vdW attractive and EDL repulsive forces leads to one maximum (primary maxima) and two minima (primary and secondary minima).[25] Colloidal stability and the rate of particle aggregation is dependent on the shape of the net DLVO potential. At the primary maxima, an energy barrier needs to be overcome by the two approaching particles before they can agglomerate.[4] As the energy barrier increases, the rate of particle association decreases, due to strong repulsive forces between the particles as they approach each other. In colloidal systems, Brownian motion controls the kinetic energy of the approaching particles, and the energies of the particles follow a Gaussian distribution. For particles of the same charge, there is a large energy barrier due to the strong electrostatic repulsion between the particles, leading to a stable dispersed colloidal system.[43,48] But in the case where the kinetic energy of the particles is large enough to dominate the energy barrier, particle aggregation occurs owing to the destabilization of the colloidal particles. The magnitude and nature of particle-particle interaction force depend on several experimental variables such as dispersion pH, particle size, nature and concentration of electrolyte ions, the solubility of surface-active species including surfactants, polymers and polyelectrolytes.[47] Destabilization of colloidal dispersion requires inducement of attraction between particles to promote maximum particle contact and the formation of large, fast settling of aggregated flocs. This is mostly achieved by several mechanisms such as double layer compression, electrostatic charge neutralization, interparticle bridging and colloidal entrapment.

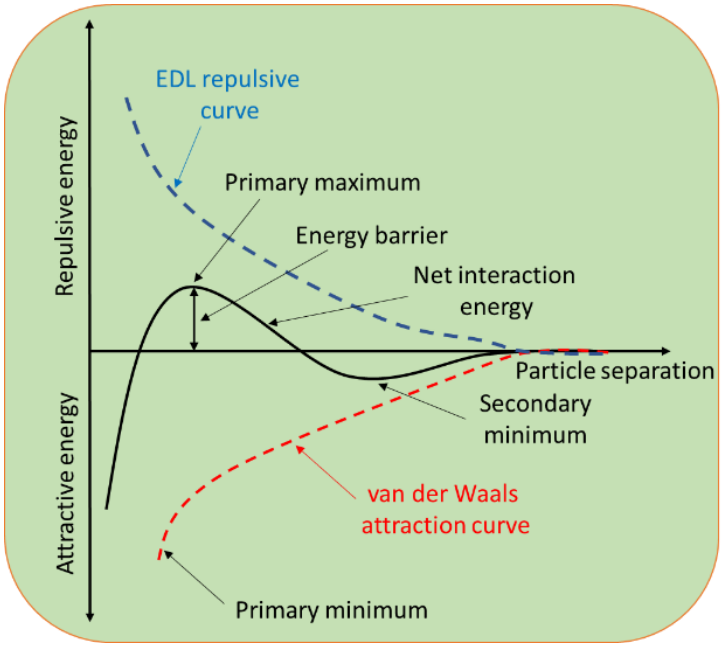

Figure 1.4: Interparticle forces as a function of particles separation distance.

2.3.2 Non-DLVO contribution to colloidal stability

Even though the DLVO theory can predict the interaction between colloidal particles and the stability of colloidal dispersion based on vdW and EDL forces, the complexity of many systems requires other forces to describe their colloidal behavior properly. As an illustration, the validity of the Hamaker constant and Stern potential estimates have been questioned for the colloidal behavior of kaolin dispersions since deviations have been reported on the classical understanding based on the DLVO theory and/or double layer theory.[49] Other non-DLVO forces that affect the interaction of colloidal system and their stability are discussed below.

2.3.2.1 Hydration effects

Hydration effects were shown experimentally and theoretically to be strong and short-range repulsive forces attributed to the affinity of the hydrophilic surfaces toward water.[49] Water monolayers tend to bind strongly to hydrophilic surfaces. Hence, in order for two hydrophilic surfaces to be in contact, they must overcome additional forces such as repulsive hydration forces, along with the vdW and EDL forces. This occurs because water molecules adjacent to the particle surface show properties indicating that molecules arrange in a more structured configuration than in the bulk water.[50] Therefore, water molecules are forced in a different configuration with

unfavorable entropy when hydrated cations or the structured water layers come into close contact with a structured water surface. The effect of such structured hydration results in repulsive forces between surfaces. Such types of hydration forces have been reported experimentally on the surfaces of clay, silica and mica.[51–53] For instance, hydration force between mica sheets have been observed to increase with an increasing number of cation hydration via a surface force apparatus.[51–53] Hydration forces have been expressed mathematically in a single exponential form according to equation (2.13).[50]

$$F_{HD} = \frac{2\pi r_1 r_2}{r_1 + r_2} K_{HD} \exp\left(-\frac{h}{\lambda}\right) \tag{2.13}$$

Here, λ is the decay length, K_{HD} is the hydration force constant (N/m) and the other variables have meanings as described above. Values of λ and K_{HD} can be experimentally obtained.[50]

2.3.2.2 Hydrophobic effects

Unlike hydration interaction, hydrophobic effects are a long-range (>10 nm) attractive force which occurs owning to two hydrophobic surfaces trying to eliminate water molecules between them.[54,55] Polar and ionic compounds can readily dissolve in water due to the polar nature of water. However, the introduction of nonpolar (hydrophobic) compounds into water or polar solvent leads to hydrophobic effects. Hydrophobic effects are the tendency of nonpolar molecules to self-associate instead of dissolving individually in water.[56] The hydrophobic effects are the driving force for aggregation or formation of micelles by amphiphilic molecules, and removal of nonpolar molecules from the aqueous environment.[57] For instance, when oil or other nonpolar molecules interact with water, the hydrogen bonding networks in water are disrupted by the nonpolar compounds and are forced to rearrange around the nonpolar moieties, which causes the formation of small cages around the individual nonpolar molecules, as shown in Figure 2.4. The cages formed are ordered structures, hence the solvent rearrangement in the ordered structures is not entropically favored.[58] However, the apolar molecules associate to form bulk structures, which reduces the number of water molecules required to form cages around them, thus, increasing the entropy of the solvent molecules.[59] The transfer of the nonpolar molecules into water is an exothermic process because of the formation of a water cage surrounding the individual hydrophobic species, resulting in the formation of hydrogen bonds between the water molecules. The formation of the individual small water cages leads to the entropy being less positive; however, the hydrophobic species self-

assemble to form bulky species and the number of water molecules required to form cages decreases, which in turn increases the entropy of the water molecules. The increased entropy is due to less ordering of the water molecules. Hydrophobic effect is a spontaneous process because the increasing entropy and exothermic nature of the process give rise to a negative value of $\Delta_{ads}G^{o}$, according to equation (2.14).[60]

$$\Delta_{ads}G^{\circ} = \Delta_{ads}H^{\circ} - T\Delta_{ads}S^{\circ} \tag{2.14}$$

Hydrophobic forces were found to be much greater than vdW forces at large distances, and it increases with increased hydrophobicity of the surface. The effect of the hydrophobic attractive force has been termed as xDLVO theory, which was added to the DLVO theory. The hydrophobic force of attraction as a function of distance for inter-particle interaction is given as:[54]

$$V_{AB}(h) = \Delta G^{\circ} \exp\left(\frac{h_o - h}{\lambda}\right) \tag{2.15}$$

Here, λ is the decay length for the molecular species in the liquid or solution state, h_o is the minimum separation distance and ΔG^{o} is the interaction energy, estimated through surface tension values obtained from contact measurements. Experimentally, the hydrophobic force determination involves direct force measurement using the Langmuir-Blodgett technique, surface force apparatus or atomic force microscope. Deviation of clay dispersion stability in the presence of multi-valent ions has been reported based on the xDLVO approach, where the variation has been attributed to hydrophobic effects.[54,55]

The biopolymer materials used in this study are considered hydrophilic due to the −OH and −NH groups on their surface, while the hydrophobic portions may reside within the biopolymer, and they will be expected to display greater hydration in water than their apolar counterparts. However, the hydrophilic nature of the materials could be changed after chemical modification towards hydrophobic properties; hence, hydrophobic effects could play a vital role in the CF process.

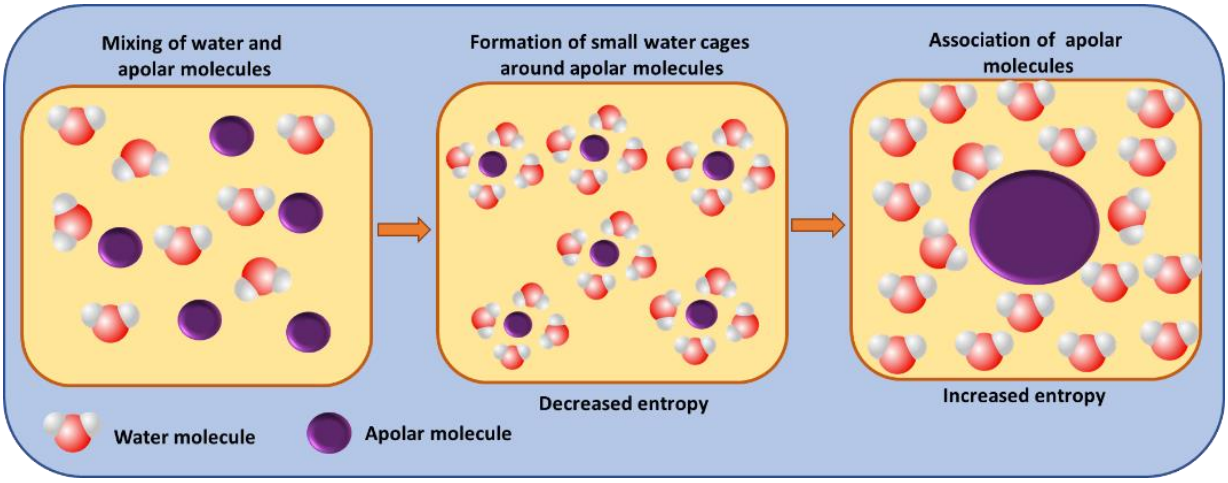

Figure 1.5: Schematic illustration of apolar association due to hydrophobic effects in an aqueous medium.

2.3.2.3 Steric/Electrostatic force

Steric force is known to be a short-range interaction arising from the adsorption of macromolecules at a surface, which has effects on a separation range comparable to twice the contour length of the hydrophobic chains of the molecules.[55,61] When macromolecules adsorb on the surface of colloidal particles, they may induce repulsive interactions, which increases the stability of the colloidal systems. Polymers such as sodium silicates, polyphosphates, and polyacrylates are usually used to enhance colloidal stability by preventing coagulation.[61–63] Non-ionic polyvinyl alcohol shifts the shear plane away from the particle surface, which reduces the magnitude of the zeta potential as well as providing polymeric steric repulsion.[63] Polyphosphates result in a negative increase of the surface charge to promote the electrostatic repulsion between the particles to induce steric stability. Both steric and electrostatic repulsion may be induced on colloidal systems when they adsorb polyacrylates, which tend to increase the stability of the colloidal system.[64] Phenomena related to entropy effects such as volume repulsion and interpenetration or osmotic pressure effects are the major cause of steric stabilization.[3,54]

2.3.2.4 Hydrogen bonding

Hydrogen bonding is a special type of dipole-dipole attractive force which occurs between two species owing to a through-space interaction such as X−H---O, as illustrated in Figure 2.5. Herein, X and O are strong electronegative atoms, where O has lone pair electrons.[65] Hydrogen bonding is energetically weaker than ionic and covalent bonds but stronger than dipole-dipole and

dispersion forces. It is the primary intermolecular force that holds water molecules together and accounts for the anomalous properties of water.[66] Hydrogen bonding is also present in organic molecules containing −OH and −NH groups.[65] For polysaccharide biopolymers such as chitosan and alginate with −OH and −NH groups, hydrogen bond formation with neutral carboxylic acid molecules and their anionic derivatives account for the major interaction that governs the coagulation-flocculation process.

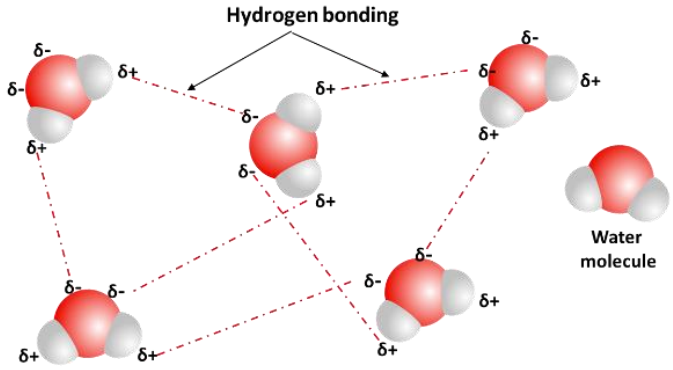

Figure 1.6: Schematic illustration of intermolecular hydrogen bonding between water molecules.

2.3.2.5 Polymer-solvent interaction

Many thermodynamic properties of polymer solutions such as solubility and phase equilibria are expressed using the polymer-solvent interaction parameter, χ. This parameter was introduced by Flory and Huggins, and it describes the interaction between solvent and polymer molecules in their lattice model of polymer solution.[67] Dissolution of a polymer in a solvent generally forms random coils, which may be described by a three-dimensional random walk. Other than the polymer-solvent interaction, there is another interaction between the polymer segments known as the interaction volume. The interaction parameter (χ) describes the enthalpy of mixing for the polymer solution. When $\chi = 0$, the solvent-polymer segment interactions and the interaction between the polymer segment are equally favored, and the solvent under this condition is called a theta-solvent (θ-solvent).[67] In a good solvent where $\chi < 0.5$, the polymer-solvent interaction is energetically favored, and the polymer segments repel each other leading to a less favorable polymer-polymer interaction. The process is known as a self-avoiding walk, and it describes the ideal state of the polymer chain where it has expanded interfacial and solution conformations. Solvent-polymer interaction is energetically less favored relative to segment-segment interaction

in a poor solvent where $\chi > 0.5$, leading to a contracted interfacial and solution conformation. Polymer-solvent interaction is temperature-dependent, and Flory-Huggins theory predicts that mixing is governed by an entropic process.[68] With water being used as the main solvent for the dissolution of the biopolymer flocculants, polymer-solvent interaction will be favored, and the polymer chain will be expanded in solution to enhance the flocculation performance since water is considered as a good solvent.

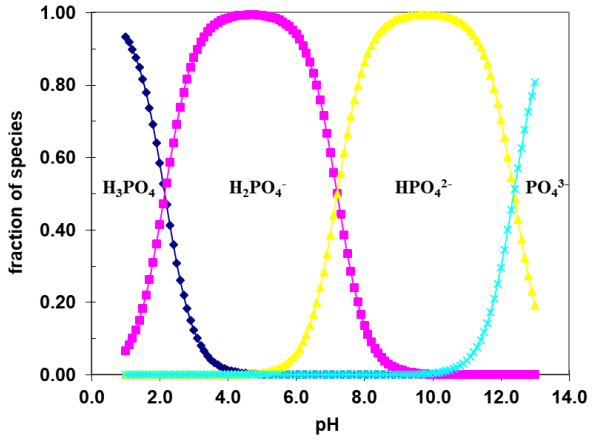

Figure 1.7: Speciation of orthophosphoric acid in aqueous medium at different pH levels.[69]

2.4 Phosphorus as an oxyanion contaminant

2.4.1 Chemistry of phosphorus

Phosphorus is among the most abundant elements (the 11th most abundant element) in the earth's crust. It has high reactivity and hence always found in combination with other elements such as oxygen.[70] Phosphorus in its elemental form has four allotropes[71] with different physical and chemical properties, which are white (or yellow), red, black and violet phosphorus. White phosphorus is very reactive because of its tetrahedral structure, causing ring strain, and it widely exists as P_4.[71] Red phosphorus; however, shows more stability since it exists as polymeric chains (P_n).[71] Heating of red phosphorus to 300 ^oC in the absence of oxygen, or under direct exposure to sunlight can lead to the formation of white phosphorus.[72] Phosphorus is an essential nutrient and used by plants for growth and development.[73] Phosphorus is found in the pentavalent state, with tetrahedral coordination to oxygen atoms or hydroxyl groups in sewage and other natural water bodies. It exists in natural water as orthophosphate (inorganic phosphate), condensed phosphate

(polyphosphate), organophosphate or phosphonate. Orthophosphate is the most abundant form of phosphorus in water. Orthophosphate undergoes speciation at different pH conditions to form H_3PO_4 (pH < 2.0), $H_2PO_4^-$ (pH ~2-7) or HPO_4^{2-} (pH ~7-11) or PO_4^{3-} (pH > 11), as shown in Figure 2.6.[69] It is evident from Figure 2.6 that $H_2PO_4^-$ and HPO_4^{2-} would dominate at the pH at which natural waters typically exist. Condensed phosphate contains two or more phosphorus atoms that are coordinated by P-O-P bonds. However, inorganic phosphate, there is P-O-C linkage present in the compound. All these forms of phosphorus in water bodies exist as soluble or dissolved species or particulate substances, as shown in Figure 2.6.[69,74] Orthophosphates are produced by natural processes and are found in sewage. Polyphosphates are used for treating boiler waters and in detergents. Organic phosphates are essential, and their occurrence may result from the breakdown of organophosphate.[75]

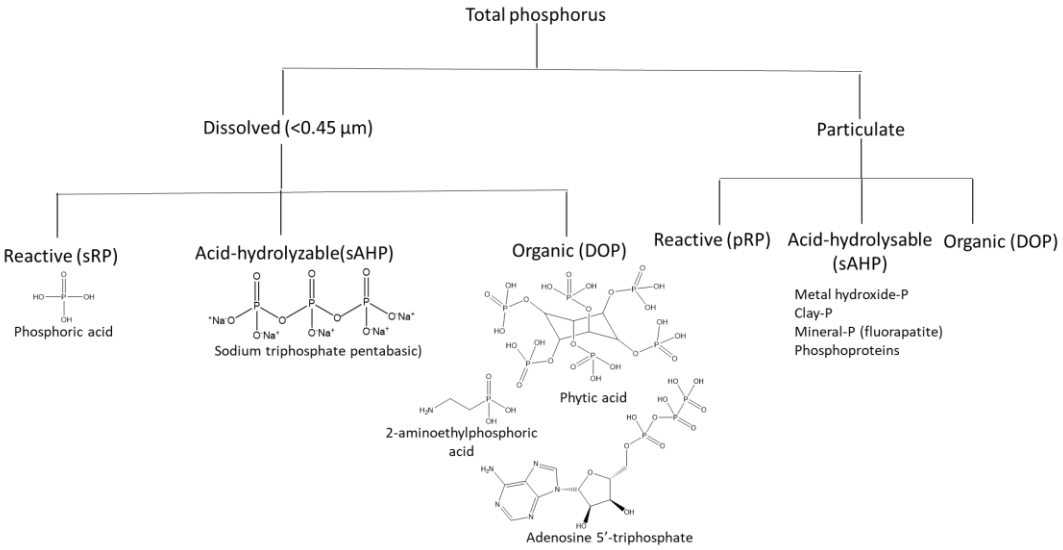

Figure 1.8: Phosphorus fractions and examples of compounds that fall under each category. (Adapted with permission from references[76,77]).

2.4.2 Sources of phosphorus in water

Under natural conditions, phosphorus is typically scarce in water because it is a nutrient and it is consumed by plants. However, anthropogenic activities have led to excessive loading of phosphorus into many water bodies. The major sources of phosphorus in water and wastewater are obtained from human, domestic and industrial waste[78] and run-off from agricultural activities, such

as the application of fertilizers to the soil for plant growth.[79] There are three primary sources of phosphorus in municipal wastewater, and their percentage levels are as follows: human excreta = 30-50%; detergents = 50 – 70 % and industrial (2 – 20 %).[80] For example, in the UK, sewage effluent and agricultural run-off are the main sources of phosphorus entering rivers, with up to 70% being attributed to sewage discharges.[81] In the United States and Canada, phosphorus loading estimates indicated that the largest anthropogenic sources of phosphorus to the environment are traced to fertilizer application, manure application, other non-point sources and wastewater treatment plant discharges.[82] In the Netherlands, about 4.2 million tons per year of phosphorus are obtained from industrial discharges, whereas; 18 million tons per year originate from domestic wastewater.[83] Similar calculations from Krakow (Poland) revealed that about 85% of the total phosphorus load is obtained from domestic sources.[80] Human wastes often contain orthophosphate and other biologically related phosphorus-containing compounds, such as nucleic acid and phospholipids. The major form of phosphorus in domestic and industrial wastewater is condensed phosphate. Natural water bodies are often contaminated by non-point sources such as natural decomposition of rocks and minerals, agricultural run-off, erosion and sedimentation, atmospheric deposition and direct input by animals. This source of contamination is usually appreciably higher than point sources of phosphate contamination.[84] Typical concentrations of the different forms of phosphorous in water are listed in Table 2.1.[69]

Table 1.1: Approximate speciation of phosphate in typical domestic wastewater influent[69]

Phosphate form	mg/L (P)	Molarity (µM)	Composition (%)
Total	10	320	100
Ortho	5	160	50
Tripoly	3	32	30
Poly	1	16	10
Organic	< 1	16	< 10

2.4.3 Global concerns for phosphorus

Phosphorus is a necessary element for life as it is found in proteins, DNAs, RNAs and enzymes. It is indispensable for the energetic metabolism (ADP/ATP) of human beings. This makes phosphorus irreplaceable in this biological function by any other element.[75] Phosphorus is a plant nutrient that is essential for plant growth, which makes it the limiting factor in plant growth.[85]

Phosphorus deficiency in the soil may inhibit plant growth; hence, it is often employed to croplands in the form of fertilizer or synthetically as single or triple superphosphate or mono-ammonium or diammonium-phosphate.[86] This phosphorus from the cropland may enter into water bodies via erosion and agricultural runoffs. However, excess levels of phosphorus in water bodies can cause eutrophication. Eutrophication leads to algal blooms, aquatic plant growth, taste and odour problems, and oxygen depletion in the water column.[87–89] Eutrophication of water bodies may be accelerated when phosphorus concentrations are between 0.1 and 0.2 mg/L. Compared to the phosphorus levels (0.2-0.3 mg/L) considered critical for plant growth, which indicates that the order and the magnitude of phosphorus in water bodies are more sensitive. Hence, small additions of phosphorus can lead to a significant change in the aquatic environment.[79]

Global usage of phosphate has significantly increased over the past years due to the continuous increase in the human population. This remarkable growth in the global population is therefore expected to increase the phosphorus required for agricultural activities. At present, 82% of total phosphorus mined is used in agriculture, while 7% are used in animal feed. The remaining 11% is used in industries such as medicine, pharmaceuticals, oils, detergents, and textiles.[89–92] It has been estimated by the Water Management Institute that the production and use of phosphorus will increase by 70% due to the growth rate of the global population.[74,89,93] This shows that that phosphorus levels in water bodies will potentially increase accordingly, which will, in turn, lead to eutrophication. Many countries around the world are concerned about phosphorus levels and the risks it poses to water quality. For instance, in the UK, the Code of Good Agricultural Practice for the protection of water quality urges that organic manure application rates must correlate with crop phosphorus uptake for rotation of soil containing more than 25 mg/L. Again, in the United States, it is required of all states to adopt the phosphorus index approach that rates the potential for phosphorus loss in runoff based on the source and transport characteristics of the site.[94] In the Netherlands, excess phosphorus in the soil has led to increased phosphorus leaching losses and environmentally acceptable nutrient losses.[83]

Phosphorus in water is usually present as dissolved phosphate. For the effective removal of dissolved phosphate, it must first be converted into a solid phase followed by the removal of this phase from the mainstream. The removal of phosphorus in wastewater has been investigated using different experimental techniques, such as adsorption[95–101], biological phosphorus removal[102–104], magnetic-based removal using Schwertmannite[105], electrocoagulation[106–108], membrane

process[109,110] and chemical precipitation.[111–113] Amongst these techniques, chemical precipitation is the most frequently used method. The advantages of the use of chemical precipitation, using salts of Fe(III) or Al as $FePO_4$ or $AlPO_4$, in the removal of phosphate are that they are relatively tolerant to toxic compounds, have lower space requirements, and, therefore, a lower installation cost. They can handle higher hydraulic loads and may be used as a pre-treatment stage for biological systems, which become more efficient in dealing with lower biochemical demand effluents.[114] Chemical precipitation is also cost-effective, flexible and simple. It can be used to assist phosphorus removal in aerated biological wastewater treatment units.[115]

Phosphorus levels in wastewater can be chemically analyzed using colorimetry, ion chromatography, or inductively coupled plasma optical emission spectroscopy, as outlined in Section A9.2.1 (Appendix A).

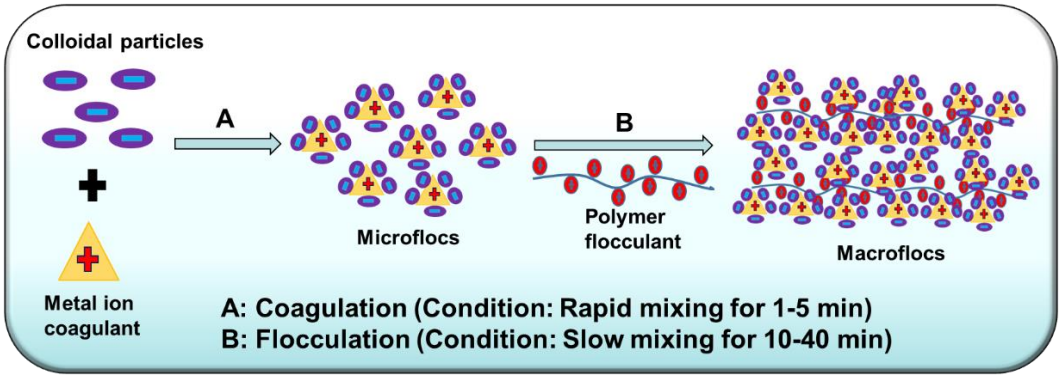

Figure 1.9: Schematic illustration of coagulation-flocculation process.[116]

2.5 Coagulation-flocculation

2.5.1 Background

Coagulation-flocculation (CF) is a physicochemical process used for separating heterogeneous (colloidal suspensions) and homogeneous (dissolved solids) mixtures.[5] The CF process has been employed in the wastewater treatment system, where it is used in primary, secondary or tertiary wastewater treatment processes. Wastewater obtained from different industries usually contain very finely suspended solids, metals, dissolved solids, colloids, inorganic and organic materials and other contaminants. The formation of particles with large mass for rapid sedimentation is problematic due to their fine size and surface charge.[5] Therefore, the removal of these contaminants from wastewater has become a global challenge for most industries in developed and

developing countries.[4,74,88,91–93,117–122] The CF process has proven to be an efficient solid-liquid separation process for the removal of suspended and dissolved solids, colloids, organic and inorganic contaminants in industrial, agricultural and municipal wastewater.[4,120–122]

Coagulation is the process by which colloids, suspended, dissolved and very fine solid particles in an aqueous environment are destabilized to ensure that they can agglomerate to form a large mass of solids for enhanced entrapment or filtration.[5,123] It usually involves neutralization of the surface charge of the colloidal particles to reduce their stability and to enhance microflocs formation. On the other hand, flocculation refers to the process in which destabilized particles undergo conglomeration via gentle agitation or stirring to form large aggregates so that they can be separated from the bulk wastewater by filtration, sedimentation, entrapment or flotation.[5,123] CF is a stepwise process where the flocculation process follows immediately after the coagulation process, as illustrated in Figure 2.7. The CF process is induced by the addition of coagulants and/or flocculants, which destabilize and aggregate the finely dispersed or dissolved particles to form macroflocs, which can settle rapidly. Common coagulants that are used are cationic metal salts such as $FeCl_3$, $FeCl_2$, $Al_2(SO_4)_3$, and $CaCl_2$, along with polyelectrolytes (polymers) which could be cationic, anionic or non-ionic that are employed as flocculant materials.[5] Generally, the colloids, suspended or dissolved particles have a negative surface charge in an aqueous medium. Hence, once the coagulant is added to the wastewater, the inorganic metal salt undergoes hydrolysis instantly at its IEP to form soluble and insoluble cationic hydroxide species, which then causes destabilization of the colloidal particles via charge neutralization and then form microflocs. The microflocs formed during the coagulation process are small and fragile and can readily break upon exposure to shear stress. Also, the flocs obtained herein, have little or no tendency to settle; hence there is a need to improve the floc properties and enhance rapid sedimentation. This is achieved by the addition of polymer flocculants or coagulant aids during the flocculation process. The flocculation process involves slow mixing or agitation to bring together and agglomerate the slow-settling microflocs to generate larger and denser flocs, hence facilitating their removal in subsequent sedimentation, filtration or flotation. Other than increasing the solidity, density and floc size, the use of the polymer flocculants significantly reduces the metal coagulant dosage required and increases the reliability of the coagulation-flocculation process and the contaminant species uptake or removal capacity.[124] Several reports have shown that the combined use of inorganic coagulants with polymer flocculants in binary or ternary systems leads to a reduced

dosage of the coagulant, reduced sludge volume and formation of larger and denser flocs with improved settling ability. In addition, the use of the polymer flocculants results in improved removal efficiency of the contaminants in wastewater.[116,125–127] The conventional method for performing the CF process in the laboratory involves the use of the jar test apparatus, as described in Section A9.2.2 (Appendix A).

2.5.2 Coagulation-flocculation kinetics

During coagulation, there is a destabilization of the colloidal particles via charge neutralization to form microflocs. The destabilized microflocs aggregate through particle-particle collision to form larger and denser flocs with a greater tendency to undergo sedimentation. The interparticle collision in the flocculation process can occur by two processes, namely, perikinetics and orthokinetics.[25]

2.5.2.1 Perikinetics flocculation

Perikinetics occurs due to the Brownian motion associated with the destabilized microflocs. The movement of the particles close enough for agglomeration to occur is controlled by Brownian motion. Perikinetic flocculation is applicable to small particles with a particle size of about 1.0 μm, where the surrounding water molecules continuously bombard them. The rate of floc population is dependent on the concentration of particles and temperature according to Smoluchowski.[128] The rate coefficient of collision for two uneven spheres with radii r_1 and r_2 is given by equation (2.16).

$$k_{12} = \frac{2k_B T}{3\eta}\left(\frac{r_1 + r_2}{r_1 r_2}\right) \tag{2.16}$$

Equation (2.16) reduces to equation (2.17) when the particles have equal radii, where k_{12} is 1.23×10^{-17} $m^3 s^{-1}$ at 25 ^oC for aqueous suspensions.

$$k_{12} = \frac{4}{2}\frac{k_B T}{\eta r} \tag{2.17}$$

During flocculation, each collision of two primary particles leads to the formation of an aggregated species; hence, there is a net loss of one particle. Therefore, the rate of decrease in the total number of particles in the early stages is given according to equation (2.18).[129]

$$\left(\frac{dn_T}{dt}\right)_{t\to 0} = -k_a\eta^2 \tag{2.18}$$

Here k_a is the rate coefficient (k_{12}) given in equation (2.17). Equation (2.18) can be integrated to obtain equation (2.19), where the total number of particle (n_T) at time t can be evaluated.[25,129]

$$n_T = \frac{n_0}{1+k_a n_0 t} = \frac{n_0}{1+ t/t_a} \tag{2.19}$$

Here, n_0 is the initial concentration, t_a is the aggregation time in which the number is reduced to one-half for small concentration. Perikinetics is only effective for small particles; hence, the rate of floc growth cannot be adequately sustained for an effective phase separation when the size of the flocs increases. Also, only minute particles can be removed in this process since the formed microflocs have poor settling properties because the process is limited by the floc size.[130,131]

2.5.2.2 Orthokinetic flocculation

Orthokinetic flocculation is based on the generation of velocity gradient within the wastewater to enhance particle interaction. In this case, a mild agitation promotes the production of the particles to form larger and denser flocs. This induces contact between the particles via bulk fluid motion (gentle motion of fluid). Herein, the rate of collision depends on the particle's nature, such as size, concentration and velocity shear gradient of the fluid.[4,132] The kinetics of particles greater than 1.0 μm are controlled by orthokinetics aggregation. Fluid molecules undergo both spatial and temporal (space and time) variation when the bulky fluid is mechanically agitated. According to Smoluchwski[128], the collision coefficient for a shear rate (velocity gradient, G) for an unequal particle is expressed according to equation (2.20)

$$k_{12} = \frac{3}{4}G\left(r_1 + r_2\right) \tag{2.20}$$

The size of the particles has a strong influence on the collision rate coefficient. When equation (2.20) is combined with equation (2.18) for a stricter condition where the primary particles have equal radii, equation (2.20) can be re-written as.[129,133]

$$\frac{dn_T}{dt} = -\frac{16}{3}\eta_T{}^2 G r^3 \tag{2.21}$$

Equation (2.21) is limited to the very early stages of aggregation, where most of the particles are still single since the rate of collision is dependent on the size of the particles. However, using the volume fraction, ϕ (*cf.* equation (2.22)), a simple transformation can be obtained, which allows equation (2.21) to be written as shown in equation (2.23):[129]

$$\phi = \frac{4\pi r^3 \eta_T}{3} \tag{2.22}$$

$$\frac{dn_T}{dt} = -\frac{4G\phi\eta_T}{\pi} \tag{2.23}$$

Equation (2.23) can be solved using integration under the condition that during the aggregation, the volume fraction remains unchanged to obtain equation (2.24).[129]

$$\frac{n_T}{n_0} = \exp\left(-\frac{4G\phi t}{\pi}\right) \tag{2.24}$$

Equation (2.24) indicates that the mean particle number will increase exponentially with time since the total particle concentration will have an exponential decrease. Compared with the perikinetic flocculation, where aggregation rises linearly with time, these two processes have a different growth rate of the aggregated particles.[4,129] The difference in the particle growth rate for perikinetics and orthokinetics is shown in Figure 2.8, where a decrease in particle number with time is shown for both cases. Figure 2.8 represents calculations for an aqueous suspension containing 1.0 μm diameter particle at a concentration of 10^{15} m^{-3} at 25 °C. Details of the perikinetic and orthokinetic flocculation processes are reviewed elsewhere.[4,25,129,132–135]

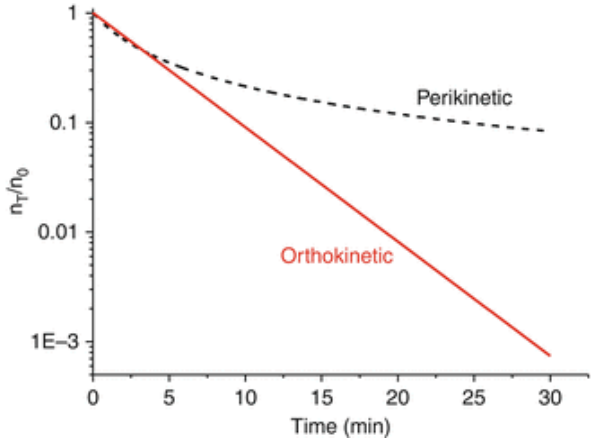

Figure 1.10: Relative decrease in total particle concentration (expressed as n_T/n_0) for perikinetic (Eq. 2.19) and orthokinetic (Eq. 2.24) aggregation (Obtained with permission from reference[129]).

2.6 Factors affecting coagulation-flocculation

2.6.1 pH effect

The efficiency of coagulation-flocculation is significantly influenced by the pH of the wastewater effluent. The surface charges of the colloidal and dissolved particles in wastewater are dependent on pH, which significantly affects the charge neutralization process.[136] Increasing the pH enhances negative charges of the colloidal and dissolved particles, whereas decreasing the pH reduces the negative surface charge. At high pH conditions, colloidal particles in an aqueous environment become more stable, which leads to reduced removal efficiency.[137] Different coagulants and flocculants show varying dependence for effective efficiency, where their solubility, precipitation and hydrolysis reaction is dependent on the pH of the solution. For instance, various hydrolysis reactions occur immediately to form aluminium hydroxide species when aluminium salt is dissolved in water, with the help of OH^- to produce different hydroxide species of aluminium, which are strongly pH dependent.[69,138–141] At pH >7, there is rapid formation of amorphous precipitates, which leads to particle entrapment via sweep-floc with reduced removal efficiency. Charge neutralization followed by adsorption is favored at low pH due to the low degree of polymerization of the aluminium, which leads to the formation of $Al(OH)_3$ precipitates, which adsorb the neutralized colloidal particles.[142] Hence, maximum CF occurs at the optimal pH, where enough dose of effective coagulant is obtained. At the optimum dosage, the effects of coagulant species can completely destabilize the suspended or dissolved particles to ensure maximum formation of microflocs. At pH above the optimal values, there is particle restabilization due to charge reversal, which reduces the removal efficiency. Ferric metal salt behaves similarly to aluminium salt under the same conditions.[142,143]

Hybrid inorganic polymer coagulants with additive in their matrix have been shown to have a wider pH performance. For instance, PA-SiC has been reported to have a wider optimal coagulation pH range (6.0-8.5) relative to that of PACl in removing oil from refinery effluent.[144] Also, PFSiS has a wider pH range (5.0-9.0) for the removal of the turbidity compared to $Fe_2(SO_4)_3$.[144] Other inorganic hybrid coagulants reported with more extensive pH coagulation range are PZSS, PAC-PDMDAAC, PFC- PDMDAAC, PAC-EP-DMA.[145] Synthetic and natural polymer flocculants are sensitive to pH variation for effective flocculation of colloidal particles. For instance, at acidic conditions below the pK_a (6.2) of chitosan, the biopolymer material undergoes protonation and becomes positively charged. Under this condition, the colloidal

particles are prone to aggregate into larger flocs due to the presence of the positively loose charged particles to bind with the negatively charged colloidal or dissolved particles.[146] On the other hand, at pH above 6.2, the surface charge of the chitosan becomes negatively charged due to deprotonation at the surface, causing electrostatic repulsion between chitosan and the colloidal particles, which would reduce flocculation efficiency via a polymer bridging mechanism. To improve flocculation properties of this natural polymers, several chemical modifications such as grating with synthetic or natural polymers, etherification and quaternization, as well as polymer composite formation, have been carried out to alter the surface charge to enhance their performance over a wide pH range.[4,121]

2.6.2 Coagulant and flocculant dosage

Coagulant and flocculant dosage are one of the most significant factors that affect the CF process. To maximize the interaction between the coagulant/flocculant and the colloidal particles, establishing an optimum dosage of the coagulant/flocculant is important.[120] Hence, the effect of coagulant/flocculant dosage on CF performance has been extensively investigated. Generally, overdosing or underdosing will lead to poor performance in flocculation; hence it is important to evaluate the optimum dosage of the coagulant or flocculant to minimize the dosing cost, sludge formation, and to obtain the optimum performance in the treatment process.[5] The effect of coagulant/flocculant dosage on CF performance has been divided into three categories.[147] (i) presence of insufficient dose of the coagulant/flocculant for the destabilization of the colloidal particles; (ii) addition of enough coagulant/flocculant to effectively destabilize the colloidal particles; and (iii) excess dosage of coagulant/flocculant leading to charge reversal effects and restabilization of the particles. Generally, the coagulant/flocculant dosage required depends on the content of the colloidal, suspended and/or dissolved particles in the wastewater. The contaminant removal efficiency is assumed to increase with increased addition of the coagulant/flocculant until it reaches an optimal value, and further addition leads to a decrease in the removal efficiency.[148] In the first category, insufficient or low dosage of the coagulant/flocculant leads to weak and incomplete charge neutralization and bridging effects; thus, the particles remain stabilized. However, at zone three, overdosing will cause sludge particles to be covered by the coagulant/flocculant, leading to the regeneration of the suspension stability of flocs, i.e., restabilization effect.[121] The presence of excess coagulant/flocculant can be observed when the applied dosage reaches an inflection point known as a critical coagulation concentration.[5] Beyond

the optimum dosage, restabilization may occur when bridge formation between adjacent particles is prohibited by the absence of adsorption sites, as most of the sites are occupied by the polymeric species.

For metal salt coagulants below the optimum dosage, destabilization of the colloidal particles occurs via ionic strength effects in terms of electrical double layer depression by oppositely charged ions, however, for greater coagulant/flocculant dosage beyond the optimum value, sweep-floc coagulation dominates.[145] Overdosing of the coagulant/flocculant often leads to a reduction in the CF efficiency, where charge patching mechanism is predominant, and the flocculation window is broadened accordingly. The use of organic cationic, anionic or non-ionic polymer flocculants results in interparticle bridging mechanism being dominant due to the presence of ─OH groups on the polymer chain and higher molecular weight of the polymer.[4] It is recommended that a lower dosage of the polymer flocculant be used to reduce organic matter content in the treated water and to reduce the sludge volume. Several reports have shown that the optimum coagulant/flocculant dosage can be evaluated from zeta potential measurement, where the optimum dosage can be indicated by the IEP (zero zeta potential) of the floc or supernatant.[120] The zeta potential of the flocs or supernatant will be negative, near-zero or positive at below the optimum dosage, at the optimum dosage and beyond the optimum dosage, respectively. The relative coagulant/flocculant dosage required for effective CF performance is dependent on the type of coagulant or flocculant, especially during charge neutralization, which is affected by the valency of the coagulant or flocculant following the Schulze-Hardy rule.[119]

2.6.3 Mixing speed and time

Coagulation-flocculation performance is significantly affected by mixing (stirring) conditions such as speed and time. In the CF process, adequate mixing is important because it enhances contact between the coagulant or flocculant with the colloidal particles in the wastewater to ensure floc formation.[119] Generally, during the CF process, two mixing rates are required, which are rapid mixing for a short time and a slow mixing for a longer time. The rapid mixing, which represents the coagulation process, ranges from 100 to 700 rpm for 0.5 to 5 min, and this process allows uniform and adequate dispersion of the coagulant into the wastewater to stabilize the colloidal system, particulate matter, and dissolved solids.[5] On the other hand, the slow mixing illustrates the flocculation process, and it ranges from 20 rpm to 100 rpm for 10 to 60 min, and this process allows gentle collision of the destabilized flocs to form macrofloc by limiting the breakdown of

aggregates via an orthokinetic flocculation process.[149] Mixing in the CF process is a critical factor because it improves the rate of adsorption of the formation of the floc owing to the increased probability of particle collision rate.[150,151] The rate of mixing (fast and slow) influences the strength and the size of the flocs as well as the flocculation efficiency. At longer fast mixing time during the coagulation process, stronger but smaller flocs are formed, but larger flocs are obtained at relatively shorter fast mixing.[152] The formation of the smaller flocs is due to the presence of lower collision efficiency of small flocs owing to increase in the shear rate and floc breakage to limiting sites. The importance of the mixing time relative to mixing speed is that it allows successful collision efficiency by ensuring adequate time for the destabilized particles to rearrange into more stable and compact flocs.[4] The coagulation efficiency has been reported to decrease when the mixing speed is too rapid, and stirring time is prolonged even though the collision frequency of the flocs is always assumed to increase with stirring time and speed.[150,151] When the mixing rate increases, the flocs are irreversibly broken into smaller particles, which reduces the CF efficiency. There is a reduced or inadequate contact between the coagulant or flocculant and the colloidal particles when the mixing speed is slow, and time is short, which results in the formation of smaller flocs with reduced resistance to shear stress and reduced CF performance.[153] Therefore, appropriate mixing time and speed is needed to ensure maximum coagulation-flocculation activity. For instance, when alum is used in wastewater treatment, the rapid mixing lead to adsorption and restabilization mechanism due to fast hydrolysis of Al species and formation of hydroxide precipitates.[4] Addition of polymer flocculant during the slow mixing period leads to formation of aggregated macroflocs via polymer bridging.[121]

2.6.4 Settling time

The efficiency of the CF process is markedly affected by the strength and settling speed of the flocs formed during the process. The ability of the flocs to settle rapidly after the CF process is largely dependent on the size of the flocs (particle size), particle density and liquid density. Using Stokes law, the settling velocity of the flocs can be estimated using equation 2.25.[154]

$$V = \frac{2gr^2(d_1 - d_2)}{9\eta} \tag{2.25}$$

Here, V is the settling velocity of the particle, r is the radius of the particle, d_1 and d_2 are the densities of the particle and the liquid, η is the coefficient of viscosity and g is the gravitational

constant. According to Stokes law, small particles will have less tendency to settle and would take a long time, compared to larger flocs. This indicates that the characteristics of the flocs has a direct influence on CF efficiency. Hence, in the CF process, the production of smaller flocs reduces the efficiency due to reduced settling velocity, fragility and the inability to separate them from the bulk treated water.[154] The size of the flocs generally depends on the type of coagulant or flocculant used and the nature of the wastewater. Generally, the use of coagulant produces microflocs with small size and fragility, hence, have poor settling ability. However, the use of flocculant is known to produce larger, denser and compact macroflocs that are more effective in settling rapidly.[4] The ability of flocculants to generate larger flocs is due to the adsorption of polymer and bridging involving long-chain polymers, which is the primary dominant mechanism. Several reports have shown that the use of natural biopolymer flocculants produces larger flocs with faster settling velocity within a short period compared to the use of inorganic coagulants such as alum and ferric chloride.[4,152,155,156] The larger molecular weight of biopolymer flocculants is known to form larger and stable flocs through rapid aggregation of particles of enough size to enhance rapid settling velocity.

2.6.5 Ionic strength

The ionic strength of a given solution is defined as a measure of the concentration of ions. The ionic strength of the medium significantly affects the structural properties of polyelectrolytes in solution and hence, the CF efficiency. As the ionic strength increases, the velocity of the polyelectrolyte solution decreases.[157,158] Also, it influences both charge density and chain conformation of ionic flocculant according to counterion condensation theory.[148] Since the solution velocity decreases as the ionic strength increases; similar charge sites are shielded and permit the polymer to fold and assume a smaller hydrodynamic volume, which is manifested in the flocculation process.[121] When the CF process is dominated by charge neutralization, increased ionic strength effectively reduces the electrical double layer of the colloidal particles in the wastewater. Also, for high molecular weight ionically charged polymer flocculants, bridging mechanism prevails as the ionic strength decreases due to an increase in the effective particle radius caused by an expansion of the polymer, as the solution viscosity decreases. Studies have shown that increasing the ionic strength for chitosan-based flocculants usually enhances the removal efficiency.[159,160]

2.6.6 Polymer molecular weight and structure

Structural factors of the polymer flocculants such as charge density, molecular weight (MW), and degree of deacetylation (DD) significantly influence the flocculation efficiency. Increasing MW of the polymer flocculant increases its hydrodynamic size according to equation (2.26).[121]

$$R^* = M_w^{\chi} \tag{2.26}$$

Here, R^* is the hydrodynamic size, M_w is the molecular weight, and χ is the polymer-solvent interaction parameter, which is characteristic of the solvent. As the relative MW increases, the more extended conformation of the macromolecular chain in water increases the bridging and sweep-floc of the polymer.[119] Effect of polymer MW on flocculation is mostly described by bridging and electrostatic patch mechanisms. Increased MW of anionic, cationic and non-ionic polyelectrolytes increase the flocculation performance via polymer bridging, irrespective of the charges on the polymer, because the polymer is adsorbed, which then extend away from the particle surface and is slower to reach equilibrium. For anionic polyelectrolytes, even though there could be repulsive interaction with the negative surface of the colloidal particles, it serves to enhance the extension of the polymer chain through mutual charge repulsion, which increases its degree of contact. Increasing the molecular weight beyond a certain point decreases the CF performance due to steric repulsion between polymer segments. Previous reports have shown that the use of high MW chitosan showed significant flocculation efficiency compared to low and medium MW chitosan in the reduction of turbidity in wastewater.[155,161,162] Native biopolymers such as chitosan, alginate, cellulose and starch have been modified chemically to increase their MW to enhance their flocculation performance.[152,161–167] In addition, for chitosan-based flocculants, increasing the DD increases the efficiency of the CF process.[161] This occurs because, as the DD increases, the number of free amine groups on the chitosan increases, leading to improved positive charge density, thus promoting both charge neutralization and bridging mechanisms by extended conformations owing to intramolecular electrostatic repulsion. The positive charge density of the polymer flocculant can be enhanced by external factors such as pH and ionic strength of the medium by changing the protonation of the polymer in solution and the counterion condensation effects.[121] Several studies have been carried out which show that the effectiveness of chitosan in the removal of colloidal and dissolved species in wastewater is dependent on its molecular weight.[161,162,166,167]

2.6.7 Temperature

The removal of colloidal, suspended and dissolved particles in wastewater by CF process requires the transport of the particles by perikinetic collision, which is temperature-dependent, as discussed in Section 2.5.2.1. Hence, the temperature has a significant influence on the CF activity since it affects the collision rate and particle transportation by altering the density and velocity of the suspension. Variation in temperature is known to change the flocculant dosage; in that, a lower flocculant dosage is required at high temperatures.[4,168] This effect is based on two phenomena. Firstly, as the temperature increases, the polymer flocculant tends to have more extended conformation owing to their improved solubility, and hence, better flocculation performance.[121] Secondly, the viscosity of the liquid medium decreases as the temperature increases, which subsequently increases the Brownian motion of the colloidal particles and enhances their collision frequency and rate, leading to the formation of larger flocs.[128] Coagulation efficiency of metal ion salts such as alum at lower temperatures is less effective due to decreased hydrolysis and precipitation kinetics, relative to fully hydrolyzed coagulants such PACl.[4] As the temperature decreases, the rate of particle aggregation is impeded and reduces perikinetic collision.[169] A recent study by You et al. (2017)[168] showed that the flocculation performance of cationic polysaccharides decrease as the temperature increased. At high temperatures, the molecular thermal motion of the flocculants intensified and trended to set itself free from obstacles of kaolin particles. However, other several reports have shown that the optimal dosages of coagulant or flocculants usually decreases as the temperature increases over a suitable range.[170,171] It has been reported that lower flocculant dosages are required in summer, whereas higher dosages are needed in winter for equal coagulation performance due to increased viscosity of the suspension and decreased Brownian motion of the colloidal particles as the temperature decreases.[171] According to Shak and Wu[172], there was a significant improvement in the removal efficiency of POME at high temperatures (up to 90 ℃) for the removal of TSS and COD when organic polymer flocculant was used. It has been postulated that when adsorption is the main mechanism of the CF process, temperature has little or no influence on the flocculation efficiency, however, the temperature has a significant effect when the CF process occurs via charge neutralization and/or particle entrapment.[172]

2.7 Coagulation-flocculation mechanisms

2.7.1.1 Charge neutralization

When inorganic mineral salts are added to wastewater, the contaminants are predominantly coagulated by charge neutralization. In this case, the positive charge on the metal ion neutralizes the negatively charged sites of the contaminant particles. However, the use of inorganic salts requires a high dosage of the salt, and subsequently, the production of a large volume of sludge. In addition, the pH of the solution is altered when inorganic salts are used in the CF process. Organic polymers can be used as a primary coagulant and give equally and perhaps better precipitation of the contaminants compared with that of the use of inorganic salts. Because contaminants in water are negatively charged, cationic polyelectrolytes are most effectively used as coagulant aids. The polymer acts as a destabilizing agent through charge neutralization and precipitation mechanism due to the electrostatic attraction between the positive charge on the polyelectrolyte and the negative charge on the contaminants. Hence the growth of microflocs to macroflocs occurs through flocculation due to the reduced surface charge of the particles (reduction of zeta potential), and accordingly, a decreased electrical repulsion force between colloidal particles, which allows the formation of van der Waals force of attraction to encourage initial aggregation of colloidal and fine suspended particles[123], as shown in Figure 2.9. Effective removal of turbidity and other dissolved contaminants such as phosphate occurs best when there is zero net charge on the particles, thus when the mobility or zeta potential of the particles is close to zero.[173] Studies have shown that polyelectrolytes with high charge density deliver more charges to the surface of the contaminants, and are more effective than those of low charge density.[123] Lower molecular weight, high charge density polyelectrolytes, such as polydiallyldimethylammonium chloride (poly-DADMAC) was shown to be a more effective coagulant. High charge density polymers tend to adsorb in a rather flat orientation, hence there is a little avenue for bridging interactions.[174]

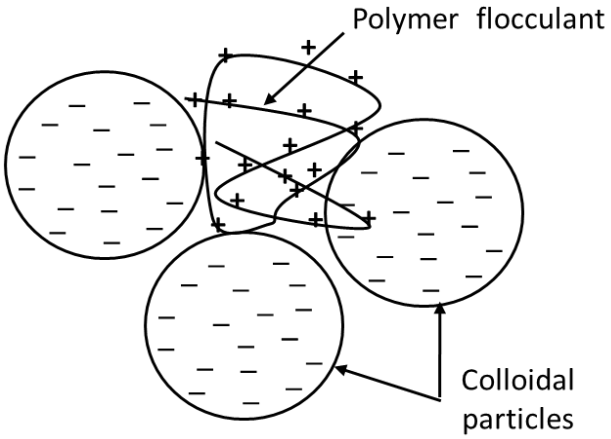

Figure 1.11: Schematic view of a charge neutralization flocculation mechanism. (Adapted with permission from reference[175]).

Electrostatic charge patching is a type of charge neutralization mechanism that occurs when the polymer dose is low.[176,177] It occurs when the particle surface is partially covered as in the initial stages of adsorption. Electrostatic patching occurs because when a highly charged cationic polyelectrolyte adsorbs on a negatively charged surface to give overall neutrality, it is not possible physically for each charged surface site to be neutralized by the cationic polyelectrolyte unit. This is because the average distance between surface sites is greater than that between the charged segments along the polymer chain. When this occurs, the polymer adsorbs, where there are domains of opposite charge of the floc to that of the polymer, resulting in a local excess of charge associated with the polymer, but leaving patches or islands of the charge of the floc[178], as shown in Figure 2.10. Flocculation occurs upon electrostatic attraction between the positive patches and the negative area, which can lead to particle attachment when they approach each other. Electrostatic charge patching depends on the condition of mixing since it occurs as soon as the polymer is added. Flocs formed from this mechanism are not as strong as those formed from bridging mechanism, and flocs may break up but reform more readily.[179] However, flocs formed from this mechanism are stronger than those formed in the presence of inorganic metal salts or by simple charge neutralization. This mechanism is favored by high molecular weight polymers, a high charge density and low ionic strength.[180]

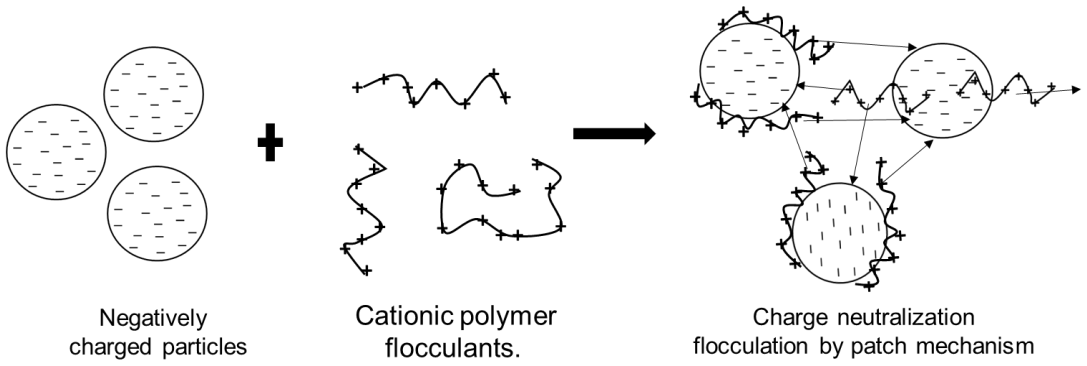

Figure 1.12: (a) Negatively charged particles. (b) Cationic flocculants. (c) Charge neutralization flocculation by patch mechanism. Arrows in (c) show the attraction of opposite charges. (Adapted with permission from reference[175]).

2.7.2 Polymer bridging

Polymer bridging involves the formation of macroflocs from microflocs produced by coagulation with inorganic metal salts or cationic polyelectrolytes through a flocculation process by the addition of polymers. In this process, polyelectrolyte bound to a floc particle has loops and dangling/tailing chains that can attach to nearby particles, as depicted in Figure 2.11a.[181] The mechanism is favored, and the best results are obtained when long-chain polymers without a high level of charge are used.[182] Usually, the characteristics of the flocs formed following the CF process will depend on the dose of the metal ion and polymer used. However, the net charge is often close to zero, slightly positive, or somewhat negative, according to zeta potential measurement. The size of the flocs is often increased by interaction with the positive sites on the flocs by anionic polyelectrolyte.[183] Bridging takes place when the adsorbed chains interact with another floc uniformly, as shown in Figure 2.11b.

In this process, electrostatic and non-electrostatic forces, cause one polymer chain to be adsorbed on two or more flocs. This occurs when the surface is partly covered, as in the initial stages of the process, or when the polymer dosage is low. It occurs immediately at the point of the addition of the polymer and is very dependent on mixing conditions.[184] Polymer bridging can give stronger macroflocs than those formed in other mechanisms. Flocs formed by this mechanism are resistant to breakage at an elevated shear level. The flocs often grow to a steady-state size, which is dependent on the applied shear or stirring speed. The stronger the flocs, the larger they can grow

at a given shear condition.[174,180] Addition of excess polymer flocculant will lead to floc breakage, as shown in Figure 2.11c, due to excess positive charges causing a reversal effect.

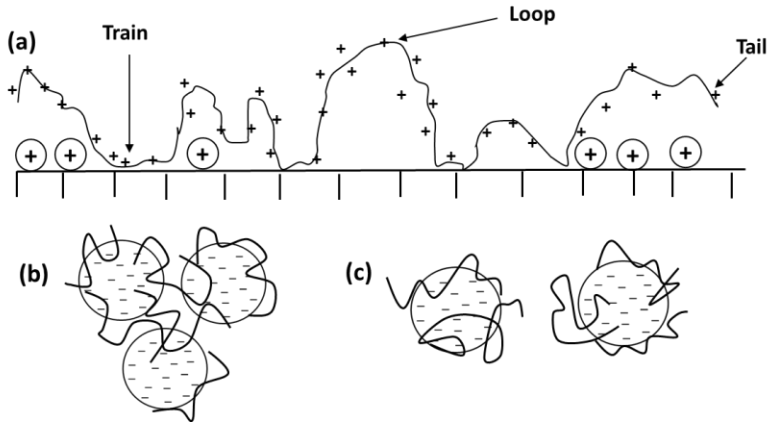

Figure 1.13: (a) Adsorption of polymer and formation of loops available for binding. (b) Polymer bridging between particles (aggregation). (c) Restabilization of colloid particles (floc breakup). (Adapted with permission from reference[175]).

2.7.3 Adsorption mechanism

Colloidal suspensions and dissolved materials, either organic or inorganic, are negatively charged; hence, when there is an affinity between polymer units and the contaminant in water, adsorption of polymer chains may occur. There is a low affinity between the polymer segment and the surface site of the contaminants because there are many attachment points on the polymer chain. Also, the adsorption affinity should be appreciable to outweigh the loss of entropy associated with polymer adsorption because an adsorbed chain will have a more restricted configuration than a random coil in a free solution.[174] Polymer adsorption is considered as a non-reversible process because the likelihood of detaching of all attached segments of a long chain polymer is negligible. According to Napper[185], polymer adsorption usually follows three distinct mechanisms: (i) attached the surface in trains (ii) projecting into the solution as tails and (iii) in the form of loops, between trains. These models of polymer adsorption are depicted in Figure 2.11a. Interaction of the polymer segments with solvent and the surface sites (contaminants) defines the measure of tail and loops and hence the effective thickness of the adsorbed polymer layer.[186]

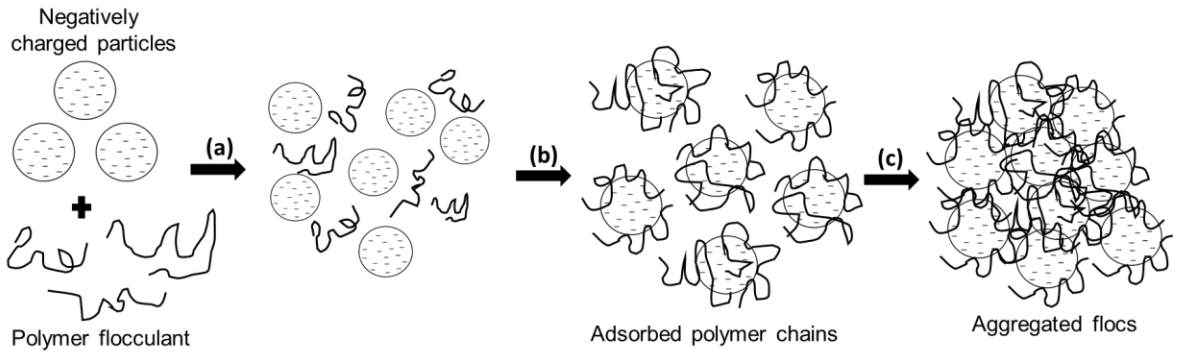

Figure 1.14: Steps involved in the flocculation of particles by adsorbing polymer. (a) mixing of negatively charged particles with polymer flocculant, (b) adsorption of polymer chains on the charged particle surface, and (c) rearrangement and aggregation of adsorbed polymer chains. (Adapted with permission from reference[178]).

Adsorption of a polymer segment onto contaminant surface sites could occur utilizing electrostatic interactions, hydrogen bonding or ion binding. In attractive electrostatic interaction, polyelectrolyte with a charge opposite to that of the surface site nearby always adsorbs strongly. Adsorption occurs because of the attractive interaction between oppositely charged ionic species.[174] Electrostatic adsorption occurs in a flat equilibrium configuration, without extensive loops and tails, especially for polymers of high charge density. Salt effects also play an important role in the electrostatic adsorption process. For example, cationic polyelectrolytes adsorbed on cellulose fibres could be desorbed by the addition of salts.[174] In the case of adsorption by hydrogen bonding, contaminants with effective hydrogen bonding surface sites could form hydrogen bonds with polymers such as polyacrylamide and polyethylene oxide as well as other natural polymers such as chitosan and alginate and their modified derivatives.[187] With regards to ion binding adsorption, anionic polyelectrolytes can adsorb onto negatively charged surfaces of the contaminants in water, even though there is electrostatic repulsion. This type of adsorption is made possible if there is a sufficient concentration of divalent metal ions present.[188] Calcium and magnesium ions can act as bridges between anionic polyelectrolytes and the negative sites on the surface of the contaminants. In the absence of a divalent cation, no flocculation takes place even at quite high ionic strength. However, polyacrylamide could be adsorbed on the surface of negatively charged species and form precipitate and be flocculated at a moderately low concentration of calcium.[189] Figure 2.12 represents the adsorption mechanism, where three processes are involved. Initially, the polymer flocculant is mixed with the negatively charged

materials. Secondly, the polymer chains are then adsorbed on the surface of the negatively charged particles via hydrogen bonding, ion binding or attractive electrostatic interaction. Finally, the adsorbed polymer chains undergo rearrangement and then flocculate via aggregation to form macroflocs.

2.8 Flocculation kinetics, adsorption isotherms and thermodynamic parameters

2.8.1 Flocculation kinetics

Studies on the adsorption kinetics and adsorption isotherms in coagulation-flocculation process is important to understand the adsorption behavior of the phosphate and the colloidal particles during the flocculation. The contact time between the bioflocculants and the contaminant species is an important parameter for the flocculation process. This is because it provides information on the flocculation kinetics of the phosphate or colloidal particles for a given initial concentration of the bioflocculants.[190] Hence, it is necessary to study the effect of the contact time on the flocculation ability of the biopolymers toward phosphate and colloidal species. Several adsorption kinetic models have been used to describe the kinetics of contaminants, such as dyes and colloidal particles, flocculation by polysaccharide-based flocculants.[191] Two kinetic models, pseudo-first-order (PFO)[192] and pseudo-second-order PSO)[193] are generally employed to model the experimental data over the process. The non-linear PFO and PSO kinetic models are defined according to equations (2.28) and (2.29), respectively.

$$q_t = q_e(1-e^{-k_1 t}) \tag{2.28}$$

$$q_t = \frac{k_2 q_e^{\,2} t}{1+k_2 q_e t} \tag{2.29}$$

Here, q_e and q_t (mg·g^{-1}) are the adsorptive removal capacity at equilibrium and variable time (t) via the flocculation process, respectively. k_1 and k_2 are the rate constants for the PFO and PSO kinetic models, respectively. Several assumptions were made in establishing these kinetic models. These include:[194] (i) adsorption occurs at specific sites, and there is no interactions between the adsorbates, (ii) the adsorption energy is independent of the surface coverage, (iii) attainment of monolayer coverage on the surface of the adsorbent that leads to maximum adsorption, (iv) the concentration of the adsorbate does not change, and (v) adsorption of the adsorbate is controlled by a first-order and second-order rate equations for the PFO and PSO models, respectively.

2.8.2 Adsorption isotherms

Flocculation adsorption phenomena can be described through isotherms. Adsorption isotherms are important for identifying the interaction of the adsorbates on the adsorbents and the optimization of the adsorbent.[195] Langmuir, Freundlich and Sips adsorption models are the most frequently used to describe flocculation processes of colloidal particles and dissolved species. In this thesis study, these models are employed to understand the adsorption processes during flocculation for single-component and multicomponent systems. Adsorption isotherm fitting with a model equation is necessary to elucidate the flocculation mechanism.

The Langmuir adsorption isotherm model assumes that adsorption occurs at specific homogeneous sites with the adsorbent, and it is given according to equation (2.30).[196]

$$q_e = \frac{q_m K_l c_e}{1 + K_l c_e} \tag{2.30}$$

Here, q_m (mg·g^{-1}) is the maximum amount of contaminant species per unit mass of adsorbent when all the binding sites are occupied (absorption capacity) and q_e (mg·g^{-1}) is the amount of contaminant species adsorbed at equilibrium. K_l (L·g^{-1}) is the equilibrium adsorption constant, which is related to the affinity of the binding sites. The equilibrium constant is related to a dimensionless constant called the separation factor or equilibrium parameter, R_l, as given according to equation (2.31). The adsorption process can be categorized into four groups based on the value of R_l. That is irreversible ($R_l = 0$), favorable ($0 < R_l < 1$), linear ($R_l = 1$) and unfavorable ($R_l > 1$).

$$R_l = \frac{1}{1 + K_l \cdot c_o} \tag{2.31}$$

The Freundlich isotherm is based on multilayer sorption by assuming that the adsorbent has a heterogeneous surface with non-uniform distribution of sorption sites.[197] The Freundlich adsorption isotherm is given by equation (2.32),

$$q_e = K_f c_e^{1/2} \tag{2.32}$$

where K_f is the Freundlich isotherm constant and is related to the adsorption capacity, and n is a dimensionless constant. It is an empirical parameter that gives valuable information on the shape of the isotherm. The adsorption process can be classified as unfavorable ($1/n > 1$), favorable ($1/n < 1$) and irreversible ($1/n = 0$).

Another important adsorption model is the Sips isotherm, which was developed by R. J. Sips during his seminal studies on the distribution of adsorption energies of the active sites on catalyst surfaces.[198] This model is composed of a combination of components of the Langmuir and Freundlich models, as given in equation (2.33).

$$q_e = \frac{q_m \left(K_s c_e\right)^{n_s}}{1+\left(K_s c_e\right)^{n_s}} \tag{2.33}$$

Here, K_s is the Sips equilibrium constant, and n_s denotes the heterogeneous nature of the adsorption process. This model is useful because it can overcome the limitations of the Freundlich model since it can predict adsorption onto heterogeneous adsorbents. When $n_s > 1$, the Sips model indicates that the adsorbent material consists of heterogeneous sites. Also, when $n_s = 1$, monolayer behavior is described, where the equation converges to the Langmuir model; however, when $n_s < 1$, it describes Freundlich model behavior. The Sips model can describe sorption processes at both high and low adsorbate concentrations.

2.8.3 Thermodynamic parameters

Thermodynamic parameters can be obtained by performing the flocculation process at different temperatures. The temperature effect on the flocculation of the oxyanion by the bioflocculants can be obtained from calculated thermodynamic parameters. The standard changes in Gibbs free energy (ΔG^o), enthalpy (ΔH^o), and entropy (ΔS^o) can be obtained according to the equations below.

$$\Delta G^o = -RT \ln K_D \tag{2.34}$$

$$\Delta G^o = \Delta H^o - T\Delta S^o \tag{2.35}$$

$$\ln K_D = \frac{\Delta S^o}{R} - \frac{\Delta H^o}{RT} \tag{2.36}$$

Here, R is the universal gas constant, T is the temperature in kelvin, and K_D is the equilibrium constant, similar to that from the Sips and Langmuir isotherms which are given according to equation (2.37).[199]

$$K_D = \frac{q_e}{c_e} \tag{2.37}$$

The value of ΔG^o can determine the spontaneity and the thermodynamic stability of the flocculation process and the flocs formed. The values of ΔH^o and ΔS^o will be able to throw more

light on the thermodynamics of the flocculation process. Values of ΔS^o will indicate whether there is an increased or a decreased randomness of the solid/solution interface during the process. The driving force (enthalpic and/or entropic) can be evaluated from the values of ΔH^o and ΔS^o.

2.9 Coagulation-flocculation of phosphate

2.9.1 Conventional inorganic coagulants

2.9.1.1 Aluminum phosphate precipitation

Aluminium containing compounds are the most widely used mineral salts for phosphate precipitation. Some of the commonly used aluminium salts are aluminium sulphate (alum), polyaluminium chloride (PACl) and sodium aluminate. Alum is the most widely used chemical, however, PACl is gaining popularity as a result of its polymeric nature and improved removal efficiency. The reaction between alum or PACl with phosphate in wastewater is complex and no clear reaction mechanism has been proposed yet.[138] Two schools of thought are available that describe the reaction between phosphate ion and aluminium ion. Firstly, it is proposed that $AlPO_4$ (s) is the major product formed and precipitated when alum is added to wastewater, according to equation (RE1):

$$Al_2(SO_4)_3 \cdot 14(H_2O) + 2PO_4^{3-} \rightarrow 2AlPO_4 \downarrow + 3SO_4^{2-} + 14H_2O \qquad \text{(RE1)}$$

Studies by Jenkins et al.[69] showed that aluminium phosphate is formed and precipitates because the chemical process is thermodynamically and kinetically favored over the formation of aluminium hydroxide complexes. However, at low phosphate concentration (< 10 mg/L), there is competition from the formation of hydroxides, which prevents the occurrence of aluminium-to-phosphate ratio necessary for aluminium phosphate precipitation.[200]

By comparison, the second school of thought proposes that the aluminium ion becomes hydrated and forms monomer and polymer species with solid products.[201] The formation of the polynuclear species involved in the dilution is a step-wise process involving a deprotonation-dehydration mechanism, as presented below:[202,203]

$$Al(OH_2)_6^{3+} \rightarrow Al(OH_2)_5(OH)^{2+} + H^+ \qquad \text{(RE2)}$$

$$2Al(OH_2)_5(OH)^{2+} \rightarrow Al_2(OH_2)_8(OH)_2^{4+} + 2H_2O \rightarrow Al_6(OH)_{12}^{6+} \cdot 12H_2O \qquad \text{(RE3)}$$

$$Al_6(OH)_{12}^{6+} \cdot 12H_2O \rightarrow Al_{10}(OH)_{22}^{8+} \cdot 16H_2O \rightarrow Al_{24}(OH)_{60}^{12+} \cdot 24H_2O \qquad \text{(RE4)}$$

$$Al_{24}(OH)_{60}^{12+} \cdot 24H_2O \rightarrow Al_{32}(OH)_{82}^{14+} \cdot 28H_2O \rightarrow Al_{54}(OH)_{144}^{18+} \cdot 36H_2O \quad \text{(RE5)}$$

The polymer hydroxyl group on the aluminum serves as an adsorption site for the phosphate ion. In summary, Aguilar et al.[204] have suggested that when an aluminium-based coagulant is added to wastewater, these processes occur: (i) phosphate ions are directly deposited on the hydrolysis products formed by the addition of alum to wastewater, and (ii) removal by the formation of insoluble phosphate salt with aluminium, according to equation (RE6).

$$Al^{3+} + H_nPO_4^{n-3} \rightarrow AlPO_4 \downarrow + nH^+ \quad \text{(RE6)}$$

This reaction is predominant at low pH values or low alum doses. Georgantas et al.[201] have shown that removal of metaphosphate ions occurs through a ligand exchange mechanism in which surface hydroxyl groups on the surface of the precipitated $Al(OH)_3$ are exchanged for phosphate ions. Phosphorus stoichiometry, according to equation (RE6), was designed based on synthetic or model wastewaters without considering the hydrolysis reaction of Al salts. Fettig et al.[205] have suggested an empirical formula, $Al_{1.4}PO_4(OH)_{1.2,}$ instead of $AlPO_4$. Hence the molar ratio of Al:P shows to have increased from 1:1 to 1.4:1 for efficient removal of phosphorus. However, the situation is different in real wastewater treatment and is more complicated than indicated by model waters. A range of competing reactions occurs when Al salt is added to wastewater, as described previously. Recent and past studies have shown that for greater and efficient percentage removal of phosphate, the required dose of aluminium increases, and that all of the doses significantly exceed the theoretical demand.[139–141,206,207] In situations of this kind, there is a combination of phosphate removal and the removal of other impurities, such as colloidal particulate materials and organic substances. The efficiency of phosphate removal has been shown to be pH dependent, and the highest percentage removal is obtained at a pH between 5.5 and 6.5.[141,208,209]

2.9.1.2 Iron phosphate precipitation

Application of iron species for the removal of dissolved phosphate in wastewater dates back to the early works of Thomas in the 1960s,[210,211] who used ferric chloride and ferric sulphate for the removal of phosphate ions in water and wastewater. The mechanism involving the reaction when Fe(III) is added to wastewater to precipitate phosphate is complicated and does not follow any simple steps, just like that of the precipitation of phosphate using Al. Ferric chloride is the most commonly used chemical for the precipitation of phosphate. $FeSO_4$ or $FeCl_2$ may be used to precipitate phosphate from wastewater.[212] However, before Fe(II) ions can precipitate phosphate

effectively, it must be converted to Fe(III) through an oxidation process. This process depends on pH, oxygen concentration, catalytic activity and the presence of inhibitory materials such as sulphur.[213] Iron (III) is known to form strong complexes with pyrophosphate and tripolyphosphate, and they are then removed by adsorption onto iron(III)-hydroxo-phosphate surfaces.[69] The efficiency of the precipitation of the oxidation product for the phosphate removal is dependent on pH, phosphate initial concentration in the wastewater, iron(III) dose and temperature.[213] Precipitation with ferric salt is most effective within a certain pH range. The optimum pH for ferric ion is 4.5 to 5.0. Studies have shown that at pH > 7, a significant amount of P_i is precipitated and removed by Fe(III) ions.[214–216] The optimum pH range for Fe(II) is between 7 and 8.[217] Studies conducted by Benedek et al.[218] on phosphorus removal in an orthophosphate system showed that the removal did not depend on pH below a Fe:PO_4 ratio of 1.5. However, above this ratio, pH had a significant effect on the removal process because there is a competition between OH^- ions and P_i for Fe(III) ions at the point of addition.[219–221] Also, the reaction of bicarbonate ions to form iron hydroxides and the need to destabilize iron phosphate, as well as other colloids, possibly account for the stoichiometric excess of Fe(III) required for the precipitation of phosphate.[69]

A simplified reaction that occurs between Fe(III) and P_i ions in wastewater is as follows:

$$FeCl_3 + PO_4^{3-} \rightarrow FePO_4 \downarrow + 3Cl^- \qquad \text{(RE7)}$$

The molar ratio of Fe:P is 1:1 and 163.5 g of $FeCl_3$ will react with 95 g of PO_4^{3-}. The weight ratio is 1.8:1 for Fe:P and 5.2:1 for $FeCl_3$:P. Based on the stoichiometry of the reaction above, it is expected the molar ratio between Fe(III) and phosphate will be unity for effective precipitation of the phosphate ion in water. However, a previous study has shown that the ratio is significantly greater than unity for efficient precipitation of the phosphate.[62] This increase in Fe(III) dosage has been attributed to the competing reaction of other contaminating species with Fe(III) against that of the P_i.[138] During P_i precipitation with Fe(III), the metal salt undergoes hydrolysis to form a range of hydrolysis species including some polymeric hydroxides. The P_i is then adsorbed on the surface of hydrolysis complexes, or they form complex with them. However, other contaminants present in the wastewater are destabilized by the hydrolyzed species leading to competing reactions. These account for why an increased amount of Fe(III) coagulant is required for the removal of P_i due to these competing reactions.

Smith et al. (2008)[215,216] have developed an alternative precipitation model for P_i removal based on experimental and theoretical modeling, which is known as the surface complexation model

(SCM). It involves the formation of hydrous ferric oxide (HFO) upon the addition of $FeCl_3$ to wastewater. The mechanism is based on geochemical reaction modeling techniques which involve precipitation of HFO, and subsequent precipitation of P_i by the HFO, where the P_i is occluded into the HFO flocs. At alkaline conditions, the addition of $FeCl_3$ to wastewater leads to the precipitation of HFO flocs. Once the HFO is formed, the removal of P_i can occur via several routes, including:[215]

i. adsorption of P_i onto HFO;
ii. co-precipitation of P_i into the HFO structure;
iii. precipitation of ferric P_i; and
iv. precipitation of mixed cation P_i (i.e., calcium, magnesium, iron, or aluminum phosphates, or hydroxyphosphates).

The SCM is based on the assumption that iron and phosphorus share an oxygen atom which can be represented by the symbolic reaction in equation (RE8) (omitting charges) where the iron oxide surface is denoted as FeOOH.

$$FeOOH + HOPO_4 \rightarrow FeOOPO_4 + H_2O \qquad \text{(RE8)}$$

Herein, the nature of the oxygen atom at the HFO surface determines the exact reaction that will occur. The type of reaction that will prevail has been summarized by the MUltiSIte surface Complexation (MUSIC) model applied to phosphate/goethite interactions.[222] This model depends on the pH of the medium due to competition for surface oxygen and phosphate oxygen by the proton. The reactive oxygen atoms are known as the active surface sites and their availability is influenced by mixing and aging conditions.[215]

Fast mixing leads to greater availability of active surface sites (shared oxygen atoms between HFO and phosphate species). However, during slow mixing, much of the HFO would form in the absence of P_i, resulting in a reduced availability of internal oxygen atoms for binding or sharing.[215,216] Freshly precipitated HFO has a very open structure and active surface sites for P_i precipitation. However, the HFO structure becomes more compact, as aging occurs in the minerals, and the surface oxygen atoms become less available for binding. At this stage, even though binding between the HFO and the P_i may occur, it will be controlled by diffusion processes, indicating that kinetics could be necessary. A study has suggested that for a longer kinetic data, there is a two-step process involved, which are fast (equilibrium) step and slow (kinetic) step.[223] The SCM mechanism is markedly affected by the structure of the HFO, which changes with time as it undergoes aging and becomes crystalline relative to its initial amorphous state. Increased density

of the amorphous HFO structure enhances P_i precipitation. This occurs because the more open amorphous structure increases the availability of the number of oxygen atoms in the HFO for the diffusion of the P_i to the active sites, where oxygen atoms in the HFO and P_i molecules can be shared via covalent bonds, hence enhancing the P_i removal efficiency.[215] On the molecular level, in a well-mixed system of ferric ions and P_i, the oxygen sharing can take place as the initial iron hydroxide oligomer precursors of the solid phase are forming; hence, there is molecular complexation of P_i by soluble hydroxide species. The HFO will contain associated phosphate occluded into the solid HFO flocs in a well-mixed system during polymerization. During poor mixing conditions, there is much less P_i occluded in the HFO, leading to an inefficient P_i precipitation.[214,224,225]

2.9.2 Natural polymer coagulant aids and flocculants

2.9.2.1 Chitosan

Chitin and its derivative, chitosan, is among the novel families of natural macromolecules whose usefulness is becoming progressively evident. Chitin is the second most abundant naturally occurring polysaccharide after cellulose.[226,227] It is obtained from the shell wall or exoskeletons as well as in the internal structure of crustaceans such as crabs, lobsters, prawns, shrimps and some fungi.[226,227] Chitin is composed of β(1→4)-linked 2-acetamido-2-deoxy-β-D-glucose (N-acetylglucosamine),[228] as shown in Figure (2.14). The amount of glucosamine groups is negligible in chitosan; hence, the acetyl groups impart low water solubility due to the extensive intra- and inter-molecular hydrogen bonding among the monomer units. Chitosan is obtained by partial alkaline deacetylation of chitin, and it is considered to be a linear polysaccharide.[229] It is a copolymer consisting of N-acetyl-D-glucosamine and glucosamine units (*cf.* Figure (2.14)). The chemical structure of chitosan contains many amine ($-NH_2$) and hydroxyl (-OH) groups. Chitosan has excellent chelating properties, and hence, able to remove heavy metal ions from water.[230] Chitosan is a cationic polyelectrolyte because the active amine groups in its structure can be protonated in an acidic medium below its pK_a value of 6.2.[121] The presence of the cationic charge on the polymer leads to strong electrostatic attraction between chitosan and anionic contaminants such as phosphate, nitrate, other metal anions, anionic dyes such as Reactive black 5.[121,167,231] Characteristic properties of chitosan are influenced by its molecular weight, degree of deacetylation and crystallinity.[232] Chitosan has been applied in the paper and pulp industry for

several purposes, such as carbonless copy paper[233], as a processing additive for surface treatment applications[234], and photographic paper.[233] It has also been applied in industries related to mixtures, coating, blends and textiles such as silk, wool, viscose and cotton.[232,235] It has also been applied in industries such as cosmetics, food, agriculture, biotechnology, dentistry, pharmaceuticals, biomedical engineering, ophthalmology and chemistry.[236–239]

In the past two decades, chitosan has been applied for the treatment of water and wastewater effluents. However, its application in water treatment has been focused on the binding of dissolved contaminants by sorption onto chitosan in the solid state.[240] But the literature is much less abundant on the use of chitosan for the removal of particulate matter and dissolved substances using chitosan in the dissolved state.[156,230,241–247] Its application in the solid state for the treatment of contaminated water has been used for chelation of metal ions in near-neutral (neutral pH) solution, the complexation of metals ions in acidic solutions and dye complexation using adsorption processes.[226,229,248]

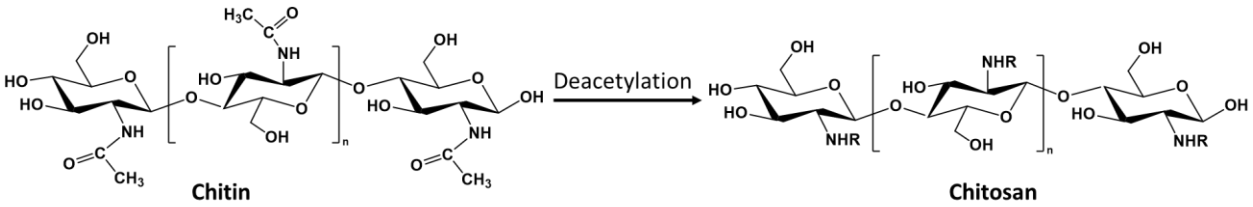

Figure 1.15: Structure of chitin and chitosan. Note: n denotes the number of monomer units and R represents H or acetyl groups depending on the degree of deacetylation.

Chitosan has unique properties that make it useful as a coagulant and/or flocculant in the removal of particulate and dissolved substances in water. It has high cationic charge density, long polymer chains, bridging of aggregate and precipitation in neutral or alkaline pH conditions.[249] It is also biodegradable and non-toxic.[227,250] It has been used effectively in the treatment of mineral and organic suspensions[251,252] and the coagulation of negatively charged contaminants in acidic solutions containing dyes[253] and humic acid[244,254] at pH above the pK_a of the macromolecule.

To study the efficiency of chitosan and design suitable experiments for chitosan coagulation and flocculation, its solubility must be considered. However, the solubility of chitosan is difficult to control.[255,256] Chitosan can be dissolved in dilute organic acids such as acetic acid and formic acid, and mineral acids such as hydrochloric acid. In an acidic solution (pH < 5), the amine groups are protonated, and the polymers become soluble. At this condition, chitosan becomes a soluble

cationic polyelectrolyte with high charge density.[232,257] Hence treatment of chitosan with acidic solution leads to protonated electrostatic interaction between polymer chains and the negatively charged contaminants.

Different reviews have been written on the application of chitosan for the removal of contaminants in water using adsorption[121,122,226,240,248,255,258,259] and membrane filtration,[260,261] respectively. Even though chitosan has been extensively used in their removal of contaminants from water, most of the studies and the reviews have centred on the recovery of suspended solids and colloidal particles as compared to the case of dissolved contaminants.[165] Bough and his co-workers[262,263], No et al.[264] and Sievers et al.[265] have independently shown that chitosan can be used to remove suspended solids effectively, turbidity and chemical oxygen demand (COD) in contaminated waters as much as 65-99%. Chitosan has been used as a flocculant and/or coagulant aid with significant performance in the removal of humic substances[244,254], metal cations[234,240,248], inorganic suspensions[243,251], proteins[266], phenolic and aromatic derivatives[267], oil and grease[163,268,269], bacteria[270] and algae[243] suspensions. The novelty of these studies is that the application of chitosan can perform better than when inorganic metal salts are used. For instance, chitosan has been shown to be more effective coagulant to remove oil residual content from palm oil mill effluent compared to alum and PACl.[268]

Guibal and his coworkers[165,248] have demonstrated that chitosan can be used effectively to treat both particulate suspension and dissolved substances. They have successfully used chitosan as a coagulant and/or flocculant in the dissolved state to remove humic substances and anionic dyes such as Reactive black 5.[251,252,265,271–274] Divakaran and Pillai have also shown that algae content in water can be reduced by using chitosan as a flocculant.[243] However, this process was found to be controlled by pH. Chitosan has also been shown to be effective in the removal of bacteria and pathogens.[270,275] Chitosan has been applied in the removal of phosphate in wastewater using different techniques or processes other than coagulation-flocculation process.[276–280]

Guilbal et al.[165] have shown that the effectiveness of chitosan in the removal of suspended and dissolved substances in water is better when it is in the dissolved state. This is because the reactivity of the amine groups increased remarkably in the aqueous phase. The application of chitosan in the dissolved state improves the accessibility and availability of reactive sites compared to the solid state.[165]

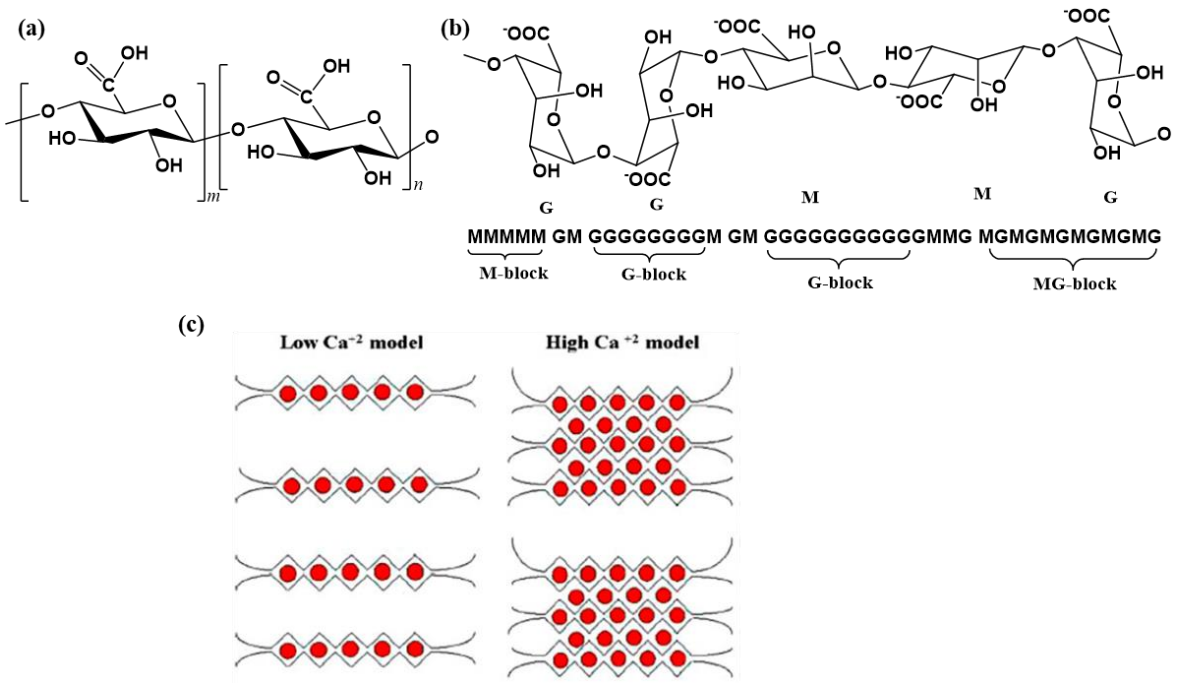

Figure 1.16: (a) Chemical structure of alginate. (b) Arrangement of G and M polymer units in alginate. (c) Egg-box model of Alginate with high and low Ca^{2+} concentrations.[281] Note: n and m represent repeating units of guluronic acid and mannuronic acid.

2.9.2.2 Alginate

Alginate is a linear naturally occurring polymeric material obtained from structural components in marine brown algae (seaweed) and also from capsular polysaccharides in soil bacterial.[282] It is anionic, possessing a negative charge. It occurs naturally in the form of calcium, magnesium and sodium salts.[283] Among all polysaccharides, it is the only one that naturally possess two carboxyl groups in each constituent unit, and exhibits diverse abilities for functional materials.[283,284] Its numerous industrial applications are related to its ability to retain water and other physical properties, such as viscoelasticity, strong stability, and gelation.[285] Another essential property of alginic acid is its ability to react with polyvalent metal cations, especially calcium ions to produce strong gel or insoluble polymers.[286]

Alginate is a linear block copolymer and is composed of β-D-mannuronate (M) and α-L-guluronate (G) units linked by β-1→4 and α-1→4 glycosidic bonds[287], as shown in Figure 2.15a. The viscoelasticity and gel formation ability of alginate is attributed to the block structure and chain length of the polymer.[282,284] The G and M monomer units in alginate can be arranged in three forms, which are depicted in Figure 2.15b;[288] (i) hydropolymeric G-blocks (polyguluronate),

where the polymer consists of only G-units, (ii) hydropolymeric M-blocks (polymannuronate) where the polymer comprises only M-units and (iii) heteropolymeric GM-block, where G and M monomer units alternate with each other. The relative abundance of these blocks in the alginate structure determines the reaction that alginate goes through especially with metal cations, and hence the nature of the final product.[289]

Even though alginate has been used for water treatment for some years[283,284,290], the study of the effect of alginate on water treatment is still at the level of infancy when compared with other biopolymers such as cellulose and chitosan. Unlike chitosan, alginate is now gaining attention in its application in wastewater treatment due to the following advantageous features. It is cost-effective, possesses no adverse health effects for handling or as an additive to drinking water, improved sludge dewatering characteristics, an effective flocculant to increase the size and weight of alum flocs, small dosage is required and does not alter the pH of the solution. It is also biodegradable and biocompactible.[152,291]

In the treatment of water with alginate, it is usually combined with Ca^{2+} solution because they form an egg-box structure, as illustrated in Figure 2.15c.[292] This gel formation property of alginate, together with other specific reactions with metal cations, makes it an industrially important biopolymer with a broad range of applications, especially in water treatment. Alginate has been used as a coagulant and coagulant aid and/or flocculant in wastewater treatment by a few researchers, as highlighted below. Wu et al.[293] have studied the effect of alginate as a coagulant aid on the coagulation behavior and floc characteristics of aluminium sulphate (alum). It was concluded that alginate enhanced the removal of color at low alum dosage than higher ones, with high flocs recoverability. The coagulation performance of alginate with ferric chloride, alum and titanium tetrachloride has been investigated by Zhao et al.[206] The results showed that when alginate is combined with an inorganic coagulant, it can remove turbidity and dissolved organic carbon. Also, the floc growth rate and floc size were significantly improved by these combinations. Devrimic et al.[294] have also used calcium alginate to remove turbidity in water. It was concluded that calcium alginate proved to be a very effective coagulant causing turbidity removal generally over 98 %. Rocher et al.[295] have also investigated the removal of organic dyes by magnetic alginate beads. It was deduced that the efficiency of the beads in the removal of dye residues in water was better than the use of inorganic salts alone and the results depended on pH, initial dye concentration and calcium content. Vijayaraghavan and Shanthakumar[295–297] have studied the application of

alginate as a coagulant for the treatment of dyes in water. They reported that the maximum Sulphur black dye removal (98.2 %) was achieved under optimum conditions of initial dye concentration of 200 mg/l, calcium concentration, 6 mg/l, and alginate dose 30 mg/l. Also, for the removal of Congo red dye, the efficiency of the coagulant was 96 % and depended on the initial pH (4-6), alginate dose (10-60 mg/l) and calcium dose (1-6 g/L) and initial concentration of the dye (50-250 mg/l). Tripathy et al. have also used alginate for effective adsorption of Pb^{2+}.[292] Recently, flocculation properties of modified alginate for the removal of dye and heavy metal ions have been investigated.[152,291,298–301]

2.9.3 Research motivation

A survey of the literature before the commencement of this Ph.D. thesis showed that several knowledge gaps exist in the field of coagulation-flocculation science and technology for the removal of dissolved species such as phosphate in the presence of colloidal species using biopolymer materials. Several reports have revealed that phosphate can be removed from wastewater using conventional inorganic coagulants as presented in Table A9.1 in Appendix A. However, no study was conducted on the removal of phosphate by coagulation-flocculation process using biopolymer materials in a homogeneous system. The closest use of biopolymer materials for the removal of phosphate is through adsorption process, in which a solid phase of the biopolymer materials and their modified forms such as beads are required for the process in a liquid-solid heterogeneous system.[95–101] Several biopolymers and biomass materials have been utilized for the removal of phosphate via adsorption process, as reported in Table A9.1. However, Guibal et al.[165] have shown that biopolymers in a homogenous liquid phase are more effective in removing suspended solids and metal ion from wastewater compared to the solid phase counterpart of the biopolymer materials because the liquid state improves the accessibility and availability of reactive sites compared to the solid state. Hence, it is proposed herein that biopolymers such as chitosan and alginate and their modified forms in a homogeneous liquid phase would be more effective in the removal of phosphate in the presence of colloidal species in ternary, binary and single-component systems. Lack of research on the removal of phosphate using biopolymer materials has led to the following knowledge gaps, which will be addressed in this thesis.

1. Understanding of the structure-activity relationship of biopolymers (e.g., chitosan and alginate) and their chemically modified forms for the removal of phosphate and colloidal materials in wastewater.
2. The effect of the structural properties and chemical composition of the biopolymer materials on the coagulation-flocculation mechanisms.
3. The effect of the structural properties and chemical composition of the biopolymer materials on the physicochemical characteristics of the flocs.

To develop improved biopolymer flocculants and an understanding of flocculation processes, the study of their structure-activity relationships is required. The flocculation efficiency depends strongly on their structural factors such as molecular weight, degree of functional group substitution as well as the type of grafting ratio. However, due to the complexity of the understanding of biopolymer structure and hydration, and complementary interactions with species of interest for removal, studies related to the flocculation of dissolved species with bioflocculants are not well established and very limited to suspended solids in water using inorganic mineral salts. This thesis will seek to develop a greater understanding of the structure-activity relationship of biopolymers (e.g., chitosan and alginate) and their chemically modified forms for the removal of phosphate and colloidal materials in wastewater.

Moreover, knowledge of the basic characteristics of the biopolymers will provide useful information on the mechanism of the flocculation process since the efficiency of the bioflocculants depends on their chemical composition and structural characteristics. The flocculation mechanisms of biopolymers are not fully understood by a systematic review of previous works.[4,120,121,302] Several mechanisms have been postulated to occur during the CF process using inorganic coagulants.[303] This thesis will also focus on understanding the mechanisms of the CF process, based on the molecular weight, structure and charge density of alginate and chitosan-based bioflocculants together with other external factors such as pH, coagulant/flocculant dosage, settling time and mixing speed and time.

Finally, studies on the characteristics of flocs that are obtained from the flocculation of colloidal suspension and dissolved particles using biopolymers are also lacking, unlike that of conventional coagulants and flocculants such as $Al_2(SO_4)_3$, PACl, $FeCl_3$, and PAM (polyacrylamide).[304–306] This is one of the major gaps this thesis focuses to address by physicochemical characterization of the bioflocculants and the flocs obtained after the CF process.

2.10 References

(1) Mewis, J.; Wagner, N. J. *Colloidal Suspension Rheology*; Cambridge University Press: Cambridge, **2011**.

(2) Sincero, Arcadio Pacquiao; Sincero, G. A. *Physical-Chemical Treatment of Water and Wastewater*, First.; CRC Press: Hoboken, 2002.

(3) Mo, S.; Shao, X.; Chen, Y.; Cheng, Z. Increasing Entropy for Colloidal Stabilization. *Sci. Rep.* **2016**, *6*, 1–7.

(4) Teh, C. Y.; Budiman, P. M.; Shak, K. P. Y.; Wu, T. Y. *Ind. Eng. Chem. Res.* **2016**, *55* (16), 4363–4389.

(5) Bratby, J. *Coagulation and Flocculation in Water and Wastewater Treatment*, Second.; IWA publishing: London, **2006**.

(6) Ndlovu, B.; Farrokhpay, S.; Forbes, E.; Bradshaw, D. *Powder Technol.* **2015**, *269*, 505–512.

(7) Murray, H. H.; Keller, W. D.; Harvey, C. C. The Diverse Industrial Applications of Kaolin. In *Kaolin Genesis and Utilization*; Clay Minerals Society, **1993**; 1–50.

(8) Murugesh Babu, K. Kaolin: Processing, Properties and Applications. *Appl. Clay Sci.* **1991**, *6*, 87–119.

(9) Hu, Y.; Liu, X. *Miner. Eng.* **2003**, *16*, 1279–1284.

(10) Teh, E. J.; Leong, Y. K.; Liu, Y.; Fourie, A. B.; Fahey, M. *Chem. Eng. Sci.* **2009**, *64* (17), 3817–3825.

(11) Ma, X.; Bruckard, W. J. *Int. J. Miner. Process.* **2010**, *94* (3–4), 111–114.

(12) Jaradat, K. A.; Darbari, Z.; Elbakhshwan, M.; Abdelaziz, S. L.; Gill, S. K.; Dooryhee, E.; Ecker, L. E. *Appl. Clay Sci.* **2017**, *150*, 163–174.

(13) Zbik, M. S.; Smart, R. S. C.; Morris, G. E. *J. Colloid Interface Sci.* **2008**, *328* (1), 73–80.

(14) Gupta, V.; Miller, J. D. *J. Colloid Interface Sci.* **2010**, *344* (2), 362–371.

(15) Kim, S.; Palomino, A. M. P *Appl. Clay Sci.* **2009**, *45* (4), 270–279.

(16) Dwari, R. K.; Mishra, B. K. *Int. J. Min. Sci. Technol.* **2019**, *29* (5), 745–755.

(17) Liu, J.; Sandaklie-Nikolova, L.; Wang, X.; Miller, J. D. *J. Colloid Interface Sci.* **2014**, *420*, 35–40.

(18) Van Oss. *Interfacial Forces in Aqueous Media*; CRC/Taylor & Francis: Boca Raton, **2006**.

(19) Tombácz, E.; Szekeres, M. *Appl. Clay Sci.* **2006**, *34* (1–4), 105–124.

(20) Kumar, N.; Andersson, M. P.; Van Den Ende, D.; Mugele, F.; Siretanu, I. *Langmuir* **2017**, *33* (50), 14226–14237.

(21) Wang, Q.; Zhu, C.; Yun, J.; Yang, G. *J. Phys. Chem. C* **2017**, *121* (48), 26722–26732.

(22) Sen Gupta, S.; Bhattacharyya, K. G. *Phys. Chem. Chem. Phys.* **2012**, *14* (19), 6698–6723.

(23) Braggs, B.; Fornasiero, D.; Ralston, J.; Smart, R. S. *Clays Clay Miner.* **1994**, *42*, 123–136.

(24) Bhattacharjee, J. H. M. S. *Electrokinetic and Colloid Transport Phenomena*; John Wiley & Sons, Inc.: Hoboken, New Jersey, **2005**.

(25) Pal, P. Physicochemical Treatment Technology. In *Industrial Water Treatment Process Technology*; Elsevier Inc., **2017**;145–171.

(26) Debye, P.; Huckel, E. *Phys. Ztschr.* **1923**, *24*, 185–206.

(27) Gouy, M. *J. Phys. Théorique Appliquée* **1910**, *9* (1), 457–468.

(28) Chapman, D. L. A *Philos. Mag.* **1913**, *25* (148), 475–481.

(29) L D Landau, J. S. Bell, M. J. Kearsley, L. P. Pitaevskii, E.M. Lifshitz, J. B. S. *Electrodynamics of Continuous Media*; Pergamon Press: New York, **1984**.

(30) Ahn Nguyen, H. J. S. *Colloidal Science of Flotation: Surfactant Science Series*; **2003**.

(31) Hunter, R. J. *Zeta Potential in Colloid Science: Principles and Applications*; Academic Press: London, **2013**; Vol. 2.

(32) Schneider, C.; Hanisch, M.; Wedel, B.; Jusufi, A.; Ballauff, M. *J. Colloid Interface Sci.* **2011**, *358* (1), 62–67.

(33) Greenwood, R.; Lapčíková, B.; Surýnek, M.; Waters, K.; Lapčík, L. *Chem. Pap.* **2007**, *61* (2).

(34) O'brien, R. W.; Cannon, D. W.; Rowlands, W. N. Electroacoustic Determination of Particle Size and Zeta Potential. *J. Colloid And Interface Science*. 1995, 406–418.

(35) Hunter, R. J.; O'Brien, R. W. *Colloids Surfaces A Physicochem. Eng. Asp.* **1997**, *126* (2–3), 123–128.

(36) O'Brien, R. W.; Beattie, J. K.; Djerdjev, A. M. *J. Colloid Interface Sci.* **2014**, *420*, 70–73.

(37) Huang, Y.; Yang, J. K.; Keller, A. A. *ACS Sustain. Chem. Eng.* **2014**, *2* (5), 1128–1138.

(38) Bakatula, E. N.; Richard, D.; Neculita, C. M.; Zagury, G. J. *Environ. Sci. Pollut. Res.* **2018**, *25* (8), 7823–7833.

(39) Cardenas-Peña, A. M.; Ibanez, J. G.; Vasquez-Medrano, R. *Int. J. Electrochem. Sci.* **2012**, *7* (7), 6142–6153.

(40) Sposito, G. On Points of Zero Charge. *Environ. Sci. Technol.* **1998**, *32* (19), 2815–2819.

(41) Trefalt, G.; Borkovec, M. Overview of DLVO Theory. *Lab. Colloid Surf. Chem. Univ. Geneva* **2014**, 1–10.

(42) Akiyama, R.; Fujino, N.; Kaneda, K.; Kinoshita, M. *Condens. Matter Phys.* **2007**, *10* (4), 587–596.

(43) Trefalt, G.; Borkovec, M. Overview of DLVO Theory. *Lab. Colloid Surf. Chem. Univ.*

Geneva **2014**, 1–10.

(44) Bhattacharjee, S.; Elimelech, M.; Borkovec, M. *Croat. Chem. Acta* **1998**, *71* (4), 883–903.

(45) Zhang, Z.; Zhao, L.; Li, Y.; Chu, M. *Math. Probl. Eng.* **2015**, *2015* (4), 1–6.

(46) Livadiotis, G.; Mccomas, D. J. *J. Plasma Phys.* **2014**, *80* (3), 341–378.

(47) Ohshima, H.; Furusawa, K. *Electrical Phenomena at Interfaces*; CRC/Taylor & Francis, **1998**.

(48) Sass, R. *Encyclopedia of Applied Electrochemistry*; 2014.

(49) Yao, J.; Han, H.; Hou, Y.; Gong, E.; Yin, W. *Math. Probl. Eng.* **2016**, *2016*.

(50) Parsegian, V. A.; Zemb, T. *Curr. Opin. Colloid Interface Sci.* **2011**, *16* (6), 618–624.

(51) Pashley, R. M. *J. Colloid Interface Sci.* **1981**, *80* (1), 153–162.

(52) Ducker, W. A.; Senden, T. J; Pashley, P. A. *Nature* **1991**, *353* (353), 2239.

(53) Pashley, R. M. *J. Colloid Interface Sci.* **1981**, *83* (2), 531–546.

(54) Grasso, D.; Subramaniam, K.; Butkus, M.; Strevett, K.; Bergendahl, J. *Rev. Environ. Sci. Biotechnol.* **2002**, *1* (1), 17–38.

(55) Liang, Y.; Hilal, N.; Langston, P.; Starov, V. *Adv. Colloid Interface Sci.* **2007**, *134–135*, 151–166.

(56) Remsing, R. C.; Patel, A. J. Hydrophobic Interactions : *J. Phys. Condens. Matter* **2002**, *14*, 9445.

(57) Meyer, E. E.; Rosenberg, K. J.; Israelachvili, J. *PNAS* **2006**, *103* (43), 15739–15746.

(58) Blokzijl, W.; Engberts, J. B. F. N. *Angew. Chemie Int. Ed. English* **1993**, *32* (11), 1545–1579.

(59) Schauperl, M.; Podewitz, M.; Waldner, B. J.; Liedl, K. R. *J. Chem. Theory Comput.* **2016**, *12*, 4600–4610.

(60) Chandle, D. *Nature* **2005**, *437* (29), 640–647.

(61) Diao, Y.; Han, M.; Lopez-Berganza, J. A.; Valentino, L.; Marinas, B.; Espinosa-Marzal, R. M. *Langmuir* **2017**, *33* (36), 8982–8992.

(62) Song, X.; Pan, Y.; Wu, Q.; Cheng, Z.; Ma, W. *Desalination* **2011**, *280* (1–3), 384–390.

(63) Farrokhpay, S.; Morris, G. E.; Fornasiero, D.; *J. Colloid Interface Sci.* **2004**, *274* (1), 33–40.

(64) Zaman, A. A.; Tsuchiya, R.; Moudgil, B. M. *J. Colloid Interface Sci.* **2002**, *256* (1), 73–78.

(65) Grabowski, J. *Chem. Rev.* **2011**, *111*, 2597–2625.

(66) Sweetman, A. M.; Jarvis, S. P.; Sang, H.; Lekkas, I.; Rahe, P.; Wang, Y.; Wang, J.; Champness, N. R.; Moriarty1, L.; Kantorovich, P. *Nat. Commun.* **2014**, *5* (May), 1–7.

(67) Flory, P. L. *Principles of Polymer Chemistry*; Ithaca, New York, **1953**.

(68) Díez, E.; Ovejero, G.; Romero, M. D.; Díaz, I. *Fluid Phase Equilib.* **2011**, *308*, 107–113.

(69) Jenkins, D.; Ferguson, J.; Menar, A. *Water Res.* **1971**, *5*, 369–389.

(70) Cooper, J.; Lombardi, R.; Boardman, D.; Carliell-Marquet, C. *Resour. Conserv. Recycl.* **2011**, *57* (January), 78–86.

(71) Pfitzner, A.; Bräu, M. F.; Zweck, J.; Brunklaus, G.; Eckert, H. *Angewandte Chemie - International Edition* **2004**, *43*, 4228–4231.

(72) Daneshgar, S.; Callegari, A.; Capodaglio, A. G.; Vaccari, D. *Resources* **2018**, *7* (2).

(73) Gilbert, N. *Nature* **2009**, *461* (8), 716–718.

(74) Cieślik, B.; Konieczka, P. *J. Clean. Prod.* **2017**, *142*, 1728–1740.

(75) Kroiss, H.; Rechberger, H.; Egle, L. *Integr. Waste Manag.* **2011**, *2* (181–214), 13.

(76) Ateeq, F. Chemical Removal of Total Phosphorus from Wastewater to Low Levels and Its Analysis, MSc. Thesis, Wilfrid Laurier University,Waterloo, Canada, **2016**.

(77) Maher, W.; Woo, L. *Anal. Chim. Acta* **1998**, *375* (1–2), 5–47.

(78) Alexander, G. C.; Stevens, R. J. *Water Res.* **1976**, *10* (9), 757–764.

(79) Daniel, T. C.; Sharpley, A. N.; Lemunyon, J. L. *J. Environ. Qual.* **1998**, *27* (2), 251–257.

(80) Rybicki, S. *Phosphorus Removal From Wastewater - A Literature Review*; **1997**.

(81) Bunce, J. T.; Ndam, E.; Ofiteru, I. D.; Moore, A.; Graham, D. W. *Front. Environ. Sci.* **2018**, *6* (February), 1–15.

(82) Litke, B. D. W. *Review of Phosphorus Control Measures in the United States and Their Effects on Water Quality*; Denver, Colorado, **1999**.

(83) Van der Molen, D. T.; Breeuwsma, A.; Boers, P. C. M. *J. Environ. Qual.* **1998**, *27* (1), 4–11.

(84) Havukainen, J.; Nguyen, M. T.; Hermann, L.; Horttanainen, M.; Mikkilä, M.; Deviatkin, I.; Linnanen, L. *Waste Manag.* **2016**, *49*, 221–229.

(85) Kahiluoto, H.; Kuisma, M.; Kuokkanen, A.; Mikkilä, M.; Linnanen, L. *Glob. Food Sec.* **2014**, *3* (1), 16–21.

(86) Kok, D. J. D.; Pande, S.; Van Lier, J. B.; Ortigara, A. R. C.; Savenije, H.; Uhlenbrook, S. *Hydrol. Earth Syst. Sci.* **2018**, *22* (11), 5781–5799.

(87) Smith, V. H.; Schindler, D. W. *Trends Ecol. Evol.* **2009**, *24* (4), 201–207.

(88) Powers, S. M.; Bruulsema, T. W.; Burt, T. P.; Chan, N. I.; Elser, J. J.; Haygarth, P. M.; Howden, N. J. K.; Jarvie, H. P.; Lyu, Y.; Peterson, H. M.; et al. *Nat. Geosci.* **2016**, *9* (5), 353–356.

(89) Némery, J.; Garnier, J. *Nat. Geosci.* **2016**, *9* (5), 343–344.

(90) MacDonald, G. K.; Bennett, E. M.; Potter, P. A.; Ramankutty, N. *Proc. Natl. Acad. Sci. U. S. A.* **2011**, *108* (7), 3086–3091.

(91) Villalba, G.; Liu, Y.; Schroder, H.; Ayres, R. U. *J. Ind. Ecol.* **2008**, *12* (4), 557–569.

(92) Cordell, D.; Drangert, J. O.; White, S. *Glob. Environ. Chang.* **2009**, *19* (2), 292–305.

(93) Li, H.; Liu, J.; Li, G.; Shen, J.; Bergström, L.; Zhang, F. *Ambio* **2015**, *44* (2), 274–285.

(94) Heathwaite, L.; Sharpley, A.; Gburek, W. *J. Environ. Qual.* **2000**, *29* (1), 158–166.

(95) Mahaninia, M. H.; Wilson, L. D. *J. Colloid Interface Sci.* **2017**, *485*, 201–212.

(96) Mahaninia, M. H.; Wilson, L. D. *J. Appl. Polym. Sci.* **2016**, *133* (5), 1–10.

(97) Mahaninia, M. H.; Wilson, L. D. *Ind. Eng. Chem. Res.* **2017**, *56* (7), 1704–1712.

(98) Luo, X.; Wu, X.; Reng, Z.; Min, X.; Xiao, X.; Luo, J. *Ind. Eng. Chem. Res.* **2017**, *56*, 9419–9428.

(99) Huang, W.; Zhang, Y.; Li, D. *J. Environ. Manage.* **2017**, *193*, 470–482.

(100) Gu, Y.; Yang, M.; Wang, W.; Han, R. *J. Chem. Eng. Data* **2019**, *64*, 2849–2858.

(101) Huang, X.; Foster, G. D.; Honeychuck, R. V; Schreifels, J. A. *Langmuir* **2009**, *25* (21), 4450–4461.

(102) Yang, Y.; Zhang, L.; Shao, H.; Zhang, S.; Gu, P.; Peng, Y. *Front. Environ. Sci. Eng.* **2017**, *11* (2), 1–6.

(103) Yang, G.; Wang, D.; Yang, Q.; Zhao, J.; Liu, Y. *Chemosphere* **2018**, *196*, 78–86.

(104) Oehmen, A.; Lemos, P. C.; Carvalho, G.; Yuan, Z.; Blackall, L. L.; Reis, M. A. M. *Water Res.* **2007**, *41*, 2271–2300.

(105) Eskandarpour, A.; Sassa, K.; Bando, Y.; Okido, M.; Asai, S. *Mater. Trans.* **2006**, *47* (7), 1832–1837.

(106) Hashim, K. S.; Jasim, N.; Shaw, A.; Phipps, D.; Kot, P.; Alattabi, A. W.; Abdulredha, M.; Alawsh, R. *Sep. Purif. Technol.* **2019**, *210*, 135–144.

(107) Lei, Y.; Geraets, E.; Saakes, M.; Weijden, R. D. Van Der; Buisman, C. J. N. *Water Res.* **2020**, *169*, 115207.

(108) Dura, A.; Breslin, C. B. *J. Electroanal. Chem.* **2019**, *846*, 113161.

(109) Jiang, J.; Inhyuk, D.; Dorji, P.; Phuntsho, S.; Hong, S.; Kyong, H. *Process Saf. Environ. Prot.* **2019**, *126*, 44–52.

(110) Tang, J.; Wang, X. C.; Hu, Y.; Pu, Y.; Huang, J.; Hao, H.; Zeng, Y.; Li, Y. *Bioresour. Technol.* **2019**, *271* (August 2018), 125–135.

(111) Ebeling, J. M.; Sibrell, P. L.; Ogden, S. R.; Summerfelt, S. T. *Aquac. Eng.* **2003**, *29* (1–2), 23–42.

(112) Dunets, C. S.; Zheng, Y. C*Hortscience* **2015**, *50* (6), 921–926.

(113) Li, T.; Dong, W.; Zhang, Q.; Xing, D.; Ai, W.; Liu, T. *J. Environ. Manage.* **2020**, *255* (October 2019), 109849.

(114) Sedlak, R. I. *Phosphorus and Nitrogen Removal from Municipal Wastewater*, Second.; Lewis Publishers: New York, USA, **1991**.

(115) Yang, K.; Li, Z.; Zhang, H.; Qian, J.; Chen, G. *Environ. Technol.* **2010**, *31* (6), 601–609.

(116) Agbovi, H. K.; Wilson, L. D. *Environ. Chem.* **2019**, *16* (8), 599–612.

(117) Childers, D. L.; Corman, J.; Edwards, M.; Elser, J. J. *Bioscience* **2011**, *61* (2), 117–124.

(118) Jarvie, H. P.; Sharpley, A. N.; Spears, B.; Buda, A. R.; May, L.; Kleinman, P. J. A. *Environ. Sci. Technol.* **2013**, *47* (16), 8997–8998.

(119) Tripathy, T.; De, B. R. *J. Phys. Sci.* **2006**, *10*, 93–127.

(120) Wei, H.; Gao, B.; Ren, J.; Li, A.; Yang, H. *Water Res.* **2018**, *143* (2015), 608–631.

(121) Yang, R.; Li, H.; Huang, M.; Yang, H.; Li, A. *Water Res.* **2016**, *95*, 59–89.

(122) Zhang, L.; Zeng, Y.; Cheng, Z. *J. Mol. Liq.* **2016**, *214*, 175–191.

(123) Lee, C. S.; Robinson, J.; Chong, M. F. *Process Saf. Environ. Prot.* **2014**, *92* (6), 489–508.

(124) Radoiu, M. T.; Martin, D. I.; Calinescu, I.; Iovu, H. *J. Hazard. Mater.* **2004**, *106B*, 27–37.

(125) Agbovi, H. K.; Wilson, L. D. *Ind. Eng. Chem. Res.* **2017**, *56* (12).

(126) Agbovi, H. K.; Wilson, L. D.; Tabil, L. G. *Ind. Eng. Chem. Res.* **2017**, *56* (1), 37–46.

(127) Agbovi, H. K.; Wilson, L. D. *Carbohydr. Polym.* **2018**, *189*, 360–370.

(128) Smoluchowski, M. von. *Z. Phys. Chem.* **1917**, *92*, 129–168.

(129) Gregory, J. *Adv. Colloid Interface Sci.* **2009**, *147–148*, 109–123.

(130) Bal, V. *J. Colloid Interface Sci.* **2020**, *564*, 170–181.

(131) Oktaviani, O.; Adachi, Y. *Colloids and Interfaces* **2019**, *3* (5), 1–13.

(132) Oyegbile, B.; Ay, P.; Narra, S. *Environ. Eng. Res.* **2016**, *21* (1), 1–14.

(133) Smoczyński, L.; Mróz, P.; Wardzynska, R.; Załeska-Chróst, B.; Dłuzyńska, K. *Chem. Eng. J.* **2009**, *152* (1), 146–150.

(134) Torkaman, M.; Bahrami, M.; Dehghani, M. *Energy and Fuels* **2017**, *31*, 11169–11180.

(135) Thomas, D. N.; Judd, S. J.; Fawcett, N. *Water Res.* **1999**, *33* (7), 1579–1592.

(136) Raynaud, M.; A, J. V.; Olivier, J.; Dieude-Fauvel, E.; Baudez, J.-C. Compression *Water Res.* **2012**, *46*, 4448–4456.

(137) Zheng, H.; Sun, Y.; Zhu, C.; Guo, J.; Zhao, C.; Liao, Y.; Guan, Q. *Chem. Eng. J.* **2013**, *234*, 318–326.

(138) Jiang, J. Q.; Graham, N. J. D. *Water SA* **1998**, *24* (3), 237–244.

(139) Guaya, D.; Valderrama, C.; Farran, A.; Armijos, C.; Cortina, J. L. *Chem. Eng. J.* **2015**, *271*, 204–213.

(140) Park, T.; Ampunan, V.; Lee, S.; Chung, E. *Chemosphere* **2016**, *144*, 2264–2269.

(141) Sadeghi, S.; Hua, G.; Min, K.; Johnson, T. J.; Gibbons, W. B. *J. Environ. Eng. (United States)* **2020**, *146* (1), 1–10.

(142) Zouboulis, A. I.; Tzoupanos, N. D. *J. Hazard. Mater.* **2009**, *162*, 1379–1389.

(143) Zhang, P.; Hahn, H. H.; Hoffmann, E. *Chemosphere* **2004**, *57*, 1489–1494.

(144) Moussas, P. A.; Zouboulis, A. I. *Sep. Purif. Technol.***2008**, *63*, 475–483.

(145) Lee, K. E.; Morad, N.; Teng, T. T.; Poh, T. *Chem. Eng. J.* **2012**, *203*, 370–386.

(146) Yang, R.; Li, H.; Huang, M.; Yang, H.; Li, A. *Water Res.* **2016**, *95* (2015), 59–89.

(147) Shammas, N. K. Coagulation and Flocculation. In *in: Environmental chemistry of dyes and pigments*; **1996**;103–139.

(148) Mohan, S. M. *J. Environ. Manage.* **2014**, *136*, 103–111.

(149) Zou, J.; Zhu, H.; Wang, F.; Sui, H.; Fan, J. *Chem. Eng. J.* **2011**, *171* (1), 350–356.

(150) Kan, C.; Huang, C.; Pan, J. R. *Colloids Surfaces A Physicochem. Eng. Asp***,2002**, *203*, 1–9.

(151) Ramphal, S.; Sibiya, S. M. *Procedia Eng.* **2014**, *70*, 1401–1410.

(152) Tian, Z.; Zhang, L.; Sang, X.; Shi, G.; Ni, C. *J. Phys. Chem. Solids* **2020**, *141* (December 2019), 109408.

(153) Vadasarukkai, Y. S.; Gagnon, G. A. *Water Res.* **2015**, *84*, 333–341.

(154) Pillai, J. *Flocculants and Coagulants: The Keys to Water and Waste Management in Aggregate Production*; Naperville, Illinois, **1997**.

(155) Teh, C. Y.; Wu, T. Y.; Juan, J. C. *Ecol. Eng.* **2014**, *71*, 509–519.

(156) Sun, Y.; Zhou, S.; Sun, W.; Zhu, S.; Zheng, H. *Sep. Purif. Technol.* **2020**, *241*, 116737.

(157) Paton-Morales, P.; Talens-Alesson, F. I. *Langmuir* **2001**, *17* (20), 6059–6064.

(158) Järnström, L.; Lason, L.; Rigdahl, M. *Colloids Surfaces A Physicochem. Eng. Asp.* **1995**, *104* (2–3), 191–205.

(159) Yang, Z.; Yuan, B.; Huang, X.; Zhou, J.; Cai, J.; Yang, H.; Li, A. *Water Res.* **2011**, *46* (1), 107–114.

(160) Li, J.; Jiao, S.; Zhong, L.; Pan, J.; Ma, Q. *Colloids Surfaces A Physicochem. Eng. Asp.* **2013**, *428*, 100–110.

(161) Bhalkaran, S.; Wilson, L. D. *Int. J. Mol. Sci.* **2016**, *17* (10).

(162) Feng, L.; Li, X.; Lu, W.; Liu, Z.; Xu, C.; Chen, Y.; Zheng, H. *Int. J. Biol. Macromol.* **2020**, *150*, 617–630.

(163) Bratskaya, S.; Avramenko, V.; Schwarz, S.; Philippova, I. *Colloids Surfaces A Physicochem. Eng. Asp.* **2006**, *275* (1–3), 168–176.

(164) Djibrine, B. Z.; Zheng, H.; Wang, M.; Liu, S.; Tang, X.; Khan, S.; Jimenéz, A. N.; Feng, L. *Int. J. Polym. Sci.* **2018**, *2018*.

(165) Guibal, E.; Van Vooren, M.; Dempsey, B. a.; Roussy, J. *Sep. Sci. Technol.* **2006**, *41* (11), 2487–2514.

(166) Guo, K.; Gao, B.; Wang, W.; Yue, Q.; Xu, X. *Chemosphere* **2019**, *215*, 214–226.

(167) Liu, Y.; Zheng, H.; Sun, Y.; Ren, J.; Zheng, X. *J. Clean. Prod.* **2020**, *249*, 119350.

(168) You, L.; Song, L.; Wang, A.; Lu, F.; Zhang, Q. *Colloids Surfaces A Physicochem. Eng. Asp.* **2017**, *520*, 841–849.

(169) Xiao, F.; Huang, J. H.; Zhang, B.; Cui, C. *Desalination* **2009**, *237* (1–3), 201–213.

(170) Chen, Y.; Liu, S.; Wang, G. *Chem. Eng. J.* **2007**, *133* (1–3), 325–333.

(171) Zhang, W.; Shang, Y.; Yuan, B.; Jiang, Y.; Lu, Y.; Qin, Z.; Chen, A.; Qian, X.; Yang, H.; Cheng, R. *J. Appl. Polym. Sci.* **2010**, *117*, 2016–2024.

(172) Shak, K. P. Y.; Wu, T. Y. *Chem. Eng. J.* **2014**, *256*, 293–305.

(173) Kleimann, J.; Gehin-Delval, C.; Auweter, H.; Borkovec, M. *Langmuir* **2005**, *21* (8), 3688–3698.

(174) Bolto, B.; Gregory, J. *Water Res.* **2007**, *41* (11), 2301–2324.

(175) Sharma, B. R.; Dhuldhoya, N. C.; Merchant, U. C. *J. Polym. Environ.* **2006**, *14* (2), 195–202.

(176) Gregory, J. *J. Colloid Interface Sci.* **1973**, *42* (2), 448–456.

(177) Kasper, D. R. Theoretical and Experimental Investigations of the Flocculation of Charged Particles in Aqueous Solutions by Polyelectrolytes of Opposite Charge, PhD Thesis, California Institute of Technology, Pasadena, California, **1971**.

(178) Bolto, B.; Gregory, J. Organic Polyelectrolytes in Water Treatment. *Water Res.* **2007**, *41*, 2301–2324.

(179) Yoon, S.-Y.; Deng, Y. *J. Colloid Interface Sci.* **2004**, *278* (1), 139–145.

(180) Sher, F.; Malik, A.; Liu, H. *J. Environ. Chem. Eng.* **2013**, *1* (4), 684–689.

(181) Lee, K. E.; Morad, N.; Teng, T. T.; Poh, B. T. *Chem. Eng. J.* **2012**, *203*, 370–386.

(182) Razali, M. A. A.; Ahmad, Z.; Ahmad, M. S. B.; Ariffin, A. *Chem. Eng. J.* **2011**, *166* (2), 529–535.

(183) Edzwald, J.; Tobiason, J. *Water Sci. Technol.* **1999**, *40* (9), 63–70.

(184) Hoogeveen, N. G.; Cohen Stuart, M. A.; Fleer, G. J. *Colloids Surfaces A Physicochem. Eng. Asp.* **1996**, *117* (1–2), 77–88.

(185) Napper, D. H. *Polymeric Stabilization of Colloidal Dispersions*; Academic Press Inc.: New York, **1983**.

(186) Dahlgren, M. A. G. *Langmuir* **1994**, *10* (29), 1580–1583.

(187) Tanneru, C. T.; Rimer, J. D.; Chellam, S. *Environ. Sci. Technol.* **2013**, *47* (9), 4612–4618.

(188) Yang, Z.; Yan, H.; Yang, H.; Li, H.; Li, A.; Cheng, R. *Water Res.* **2013**, *47* (9), 3037–3046.

(189) Lipatov, Y.; Chornaya, V.; Todosijchuk, T.; Dudarenko, G. *J. Colloid Interface Sci.* **2005**, *285* (2), 525–531.

(190) Singh, R. P.; Pal, S.; Rana, V. K.; Ghorai, S. *Carbohydr. Polym.* **2013**, *91* (1), 294–299.

(191) Guibal, E.; Roussy, J. *React. Funct. Polym.* **2007**, *67* (1), 33–42.

(192) Ho, Y. S.; McKay, G. *Chem. Eng. J.* **1998**, *70* (2), 115–124.

(193) Ho, Y. S.; McKay, G. *Process Biochem.* **1999**, *34* (5), 451–465.

(194) Tan, K. L.; Hameed, B. H. *J. Taiwan Inst. Chem. Eng.* **2017**, *74*, 25–48.

(195) Kono, H.; Kusumoto, R. *J. Water Process Eng.* **2015**, *7*, 83–93.

(196) Langmuir, I. *J. Am. Chem. Soc.* **1916**, *252*, 2221–2295.

(197) Freundlich, H. M. F. *Z. Phys. Chem.* **1909**, *57*, 385–470.

(198) Sips, R. *J. Chem. Phys.* **1948**, *18* (5), 490–495.

(199) Sari, Ahmet Tuzen, Mustafa Uluozlu, Dogan Ozgur Soylak, M. *Biochem. Eng. J.* **2007**, *37*, 151–158.

(200) Stumm, W., Morgan, J. J. *Aquatic Chemistry — An Introduction Emphasizing Chemical Equilibrist in Natural Waters*; Wiley-Interscience: Hoboken, New Jersey, **1996**.

(201) Georgantas, D. A.; Grigoropoulou, H. P. *J. Colloid Interface Sci.* **2007**, *315* (1), 70–79.

(202) Georgantas, D. A.; Grigoropoulou, H. P. *Glob. NEST J.* **2006**, *8* (2), 121–130.

(203) Nail, S. L.; White, J. O. E. L.; Hem, S. L. *J. Pharm. Sci.* **1976**, *68* (8), 1188–1191.

(204) Aguilar, M. I.; Sáez, J.; Lloréns, M.; Soler, A.; Ortuño, J. F. *Water Res.* **2002**, *36* (11), 2910–2919.

(205) Fettig, J.; Ratnaweera, H.; Odegaard, H. *Water Supply* **1990**, *8*, 19–26.

(206) Zhao, Y. X.; Wang, Y.; Gao, B. Y.; Shon, H. K.; Kim, J.-H.; Yue, Q. Y. *Desalination* **2012**, *299*, 79–88.

(207) Low, F.; Study, A. C.; Łopata, M.; Augustyniak, R.; Grochowska, J.; Parszuto, K.; Tandyrak, R. *Water* **2019**, *11*, 1812.

(208) Tibebe, D.; Kassa, Y.; Bhaskarwar, A. N. *BMC Chem.* **2019**, *13* (1), 1–14.

(209) Munir, M. T.; Li, B.; Boiarkina, I.; Baroutian, S.; Yu, W.; Young, B. R. *Bioresour. Technol.* **2017**, *239*, 171–179.

(210) Thomas, E. A. *Vierteljahrsch Naturf. Ges. Zurich* **1965**, *110*, 419.

(211) Thomas, E. A. *Vertl. jahrsch. Naturf. Ges. Zurich* **1966**, *111*, 309.

(212) Shannon, M. A.; Bohn, P. W.; Elimelech, M.; Georgiadis, J. G.; Marĩas, B. J.; Mayes, A. M. *Nature* **2008**, *452* (7185), 301–310.

(213) Yeoman, S.; Stephenson, T.; Lester, J. N.; Perry, R. *Environ. Pollut.* **1988**, *49* (3), 183–233.

(214) Chakraborty, T.; Balusani, D.; Smith, S.; Santoro, D.; Walton, J.; Nakhla, G.; Ray, M. B. *Sep. Purif. Technol.* **2020**, *231*, 115894.

(215) Smith, S.; Takács, I.; Murthy, S.; Daigger, G. T.; Szabó, A. *Water Environ. Res.* **2008**, *80* (5), 428–438.

(216) Szabó, A.; Takács, I.; Murthy, S.; Daigger, G. T.; Licskó, I.; Smith, S. *Water Environ. Res.* **2008**, *80* (5), 407–416.

(217) Suschka, J.; Machnicka, a.; Poplawski, S. **2001**, *22* (11), 1295–1301.

(218) Benedek, A.; Hamielec, A. E.; Bancsi, J. J.; Ishige, T. *Assessment of Polyelectrolytes for Phosphorus Removal*; **1976**.

(219) Blatter, M.; Vermeille, M.; Furrer, C.; Pouget, G.; Fischer, F. *ACS Sustain. Chem. Eng.* **2019**, *7* (6), 5856–5866.

(220) Wilfert, P.; Kumar, P. S.; Korving, L.; Witkamp, G. J.; Van Loosdrecht, M. C. M. *Environ. Sci. Technol.* **2015**, *49* (16), 9400–9414.

(221) Zahrim, A. Y.; Dexter, Z. D.; Joseph, C. G.; Hilal, N. *J. Water Process Eng.* **2017**, *16*, 258–269.

(222) Geelhoed, J. S.; Hiemstra, T.; Van Riemsdijk, W. H. *Geochim. Cosmochim. Acta* **1997**, *61* (12), 2389–2396.

(223) Makris, K. C.; El-Shall, H.; Harris, W. G.; O'Connor, G. A.; Obreza, T. A. *J. Colloid Interface Sci.* **2004**, *277* (2), 417–423.

(224) Gray, H. E.; Powell, T.; Choi, S.; Smith, D. S.; Parker, W. J. *Water Res.* **2020**, *182*, 115968.

(225) Hauduc, H.; Takács, I.; Smith, S.; Szabo, A.; Murthy, S.; Daigger, G. T.; Spérandio, M. *Water Res.* **2015**, *73*, 157–170.

(226) Gerente, C.; Lee, V. K. C.; Cloirec, P. Le; McKay, G. *Crit. Rev. Environ. Sci. Technol.* **2007**, *37* (1), 41–127.

(227) Kaya, M.; Mujtaba, M.; Ehrlich, H.; Salaberria, A. M.; Baran, T.; Amemiya, C. T.; Galli, R.; Akyuz, L.; Sargin, I.; Labidi, J. *Carbohydr. Polym.* **2017**, *176*, 177–186.

(228) Aranaz, I.; Mengíbar, M.; Harris, R.; Paños, I.; Miralles, B.; Acosta, N.; Galed, G.; Heras, A. *Curr. Chem. Biol.* **2009**, *3*, 203–230.

(229) Mohammadzadeh Pakdel, P.; Peighambardoust, S. J. *Carbohydr. Polym.* **2018**, *201* (August), 264–279.

(230) Lichtfouse, E.; Morin-Crini, N.; Fourmentin, M.; Zemmouri, H.; do Carmo Nascimento, I. O.; Queiroz, L. M.; Tadza, M. Y. M.; Picos-Corrales, L. A.; Pei, H.; Wilson, L. D.; et al. *Environ. Chem. Lett.* **2019**, *17* (4), 1603–1621.

(231) George, A.; Sanjay, M. R.; Sriusk, R.; Parameswaranpillai, J.; Siengchin, S. *Int. J. Biol. Macromol.* **2020**, *154*, 329–338.

(232) Rinaudo, M. *Prog. Polym. Sci.* **2006**, *31* (7), 603–632.

(233) Song, Z.; Li, G.; Guan, F.; Liu, W. *Polymers (Basel).* **2018**, *10* (4).

(234) Talukdar, M. I.; Hasnine, M. T. *Int. Res. J. Environ. Sci.* **2014**, *3* (3), 5–10.

(235) Enescu, D. *Rom. Biotechnol. Lett.* **2008**, *13* (6), 4037–4048.

(236) El-Hefian, E. A.; Nasef, M. M.; Yahaya, A. H. *J. Chem. Soc. Pakistan* **2014**, *36* (1), 11–27.

(237) Harish Prashanth, K. V.; Tharanathan, R. N. *Trends Food Sci. Technol.* **2007**, *18* (3), 117–131.

(238) Kumar, M. N. V. R.; Muzzarelli, R. A. A.; Muzzarelli, C.; Sashiwa, H.; Domb, A. J. *Chem. Rev.* **2004**, *104* (12), 6017–6084.

(239) Prabaharan, M.; Mano, J. F. *Drug Deliv.* **2004**, *12* (October), 41–57.

(240) Varma, A. .; Deshpande, S. .; Kennedy, J. . *Carbohydr. Polym.* **2004**, *55* (1), 77–93.

(241) Huang, C.; Chen, Y. *J. Chem. Technol. Biotechnol.* **1996**, *66* (3), 227–232.

(242) Gassara, F.; Antzak, C.; Ajila, C. M.; Sarma, S. J.; Brar, S. K.; Verma, M. *J. Food Eng.* **2015**, *166*, 80–85.

(243) Divakaran, R.; Sivasankara Pillai, V. N. *Water Res.* **2002**, *36* (9), 2414–2418.

(244) Bratskaya, S. Y.; Avramenko, V. A.; Sukhoverkhov, S. V.; Schwarz, S. *Colloid J.* **2002**, *64* (6), 681–686.

(245) Sharma, B. R.; Dhuldhoya, N. C.; Merchant, U. C. *J. Polym. Environ.* **2006**, *14*, 195–202.

(246) Yang, Z.; Degorce-Dumas, J. R.; Yang, H.; Guibal, E.; Li, A.; Cheng, R. *Environ. Sci. Technol.* **2014**, *48* (12), 6867–6873.

(247) Zeng, D.; Wu, J.; Kennedy, J. F. *Carbohydr. Polym.* **2008**, *71* (1), 135–139.

(248) Guibal, E. *Sep. Purif. Technol.* **2004**, *38* (1), 43–74.

(249) Renault, F.; Sancey, B.; Badot, P. M.; Crini, G. *Eur. Polym. J.* **2009**, *45* (5), 1337–1348.

(250) Kanmani, P.; Aravind, J.; Kamaraj, M.; Sureshbabu, P.; Karthikeyan, S. *Bioresour. Technol.* **2017**, *242*, 295–303.

(251) Roussy, J.; Van Vooren, M.; Guibal, E. *J. Dispers. Sci. Technol.* **2005**, *25* (5), 663–677.

(252) Roussy, J.; Van Vooren, M.; Dempsey, B. A.; Guibal, E. *Water Res.* **2005**, *39* (14), 3247–3258.

(253) Xin, C.; Hui-li, S.; Jia-hui, P. *Ocean Sci. J.* **2006**, *226* (4), 221–226.

(254) Ma, J.; Fu, K.; Jiang, L.; Ding, L.; Guan, Q.; Zhang, S.; Zhang, H.; Shi, J.; Fu, X. *Sep. Purif. Technol.* **2017**, *181*, 201–212.

(255) Choi, C.; Nam, J. P.; Nah, J. W. *J. Ind. Eng. Chem.* **2016**, *33*, 1–10.

(256) Giraldo, J. D.; Rivas, B. L. *Polym. Bull.* **2020**, No. 0123456789.

(257) Kurita, K. *Mar. Biotechnol.* **2006**, *8* (3), 203–226.

(258) Crini, G. *Prog. Polym. Sci.* **2005**, *30*, 38–70.

(259) Vakili, M.; Deng, S.; Cagnetta, G.; Wang, W.; Meng, P.; Liu, D.; Yu, G. *Sep. Purif. Technol.* **2019**, *224*, 373–387.

(260) Cooper, A.; Oldinski, R.; Ma, H.; Bryers, J. D.; Zhang, M. *Carbohydr. Polym.* **2013**, *92* (1), 254–259.

(261) Li, L.; Li, Y.; Yang, C. *Carbohydr. Polym.* **2016**, *140*, 299–307.

(262) Bough, W. A.; Shewfelt, A. L.; Salter, W. L. *Poult. Sci.* **1975**, *54* (4), 992–1000.

(263) Bough, W. A.; Salter, W. L.; Wu, A. C. M.; Perkins, B. E. *Biotechnol. Bioeng.* **1978**, *20* (12), 1931–1943.

(264) No, H.K. ; Meyers, S. P. *Rev. Environ. Contam. Toxicol.* **2000**, *163*, 1–27.

(265) Sievers, D. M.; Jenner, M. W.; Hanna, M. W. *Am. Soc. Agric. Eng.* **1991**.

(266) Gamage, A.; Shahidi, F. *Food Chem.* **2007**, *104* (3), 989–996.

(267) Zheng, S.; Yang, Z.; Jo, D. H.; Park, Y. H. *Water Res.* **2004**, *38* (9), 2315–2322.

(268) Ahmad, A. L.; Sumathi, S.; Hameed, B. H. *Chem. Eng. J.* **2006**, *118* (1–2), 99–105.

(269) Ahmad, A.; Ismail, S.; Bhatia, S. *Environ. Sci. Technol.* **2005**, *39* (8), 2828–2834.

(270) Al-Manhel, A. J.; Al-Hilphy, A. R. S.; Niamah, A. K. *J. Saudi Soc. Agric. Sci.* **2018**, *17* (2), 186–190.

(271) Szyguła, A.; Guibal, E.; Ruiz, M.; Sastre, A. M. *Colloids Surfaces A Physicochem. Eng. Asp.* **2008**, *330* (2–3), 219–226.

(272) Szyguła, A.; Guibal, E.; Palacín, M. A.; Ruiz, M.; Sastre, A. M. *J. Environ. Manage.* **2009**, *90* (10), 2979–2986.

(273) Roussy, J.; Van Vooren, M.; Guibal, E*J. Appl. Polym. Sci.* **2005**, *98* (5), 2070–2079.

(274) Vogelsang, C.; Andersen, D. O.; Hey, A.; Håkonsen, T.; Jantsch, T. G.; Müller, E. D.; Pedersen, M. A.; Vårum, K. M. *Water Sci. Technol. Water Supply* **2004**, *4* (5), 121–129.

(275) Abebe, L. S.; Chen, X.; Sobsey, M. D. *Int. J. Environ. Res. Public Health* **2016**, *13* (3).

(276) Filipkowska, U.; Jóźwiak, T.; Szymczyk, P. *Prog. Chem. Appl. Chitin its Deriv.* **2014**, *19* (1), 5–14.

(277) Fierro, S.; del Pilar Sánchez-Saavedra, M.; Copalcúa, C. *Bioresour. Technol.* **2008**, *99* (5), 1274–1279.

(278) Liu, X.; Zhang, L. *Powder Technol.* **2015**, *277*, 112–119.

(279) Szymczyk, P.; Filipkowska, U.; Jóźwiak, T.; Kuczajowska-Zadrożna, M. *Prog. Chem. Appl. Chitin its Deriv.* **2016**, *21*, 192–202.

(280) Wang, X.; Lü, S.; Gao, C.; Feng, C.; Xu, X.; Bai, X.; Gao, N.; Yang, J.; Liu, M.; Wu, L. *ACS Sustain. Chem. Eng.* **2016**, *4* (4), 2068–2079.

(281) Simpson, N. E.; Stabler, C. L.; Simpson, C. P.; Sambanis, A.; Constantinidis, I. *Biomaterials* **2004**, *25* (13), 2603–2610.

(282) Pawar, S. N.; Edgar, K. J. Alginate Derivatization: *Biomaterials* **2012**, *33* (11), 3279–3305.

(283) Salehizadeh, H.; Yan, N.; Farnood, R. Flocculants. *Biotechnol. Adv.* **2018**, *36* (1), 92–119.

(284) Yang, J. S.; Xie, Y. J.; He, W. *Carbohydr. Polym.* **2011**, *84* (1), 33–39.

(285) Saranya, P.; Ramesh, S. T.; Gandhimathi, R. *Desalin. Water Treat.* **2014**, *52* (31/33), 6030–6039.

(286) Salehizadeh, H.; Yan, N. *Biotechnol. Adv.* **2014**, *32* (8), 1506–1522.

(287) Lee, K. Y.; Mooney, D. J. *Prog. Polym. Sci.* **2012**, *37* (1), 106–126.

(288) Szekalska, M.; Puciłowska, A.; Szymańska, E.; Ciosek, P.; Winnicka, K. *Int. J. Polym. Sci.* **2016**, *2016*.

(289) Ikeda, A.; Takemura, A.; Ono, H. *Carbohydr. Polym.* **2000**, *42*, 421–425.

(290) Tripathy, T.; Pandey, S. .; Karmakar, N. .; Bhagat, R. .; Singh, R. *Eur. Polym. J.* **1999**, *35* (11), 2057–2072.

(291) Tian, Z.; Zhang, L.; Ni, C. *Environ. Sci. Pollut. Res.* **2019**, *26* (31), 32397–32406.

(292) Tripathy, T.; Kolya, H.; Jana, S. *J. Polym. Environ.* **2018**, *26* (3), 926–937.

(293) Wu, C.; Wang, Y.; Gao, B.; Zhao, Y.; Yue, Q. *Sep. Purif. Technol.* **2012**, *95*, 180–187.

(294) Devrimci, H. A.; Yuksel, A. M.; Sanin, F. D. *Desalination* **2012**, *299*, 16–21.

(295) Rocher, V.; Bee, A.; Siaugue, J.-M.; Cabuil, V. *J. Hazard. Mater.* **2010**, *178* (1–3), 434–439.

(296) Vijayaraghavan, G.; Shanthakumar, S. *Prog. Sustain. Energy* **2015**, *34* (5), 1427–1434.

(297) Vijayaraghavan, G.; Shanthakumar, S. *Desalin. Water Treat.* **2016**, *57* (14), 6384–6392.

(298) Babu, N. A.; Krishna Mohan, G. V.; Kalpana, K.; Ravindhranath, K. *J. Anal. Methods Chem.* **2017**, *2017*.

(299) Benettayeb, A.; Guibal, E.; Morsli, A.; Kessas, R. *Chem. Eng. J.* **2017**, *316*, 704–714.

(300) Tian, Z.; Zhang, L.; Shi, G.; Sang, X.; Ni, C. *J. Appl. Polym. Sci.* **2018**, *135* (31), 1–7.

(301) Zhang, Q.; Wang, D.; Bei, Y.; Ren, S.; Fang, G. *BioResources* **2013**, *8* (3), 3544–3555.

(302) Salehizadeh, H.; Yan, N. *Biotechnol. Adv.* **2014**, *32* (8), 1506–1522.

(303) Feng, J.; Yang, Z.; Zeng, G.; Huang, J.; Xu, H.; Zhang, Y.; Wei, S.; Wang, L. *Bioresour. Technol.* **2013**, *148*, 414–421.

(304) Aktas, T. S.; Fujibayashi, M.; Maruo, C.; Nomura, M.; Nishimura, O. *Desalin. Water Treat.* **2013**, *51* (22–24), 4729–4735.

(305) Huang, X.; Gao, B.; Zhao, S.; Sun, S.; Yue, Q.; Wang, Y.; Li, Q. *RSC Adv.* **2016**, *6* (55), 49469–49477.

(306) Zhao, H.; Hu, C.; Zhang, D.; Liu, H.; Qu, J. *PLoS One* **2016**, *11* (1), 1–17.

CHAPTER 3

3 Biopolymer flocculants and oat hull biomass to aid the removal of orthophosphate in wastewater treatment[1]

Description

This research study is directed towards investigation of the flocculation properties of natural polymer flocculants in comparison to inorganic mineral salt coagulants for the removal of phosphate in synthetic wastewater. The bioflocculants of interest are chitosan, alginate and oat hull biomass. Herein, the flocculant materials were used as obtained from Prof. L. Tabil without any chemical modification. The flocculation results show that a combination of alginate, chitosan and alum (coagulant) in a ternary system is more effective in removing the phosphate relative to binary (alum and alginate or alum and chitosan) and single-component systems. A binary system consisting of alum and oat hull biomass showed significant improvement in the flocculation process towards the phosphate removal. The results indicate that the biopolymer materials have tunable properties for the removal of dissolved nutrients.

Author's contribution

Lee D. Wilson and I conceived the project. I performed all the experimental work, data processing and analysis, and wrote the first draft of the manuscript as well as making further revisions where and when necessary on subsequent drafts. Dr. L.D. Wilson was responsible for the supervision of the project, editorial guidance for revision of the manuscript drafts, and corresponding author. Dr. Lope G. Tabil supplied the oat hull biomass used in the experiment and helped with editorial advice. Permission was obtained from all contributing authors before the inclusion of the manuscript in this thesis.

[1] Reproduced in part with permission from Agbovi, H. K.; Wilson, L. D.; Tabil, L. G. *Ind. Eng. Chem. Res*. 2017, 56 (1), 37–46. Copyright 2017 American Chemical Society.

Relation of Chapter 3 to Overall Objective of this Project

The importance of this research was significant toward developing and understanding the flocculation properties of natural polymer and biomass materials for the removal of dissolved nutrients such as phosphate. This project satisfies the first theme (flocculation efficacy of combined biopolymer-metal salt system towards dissolved phosphate removal from wastewater in single, binary and ternary CF system) of the thesis research. The significance of this work relates to the overall objective of the research project because this research study demonstrated that the biopolymer flocculants are more efficient in a ternary system in removing phosphate in wastewater. The CF process depends on several factors, and it is controlled by charge neutralization and polymer-bridging mechanisms, which supports hypotheses 2 and 5 introduced in Chapter 1.

3.1 Introduction

Phosphorous is a critical contaminant in water bodies and represents a primary environmental concern at elevated levels for many countries globally, mainly when wastewater contains *ca*. 10 mg/L to 20 mg/L of total phosphorus.[1] While phosphate is an essential micronutrient in water, elevated levels lead to the growth of algae in water bodies. Thus, many countries regulate phosphate at threshold levels below 0.05 mg/L to reduce eutrophication.[2,3] The removal of dissolved orthophosphate (P_i) generally involves precipitation, followed by removal from the aqueous phase. Removal of P_i has been studied by various methods such as adsorption[4], bioremediation[5], electro-coagulation[6], membrane processes[7] and chemical precipitation.[8,9]

The use of inorganic salts such as, aluminium sulphate (alum) and ferric chloride to precipitate phosphate have been widely utilized due to their cost effectiveness and ready availability.[10] However, these mineral salts have some disadvantages that include higher dosage, ineffectiveness at lower temperature, pH-dependent performance, excessive sludge production, and potential toxicity to human health.[11] The utility of synthetic polymers as flocculants and/or coagulant aids for the removal of phosphate species in wastewater was reported.[8] Polymer flocculants have advantages over inorganic electrolytes that relate to greater flocculation efficiency, large floc formation with high density, high mechanical strength, and favorable settling properties. Biopolymer flocculants also possess useful properties over a wide pH range and yield reduced amounts of sludge without metal (aluminium) residuals whilst maintaining the alkalinity of water.

By contrast, synthetic polymers are non-biodegradable, relatively expensive and pose potential biological toxicity and mutation.[12] The use of binary and ternary systems has several advantages: cost efficiency, biodegradability, biocompatibility, reduced toxicity, with minimal production of pollutants and side effects.[13]

Chitosan is a linear polysaccharide copolymer that consists of N-acetyl-D-glucosamine and glucosamine units with variable acetylation (*cf.* Figure 3.1a). Alkaline hydrolysis of chitin yields chitosan where its properties relate to the degree of deacetylation of chitin.[14] At slightly acidic pH conditions near or below the pK_a of chitosan, a cationic form exists due to protonation of the amine groups. In turn, favorable electrostatic interactions occur with anionic species such as phosphate and arsenate[15], as evidenced by the use of chitosan as an adsorbent for the removal of contaminants in water treatment.[16] By comparison, there are sparse reports where chitosan is used for the removal of particulate matter and dissolved substances in a homogeneous solution.[17–20] Chitosan has unique properties as a coagulant and/or flocculant due to its pH-dependent charge density, variable molecular weight, along with its chelation and aggregation behavior at pH conditions above its pK_a value.[12] The unique physicochemical properties of chitosan along with biodegradability, biocompatibility, metal chelation and low toxicity favor its utility as a biopolymer flocculant.[13,21] Chitosan has been used for the removal of P_i in wastewater using different techniques or processes besides coagulation and flocculation.[22–27] Teh and Wu have also shown that the amount of sludge produced using chitosan was significantly lesser as compared to alum.[28]

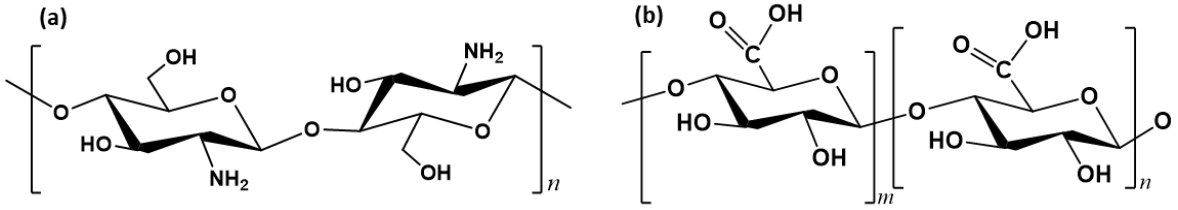

Figure 3.1: Chemical structures of (a) chitosan and (b) alginate, where *m* and *n* denote the degree of polymerization.

Alginate is a natural and linear biopolymer obtained from marine brown algae (seaweed) and capsular polysaccharides found in soil bacteria. Alginate is an anionic block copolymer at pH values above its pK_a (3.5). The alginate biopolymer is composed of β-D-mannuronate (M) and α-L-guluronate (G) units linked by β-1→4 and α-1→4 glycosidic bonds (*cf.* Figure 3.1b).[29] The G

and M monomer units of alginate can be arranged in several forms, hydropolymer G-/M-blocks and heteropolymer GM-blocks. Alginate contains carboxylic acid groups on each monomer unit, where the ability to chelate with reactive polyvalent metal cations contributes to its utility in the treatment of water.[30] Alginate, as a bioflocculant in wastewater treatment, was studied by Wu et al.[31], where it was used as a coagulant aid with aluminium sulphate to test its coagulation and floc properties. Similar studies were carried out using alginate with ferric chloride, alum and titanium tetrachloride by Zhao et al.[31,32] Devrimici et al.[33] used calcium alginate to remove turbidity in water, while Rocher et al.[34] examined the removal of organic dyes by magnetic alginate beads. Vijayaraghavan and Shanthakumar[35,36] studied the utility of alginate as a coagulant for the treatment of dyes in wastewater.

Oat hulls are rich in fibre content relative to wheat and corn bran[37], where the cellulose content of such biomaterials are of interest in wastewater treatment. Oat hull contains polysaccharides composed of D-glucose monomer units with variable linkages, β-1,3- or β-1,4-linkages.[38] Studies by Bernardo et al. have shown that the functional groups of oat hull relate to its utility as a bioflocculant, where the pK_a values cover a suitable range of functional groups; carboxyl (3.6 – 4.1), amines (6.6 – 7.2) and the hydroxyl groups (9.1 – 12.6)].[39] The -COOH and -OH groups reveal that cellulose, hemi-cellulose, pectin and lignin fractions coexist in oat hull biomass.[39] Up to the present time, oat hulls have not been reported as effective flocculant aids for the removal of contaminants in wastewater. A recent study on the application of oat hulls as a flocculant relates to grafted oatmeal.[40] Other studies have employed oat hulls as adsorbent biomass for the removal of chromium ions[39,41] and arsenic (V) species.[40] Herein, oat hulls are examined for use as an additive to aid the coagulation-flocculation process for the removal of phosphate species in water.

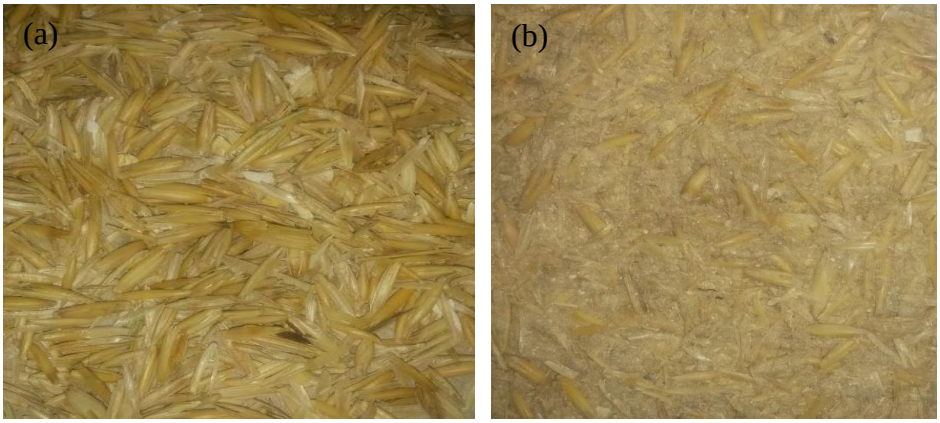

Figure 3.2: Optical images of (a) refined and (b) unrefined oat hull biomass.

The objective of this study is to report on the removal efficacy of dissolved orthophosphate from simulated wastewater using mixtures containing the coagulant (alum) and biopolymer flocculants (alginate and chitosan), and a biomass additive (oat hull). Various single and multicomponent systems were compared: *i*) single (alum, chitosan or alginate), *ii*) binary (alum + chitosan or alum + alginate), and iii) ternary (alum + alginate + chitosan) coagulant-flocculant systems to evaluate the P_i removal properties and the role of synergistic effects. This study contributes to the field of biomaterials in several ways through the use of alum/chitosan/alginate ternary systems for the removal of phosphate over the removal efficacy of single and binary systems, as evidenced by variable P_i removal at variable concentration and pH conditions.

3.2 Materials and experimental procedures

3.2.1 Materials and chemicals

All chemicals were of analytical reagent (AR) grade. Hydrated ferric chloride ($FeCl_3 \cdot 6H_2O$), anhydrous monobasic potassium phosphate (KH_2PO_4), NaOH (aq), HCl (aq), vanadate molybdate reagent (aq), medium viscosity sodium alginate, chitosan (medium molecular weight, 85% deacetylation) and aluminium sulphate (alum) were purchased from Sigma-Aldrich, Oakville, Ontario, Canada. Oat hulls (unrefined), a by-product of oat processing was procured from Richardson Milling Ltd., Martensville, SK, Canada. The oat hulls were cleaned using a sieving machine and an aspirator to remove other parts of the oat grain to yield refined oat hulls. Refined and unrefined oat hulls (*cf.* Figure 3.2) were ground using a knife mill (Retsch GmbH 5657 HAAN, Germany) fitted with a 2.7 mm sieve.

3.2.2 Analytical method

Phosphate, alum and alginate stock solutions were prepared by dissolving their respective salts in ultrapure water (18.2 MΩ·cm at 25 °C). A standard chitosan solution was prepared with 0.01 M HCl solution. A phosphate calibration curve was obtained using a vanadate molybdate colorimetric method (λ = 420 nm) using a double beam UV–Vis CARY-100 spectrophotometer at pH 6.5[42], as shown in Figure A9.2 (Appendix A). Details of the analytical determination of phosphate using colorimetry have been discussed in Section A9.2.2 in Appendix A. The coagulation-flocculation experiments were performed using a conventional jar test apparatus with a six-plate (6 × 2000 ml) jar system with stirrers (Phipps & Bird; Richmond, VA., USA). Single, binary and ternary systems were studied. Initially, P_i solutions were added to the various jars of the setup with a volume of

1.0 L. 5.0 ml of the phosphate solution was sampled and prepared for UV-Visible analysis by adding 1.0 ml of vanadate molybdate reagent. After the addition of the reagent to the P_i-containing sample, the yellow color was allowed to develop for 20 min before the UV-Vis measurements. The pH of the P_i solution (*ca* 25 mg/L) was adjusted using 0.1 M NaOH or 0.1 M HCl to the desired value. For the single systems, the coagulant (or coagulant aid) was added to the P_i solution followed by rapid stirring for 3 min, followed by continuous slow mixing for 20 min. For the binary systems, the alum was added to the P_i solution with rapid stirring for 3 min, followed by slow stirring for 20 min. The flocculant was added within the first 5 min of the slow mixing. In ternary systems, alum was added to the P_i solution followed by rapid stirring for 3 min, followed by slow stirring for 20 min. The flocculants were added within the first 10 min of the slow mixing step. After the rapid mixing, the solution was allowed to settle for 30 min, where the rapid and slow mixing was 295 rpm and 25 rpm, respectively. After the settling period, 5.0 ml of the solution was sampled from the top region and prepared for UV-Vis analysis. The P_i levels were estimated before and after the coagulation-flocculation process. The solution pH was measured after the 30 min settling period. Figure 3.3 illustrates the sequence of steps used for the study of the CF process.

With reference to the binary system containing oat hulls (unrefined or refined) and alum, a standard dosage was prepared by soaking the finely ground powder, with a particle size of 50 µm, in Millipore water and stirred for 30 min. The coagulation-flocculation process was carried out using the same experimental design, according to Figure 3.3. However, the alginate and/or chitosan flocculants were replaced with the oat hull suspension to afford a binary system, consisting of alum and oat hulls.

All experiments were performed in triplicate, where the average value and the standard deviation are reported. The P_i removal was estimated using equation (3.1).[42]

$$\%\,\mathrm{P}_{r\,removal} = \frac{C_o - C_e}{C_o} \cdot 100\% \tag{3.1}$$

C_o and C_e refer to the P_i concentration before and after the coagulation-flocculation process, respectively. The raw experimental data obtained herein are presented in Tables A9.2 to A9.5 in Appendix A.

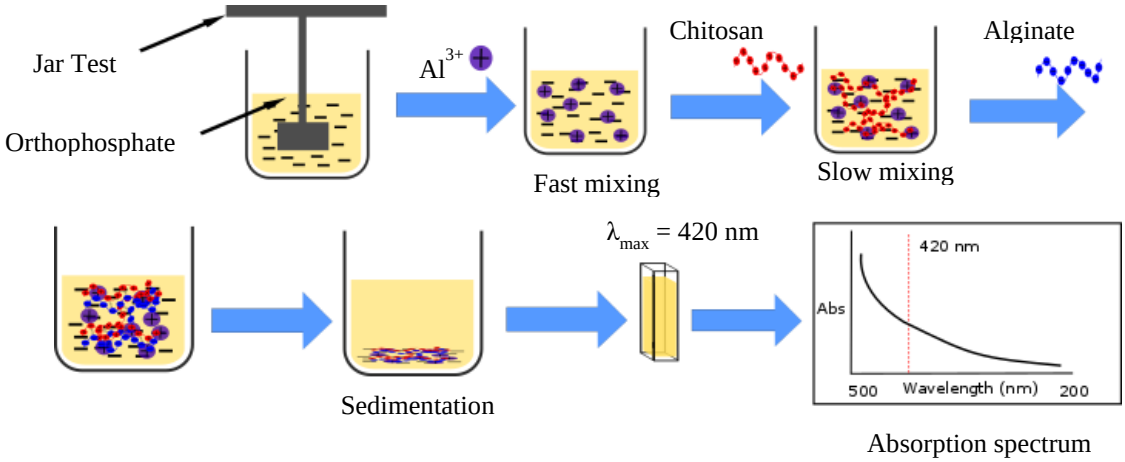

Figure 3.3: Schematic diagram of the step-wise procedure for the coagulation-flocculation process and experimental setup.

Table 3.1: Comparison of the removal of phosphate in water and wastewater using inorganic salts

Wastewater Source	Coagulant / Flocculant	Optimum dosage (mg/L)	Optimum pH	Efficiency (%)	Reference
SW	Alum* + Alg + Chi	35	5.5 - 7.0	85 ± 0.7	This work
SW	Alum	30	5.5 - 7.0	67 ± 0.3	This work
SW	Alum and $CaCl_2$	80, 60	6	85	Mohammed and Shanshool[8]
SW	PACl	6	N/A	94.6	Chen and Luan[43]
AW	Alum and $FeCl_3$	90	7.1	89, 93	Ebeling et al.[44]
SS	Alum	10	5.7 - 5.9	92	Banu et al.[45]
MW	Alum and $FeCl_3$	13	N/A	80	An et al.[46]

* Flocculant dosage was varied while keeping the other constants.
Chi and Alg represent Chitosan and Alginate, respectively.
SW: Synthetic wastewater; MW: Municipal wastewater; AW: Agricultural wastewater.
Optimum pH and optimum dosage are the pH and coagulant/flocculant dosage at which there is maximum P_i removal, respectively.

3.3 Results and discussion

3.3.1 Single-component systems

3.3.1.1 Effect of alum

The results in Figure 3.4 were obtained by singly varying the respective dose of alum, alginate and chitosan to understand their individual effect on the orthophosphate (P_i) removal. The blue curve in Figure 3.4 represents the effect of alum dosage at an initial orthophosphate level of *ca*. 10 mg/L at pH of 5-6. An alum dosage of 5.0 mg/L was able to lower the P_i level by 45%. As the dosage of the alum increased, the efficiency of the P_i removal increased steadily until it reached a maximum level of 67% at 35 mg/L. After this point, the P_i removal decreased to 56% at 50 mg/L, where it remained constant as the alum dosage increased. The decreasing efficiency of P_i removal beyond the optimal dosage was attributed to the stabilization of the P_i solution.[47] As the alum dosage increases, the pH shifts to an unfavorable range for P_i removal, leading to a decrease in the removal efficiency. In Figure 3.4b, the Al/P molar ratios range from 0.5 to 5.0, with optimal P_i removal at a molar ratio of 3.5. This ratio is within the expected range of Al/P molar ratio for effective P_i removal. The pH of the phosphate solution after coagulation-flocculation process was found to be in the alkaline region (8.0 – 9.5) compared to the initial phosphate solutions.

The reaction between alum with P_i in wastewater likely involves complex formation and charge stabilization with no precise flocculation mechanism proposed thus far. $AlPO_4(s)$ is an insoluble product formed when alum combines with P_i, (*cf*. equation (3.2)), in agreement with the report of Jenkins et al.[48] Aluminium phosphate precipitates because the ion association process is thermodynamically and kinetically favored over the formation of aluminium hydroxide species.

$$Al_2(SO_4)_3 \cdot (H_2O)_{14\,(aq)} + 2\ PO_4^{3-}{}_{(aq)} \rightarrow 2\ AlPO_{4(s)} \downarrow + 3\ SO_4^{2-}{}_{(aq)} + 14\ H_2O_{(l)} \qquad (3.2)$$

The optimum dosage of 35 mg/L obtained herein at an initial P_i dose of 10-11 mg/L is lower when compared to values reported in literature (*cf*. Table 3.1). For example, Mohammed and Shanshool[8] reported an optimal dosage of 80 mg/L, while Ebeling et al.[44] reported 90 mg/L for alum while Banu et al.[45] report 80 mg/L for alum at different pH conditions and initial P_i concentrations.

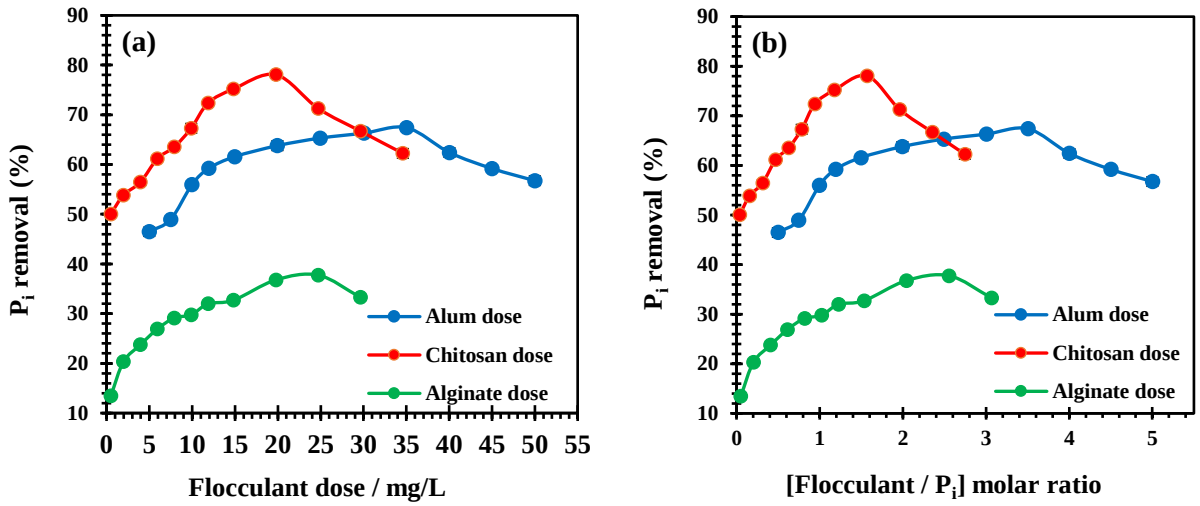

Figure 3.4: Phosphate removal (%) as a function of (a) single coagulant/flocculant dosage and (b) [flocculant / P_i] molar ratio. Initial phosphate concentration is *ca.* 10-11 mg/L.

Table 3.2: Comparison of the removal of phosphate in water and wastewater using biopolymer flocculants

Water Source	Flocculant	Optimum Dosage (mg/L)	Optimum pH	Efficiency (%)	Reference
SW	Chi	20	6.2 - 7.0	78 ± 0.1	This work
SW	Alg	25	5.7 - 7.0	38 ± 0.2	This work
SW	Chi* + Alum	49	5.8 - 7.0	88 ± 0.8	This work
SW	Al* + Alum	59	5.8 - 7.0	80 ± 0.8	This work
SW	Chi* + Alg +Alum	15	5.5 - 7.1	98 ± 0.7	This work
SW	Alg* + Chi +Alum	16	5.5 - 7.2	98 ± 1.2	This work
Struvite	Chi and Alg	10, 20	N/A	80	Latifian et al.[25]
SW	Chi	N/A	7.5 - 7.9	60	Fierro et al.[24]
SW	Chi	N/A	4.0	30	Filipkowska[23]
SW	Polydiallyldimethyl-ammonium chloride	0.5	8.0	59	Chen and Luan[43]
MW	Chi	60	9.5	89	Dunets and Zheng[19]
	Starch	24		86	
	Guar gum	24		82	

* Flocculant dosage was varied while keeping the other constants. Chi and Alg represent chitosan and alginate, respectively. SW: Synthetic wastewater; MW: Municipal wastewater. Optimum pH and optimum dosage are the pH and coagulant/flocculant dosage at which there is maximum P_i removal, respectively.

3.3.1.2 Effect of chitosan

The effect of chitosan dosage on P_i removal is shown in Figure 3.4 (red curve) at initial P_i levels of 10-11 mg/L at pH of 5-6. An increase in chitosan dosage from 0.5 mg/L to 20 mg/L enhanced the removal of P_i from 50% to 78%. Further addition of chitosan led to a decrease in the efficiency of the P_i to 62% at 35 mg/L of chitosan. As the dosage of the chitosan increased beyond the optimum dosage, precipitation of dissolved P_i occurs. However, the excess addition of chitosan resulted in restabilization as positively charged colloidal particles with a corresponding reduction in P_i removal, as shown in Scheme 3.1. An increase in the dosage of the chitosan beyond the optimal dosage limit leads to an increase in the amount of cationic charge in the solution. An appropriate amount of cation species is required to neutralize the P_i anion species. The charge neutralization process relates to the agglomeration of the P_i containing particulates by a bridging mechanism with eventual settling of the floc. However, a reverse effect occurs when excess of cationic species is present in the solution. The excess positive charge stabilizes the neutral P_i containing aggregates and the macroflocs undergo repulsive interactions, resulting in a progressive decrease in the P_i removal efficiency, as shown in Scheme 3.1. Similar results were reported by Roussy et al.[49] as well as Huang and Chen[50]. In Figure 3.4b, the chitosan to P_i mole ratio ranged from 0.04 to 2.74, with optimal P_i removal at 1.57.

In Table 3.2, the results of the present study compare to previous results, where it is noted that the P_i removal herein is greater relative to the solid phase when chitosan is dissolved in bulk solution. Filipkowska et al.[23] obtained 30% removal, while Fierro et al.[24] had 60% P_i removal when chitosan was used as dispersed solid forms. Guibal et al.[51] reported the effectiveness of chitosan for the removal of suspended and dissolved substances when it is used in its dissolved form. This relates to the greater reactivity of the amine groups when chitosan is dissolved in bulk solution. The application of aqueous chitosan improves the accessibility and kinetics of the process relative to the dispersed solid forms of chitosan due to ionization of amine group.[51] Also, dissolved chitosan has more rapid kinetics of mixing (mass transfer effects). Charge neutralization is a key step in the process of coagulation and/or flocculation, followed by polymer bridging, in agreement with results obtained herein, as depicted in Scheme 3.1. Usually, the type of mechanism is governed by the pH, coagulant dose and the type of contaminants.[52] As well, it is known that P_i and other structurally related oxyanions such as, arsenate have favorable affinity to chitosan and its modified forms.[15,26,53]

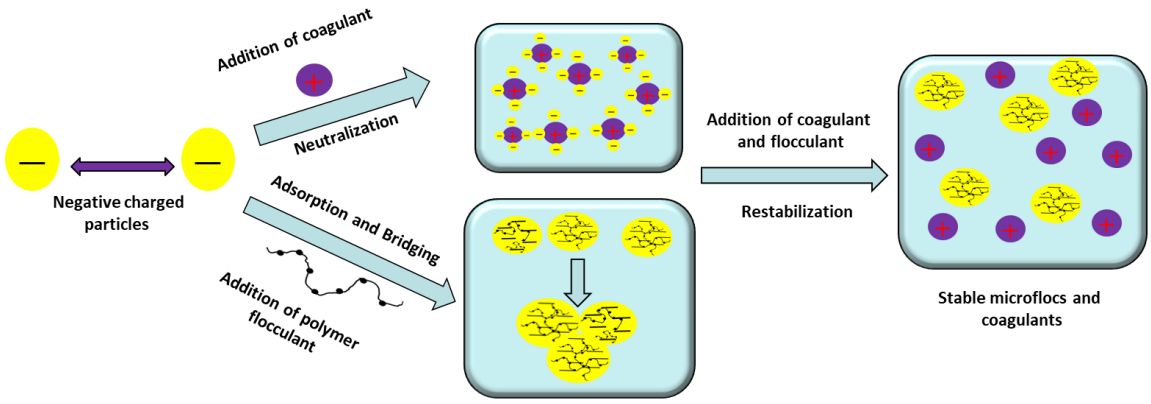

Scheme 3.1: Illustration of the coagulation flocculation mechanism.

3.3.1.3 Effect of alginate

The influence of alginate dose on the removal of P_i is shown in Figure 3.4 (green curve). The use of alginate alone showed poor P_i removal efficiency. For instance, an alginate dose of 0.5 mg/L had a low P_i removal (13%), where it increased gradually up to an optimum dose of 25 mg/L to a higher P_i removal (39%). Alginate is an anionic polyelectrolyte and P_i is also negatively charged at these conditions, resulting in electrostatic repulsions in solution and stabilization of unbound P_i. However, the biopolymer nature of the alginate favors removal of P_i by a bridging and ion binding adsorption mechanism, especially when used in combination with a cationic polyelectrolyte such as chitosan, as illustrated in Scheme 3.1. In Figure 3.4b, the alginate to phosphate molar ratio ranges from 0.04 to 3.07, with optimal P_i removal at a molar ratio of 2.56.

3.3.2 Binary system

The P_i removal efficiency was also studied by combining alum with chitosan or alginate (Figure 3.5). The P_i removal for the alum-chitosan combination (at constant alum dose of 30 mg/L) increased gradually from 68% to 88% at 49 mg/L and then remained stable with a further increase in the chitosan dosage, as depicted by the red curve in Figure 3.5a. Comparing this result to the chitosan data in Figure 3.4, the P_i removal for the binary system is ~10% greater than the single-component system at comparable optimal dosage values. The single-component system had a maximum efficiency of 78% with an optimal dosage of 20 mg/L, where the initial phosphate dose was ~10 mg/L. In Figure 3.5b, the chitosan to P_i mole ratio at a constant alum dose for optimal P_i removal was 2.22. In Figure 3.4b, the chitosan to P_i molar ratio (without alum) for optimal removal

was 3.50. This indicates that the combined use of alum and chitosan has synergistic effects with enhanced P_i removal. For example, Shak and Wu have found that the binary system consisted of alum and seed gum also yielded significant removals of total suspended solids and chemical oxygen demand from the real industrial wastewater.[54]

Similarly, the alum-alginate binary system had an optimum dosage of 59 mg/L with 80% P_i removal. As compared to the single-component system in Figure 3.4, an optimal dosage was obtained using P_i at 25 mg/L with a maximum P_i removal of 39%. This illustrates that the binary system displays greater P_i removal over the single-component system. Alginate possesses excess negative charge in solution, which results in floc stabilization with decreased P_i removal of the alum-alginate binary system. Similar results have been presented for the removal of dyes, turbidity and other substances using alginate together with inorganic salts.[31–33,35,36,55–57]

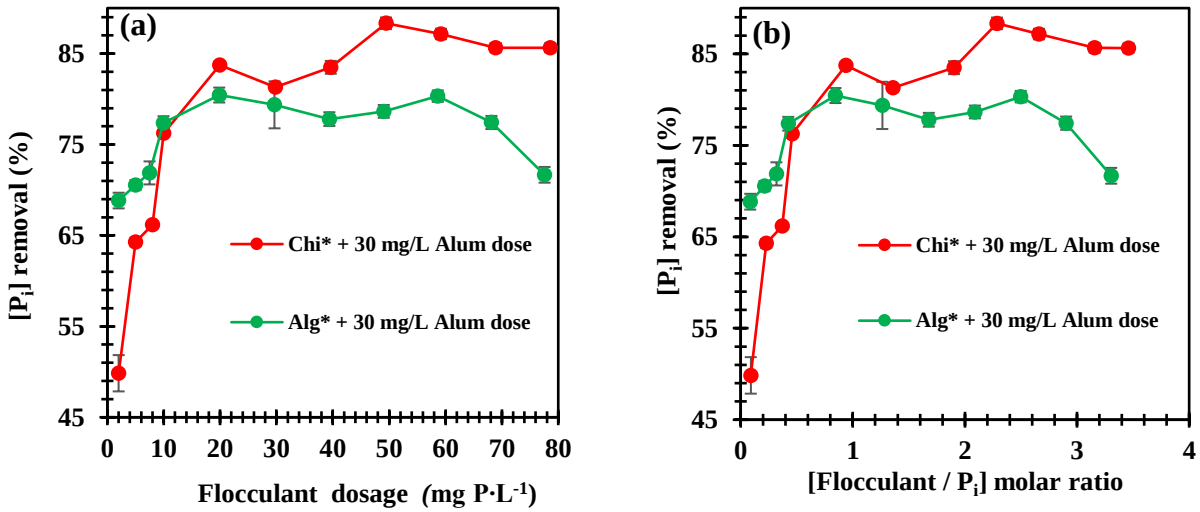

Figure 3.5: Phosphate removal (%) as a function of (a) binary coagulant/flocculant dosage and (b) [Alum / P_i] molar ratio. Flocculant with an asterisk (*) had varied dosage while the concentration of Alum was kept at 30 mg/L. The phosphate dosage was *ca.* 23 mg/L.

3.3.3 Ternary system

The results in Figure 3.6 indicate that the P_i removal occurred using a combination of alginate, alum and chitosan (ternary system). However, two parameters were held constant while varying the other component. For instance, the alum dosage was varied, while the chitosan and alginate dosage was fixed at 10 mg/L. Similarly, the alum (30 mg/L) and alginate (10 mg/L) dosage were fixed, while the chitosan dosage varied. Following the same approach, the dosage of alginate was

varied while the level of alum (30 mg/L) and chitosan (10 mg/L) were fixed. The P_i concentration was kept at 10-11 mg/L throughout the process unless indicated otherwise.

The blue curve in Figure 3.6 represents the effect of alum dosage variation, where a dosage of 2.0 mg/L resulted in a reduction of P_i levels by 62% in the presence of chitosan and alginate. As the dosage of the alum increased, the efficiency of the P_i removal effect rose steadily until it reached a maximum (82%) at 30 mg/L. Beyond this point, the efficiency of P_i removal decreased to 70% at 40 mg/L and remained constant with increasing alum dosage. In Figure 3.6b, the alum to P_i molar ratio was 1.40, while the chitosan and alginate were fixed to achieve optimal P_i removal. The P_i removal was greater for the ternary system over the single and binary systems. The advantage of the addition of organic flocculants is shown by a comparison of the optimum dosage from this study to independent results in Table 3.1. The presence of chitosan and alginate as a coagulant-flocculant system leads to the formation of macroflocs after alum undergoes coagulation with the dissolved P_i to form microflocs.

The effect of chitosan dosage on the P_i removal without pH adjustment at a fixed dosage of alum and alginate is shown in Figure 3.6 (red curve). An increase in chitosan dosage up to 15.8 mg/L increased the P_i removal from 88% to 98.8%. Further addition of chitosan led to a decrease in the P_i removal to 92% at 30 mg/L of chitosan. In Figure 3.6b, the chitosan to P_i molar ratio at a constant alum and alginate dose for optimal P_i removal is 1.40, which is significantly lower than values obtained from the single and binary systems.

The influence of alginate at fixed dosages of alum and chitosan on the removal of P_i in the ternary system is shown in Figure 3.6a (green curve). When alginate is above its pK_a value of 3.6, it interacts favorably with cationic species such as protonated chitosan to form aggregates which result in precipitation of P_i anions.[33] Similar to chitosan, the efficiency of the P_i removal increased with alginate dosage until an optimum dosage is reached at 15.0 mg/L with an efficiency of 98%. Beyond this optimum level, further addition of alginate results in a decrease in the P_i removal level. Similar to chitosan, the alginate to phosphate molar ratio was 1.39, while the alum and chitosan levels were fixed to achieve variable P_i removal. The effect is significantly higher over that obtained for the single component and binary systems. While alginate is an anionic polyelectrolyte, it associates with chitosan via electrostatic cross-linking effects to yield aggregates[58], which facilitate microfloc formation between phosphate and alum. In the absence of chitosan in the solution, further addition of alginate beyond the optimum dosage results in charge stabilization

due to the formation of negatively charged colloidal suspensions, which lowers P_i removal. The ternary system favors efficient P_i removal relative to the binary and single-component systems, as reported in Table 3.3.

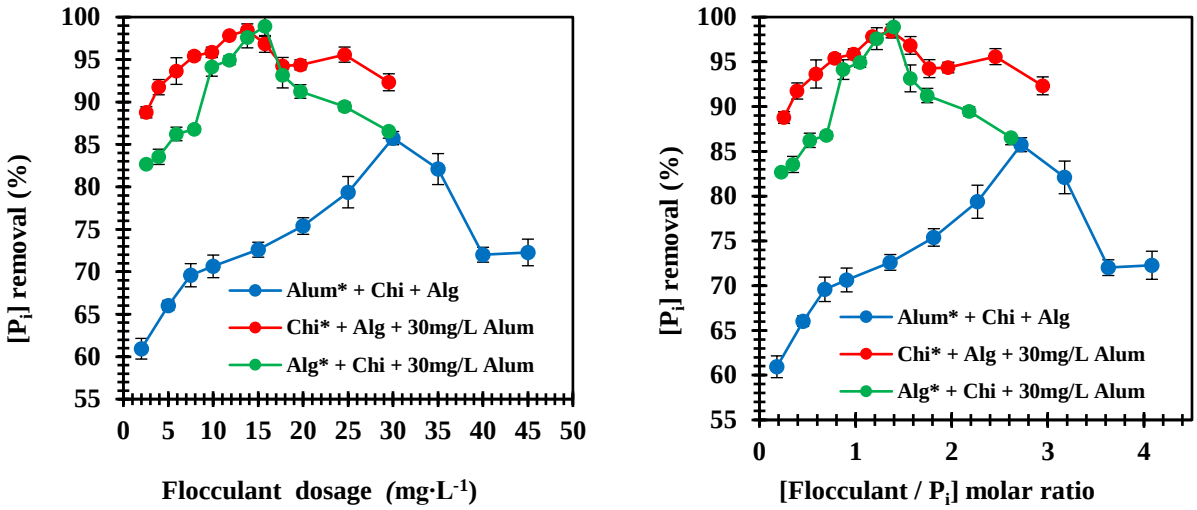

Figure 3.6: Phosphate removal (%) at variable conditions: (a) ternary coagulant/flocculant dosage and (b) [flocculant / P_i] molar ratio. Initial phosphate concentration was *ca.* 10-11 mg/L. Coagulant/Flocculant with an asterisk (*) was varied while the others were kept constant. Chi and Alg are chitosan and alginate, respectively.

Table 3.3: Phosphate removal in water using different flocculant systems

Wastewater Source	Flocculant /Adsorbent	Optimum Dosage (g/L)	[Flocculant / P_i] molar ratio	Efficiency (%)
SW	Alum	35	3.5	67 ± 0.3
SW	Alum* + Alg + Chi	30	2.6	85 ± 0.8
SW	Chi	20	1.6	78 ± 0.1
SW	Alg	25	2.6	38 ± 0.2
SW	Chi* + Alum	49	2.2	88 ± 0.8
SW	Alg* + Alum	59	2.7	80 ± 0.8
SW	Chi* + Alg +Alum	15	1.4	98 ± 0.8
SW	Alg* + Chi + Alum	16	1.4	98 ± 1.2

* Flocculant dosage was varied while keeping the other constants.
Chi and Alg represent Chitosan and Alginate, respectively. SW: Synthetic wastewater

3.3.4 pH effects on phosphate removal

P_i removal in water is highly pH dependent, as shown by the dependence of P_i removal on pH by the additions of 0.1 M NaOH or 0.1 M HCl at different initial dosage levels of P_i in Figure 3.7a. The CF process was performed using the optimized condition of the ternary system: alum (30 mg/L), alginate (15 mg/L), and chitosan (15 mg/L). Alum precipitates phosphate to form $AlPO_4$, while the chitosan and the alginate biopolymers are cationic and anionic species at these conditions. The biopolymers formed cross-linked aggregates which enhance the P_i removal via precipitation of $AlPO_4$, and related adsorption effects. The influence of pH on the P_i removal followed a similar trend independent of the initial P_i dosage level. The efficiency increased from pH 2 and reached optimum removal near pH 6-7. Thereafter, the efficiency decreased as the pH increased to pH 10. As alum is added to the P_i-containing-water, a fraction of the alum was precipitated as the hydroxide species, and H^+ was released according to equation (3.3).

$$Al^{3+}_{(aq)} + 3\ H_2O_{(l)} \rightarrow Al(OH)_{3(s)} \downarrow + 3\ H^+_{(aq)} \qquad (3.3)$$

The Al^{3+} ions are soluble below pH 5.5 and do not precipitate during the dissolution process. In addition, aluminium phosphate ($AlPO_4$) species are formed which are soluble at pH 6 to 7.[59] Above pH 7, the addition of alum forms a soluble complex ($[Al(OH)_4]^-$), where the efficiency of the coagulation-flocculation process is decreased.[60] The solution pH after the addition of the alum is more critical than the initial pH, especially for low alkalinity wastewater.[45] The addition of the alum to low alkalinity water likely results in lower pH, which shifts to an optimum range (pH 6-7), as reported for efficient P_i removal.[61] From the results in Figure 3.7a, P_i removal occurs at lower dosage at an optimum pH (pH 7). Higher P_i levels reveal optimal removal at pH 6-7, and these results are in agreement with other reports.[8,45,62]

P_i removal has a strong dependence on the relative chitosan dosage due to its cationic nature. The amine groups of chitosan are deprotonated at higher pH values, especially at conditions above pH 6.5, since the pK_a value of chitosan is near 6.2. Chitosan does not associate favorably with phosphate via attractive ion-ion interactions at these conditions. By contrast, attractive ion-ion interactions occur below pH 6.2 due to association of chitosan/phosphate (cation/anion) complexes. Excess cationic chitosan species in solution may result in colloidal stabilization at lower pH values.

3.3.5 Effect of initial phosphate dosage

Although pH plays a significant role in P_i removal, the dependence of the initial P_i dosage on the efficacy of the coagulation-flocculation process requires further study. Figure 3.7b depicts the effect of variable P_i dosage on P_i removal at optimal pH conditions. In Figure 3.7b, P_i removal was lower relative to other systems at higher dosage levels when the P_i was fixed at 6.5 mg/L. At low P_i concentration (< 10 mg/L), there is competition due to the formation of hydroxides, which prevents the formation of precipitates since the Al^{3+}/P_i ratio does not favor precipitation at this condition due to the greater K_{sp} value of $Al(OH)_3$ (1.8×10^{-5}) relative to that of $AlPO_4$ (6.3×10^{-19}).[13] However, a greater P_i dosage (10 mg /L - 55 mg/L) indicates there is a minor effect on the efficiency of the coagulation-flocculation process. The P_i removal at variable P_i levels (10 mg/L – 55 mg/L) varies from 96 to 98% at the optimum pH, as shown in Figure 3.7b. A P_i dosage of 16.5 mg/L resulted in the highest P_i removal, where typical P_i levels for contaminated wastewater lie in a similar range (10 to 20 mg/L). Hence, the coagulation-flocculation process is effective for P_i removal in water at relevant levels of P_i found in aquatic and industrial wastewater. With the exception of the lower P_i dosage (< 10 mg/L), it can be concluded that an increase in the P_i concentration does not affect the level of P_i removal. Hence, highly contaminated wastewater laden with P_i above reported literature values could be effectively treated using the conditions reported above.

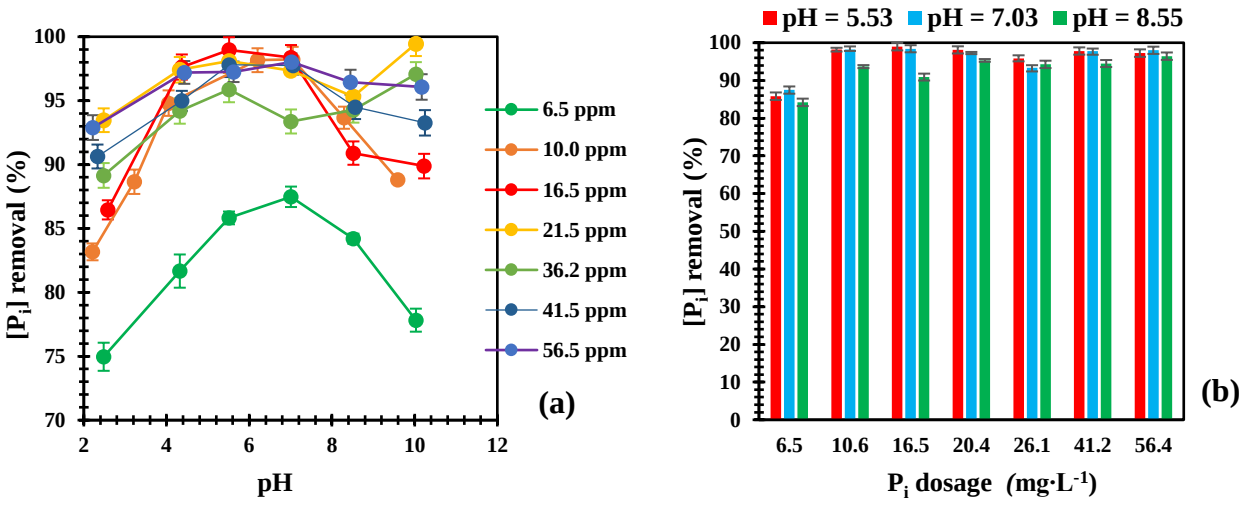

Figure 3.7: (a) Effect of pH on P_i (%) in wastewater. The effects of the initial levels of phosphate (ppm) in wastewater on its removal efficiency systems. (b) Effect of phosphate dosage on the P_i (%) in a coagulation-flocculation experiment at variable pH values.

3.3.6 Oat hulls as coagulant aids

Herein, oat hull suspensions were studied in combination with alum, where the role of oat hulls as a coagulant aid for removal of dissolved P_i in water was evaluated. The efficiency of the oat hulls (refined and unrefined) single-component and alum-oat hull binary systems for the removal of P_i using coagulation-flocculation process is presented in Figure 3.8(a & b), at an initial P_i dosage of 25 mg/L. The combinatorial effect of the alum-oat hull binary systems is significantly more efficient in the removal of the P_i than the use of the single component oat hull for the same effect, as observed in Figure 3.8(a & b). Flocculation process was observed to be more effective for the refined oat hull than the unrefined sample in both cases. For the binary systems, as the oat hull dosage reached 0.93 g/L, the P_i removal was 83% (refined oat hull) and 77% (unrefined oat hulls) at an initial P_i dosage of 25 mg/L. Refined oat hulls showed greater P_i removal that increased to 95% at 1.5 g/L with decreased P_i removal to 92% at 1.6 g/L. Thereafter, it grew steadily to 98% at 1.9 g/L and remained constant (95%) up to 2.4 g/L. By comparison, the P_i removal for the unrefined oat hull increased sharply to 92% at 1.8 g/L and decreased to 85% at 1.9 g/L. Thereafter, it increased slightly to 89% at 2.1 g/L and remained constant thereafter.

The effect of the oat hull on P_i removal relative to the coagulant (alum) was determined, as shown in Figure 3.8c. Accordingly, oat hulls may serve as an effective flocculant aid. In Figure 3.8c, it is evident that the flocculation efficacy for the refined oat hulls increased from 56% at 0.93 g/L compared with 63% at 1.5 g/L for an initial P_i level of 25 mg/L. P_i removal remained nearly constant (63%) up to 2.4 g/L. In the case of the unrefined oat hulls, the P_i removal increased from 48% to 0.93 g/L to 61% at 1.7g/L and remained constant up to 2.4 g/L when the initial P_i level was 25 mg/L. Comparing these results with those reported for other biomass materials in Table 3.4 reveals the utility of oat hulls as suitable coagulant aids for P_i removal in water.

The removal mechanism for the flocculation of P_i with oat hulls may relate to enhanced polymer bridging and/or adsorption processes, as illustrated in Scheme 3.1, along with synergistic effects. Polymer bridging involves the nucleation of micro- to macro-flocs due to the coagulation of alum upon the addition of oat hulls. In this process, the electrolyte species are bound to domains which can associate with other particles.[63] The mechanism is favored, and optimal results are obtained when long-chain polymers or biomass materials without a high level of ionic charge are used.[64] Here, the cellulose and the hemicellulose fractions of the oat hull are uncharged at these pH conditions which may favor the formation of flocs with other species by polymer-bridging effects.

The flocs formed after the coagulation process depends on the metal salt dose, where the floc size increases the interaction between polyelectrolytes of opposite charge.[65] Bridging takes place when the adsorbed chains interact favorably with domains of another floc in a uniform manner, as depicted in Scheme 3.1. In this process, Coulombic and dispersion forces cause the biomass (oat hull) biopolymers to co-adsorb onto two or more flocs. This occurs when the surface is partly covered, during the initial stages of the process, when the polymer dosage is low. The effect occurs immediately upon addition of the biomass and depends on the mixing conditions.[66]

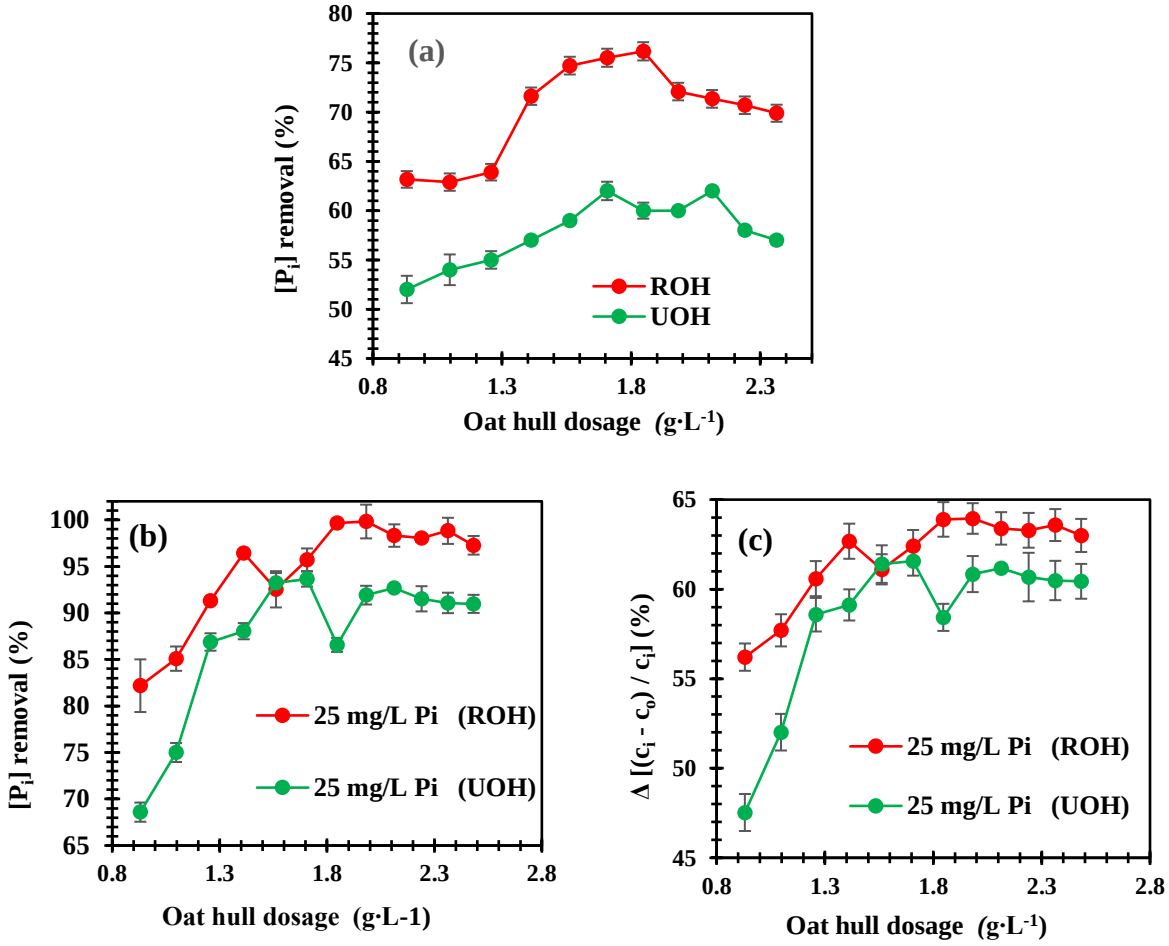

Figure 3.8: (a) P_i removal (%) in water as a function of only oat hull flocculant. (b) P_i removal (%) in water as a function of alum-oat hull flocculant system (c) The change of P_i removal (%) in water as a function of oat hull dosage. UOH is the unrefined oat hull and ROH is the refined oat hull. Alum dosage was kept at 30 mg/L and the initial P_i dosage was 25.0 mg/L in (b) and (c).

Table 3.4: Efficiency of P_i removal using different biopolymer materials

Wastewater Source	Flocculant /Adsorbent	Optimum Dosage (g/L)	[P_i] (mg/L)	Efficiency (%)	Reference
SW	Unrefined oat hull	1.7	25	62 ± 0.9	This work
SW	Refined oat hull	1.8	25	76 ± 1	This work
SW	Unrefined oat hull + alum	1.8	25	93 ± 1	This work
SW	Refined oat hull + alum	1.8	25	99 ± 2	This work
SW	Fly ash and bottom ash	3.4 & 9.1	20	97	Barbosa et al.[67]
SW	Fly ash and bottom ash	34.5 & 46.6	20	90	Barbosa et al.[67]
SW	$La(OH)_3$ modified pine needles	0.7	10	65	Wang et al.[68]
SW	Wheat straw biochars	6.0	3 - 11	88	Li et al.[69]
SW	Carbon residue	5.0	25	25	Kilpimaa et al.[70]
SW	Sugarcane bagasse	16.0	50	11	Hena et al.[71]

SW: Synthetic wastewater

3.4 Conclusions

Coagulation-flocculation of orthophosphate (P_i) using alum in conjunction with biopolymers (chitosan and alginate), along with oat hull biomass are reported in this study. The efficiency of the P_i removal was related to the dosage of the coagulant-flocculant system. Variable alum dosing in the alum-chitosan-alginate ternary system revealed an optimum alum dosage of 30 mg/L when the initial P_i level was 10-11 mg/L. P_i removal was more effective for the ternary system relative to the binary and single-component systems. The binary system (alum/alginate or alum/chitosan) had a lower P_i removal (80% and 88%) relative to the ternary systems (98%). The presence of flocculants and the smaller value of alum to phosphate molar ratios (Table 3.3) indicate that the P_i removal depends on pH, with an optimum value at pH 6–7, in agreement with a process that occurs by charge neutralization and polymer-bridging, as shown in Scheme 3.1. The initial level of P_i was found to be relatively independent of the P_i removal efficacy. Refined and unrefined oat hulls aid the flocculation process by further removal of dissolved P_i. Variable P_i removal occurs for the refined (99%) and unrefined (93%) oat hulls at an initial P_i dosage of 25 mg/L in the binary systems. By considering other properties of alginate and chitosan such as sorption and chelation of metal ions, biocompatibility, biodegradability, non-toxic nature and antimicrobial activity, the

use of such biopolymers can enhance P_i removal. The availability and abundance of oat hull biomass reveal its utility for wastewater treatment, as evidenced by lowered cost and enhanced pollutant removal when used in conjunction with conventional flocculation-coagulation processes.

3.5 References

(1) Rybicki, S. *Phosphorus Removal From Wastewater - A Literature Review*; 1997.

(2) Benyoucef, S.; Amrani, M. *Desalination* **2011**, *275* (1–3), 231.

(3) Painting, S. J.; Devlin, M. J.; Malcolm, S. J.; Parker, E. R.; Mills, D. K.; Mills, C.; Tett, P.; Wither, a.; Burt, J.; Jones, R.; Winpenny, K. *Mar. Pollut. Bull.* **2007**, *55* (1–6), 74.

(4) Sø, H. U.; Postma, D.; Jakobsen, R.; Larsen, F. *Geochim. Cosmochim. Acta* **2011**, *75* (10), 2911.

(5) Gautam, R. K.; Banerjee, S.; Gautam, P. K.; Chattopadhyaya, M. C. *Adv. Environ. Res.* **2014**, *36*, 1.

(6) Bektaş, N.; Akbulut, H.; Inan, H.; Dimoglo, A. *J. Hazard. Mater.* **2004**, *106* (2–3), 101.

(7) Peleka, E. N.; Mavros, P. P.; Zamboulis, D.; Matis, K. A. *Desalination* **2006**, *198* (1–3), 198.

(8) Mohammed, S. A. M.; Shanshool, H. A. *Iraqi J. Chem. Pet. Eng.* **2009**, *10* (2), 35.

(9) Sowmya, A.; Meenakshi, S. *Desalin. Water Treat.* **2014**, *52* (13–15), 2583.

(10) Teh, C. Y.; Budiman, P. M.; Shak, K. P. Y.; Wu, T. Y. *Ind. Eng. Chem. Res.* **2016**, *55* (16), 4363.

(11) Tzoupanos, N. D.; Zouboulis, A. I. *6th IASME/WSEAS Int. Conf. HEAT Transf. Therm. Eng. Environ.* **2008**, 309.

(12) Renault, F.; Sancey, B.; Badot, P. M.; Crini, G. *Eur. Polym. J.* **2009**, *45* (5), 1337.

(13) Bratby, J. Coagulation and Flocculation with an Emphasis on Water and Wastewater Treatment; *Uplands Press Ltd.*, **1980**, 55.

(14) Zemmouri, H.; Drouiche, M.; Sayeh, A.; Lounici, H.; Mameri, N. *Energy Procedia* **2013**, *36*, 558.

(15) Pratt, D. Y.; Wilson, L. D.; Kozinski, J. A. *J. Colloid Interface Sci.* **2013**, *395*, 205.

(16) Varma, A. .; Deshpande, S. .; Kennedy, J. . *Carbohydr. Polym.* **2004**, *55* (1), 77.

(17) Divakaran, R.; Pillai, V. N. S. *J. Appl. Phycol.* **2002**, *14* (5), 419.

(18) Bratskaya, S. Y.; Avramenko, V. A.; Sukhoverkhov, S. V.; Schwarz, S. *Colloid J.* **2002**, *64*

(6), 681.

(19) Dunets, C. S.; Zheng, Y. *Hortscience* **2015**, *50* (6), 921.

(20) Fortin–Chevalier, T.; Leduc, R. *Int. J. Environ. Waste Manag.* **2014**, *14* (4), 358.

(21) Crini, G.; Badot, P.-M. *Prog. Polym. Sci.* **2008**, *33* (4), 399.

(22) Aguilar-May, B.; Del Pilar Sánchez-Saavedra, M. *J. Appl. Phycol.* **2009**, *21* (3), 353.

(23) Filipkowska, U.; Jóźwiak, T.; Szymczyk, P. *Prog. Chem. Appl. Chitin its Deriv.* **2014**, *19* (1), 5.

(24) Fierro, S.; del Pilar Sánchez-Saavedra, M.; Copalcúa, C. *Bioresour. Technol.* **2008**, *99* (5), 1274.

(25) Latifian, M.; Liu, J.; Mattiasson, B. *Environ. Technol.* **2014**, *35* (18), 2289.

(26) Mahaninia, M. H.; Wilson, L. D. *J. Appl. Polym. Sci.* **2016**, *133* (5), 1.

(27) Mohamed, M. H.; Wilson, L. D. *Adsorption* **2016**, *22*, 1025.

(28) Teh, C. Y.; Wu, T. Y. *Chem. Eng. Trans.* **2014**, *39*, 1603.

(29) Lee, K. Y.; Mooney, D. J. *Prog. Polym. Sci.* **2012**, *37* (1), 106.

(30) Kim, S.-K. *Marine Carbohydrates: Fundamentals and Applications, Part 2*; Elsevier Science, 2014; Vol. 73.

(31) Wu, C.; Wang, Y.; Gao, B.; Zhao, Y.; Yue, Q. *Sep. Purif. Technol.* **2012**, *95*, 180.

(32) Zhao, Y. X.; Wang, Y.; Gao, B. Y.; Shon, H. K.; Kim, J.-H.; Yue, Q. Y. *Desalination* **2012**, *299*, 79.

(33) Devrimci, H. A.; Yuksel, a. M.; Sanin, F. D. *Desalination* **2012**, *299*, 16.

(34) Rocher, V.; Bee, A.; Siaugue, J.-M.; Cabuil, V. *J. Hazard. Mater.* **2010**, *178* (1–3), 434.

(35) Vijayaraghavan, G.; Shanthakumar, S. *Environ. Prog. Sustain. Energy* **2015**, *34* (5), 1427.

(36) Vijayaraghavan, G.; Shanthakumar, S. *Desalin. Water Treat.* **2015**, *3994*, 1.

(37) Galdeano, M. C.; Grossmann, M. V. E. *Ciênc. Tecnol. Aliment. Campinas* **2006**, *26* (1), 123.

(38) Bharti, S.; Mishra, S.; Sen, G. *Carbohydr. Polym.* **2013**, *93* (2), 528.

(39) Bernardo, G. R. R.; Rene, R. M. J.; Alfaro-De la, A. D. la T. *J. Hazard. Mater.* **2009**, *170* (2–3), 845.

(40) Chuang, C. L.; Fan, M.; Xu, M.; Brown, R. C.; Sung, S.; Saha, B.; Huang, C. P. *Chemosphere* **2005**, *61* (4), 478.

(41) Gardea-Torresdey, J. L.; Tiemann, K. J.; Armendariz, V.; Bess-Oberto, L.; Chianelli, R. R.; Rios, J.; Parsons, J. G.; Gamez, G. *J. Hazard. Mater.* **2000**, *80* (1–3), 175.

(42) Patel, H.; Vashi, R. T. *J. Saudi Chem. Soc.* **2012**, *16* (2), 131.

(43) Chen, J.; Luan, Z. *Fresenius Environ. Bull.* **2010**, *19* (10), 2200.

(44) Ebeling, J. M.; Sibrell, P. L.; Ogden, S. R.; Summerfelt, S. T. *Aquac. Eng.* **2003**, *29* (1–2), 23.

(45) Banu, R. J.; Do, K. U.; Yeom, I. T. *Int. J. Environ. Sci. Technol.* **2007**, *5* (1), 93.

(46) An, J.-S.; Back, Y.-J.; Kim, K.-C.; Cha, R.; Jeong, T.-Y.; Chung, H.-K. *Environ. Technol.* **2014**, *35* (13–16), 1668.

(47) Ahmad, A. L.; Sumathi, S.; Hameed, B. H. *Chem. Eng. J.* **2006**, *118* (1–2), 99.

(48) Jenkins, D.; Ferguson, J.; Menar, A. *Water Res.* **1971**, *5*, 369.

(49) Roussy, J.; Van Vooren, M.; Guibal, E. *J. Dispers. Sci. Technol.* **2005**, *25* (5), 663.

(50) Huang, C.; Chen, Y. *J. Chem. Technol. Biotechnol.* **1996**, *66* (3), 227.

(51) Guibal, E.; Van Vooren, M.; Dempsey, B. a.; Roussy, J. *Sep. Sci. Technol.* **2006**, *41* (11), 2487.

(52) Huang, C. *Water Res.* **2000**, *34* (3), 1057.

(53) Poon, L.; Younus, S.; Wilson, L. D. *J. Colloid Interface Sci.* **2014**, *420*, 136.

(54) Shak, K. P. Y.; Wu, T. Y. *Ind. Crops Prod.* **2015**, *76*, 1169.

(55) Vijayaraghavan, G.; Shanthakumar, S.; Division, E. E.; Sciences, B. In *International Conference on Recent Advancement in Chemical Environmental & Energy Engineering*; 2014; pp 1–5.

(56) Zhao, Y. X.; Gao, B. Y.; Wang, Y.; Shon, H. K.; Bo, X. W.; Yue, Q. Y. *Chem. Eng. J.* **2012**, *183*, 387.

(57) Zhao, Y. X.; Gao, B. Y.; Shon, H. K.; Wang, Y.; Kim, J. H.; Yue, Q. Y.; Bo, X. W. *Bioresour. Technol.* **2012**, *108* (0), 45.

(58) Xue, C.; Wilson, L. D. *Carbohydr. Polym.* **2015**, *132*, 369.

(59) Sedlak, R. I. *Phosphorus and nitrogen removal from municipal wastewater*, Second.; Lewis Publishers: New York, USA, 1991.

(60) Teh, C. Y.; Wu, T. Y.; Juan, J. C. *Ind. Crops Prod.* **2014**, *56*, 17.

(61) Lević, L.; Gyura, J.; Djurić, M.; Kuljanin, T. *Eur. Food Res. Technol.* **2005**, *220* (1), 70.

(62) Kurita, K. *Mar. Biotechnol.* **2006**, *8*, 203.

(63) Lee, C. S.; Robinson, J.; Chong, M. F. *Process Saf. Environ. Prot.* **2014**, *92* (6), 489.

(64) Razali, M. A. A.; Ahmad, Z.; Ahmad, M. S. B.; Ariffin, A. *Chem. Eng. J.* **2011**, *166* (2), 529.

(65) Edzwald, J.; Tobiason, J. *Water Sci. Technol.* **1999**, *40* (9), 63.

(66) Hoogeveen, N. G.; Cohen Stuart, M. A.; Fleer, G. J. *Colloids Surfaces A Physicochem. Eng. Asp.* **1996**, *117* (1–2), 77.

(67) Barbosa, R.; Lapa, N.; Lopes, H.; Morujo, A.; Mendes, B. *Water Sci. Technol.* **2013**, *68* (9), 2019.

(68) Wang, X.; Liu, Z.; Liu, J.; Huo, M.; Huo, H. *PLoS One* **2015**, *10* (12), 1.

(69) Li, J.; Lv, G.; Bai, W.; Liu, Q.; Zhang, Y.; Song, J. *Desalin. Water Treat.* **2016**, *57*, 4681.

(70) Kilpimaa, S.; Runtti, H.; Kangas, T.; Lassi, U.; Kuokkanen, T. *Chem. Eng. Res. Des.* **2014**, *92* (10), 1923.

(71) Hena, S.; Atikah, S.; Ahmad, H. *Int. J. Eng. Sci.* **2015**, *4* (1), 51.

CHAPTER 4

4 Flocculation optimization of orthophosphate with $FeCl_3$ and alginate using the Box-Behnken response surface methodology[2]

Description

In this research, coagulation-flocculation (CF) optimization was performed using the Box-Behnken experimental design and response surface methodology (BBD-RSM) on a binary system consisting of alginate and ferric chloride ($FeCl_3$) for the removal of orthophosphate (P_i). $FeCl_3$ was chosen over alum due to the health concerns associated with the use of aluminium in wastewater and water treatment. Several factors affecting the CF process were optimized and their individual and interactive effects on P_i removal were investigated. Optimal CF conditions were obtained, which showed comparable results for both experimental and predicted values of P_i removal. The alginate-$FeCl_3$ binary system also displayed maximum adsorption towards P_i in accordance with the flocculation kinetics and adsorption results.

Author's contribution

Lee D. Wilson and I conceived the project. I performed all the experimental work, data processing and analysis, and wrote the first draft of the manuscript as well as making further revisions where and when necessary on subsequent drafts. Dr. L.D. Wilson was responsible for the supervision of the project, editorial guidance for revision of the manuscript drafts, and corresponding author. Permission was obtained from all contributing authors before the inclusion of the manuscript in this thesis.

Relation of Chapter 4 to Overall Objective of this Project

This research builds upon the demonstrated utility of native biopolymer flocculants combined with metal ion coagulant in a binary system for improved removal of phosphate. It relates to the overall objective of this thesis per the first theme (flocculation efficacy of combined biopolymer-metal salt system towards dissolved phosphate removal in wastewater in single, binary and ternary

[2] Reproduced in part with permission from Agbovi, H. K.; Wilson, L. D. *Ind. Eng. Chem. Res*. 2017, 56 (12), 3145–3155. Copyright 2017 American Chemical Society.

CF system). Herein, CF optimization study was performed on $FeCl_3$-alginate binary system using the BBD-RSM for the removal of orthophosphate, P_i. The BBD-RSM was employed to provide an empirical relationship between the response function (P_i) and the independent variables (CF factors). The validity of the predicted response function was confirmed by experimental data, which showed comparable results. This study relates to the first theme and supports hypotheses 2, 4 and 6, discussed in Chapter 1.

4.1 Introduction

Phosphorus is an essential plant nutrient for growth and development, where it exists in aquatic systems as orthophosphate, polyphosphate or organophosphate. Major sources of phosphate in water and wastewater originate from human, domestic and industrial waste, as well as fertilizer effluent run-off from agricultural activities.[1] Municipal wastewater may contain *ca*. 10 mg/L to 20 mg/L of total phosphorus.[2] Although phosphate is an essential micronutrient in water, elevated levels lead to eutrophication and excessive algae growth in water.[3] To address eutrophication, phosphorus effluent is regulated to levels below 0.05 mg/L.[4] In Ontario, Canada, a total phosphate limit of 0.1 mg/L is usually imposed on industry (e.g., fertilizer, detergent, municipal and institutional sewage treatment processing) discharge to surface water to prevent damage to aquatic ecosystems.[5] Thus, water treatment technology is required to reduce phosphate in municipal and industrial wastewater effluent drastically. The removal of orthophosphate (P_i) in wastewater has been examined by different methods: adsorption[6–9], biological removal[10,11], electro-coagulation[12], membrane processes[13] and chemical precipitation.[14,15]

Among these various methods, coagulation-flocculation has attracted attention for primary and secondary water treatment due to its efficiency, simplicity and relatively low cost.[16] Conventional CF process involves addition of commercially available coagulants and/or flocculants such as alum, lime, ferric chloride or ferric sulphate to the wastewater to precipitate the contaminants. The solid by-products from the process are then removed by sedimentation and/or filtration.[17] Among the inorganic coagulants, ferric chloride has a widespread application over alum because of its effectiveness in contaminant removal from water. Addition of ferric chloride to water results in a hydrolysis reaction to form iron (III) hydroxide precipitates. The iron (III) hydroxide solid particles have a high affinity towards many contaminants in wastewater, such as phosphate, arsenic and sulphide species. Hsu[18] has shown that Fe^{3+} has a stronger affinity for precipitating PO_4^{3-} and a

stronger hydrolyzing power than Al^{3+}. In contrast with aluminium-based coagulants such as alum, ferric chloride has no significant adverse health effects in wastewater treatment.[19]

Inorganic salts are widely used to precipitate phosphate due to their cost effectiveness and readily availability. However, mineral salts pose several disadvantages, such as large dosage requirements, ineffectiveness at lower temperatures, pH dependent performance, sludge production and human health concerns.[20] Even though the inorganic coagulants have several disadvantages as coagulants, studies have shown that when they are used as coagulants together with other polymeric flocculants or coagulant aids, the disadvantages can be offset or eliminated. A smaller dosage of the inorganic coagulants is realized in the case of binary or ternary coagulant-flocculant systems. In addition, the inorganic coagulants can function synergistically with the biopolymer materials, which contribute to reduced sludge volume and greater mechanical stability of the sludge by-products from the flocculation process.[21–25] The use of synthetic polymer flocculants and/or coagulant aids, such as polyacrylamide, poly(diallyldimethyl) ammonium chloride and poly(styrene) derivatives for the removal of contaminants in wastewater are known.[15] Polymer flocculants have advantages over the use of inorganic salts that include greater contaminant removal efficiency, ability to form large flocs with high density, higher mechanical strength, and favorable settling properties, as discussed in Chapter 3. Polymers possess useful properties over a wide pH range and yield less sludge without metal residuals whilst maintaining the alkalinity of water. By contrast, synthetic polymers are non-biodegradable, relative higher cost, and pose potential biological toxicity.[26] The development of coagulant aid and biopolymer flocculants in binary systems have several advantages such as being cost effective, biodegradability, biocompatibility, reduced toxicity, with minimal production of pollutants.[27] The application of biopolymer flocculants such as alginate, chitosan, cellulose and biomass materials offer benefits to water treatment based on their renewable nature, biodegradability, innocuous waste production, and tunable efficiency.[26]

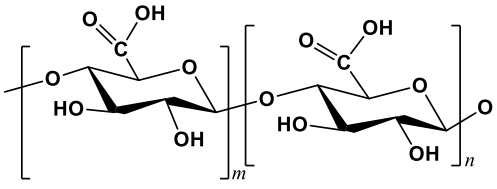

Figure 4.1: Chemical structure of alginate, where *m* and *n* denote the degree of polymerization.

Alginate has significant potential as a coagulant aid for wastewater treatment. It is a linear biopolymer obtained from marine brown algae (seaweed) and capsular polysaccharides typically found in soil bacteria.[28] Alginate is an anionic block copolymer above its pK_a value (3.5), that is composed of β-D-mannuronate (M) and α-L-guluronate (G) units linked by β-1→4 and α-1→4 glycosidic bonds, as shown in Figure 4.1.[29] Alginate contains carboxylic acid groups on each monomer unit thus possesses diverse functionality in water treatment such as chelation with reactive polyvalent metal cations.[30] Alginate has been studied as a flocculant in wastewater treatment, where Wu et al. have studied the effect of alginate as a coagulant aid in conjunction with alum.[22] The coagulation performance of alginate with metal salts such as ferric chloride, alum, titanium tetrachloride and polyaluminium chloride was reported by Zhoa et al.[24,25] Devrimic et al.[30] have used calcium alginate to reduce turbidity in water, while alginate was studied for the color removal in textile effluent as a coagulant for dye species.[21] These reports indicate that combined use of alginate and metal ions have synergetic effects on contaminant removal efficacy.

The algal form of alginate is a coagulant aid for wastewater treatment in the removal of phosphate has not been reported in the open literature. This study aims to optimize the coagulation-flocculation potential of alginate in conjunction with ferric chloride for the removal of phosphate along with the Box-Behnken Design (BBD) and the response surface methodology (RSM). The BBD method is an efficient and widely used approach in experimental design.[31] RSM is aimed at the factorial design for determining the optimal operational conditions for a given system to meet regulatory requirements.[32] In addition, binary coagulant-flocculant systems such as alginate with ferric chloride have potential cost reduction advantages due to the reduced dosage, enhancement of the flocculation activity, and potential risk reduction to human health.

4.2 Materials and methods

4.2.1 Materials

All chemicals were of analytical reagent (AR) grade. Hydrated ferric chloride ($FeCl_3 \cdot 6H_2O$), anhydrous monobasic potassium phosphate (KH_2PO_4), NaOH (aq), HCl (aq), vanadate molybdate reagent (aq) and medium viscosity sodium alginate were purchased from Sigma-Aldrich (Oakville, ON. Canada). The coagulation-flocculation experiments were carried out using a six-plate conventional Jar-test apparatus, originally developed by Phipps & Bird with six parallel stirrers.

4.2.2 Coagulation-flocculation experiment

Standard orthophosphate (P_i), ferric chloride and alginate aqueous stock solutions were prepared by dissolving in deionized and distilled water. A calibration curve of P_i was obtained using a vanadate molybdate colorimetric method at a wavelength of 420 nm at pH 6.5.[33] The coagulation-flocculation was performed, based on the experimental design matrix obtained from the BBD and the RSM, using a program-controlled conventional jar test apparatus with six-2 L jars and stirrers. Approximately, 1 L of simulated P_i containing sample was added to the jar tester and 5.0 ml of the P_i solution was sampled and used for UV-Visible analysis by adding 1.0 ml of vanadate molybdate reagent. After addition of the reagent to the P_i sample, a yellow colored complex developed after 20 min before recording the UV-Vis absorbance. The pH of the P_i solution was adjusted using 0.1 M NaOH or 0.1 M HCl to the desired value according to the experimental design. The CF experiment was carried out by adopting the procedure described in Section 3.2.2 in Chapter 3. A pre-determined amount of the coagulant (ferric chloride) was added to the solution, followed by rapid stirring for 3 min at 295 rpm. Thereafter, the stirring rate was reduced to 25 rpm for 20 min. During this period, the alginate (flocculant) was added within the first 5 min. The stirring was then stopped where different settling times (10 – 60 min) were tested. Following the settling time, a 5.0 ml aliquot of the solution was sampled from the top and prepared for UV-Vis analysis for P_i using the colorimetric method discussed above. The pH of all the solutions was measured after the appropriate settling period. The aqueous concentration of P_i before (c_o) and after (c_e) the CF experiment was determined, as described above. The experiments were performed in triplicate, where the average value and the standard deviation are reported. The orthophosphate removal ($P_{i\ removal}$, %) and the removal capacity (P_i; $mg \cdot g^{-1}$) was calculated by equations (4.1) and (4.2), respectively.[33]

$$\%\,P_{i\,removal} = \frac{c_o - c_e}{c_o} x100\% \tag{4.1}$$

$$q_e = \frac{(c_0 - c_e)\,xV}{m} \tag{4.2}$$

Here, c_0 and c_e are the initial and equilibrium concentrations of P_i in solution (mg/L), V is the volume (L) and m is the mass of the $FeCl_3$-alginate flocculant system (g).

Table 4.1: Levels of each variable for the Box-Behnken experimental design

Independent variable	Unit	Symbol	Coded level		
			Low (-1)	Middle (0)	High (+1)
pH		*x*	2	6.1	10
Alginate dose	mg/L	*z*	0.5	7.8	15
Settling time	min	*m*	10	35	60
$FeCl_3$ dose	mg/L	*n*	10	12	15

4.2.3 Box-Behnken experimental design

The traditional method of coagulation-flocculation involves changing one factor at a time and requires many experiments which may be time-consuming, often leading to low optimization efficiency. To address this problem, the design of experiment (DOE) was used to study the effect of the independent variables (CF factors) and their responses using a minimum number of experiments. RSM is a collection of statistical and mathematical methods which are useful for developing, improving, and optimizing processes.[34–36] The selection of an adequate experimental design is a key consideration in experimental optimization. The Box-Behnken Design (BBD) method was employed to obtain the optimum $P_{i,removal}$. The BBD is an independent, rotatable quadratic design with no embedded factorial or fractional factorial points where the variable combinations are at the mid-points of the edges of the variable space and at the center.[37] The BBD requires fewer treatment combinations than the central composite design, especially in cases with three or four factors, and is less expensive to perform. The BBD allows efficient estimation of the first- and second-order coefficients and does not have axial points. Thus, it is certain that all design points fall within a safe operating zone. The BBD approach ensures that not all factors are set at their high levels at the same time. This affords identification of significant effects of interaction for batch studies.[37–40]

Preliminary experiments indicate that important variables affecting $P_{i,removal}$ include ferric chloride dosage, alginate dosage, pH and settling time. These variables were evaluated to optimize $P_{i,removal}$. $FeCl_3$ dosage was varied between 10 mg/L and 15 mg/L, alginate dosage (0.5 mg/L to 15 mg/L), pH (2 to 10), and settling time (10 to 60 min). In Table 4.1, the experimental design had four variables (*x*, *z*, *m*, and *n*) for pH, alginate dosage, settling time and $FeCl_3$ dosage, respectively, each at three levels, coded as -1, 0 and +1, for low, middle and high values, respectively. Twenty-seven experiments were carried out according to the statistical matrices developed by the RSM, in order to account for variability of the independent variables on $P_{i,removal}$. The experimental data

was fit using a non-linear regression method using a second order polynomial to identify significant coefficient terms. The application of RSM provides an empirical relationship between the response function and the independent variables. The quadratic response model is based on all linear terms, square terms, and linear interaction terms, according to equation (4.3).[41]

$$Y = b_{\circ} + \sum b_i x_i + \sum b_{ii} x_{ii}^{\ 2} + \sum b_{ij} x_{ij} \tag{4.3}$$

Here, Y is the predicted response ($P_{i,removal}$ efficiency) b_o is the model constant, b_i is the linear coefficient, b_{ii} is the quadratic effect of the input factor x_{ii}, b_{ij} is the linear interaction effect between the input factors x_i and x_j.

The response function coefficients were determined by regression using the experimental data and the Statgraphics XVII-X64 regression program. The response functions for phosphate removal (%) was approximated by the standard quadratic polynomial equation in equation (4.4). Equation (4.4) describes the regression model of the system, including the interaction terms.[41]

$$\begin{aligned} Y = {} & b_0 + b_1 x + b_2 \mathrm{z} + b_3 \mathrm{m} + b_4 n + b_{11} x^2 + b_{12} xz + b_{13} xm + b_{14} \mathrm{xn} + b_{22} z^2 + b_{23} zm \\ & + b_{23} zn + b_{33} m^2 + b_{34} mn + b_{33} n^2 \end{aligned} \tag{4.4}$$

Y is the predicted response, phosphate removal (%); x, z, m and n are the coded levels of the independent variables: pH, alginate dosage, settling time and $FeCl_3$ dosage, respectively. The regression coefficient, b_0 denotes the intercept term; b_1, b_2, b_3 and b_4 represent the linear coefficients; b_{12}, b_{13}, b_{14}, b_{23}, b_{24}, and b_{34} represent the interaction coefficients and b_{11}, b_{22}, b_{33} and b_{44} denote the quadratic coefficients. Analysis of variance (ANOVA) was employed to perform diagnostic tests on the adequacy of the proposed model. The ANOVA test estimates the suitability of the response functions and the significance of the effects of the independent variables.

4.3 Results and discussion

4.3.1 Box-Behnken analysis

The Box–Behnken Design for statistical analysis and the response surface methodology was employed to investigate the effects of the four independent variables on the response function, and determination of the optimal conditions to maximize P_i removal (%). The independent variables were pH (x), alginate dosage (z), settling time (m) and $FeCl_3$ dosage (n). The experimental design involved four variables (x, z, m, and n), each at three levels, coded as -1, 0 and +1, for low, middle and high values, as shown in Table 4.1 The optimization procedure comprises study of the response of the statistically designed combinations, estimating the coefficients by fitting the experimental

data to the response functions, predicting the response of the fitted model and *goodness-of-fit* of the model.[37,38] The results for the P_i removal efficiency are listed in Table A9.6 in Appendix A. The coefficients of the response function for the dependent variables were determined by correlating the experimental data with the response functions using Statgraphics XVII-X64 regression program. Different response functions and the respective coefficients are described by equation (4.5).

$$Y = -95.4 + 17.2x + 0.260z + 0.611m - 1.53 - 1.53x^2 + 0.172xz - 0.0022xm - 0.329xn - 0.0982z^2 - 0.00317zm + 0.0361zn - 0.0117m^2 + 0.0234mn - 0.8746n^2 \quad (4.5)$$

Statistical testing of the model was performed with the Fisher's statistical test for analysis of variance (ANOVA). The ANOVA test for the P_i removal is presented in Table 4.2. The ANOVA test estimates the suitability of the response functions and the significance of the effects of the independent variables. Student's *t*-test and *p*-values were checked to determine the statistical significance of the BBD-RSM variables and their interactions (combination of two codes or variables) at variable probability values.[42] A large value of F, according to ANOVA test, indicates that most of the variables in the response can be explained by the regression equation, and probability value (*p* values) less than 0.05 are considered to be statistically significant. The ANOVA results indicate that the second order polynomial equation adequately represents the actual relationship between the response function (P_i removal efficiency) and the independent variables ($FeCl_3$ dose, alginate dose, pH and setting time). The F-value model was 250.82, implied the model was significant. Values of *p* less than 0.05 indicated that the model terms were significant, and values greater than 0.05 were considered statistically insignificant.

Figure 4.2 is a Pareto plot that depicts the standardized effect variables based on the *t* values of the independent variables, along with quadratic and interaction effects. The length of each bar in Figure 4.2 represents the standardized effect of that variable on the response function ($P_{i,removal}$), and the alpha level of 0.05 was employed to evaluate the statistical significance.

The selected 1st-order and 2nd-order variables were shown to be statistically insignificant except pH (*x*), x^2, according to the Pareto plot in Figure 4.2 and Table 4.2. Also, for the interactive variables, *xz*, *xn*, and *mn* were found to be insignificant, whereas; *xm*, *zn* and *zm* are statistically significant. The insignificant variables were identified because the Pareto bars for these variables are below the reference line, as shown in Figure 4.2, and their *p* values are relatively high (*p* >

0.05), as listed in Table 4.2. The quadratic term for pH (x^2) is the most significant component of the regression model for the present application. The pH was also identified by the linear terms among the independent variables that had a significant effect on the $P_{i,removal}$ efficiency. Moreover, each bar in the plot represents an absolute standardized effect. Values in grey display positive effects while those in black have negative effects on the response variable.

The *goodness-of-fit* by the regression model was evaluated by coefficients of R^2, adjusted R^2, standard error of estimate and mean absolute error (MAE). The R^2 statistic indicates that the model as fitted explains 99.6% of the variable $P_{i,removal}$ efficiency. The adjusted R^2 statistic (99.2%) is more suitable for comparing models with independent variables. The standard error of estimate shows the standard deviation of the residuals to be 1.42. The MAE was 0.77 and is the average value of the residuals. The accuracy of the regression model was checked by the parity and residual plots in Figure 4.3. Figure 4.3(a) illustrates the plots of the predicted P_i removal (%) versus measured values. Most of the data are distributed near the straight line where the measured and predicted $P_{i,removal}$ are the same and indicates that the regression model is able to predict these values. These plots provide information on the fit criteria contained in the residuals. In Figure 4.3(b), the maximum deviation between the predicted and the measured $P_{i,removal}$ is below 3.0% and reveals a good correlation between the predicted and the measured values.

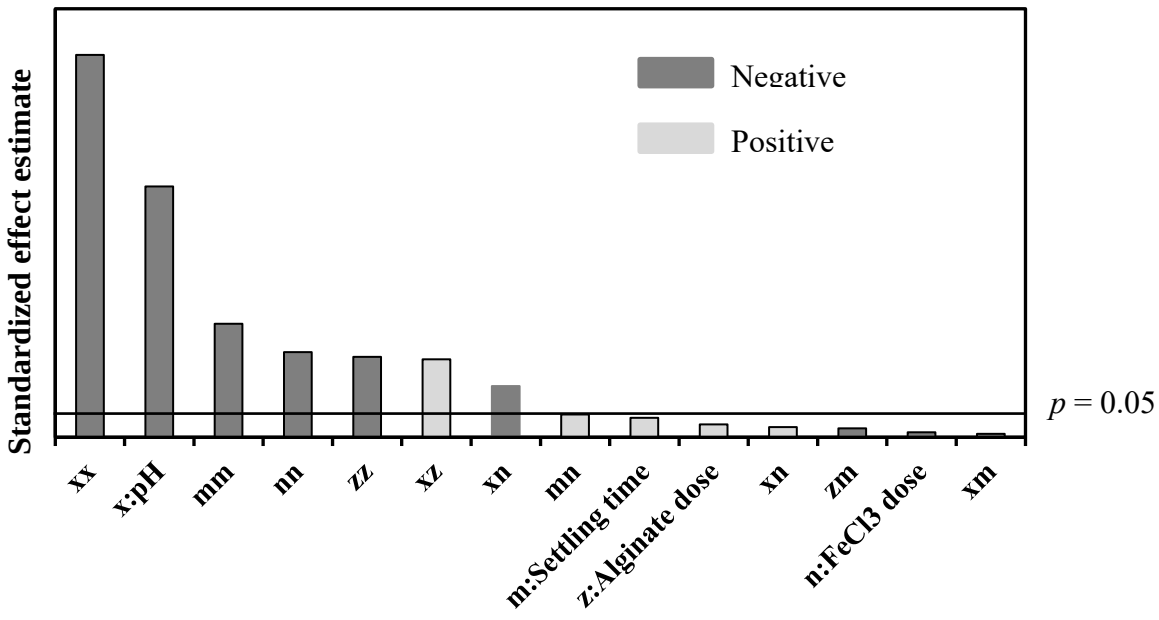

Figure 4.2: Pareto chart showing the standardized effects of variables on phosphate removal efficiency.

Table 4.2: Analysis of variance (ANOVA) results of phosphate removal efficiency as a function of pH, $FeCl_3$ dosage, alginate dosage and settling time

Source	Sum of squares	Degree of freedom	Mean square	*F*-Ratio	*p*-value	Remarks
x	3110	1.0	3110	1540	0.000	Significant
z	8.234	1.0	8.234	4.080	0.066	Insignificant
m	18.78	1.0	18.78	9.300	0.010	Significant
n	1.248	1.0	1.248	0.620	0.447	Insignificant
xx	3212	1.0	3212	1591	0.000	Significant
xz	100.2	1.0	100.2	49.63	0.000	Significant
xm	0.198	1.0	0.198	0.100	0.760	Insignificant
xn	43.23	1.0	43.23	21.41	0.001	Significant
zz	142.1	1.0	142.1	70.40	0.000	Significant
zm	1.323	1.0	1.323	0.660	0.434	Insignificant
zn	1.716	1.0	1.716	0.850	0.375	Insignificant
mm	283.1	1.0	283.1	140.24	0.000	Significant
mn	8.585	1.0	8.585	4.250	0.062	Insignificant
nn	159.4	1.0	159.4	78.93	0.000	Significant
Total error	24.23	12	2.019			
Total (corr.)	6609	26				

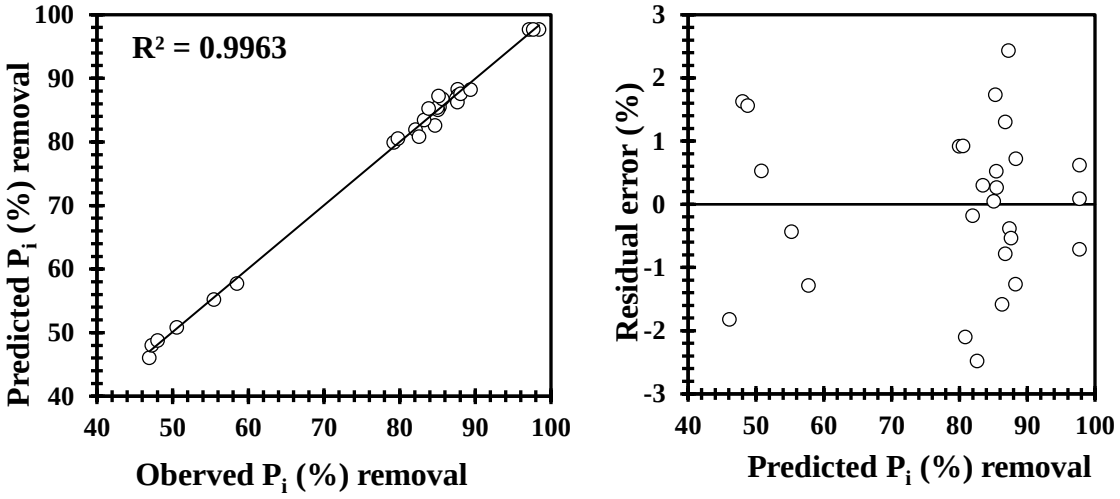

Figure 4.3: (a) Parity plot showing the correlation between the predicted and experimental values of phosphate removal efficiency (b) Percent error as a function of predicted phosphate removal.

4.3.2 Main effect plots

Figure 4.4 displays a plot of the main effects and the independent variables for the $P_{i,removal}$ efficiency. The main effect plots are used to depict a preliminary conclusion about effects of the

flocculation variables. The role of independent variables; pH, $FeCl_3$ dose, alginate dose, and settling time on the response function are shown in Figure 4.4. The effect of pH in Figure 4.4(a) is significant on the $P_{i,removal}$, where optimum removal was obtained at 4.7, with a sharp decrease in the slope as the pH increases. As the $FeCl_3$ and alginate dosage increases (Figure 4.4 (c & d)), the removal efficiency increases until an optimum dose is obtained at 12.5 mg/L and 7.5 mg/L, respectively. An increase in their respective dosages beyond the optimum level leads to a decrease in the response function. The settling time does not appear to have any considerable influence on the response function, since there is no significant variation in the $P_{i,removal}$ efficiency with time, as depicted in Figure 4.4(b). Employing the main effect to evaluate the response function is problematic because the interaction between different independent factors may affect the response variable. Hence, the effect of the interaction variables is discussed in the next section.

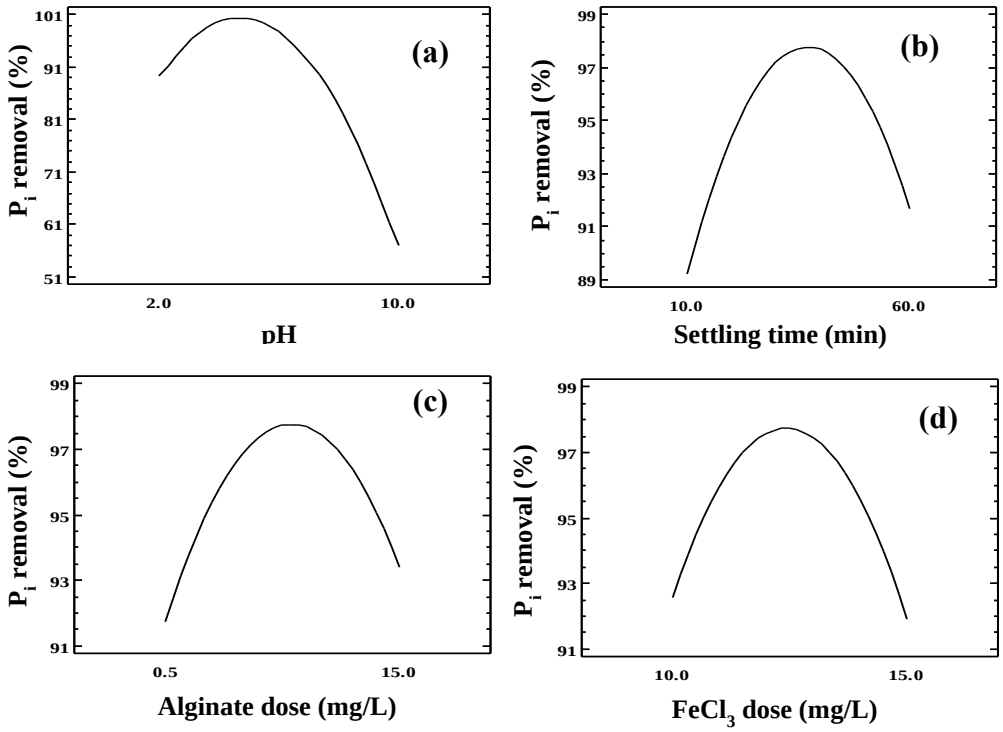

Figure 4.4: Main effects plot of (a) initial pH, (b) settling time (c) alginate dose and (d) $FeCl_3$ dose on phosphate removal efficiency.

4.3.3 The interactive effects of variables on phosphate flocculation

The three-dimensional (3D) response surface plots and 2D contour plots in Figure 4.5 were obtained from the model-predicted response by keeping two independent variables constant at the optimal level while varying the other two terms within the experimental conditions. The response surface is a graphical representation of the regression equation for visualization of the relationship between the response and experimental levels of each variable.[43] These plots are useful to assess the interactive relationship between the independent variables and the response function. The obvious peak in the response surfaces indicates that the optimal conditions were exactly located inside the design boundary. The elliptical contour plots show significant interactive effects on $P_{i,removal}$ efficiency between any two variables. In other words, there are significant interactive effects on the response variables between $FeCl_3$ and alginate dosage, $FeCl_3$ dosage and pH, $FeCl_3$ dosage and settling time, alginate dosage and settling time, pH and settling time, as well as alginate dosage and pH. The interactive effects between different variables are presented and discussed below.

The response surface and contour plots for the interaction between pH and $FeCl_3$ dose at the optimal levels of alginate dose and settling time are presented in Figure 4.5(i). Between pH 1.0 and 4.7, the $P_{i,removal}$ increased from 62.5 to 99%. However, as the pH increases further, the removal efficiency decreases significantly. At pH 10 and $FeCl_3$ dose of 15.0 mg/L, the $P_{i,removal}$ is 55%. At pH 2 and $FeCl_3$ dose of 12 mg/L, the $P_{i,removal}$ was 77.5%. This is expected because pH plays an important role in the CF process. Charge neutralization on hydrolysis products and the precipitation of hydroxides of Fe(III) can be controlled by pH variations. Phosphate has anionic surface charge, where hydrolysis products of the ferric chloride can neutralize the P_i charge. Therefore, charge neutralization is a likely mechanism for $P_{i,removal}$, where adsorption and sweeping may be considered as possible removal mechanisms due to the presence of alginate. The P_i precipitation by the hydrolysis products of Fe(III) could be controlled by surface complexation mechanism, as discussed in Chapter 2. In acidic media at low pH, protonation may occur, resulting in reduced charge density, which leads to self-aggregation of P_i where less coagulant is required. For instance, at fixed pH, an increase of the $FeCl_3$ dose leads to greater $P_{i,removal}$ until an optimum dose of 12.5 mg/L which decreases gradually as the $FeCl_3$ dose increases further.

$P_{i,removal}$ was studied as a function of pH and alginate dose is presented in Figure 4.5(iia) as 3D and 2D plots, respectively. The plots indicate that the optimal regions for the two interacting

variables are located within the design boundary. At constant alginate dosage such as 6.0 mg/L, the $P_{i,removal}$ increases until an optimum pH condition is obtained. As the pH increases beyond the optimum level, the $P_{i,removal}$ decreases significantly. By comparison, the alginate dose increased at constant pH where the $P_{i,removal}$ increases steadily with an optimum dose of 7.75 mg/L and decreases as the alginate dose increases beyond the optimal level. As pH and alginate dose were increased, the $P_{i,removal}$ increased, while a decrease in $P_{i,removal}$ occurs as the pH and alginate dose increase beyond their optimal values.

Figure 4.5(iii) shows the effect of variable pH and settling time at the optimal levels of $FeCl_3$ and alginate dosage on the $P_{i,removal}$. At constant pH, greater $P_{i,removal}$ occurred with longer settling time until it reached an optimal value at 37 min, and a sharp decrease with a further increase in settling time. During the long contact time, the P_i species were destabilized which led to the formation of large flocs with excellent settling ability. However, beyond the optimal settling time, restabilization of the flocs occurred that resulted in lower $P_{i,removal}$. On the other hand, an increase in pH at constant settling time yielded greater $P_{i,removal}$, where the response variable decreased as the pH increased beyond the optimal level. As the pH and settling time decreased or increased beyond their optimal level, the $P_{i,removal}$ was lower relative to the optimal conditions.

Figure 4.5(iv) represents the response surface and contour plots for $P_{i,removal}$ at optimal levels of pH and settling time, and variable $FeCl_3$ and alginate dosage within the experimental design. The interactive effect of the alginate and $FeCl_3$ dosage does not appear to strongly affect $P_{i,removal}$. Greater removal efficiency (> 92%) was obtained at all conditions. The greater P_i removal efficiency could be associated with several mechanisms such as, charge neutralization, surface complexation, polymer bridging and adsorption. The response surface plot shows a clear maximum, indicating that the optimum condition for $P_{i,removal}$ is well within the experimental design boundary conditions. At the optimum pH, metal hydroxide of the iron neutralizes the phosphate through charge neutralization. The $FePO_4$ precipitate is swept and then adsorbs the alginate polyelectrolyte species through sweeping and ion-binding adsorption mechanisms.[44]

Figure 4.5(v) depicts the response surface and contour plots for $P_{i,removal}$ at optimal levels of pH and $FeCl_3$ dose, with variable alginate dose and settling time for the experimental design. From Figure 4.5(v), at constant alginate dose, the $P_{i,removal}$ increases from 10 to 37 min. However, beyond the optimal settling time, the $P_{i,removal}$ remains virtually constant. Greater removal (85-92%) was obtained at all working conditions. This implies that the interaction between settling and alginate

dosage within the specified range does not have a significant impact on $P_{i,removal}$. Similar results were observed for the variation between settling time and $FeCl_3$ dose, as shown in Figure 4.5(vi).

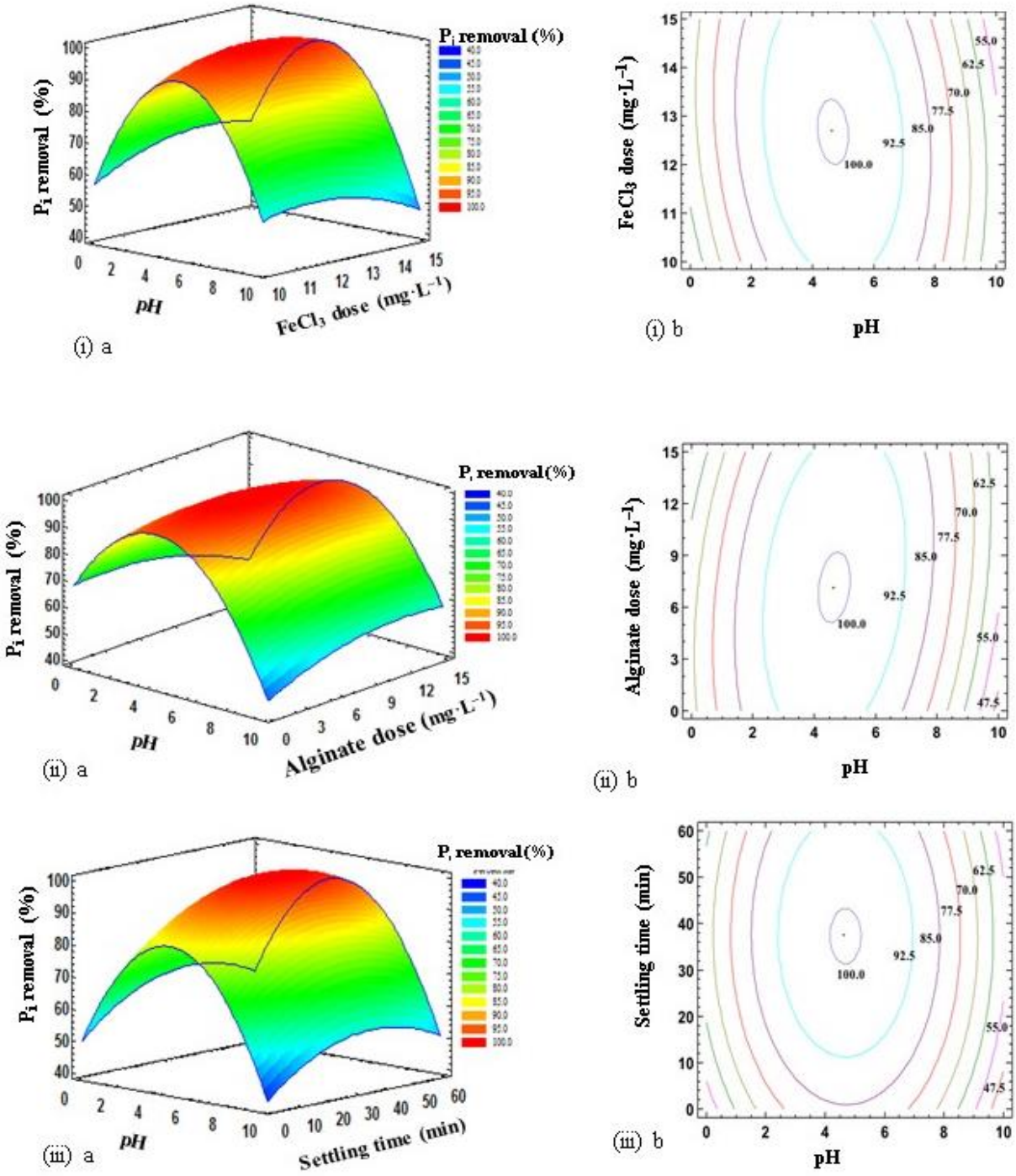

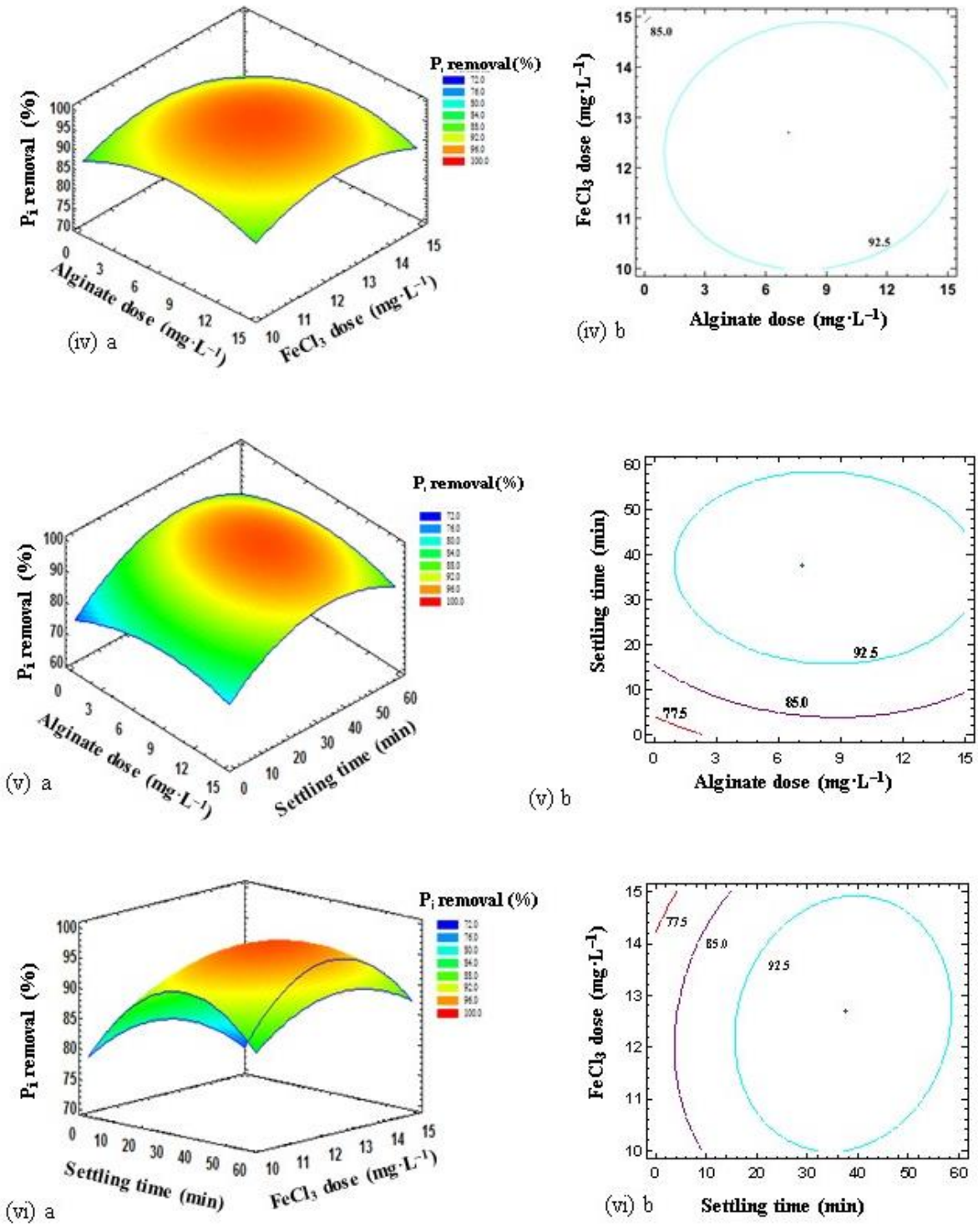

Figure 4.5: (a) 3D Box-Behnken response surface and (b) 2D contour plots of P_i removal as a function of (i) pH and $FeCl_3$; (ii) pH and alginate dose; (iii) pH and settling time; (iv) alginate dose and $FeCl_3$ dose; (v) alginate dose and setting time; (vi) setting time and $FeCl_3$ dose.

Table 4.3: Results of validation experiments under optimized conditions

Test	Independent variable				P_i Removal (%)	
	pH	$FeCl_3$ dose (mg/L)	Alginate dose (mg/L)	Settling time (minutes)	Experimental value	Estimated value
1	4.6	13	7.1	37	99.7 ± 0.7	99.6
2	3.0	10	3.0	15	85.4 ± 0.9	85.7
3	4.0	11	5.0	25	90.1 ± 1.8	90.5
4	5.0	12	7.0	35	94.7 ± 0. 5	95.1
5	6.0	13	9.0	45	94.4 ± 0.9	94.3
6	9.0	14	12	55	74.6 ± 0.9	74.8

4.3.4 Confirmation and validation

The validity of the statistical methodology in estimating the P_i removal efficiency was confirmed by carrying out additional experiments in triplicate at the predicted optimized levels obtained from the solution of equation (4.5), and five other conditions within the range of the experimental design. The selected conditions for the pH, $FeCl_3$ dosage, alginate dosage and settling time are listed in Table 4.3, along with the predicted and the measured results. The $P_{i,removal}$ determined experimentally was 99.7 ± 0.7%, which is significantly close to the predicted optimal $P_{i,removal}$ (99.6%). As shown in Table 4.3, the measured and the estimated values of $P_{i,removal}$ obtained from RSM are in good agreement. The result verifies that the RSM approach is useful for optimizing the operational conditions of the CF process. As well, RSM enables prediction of an empirical relationship between the response factor and the independent variables. Table A9.7 in Appendix A represents a comparison between the removal of P_i using a different coagulant and/or flocculant system. The results show that the P_i removal at the optimized conditions herein for the binary Fe(III)-alginate coagulant-flocculant system is significantly greater when compared with other coagulant-flocculant systems.

4.3.5 Flocculation kinetics

The contact time between the orthophosphate (P_i) and the flocculant is a significant factor in understanding the flocculation process and the flocculation kinetics of P_i at fixed initial flocculant dosage.[47,48] Figure 4.6 illustrates the effect of contact time on the flocculation ability of Fe(III)-alginate flocculant with P_i at the RSM optimized conditions. The flocculation process is divided into three regions. In the first region, there is a rapid increase in the flocculation up to 15 min, it then increases steadily until a dynamic equilibrium is reached at 35 min and remains nearly

constant thereafter. The behavior in the first region is due to electrostatic interaction between the phosphate and the ferric cations, leading to charge neutralization. P_i is negatively charged and favors interaction with metal cation species to neutralize its surface charge. The trivalent iron metal cation may act as a cross-linker along the alginate chain to form a stable gel which leads to adsorption of P_i.[47,48] In the second region, there is a gradual increase in the flocculation efficacy as a result of a reduced effective cationic charge on the flocculant surface. The third region illustrates that the dynamic equilibrium for the floc formation is *ca*. 35 min, in agreement with the RSM model. Similar results for the removal of dyes using such polysaccharide-based flocculants were reported by Kono et al.[49]

The kinetics of the flocculation process was examined at the optimized conditions. The adsorption kinetics of P_i with the Fe(III)-alginate flocculant system was investigated using pseudo-first-order (PFO) and pseudo-first-order (PSO) kinetic models. The PFO kinetic model assumes that the sorption rate decreases linearly as the adsorption rate increases.[50,51] By comparison, the PSO kinetic model assumes that the rate-limiting step involves interaction between the adsorbent and adsorbate is often applied to describe an adsorption process.[51,52] The PFO and PSO kinetic models are shown in equations (4.6) and (4.7), respectively.

$$q_t = q_e(1-e^{-k_1 t}) \tag{4.6}$$

$$q_t = \frac{k_2 q_e^{\,2} t}{1+k_2 q_e t} \tag{4.7}$$

Here, q_e and q_t are the amount of phosphate adsorbed (mg/g) at dynamic equilibrium and at time t. k_1 and k_2 are the rate constants for the PFO and PSO kinetic models, respectively. k_1, k_2 and q_e were estimated using non-linear regression fitting according to equations (4.6) and (4.7). The "best fit" criterion between the experimental data and the kinetic models was determined by minimizing the absolute sum of squares of errors (SSE) by equation (4.8).

$$SSE = \sum \sqrt{\frac{(q_{e,i} - q_{c,i})^2}{N}} \tag{4.8}$$

Here, $q_{e,i}$ is the experimental value and $q_{c,i}$ is the calculated or predicted value, according to the kinetic model and N is the number of experimental data points.

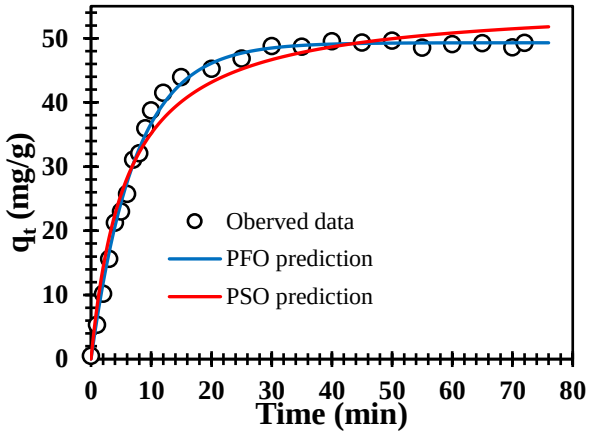

Figure 4.6: Flocculation kinetics of P_i removal in aqueous solution at variable time intervals, where c_o = 10.0 mg/L.

Figure 4.6 illustrates the kinetic results of the flocculation of P_i with the Fe(III)-alginate flocculant system. The blue and red curves in Figure 4.6 represent the theoretical PFO and PSO kinetic models, respectively. In Figure 4.6, the $P_{i,removal}$ is well described by both PSO and PFO kinetic models. Values of k_1, k_2, q_e and R^2 obtained from the regression analysis are listed in Table 4.4. The correlation coefficient (R^2) for the PFO model (R^2 = 0.998) exceeds that of the PSO model (R^2 = 0.988). Also, it is evident that the predicted values of q_e determined by the PFO model agrees well with the experimental values relative to the PSO kinetic model. In addition, the rate constant of the PFO (k_1) model is significantly greater than that of the PSO (k_2) model. This PFO adsorption mechanism describes the flocculation of phosphate by Fe(III)-alginate, according to the PFO model. The adsorption of P_i by the flocculant system indicates that the sorption rate decreases linearly as the adsorption rate increases, Similar results were reported for the flocculation of anionic dyes and arsenates by polysaccharide-based flocculants.[45,46,53,54] The rapid equilibrium process at 35 min is shown in Figure 4.6, indicating that P_i species interact with the outermost surface of the flocculant system.

Table 4.4: Pseudo-First-Order (PFO) and Pseudo-Second-Order (PSO) kinetic variables for P_i removal in aqueous solution at optimized flocculation condition. c_o (P_i) = 10.0 mg/L

Model	Q_t (mg·g^{-1})	k · 10^3	R^2
PFO	49.3 ± 0.3	136.7 ± 3.1 min^{-1}	0.998
PSO	556.7 ± 1.1	3.1 ± 0.3 g·mg^{-1}·min^{-1}	0.988

4.3.6 Adsorption isotherms

Adsorption processes in CF systems can be described through graphical isotherms. Adsorption isotherms provide insight concerning the interaction between adsorbates and adsorbents at the optimization conditions.[49] The Langmuir[55], Freundlich[56] and Sips[57] isotherm models are the most frequently used to describe adsorption during a flocculation processes of colloidal particles. In this study, the adsorption isotherm models were used to understand the adsorption processes to elucidate the flocculation mechanism.

The Langmuir adsorption isotherm model is based on the assumption that adsorption occurs at specific homogeneous sites with the adsorbent and is described by equation (4.9).

$$q_e = \frac{K_l q_m c_e}{1 + K_l c_e} \tag{4.9}$$

Here, q_m (mg·g^{-1}) is the monolayer adsorption of P_i per unit mass of Fe(III)-alginate adsorbent and q_e is the amount of adsorbed P_i (mg·g^{-1}). K_l (Lg^{-1}) is the equilibrium adsorption constant, which is related to the affinity of the binding sites and is related to a dimensionless constant called the separation factor or equilibrium variable, R_l, according to equation (4.10). The adsorption process can be categorized into four groups based on the value of R_l: irreversible (R_l = 0), favorable (0 < R_l < 1), linear (R_l = 1) and unfavorable (R_l > 1).

$$R_l = \frac{1}{1 + K_l c_0} \tag{4.10}$$

The Freundlich isotherm model accounts for multilayer sorption by assuming that the adsorbent has a heterogeneous surface with non-uniform distribution of sorption sites. The Freundlich adsorption isotherm is described by equation (4.11).

$$q_e = K_f c_e^{1/n} \tag{4.11}$$

K_f is the Freundlich isotherm constant which relates to the adsorption capacity and n is a dimensionless constant. The empirical exponent variable gives valuable information on the shape of the isotherm, where the adsorption process may be classified as unfavorable ($1/n > 1$), favorable ($1/n < 1$), and irreversible ($1/n = 0$).

The Sips isotherm model (equation (4.12)) shares features of the Langmuir and Freundlich isotherms. At low adsorbate concentrations, it converges to a Freundlich isotherm. At high adsorbate concentration (or n = 1), the model reduces to a Langmuir isotherm.[58]

$$q_e = \frac{K_s q_m c_e^{n_s}}{1 + K_s c_e^{n_s}} \tag{4.12}$$

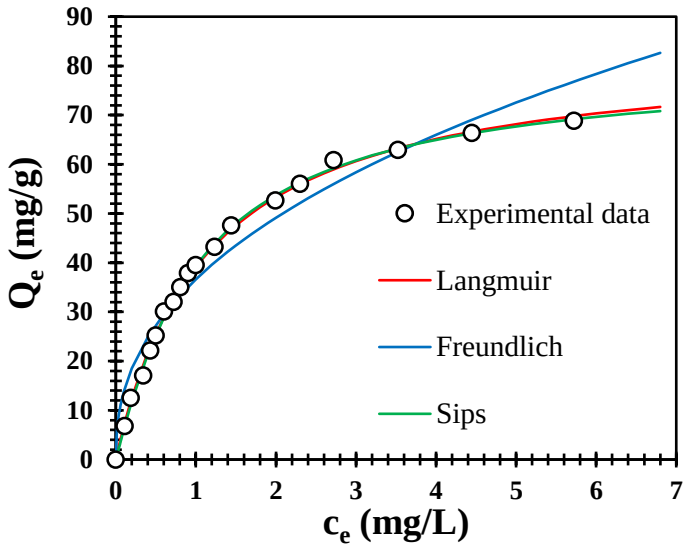

Figure 4.7: The adsorption isotherm of phosphate by combined $FeCl_3$ and alginate at optimized flocculation condition. Initial phosphate concentration (1.0 – 20.0) mg/L.

Figure 4.7 is the adsorption isotherm for the removal of P_i by Fe(III)-alginate. The experimental data were fit by the Langmuir, Freundlich and Sips isotherm models. The fitted lines through the data represent the *goodness-of-fit* of the isotherm models employed herein, where the variables are listed in Table 4.5. According to the results in Figure 4.7 and Table 4.5, the removal of P_i by the Fe(III)-alginate system is well-described by the Langmuir and Sips models. The dimensionless constant, R_l obtained from the Langmuir (0.054) and Sips (0.049) models indicate favorable adsorption of phosphate. Also, the monolayer adsorption capacity (q_m; mg/g) for P_i is given in parentheses at the optimized conditions: Langmuir (83.6±1.02) and Sips (80.3±1.88) isotherm models. The values obtained from the Langmuir and Sips models are in good agreement, where

the Langmuir model is considered more reliable due to its relative simplicity and favorable *goodness-of-fit* for the Fe(III)-alginate isotherm system. As well, the exponent term (n_s) is near unity which implies that the Sips isotherm converges with the Langmuir model when $n_s = 1$. Thus, it can be inferred that the flocculation of orthophosphate by Fe(III)-alginate follows a homogeneous mechanism based on the charge neutralization reaction between the anionic P_i and the ferric cation.

The dimensionless constant, n^{-1} in the Freundlich model, exceeds unity (2.4 ± 0.1) and indicates that the adsorption process is not favorable. The Langmuir adsorption constant, K_l is 0.88 ± 0.01 mg/L, where this describes the adsorption process of P_i adsorbed on Fe(III)-alginate. This shows that the flocs formed from the interaction between P_i with Fe(III)-alginate have stronger stability in solution. The flocculation of P_i species by Fe(III)-alginate system follows a homogeneous mechanism based on the charge neutralization reaction between the anionic P_i and the ferric cation species. The flocculation isotherm would be described by the Freundlich model if other interactions occur besides electrostatic processes during flocculation. The Freundlich isotherm model is often used to describe heterogeneous adsorption systems.[59]

Table 4.5: Langmuir, Freundlich and Sips adsorption isotherm coefficients for the flocculation of phosphate by combined $FeCl_3$ and alginate at pH 4.7

Adsorption Model	**Variable**	
Langmuir	q_t (mg/g)	84 ± 1
	K_l (L/mg)	0.88 ± 0.03
	R_l	0.054
	R^2	0.998
Freundlich	n	2.4 ± 0.1
	K_f (L/mg)	37 ± 1
	R^2	0.959
Sips	q_t (mg/g^1)	80 ± 2
	Ks (L/mg)	0.97 ± 0.05
	n	1.1 ± 0.1
	R_l	0.049
	R^2	0.998

4.3.7 Mechanism

The use of chemical precipitation for the removal of soluble impurities or nutrients in water depends on the nature of the complexes formed. The mechanism of chemical P_i removal involves

a combined process of coagulation and precipitation that is influenced by solution conditions such as pH and initial concentration. The mechanism of P_i removal by chemical precipitation, generally involves two steps, which is known as the surface complexation model:[60]

i. Formation of metal-hydroxide-phosphate complex, $M(OH)_{3-x}(PO_4)_x$. These complexes either act as centers of precipitation of phosphate ions on the M(III) hydrolysis species or absorbed onto positively charged M(III) hydrolysis species.
ii. Adsorption of phosphate ions onto the M(III) hydrolysis species followed by separation via sedimentation and/or filtration.

The mechanism involving the reaction when Fe(III) is added to wastewater to precipitate P_i species is complex and does not follow any simple single steps.[61] The efficiency of the precipitation of the oxidation product for P_i removal depends on pH, initial P_i concentration in the wastewater, iron (III) dose and temperature.[1] Precipitation with ferric salt is most effective within certain pH range. The optimum pH for ferric ion is 4.0 to 5.0.[62] A simplified reaction that occurs between Fe(III) and phosphate ions in wastewater is described by equation (4.13), where $FePO_4$ is precipitated with K_{sp} value of 1.3×10^{-22}.

$$FeCl_3 + PO_4^{3-} \rightarrow FePO_4 \downarrow + 3Cl^- \quad (4.13)$$

As ferric chloride is added to the wastewater containing P_i, the contaminants are predominantly coagulated by charge neutralization and/or surface complexation. In this case, the positive charge on the metal ion neutralizes the negatively charged sites of the P_i particles. However, the use of inorganic salts requires a higher salt dosage with the subsequent production of large sludge volume. In addition, the pH of the solution is altered when inorganic salts are used in the coagulation process. Organic polymers such as alginate may be used as coagulant aids to yield enhanced precipitation of the contaminants compared with that of the sole use of ferric chloride. Alginate acts as a destabilizing agent through charge neutralization and precipitation (surface complexation) mechanisms due to the electrostatic attraction between the positive charges on the polyelectrolyte and the negative charge on P_i. Hence, the growth of micro- to macro-flocs occurs via flocculation due to the reduced surface charge of the particles, leading to decreased electrostatic repulsion. Effective removal of P_i is favored when the zeta-potential of particles is close to zero, as demonstrated elsewhere.[63] The high charge density of alginate imparts a greater charge to the surface of the contaminant species leading to greater removal efficiency.[64] High charge density polymers adsorb as a well-defined monolayer orientation with reduced bridging interactions.[65] The

charge neutralization mechanism enables flocculation among particles with a reduced surface charge (reduction of zeta potential). Hence, a decreased electrostatic repulsion between colloidal particles which favor van der Waals interactions to allow for initial aggregation of colloidal and fine suspended materials as a microfloc.[64]

At a higher dosage of alginate, there is greater P_i removal efficiency for the same $FeCl_3$ dose and pH, as reported in Table A9.6 (Appendix A). This effect results due to ion-binding adsorption of P_i species onto the Fe(III)-alginate surface via the surface complexation model. The adsorption affinity between the polymer and P_i is likely appreciable and outweighs the loss of entropy associated with polymer because an adsorbed chain will have a more restricted configurational state than a random coil in free solution.[65] The mechanism of this flocculation process is an ion-binding adsorption process that occurs between the hydroxyl polar functional groups of alginate or charged sites on the polymer backbone and the anionic surface of the phosphate. Adsorption of P_i onto alginate occurs when there are sufficient ferric ions present since Fe(III) can act as a bridge between alginate and P_i. In the absence of a Fe(III) cation, limited flocculation occurs even at high ionic strength, as observed in Chapter 3.

4.4 Conclusion

Optimization of a coagulation-flocculation process for orthophosphate (P_i) removal in aqueous medium was investigated using a jar test system. The RSM using the Box-Behnken design method was used to optimize the conditions for maximum P_i removal. The $FeCl_3$ and alginate dosage, along with pH and settling time were determined as significant factors to yield optimal $P_{i,removal}$. The predicted quadratic polynomial model by the RSM method can be used to estimate the $P_{i,removal}$ over the range of experimental variables. Optimal conditions for the CF process occurred at pH 4.6, $FeCl_3$ (12.5 mg/L), alginate dosage (7.3 mg/L) and settling time (37 min), where the $P_{i,removal}$ was 99.7±0.7%. This study shows good agreement between experimental results and the RSM predictions, and further illustrates that the RSM can be used to model and optimize coagulation-flocculation processes for phosphate removal.

The results for the optimized conditions indicate that $P_{i,removal}$ occurs via adsorption of P_i by the Fe(III)-alginate flocculant system. Greater $P_{i,removal}$ occurred at acidic versus alkaline conditions. The variable $P_{i,removal}$ relates to the electrostatic interaction between orthophosphate anion species and the flocculant system. Kinetic adsorption profiles show uptake within 35 min where the

experimental results are well described by the pseudo-first-order kinetic model and Langmuir isotherm model at equilibrium conditions. The maximum adsorption capacity of Fe(III)-alginate for P_i was obtained as 83.6 ± 1.02 mg/g. Electrostatic charge neutralization and ion-binding adsorption and surface complexation mechanisms were found to control the flocculation process. The results of this study will contribute to the further development of advanced water treatment processes for the controlled removal of other waterborne oxyanion species.

4.5 References

(1) Yeoman, S.; Stephenson, T.; Lester, J. N.; Perry, R. *Environ. Pollut.* **1988**, *49* (3), 183–233.

(2) Rybicki, S. *Phosphorus Removal From Wastewater - A Literature Review*; 1997.

(3) Painting, S. J.; Devlin, M. J.; Malcolm, S. J.; Parker, E. R.; Mills, D. K.; Mills, C.; Tett, P.; Wither, a.; Burt, J.; Jones, R.; Winpenny, K. *Mar. Pollut. Bull.* **2007**, *55* (1–6), 74–90.

(4) Benyoucef, S.; Amrani, M. *Desalination* **2011**, *275* (1–3), 231–236.

(5) MOEE. Provision and operation of phosphorus removal facilities at municipal, institutional and private sewage treatment works; Ontario, Canada, **1994**, 1–89.

(6) Mahaninia, M. H.; Wilson, L. D. *J. Appl. Polym. Sci.* **2016**, *133* (5), 1–10.

(7) Filipkowska, U.; Jóźwiak, T.; Szymczyk, P. *Prog. Chem. Appl. Chitin its Deriv.* **2014**, *19* (1), 5–14.

(8) Sø, H. U.; Postma, D.; Jakobsen, R.; Larsen, F. *Geochim. Cosmochim. Acta* **2011**, *75* (10), 2911–2923.

(9) Yan, L. G.; Xu, Y. Y.; Yu, H. Q.; Xin, X. D.; Wei, Q.; Du, B. *J. Hazard. Mater.* **2010**, *179* (1–3), 244–250.

(10) Sathasivan, A. In *Encyclopedia of life support systems*; McGraw Hill Professional, 2010; pp 1–16.

(11) Gautam, R. K.; Banerjee, S.; Gautam, P. K.; Chattopadhyaya, M. C. *Adv. Environ. Res.* **2014**, *36*, 1–23.

(12) Inan, H.; Alaydın, E. *Desalin. Water Treat.* **2014**, *52* (7–9), 1396–1403.

(13) Peleka, E. N.; Mavros, P. P.; Zamboulis, D.; Matis, K. a. *Desalination* **2006**, *198* (1–3), 198–207.

(14) Dunets, C. S.; Zheng, Y. *Hortscience* **2015**, *50* (6), 921–926.
(15) Mohammed, S. A. M.; Shanshool, H. A. *Iraqi J. Chem. Pet. Eng.* **2009**, *10* (2), 35–42.
(16) Quinlan, P. J.; Tanvir, A.; Tam, K. C. *Carbohydr. Polym.* **2015**, *133*, 80–89.
(17) Tripathy, T.; De, B. R. *J. Phys. Sci.* **2006**, *10*, 93–127.
(18) Pa Ho Hsu. *Water Res.* **1976**, *10* (10), 903–907.
(19) Yang, K.; Li, Z.; Zhang, H.; Qian, J.; Chen, G. *Environ. Technol.* **2010**, *31* (6), 601–609.
(20) Tzoupanos, N. D.; Zouboulis, A. I. *6th IASME/WSEAS Int. Conf. HEAT Transf. Therm. Eng. Environ.* **2008**, 309–317.
(21) Vijayaraghavan, G.; Shanthakumar, S. *Desalin. Water Treat.* **2016**, *57* (14), 6384–6392.
(22) Wu, C.; Wang, Y.; Gao, B.; Zhao, Y.; Yue, Q. *Sep. Purif. Technol.* **2012**, *95*, 180–187.
(23) Zhao, Y. X.; Gao, B. Y.; Shon, H. K.; Wang, Y.; Kim, J. H.; Yue, Q. Y.; Bo, X. W. *Bioresour. Technol.* **2012**, *108* (0), 45–54.
(24) Zhao, Y. X.; Gao, B. Y.; Wang, Y.; Shon, H. K.; Bo, X. W.; Yue, Q. Y. *Chem. Eng. J.* **2012**, *183*, 387–394.
(25) Zhao, Y. X.; Wang, Y.; Gao, B. Y.; Shon, H. K.; Kim, J.-H.; Yue, Q. Y. *Desalination* **2012**, *299*, 79–88.
(26) Renault, F.; Sancey, B.; Badot, P. M.; Crini, G. *Eur. Polym. J.* **2009**, *45* (5), 1337–1348.
(27) Sharma, B. R.; Dhuldhoya, N. C.; Merchant, U. C. *J. Polym. Environ.* **2006**, *14* (2), 195–202.
(28) Saranya, P.; Ramesh, S. T.; Gandhimathi, R. *Desalin. Water Treat.* **2014**, *52* (31/33), 6030–6039.
(29) Lee, K. Y.; Mooney, D. J. *Prog. Polym. Sci.* **2012**, *37* (1), 106–126.
(30) Devrimci, H. A.; Yuksel, A. M.; Sanin, F. D. *Desalination* **2012**, *299*, 16–21.
(31) Ferreira, S. L. C.; Bruns, R. E.; Ferreira, H. S.; Matos, G. D.; David, J. M.; Brandão, G. C.; da Silva, E. G. P.; Portugal, L. A.; Dos Reis, P. S.; Souza, A. S.; dos Santos, W. N. L. *Anal. Chim. Acta* **2007**, *597* (2), 179–186.
(32) Montgomery, D. C. *Design and analysis of experiments*, 9th ed.; Wiley: Hoboken, New Jersey, 2017.
(33) Patel, H.; Vashi, R. T. *J. Saudi Chem. Soc.* **2012**, *16* (2), 131–136.
(34) Aslan, N.; Cebeci, Y. *Fuel* **2007**, *86*, 90–97.
(35) Aslani, H.; Nabizadeh, R.; Nasseri, S.; Mesdaghinia, A.; Alimohammadi, M.; Mahvi, A.

H.; Rastkari, N.; Nazmara, S. *Desalin. Water Treat.* **2016**, *3994*, 1–12.

(36) Bezerra, M. A.; Santelli, R. E.; Oliveira, E. P.; Villar, L. S.; Escaleira, L. A. *Talanta* **2008**, *76* (5), 965–977.

(37) Usharani, K.; Lakshmanaperumalsamy, P. *J. Microbiol. Biotechnol. Food Sci.* **2016**, *05* (06), 534–547.

(38) Usharani, K.; Muthukumar, M. *Int. J. Environ. Sci. Technol.* **2013**, *10* (3), 591–606.

(39) Rakić, T.; Kasagić-Vujanović, I.; Jovanović, M.; Jančić-Stojanović, B.; Ivanović, D. *Anal. Lett.* **2014**, *47* (8), 1334–1347.

(40) Zolgharnein, J.; Shahmoradi, A.; Ghasemi, J. B. *J. Chemom.* **2013**, *27*, 12–20.

(41) Jain, M.; Garg, V. K.; Kadirvelu, K. *Bioresour. Technol.* **2011**, *102* (2), 600–605.

(42) Yetilmezsoy, K.; Demirel, S.; Vanderbei, R. J. *J. Hazard. Mater.* **2009**, *171* (1–3), 551–562.

(43) Trinh, T. K.; Kang, L.-S. *Environ. Eng. Res.* **2010**, *15* (2), 63–70.

(44) Bratby, J. *Coagulation and Flocculation in Water and Wastewater Treatment*, Second.; IWA publishing: London, 2006.

(45) Singh, R. P.; Pal, S.; Rana, V. K.; Ghorai, S. *Carbohydr. Polym.* **2013**, *91* (1), 294–299.

(46) Lin, Q.; Qian, S.; Li, C.; Pan, H.; Wu, Z.; Liu, G. *Carbohydr. Polym.* **2012**, *90* (1), 275–283.

(47) Rezende, R.; Bártolo, P.; Mendes, A.; Filho, R. *8th Int. Conf. Chem. Process Eng.* **2007**, *11*, 509–514.

(48) Simpson, N. E.; Stabler, C. L.; Simpson, C. P.; Sambanis, A.; Constantinidis, I. *Biomaterials* **2004**, *25* (13), 2603–2610.

(49) Kono, H.; Kusumoto, R. *J. Water Process Eng.* **2015**, *7*, 83–93.

(50) Lagergren, S. *K. Sven. Vetensk. Sakademiens Handl.* **1898**, *24* (1–39), 2474–2479.

(51) Zhen, Y.; Ning, Z.; Shaopeng, Z.; Yayi, D.; Xuntong, Z.; Jiachun, S.; Weiben, Y.; Yuping, W.; Jianqiang, C. *ACS Appl. Mater. Interfaces* **2015**, *7* (44), 24446–24457.

(52) Ho, Y. S.; McKay, G. *Process Biochem.* **1999**, *34* (5), 451–465.

(53) Guibal, E.; Roussy, J. *React. Funct. Polym.* **2007**, *67* (1), 33–42.

(54) Kwok, K. C. M.; Koong, L. F.; Chen, G.; McKay, G. *J. Colloid Interface Sci.* **2014**, *416*, 1–10.

(55) Langmuir, I. *J. Am. Chem. Soc.* **1916**, *252*, 2221–2295.

(56) Freundlich, H. M. F. . *Z. Phys. Chem.* **1909**, *57*, 385–470.

(57) Sips, R. *J. Chem. Phys.* **1948**, *18* (5), 490–495.

(58) Ho, Y. S.; Porter, J. F.; Mckay, G. *Water, Air, Soil Pollut.* **2002**, *141* (1–4), 1–33.

(59) Crini, G. *Dye. Pigment.* **2008**, *77* (2), 415–426.

(60) Jiang, J. Q.; Graham, N. J. D. *Water SA* **1998**, *24* (3), 237–244.

(61) Jenkins, D.; Ferguson, J.; Menar, A. *Water Res.* **1971**, *5*, 369–389.

(62) Suschka, J.; Machnicka, a.; Poplawski, S. *Environ. Technol.* **2001**, *22* (11), 1295–1301.

(63) Kleimann, J.; Gehin-Delval, C.; Auweter, H.; Borkovec, M. *Langmuir* **2005**, *21* (8), 3688–3698.

(64) Lee, C. S.; Robinson, J.; Chong, M. F. *Process Saf. Environ. Prot.* **2014**, *92* (6), 489–508.

(65) Bolto, B.; Gregory, J. *Water Res.* **2007**, *41* (11), 2301–2324.

CHAPTER 5

5 Design of amphoteric chitosan flocculants for phosphate and turbidity removal in wastewater[3]

Description

In this chapter, an amphoteric flocculant (CMC-CTA) was synthesized by quaternizing 3-chloro-2-hydroxypropyl trimethylammonium chloride (CTA) onto carboxymethyl chitosan (CMC). The structure of CMC-CTA was supported by various characterization methods. The dual removal of T_i and P_i by flocculation was achieved using CMC-CTA, chitosan (CHI) and CMC, with (and without) $FeCl_3$ coagulant in a binary and single-component systems, where the effects of several factors affecting the CF process were investigated. The results revealed modification of native chitosan according to the synthetic procedure, produced polymers with improved functional and flocculation properties when combined with $FeCl_3$ in a binary system for P_i and T_i removal in an aqueous medium.

Author's contribution

Lee D. Wilson and I conceived the project. I performed all the experimental work, data processing and analysis, and wrote the first draft of the manuscript as well as making further revisions where and when necessary on subsequent drafts. Dr. L.D. Wilson was responsible for the supervision of the project, editorial guidance for revision of the manuscript drafts, and corresponding author. Permission was obtained from all contributing authors before the inclusion of the manuscript in this thesis.

Relation of Chapter 5 to Overall Objective of this Project

An amphoteric chitosan-based flocculant material was prepared and characterized using physicochemical methods related to flocculation properties. The study reported in this chapter refers to the second theme (synthesis, characterization, and flocculation properties of high

[3] Reprinted in part with permission from Agbovi, H. K.; Wilson, L. D. *Carbohydr. Polym*. 2018, 189, 360–370. Copyright 2018 Elsevier.

molecular weight chitosan-based amphoteric flocculant for P_i and T_i removal in a single-component and binary systems) of the thesis research. It also addresses the hypotheses 1, 2, and 3 mentioned in Chapter 1. Herein, the increased molecular weight of the chitosan after the modification increased the flocculation efficiency. Also, several external conditions were observed to influence the flocculation properties of the flocculants. Additionally, the flocculation was well described by pseudo-first-order and pseudo-second-order kinetic models for P_i and T_i removal, respectively.

5.1 Introduction

Environmental contamination from the discharge of domestic, municipal, and industrial wastewaters has become a serious concern for developed and developing nations. Uncontrolled discharge of effluents leads to pollution of groundwater, rivers, and lakes.[1,2] Phosphorus is a key environmental pollutant that has relatively high-water mobility, especially as orthophosphate (P_i), polyphosphate, phosphonate and/or organophosphate species. Orthophosphate (P_i) is a common form of phosphorus that often exceeds organophosphate levels in wastewater.[3] In countries where agriculture and animal husbandry are primary industries, the accumulation of phosphorous in water bodies and soils relates to uncontrolled run-off from domestic/industrial waste and fertilizer effluent from agricultural activities.[4] While phosphate is an essential micronutrient, municipal wastewater may contain *ca*. 10 mg/L to 20 mg/L of total phosphorus.[5] Untreated phosphorous-containing effluent may lead to eutrophication and excessive algae growth in lakes and rivers.[6] In general, effluent is regulated to levels below 0.5 mg/L[7], where discharge limits (mg/L) are controlled, as follows: USA (0.5 – 1.0), India (5.0), France (1.0 – 2.0) , Tunisia (10.0), Canada (0.1), Ghana (2.0), and Japan (16.0) mg/L.[7–11]

The controlled removal of P_i and T_i in wastewater was reported using adsorption[12–15], biological removal[16,17], electro-coagulation[1,2], membrane processes[18], and chemical precipitation methods.[19,20] In particular, coagulation-flocculation has attracted attention for primary and secondary water treatment due to its efficiency, simplicity and relatively low cost.[21] Commercial CF processes often use agents such as alum, lime, ferric chloride or ferric sulphate for removal of suspended contaminants, where typical precipitate removal occurs by sedimentation and/or filtration.[22] Ferric chloride has widespread use as an effective coagulant, where it is known to have a high affinity with many waterborne species such as phosphate, arsenate and nitrate. In contrast

to alum-based coagulants, ferric chloride is an alternative coagulant for wastewater treatment that has no reported adverse health effects for wastewater treatment.[23] The disadvantages of alum-based systems are discussed in detail in Chapter 3 and elsewhere.[20,24,25] By contrast, as discussed previously in Chapter 2, biopolymer coagulant aids and flocculant systems such as chitosan, and alginate, possess advantages over conventional synthetic polymer/inorganic salt systems. For example, greater contaminant removal efficiency, large floc formation with high density, higher mechanical strength, and favorable settling properties over a wide pH range that yield less sludge without secondary metal pollution even at alkaline conditions. Biopolymers are relatively cost-effective, biodegradable, biocompatible, and may be designed with tunable performance with less secondary pollutant formation.[26]

Chitosan is a linear polysaccharide copolymer that consists of N-acetyl-D-glucosamine with variable deacetylation based on its preparation.[27] At slightly acidic pH conditions, near or below the pK_a (6.2) of chitosan, protonation of the amine group occurs with favorable interaction with anion species. Chitosan has been used for the removal of phosphate and arsenic species in wastewater using different techniques or processes apart from coagulation and flocculation.[12,14,15,28,29] In contrast, there are sparse reports on chitosan for the removal of suspended and dissolved solids.[19,30,31] The unique properties of chitosan as a coagulant and/or flocculant were reported in Chapter 2, and include greater contaminant removal efficiency, large floc formation with high density, higher mechanical strength, and favorable settling properties. The relative solubility of chitosan relates to its efficiency as a flocculant, especially at lower pH since it is relatively water insoluble above its pK_a and in most organic solvents. Modified chitosan materials may have wider applications,[23,32–35] especially amphoteric forms that contain quaternary ammonium groups. Synthetic modification of chitosan with 3-chloro-2-hydroxypropyl trimethylammonium chloride (CTA) and carboxymethyl groups improve water solubility over wider pH conditions. Amphoteric materials possess favorable charge neutralization of negatively charged species and colloidal suspensions.[30,36–39] Yang et al. have shown that CTA-chitosan is more effective in turbidity removal.[40,41] By contrast, amphoteric chitosan-based flocculants have not been reported for removal of turbidity and dissolved solids such as phosphate in wastewater at the time of this report.

This study reports on the co-removal efficacy of dissolved orthophosphate (P_i) and turbidity (T_i) from simulated wastewater using a biopolymer-metal salt system. The coagulant-flocculants

studied herein contain a coagulant (ferric chloride) and biopolymer flocculants (chitosan (CHI), carboxymethyl chitosan (CMC) and grafted 3-chloro-2-hydroxypropyl trimethylammonium chloride CMC (CMC-CTA)). This study contributes to the field of biomaterials by using a binary system for T_i with P_i removal and a comparison with single-component systems at variable concentration and pH. This study contributes to binary-flocculant systems with improved efficiency and sustainability by reduction of coagulant and flocculant dosage, enhancement of the flocculation activity, and sustainability by reducing secondary pollution, as compared with conventional synthetic flocculant systems.

5.2 Materials and methods

5.2.1 Materials and Chemicals

All chemicals were of analytical reagent (AR) grade. Hydrated ferric chloride ($FeCl_3 \cdot 6H_2O$), anhydrous monobasic potassium phosphate (KH_2PO_4), NaOH (aq), HCl (aq), vanadate molybdate reagent, chitosan (medium molecular weight, 85% deacetylation), monochloroacetic acid, ethyl alcohol, isopropanol, 3-chloro-2-hydroxypropyl trimethylammonium chloride (CTA) and spectroscopic grade potassium bromide (KBr) were purchased from Sigma-Aldrich, Oakville, Ontario, Canada. All materials were used as received unless specified otherwise.

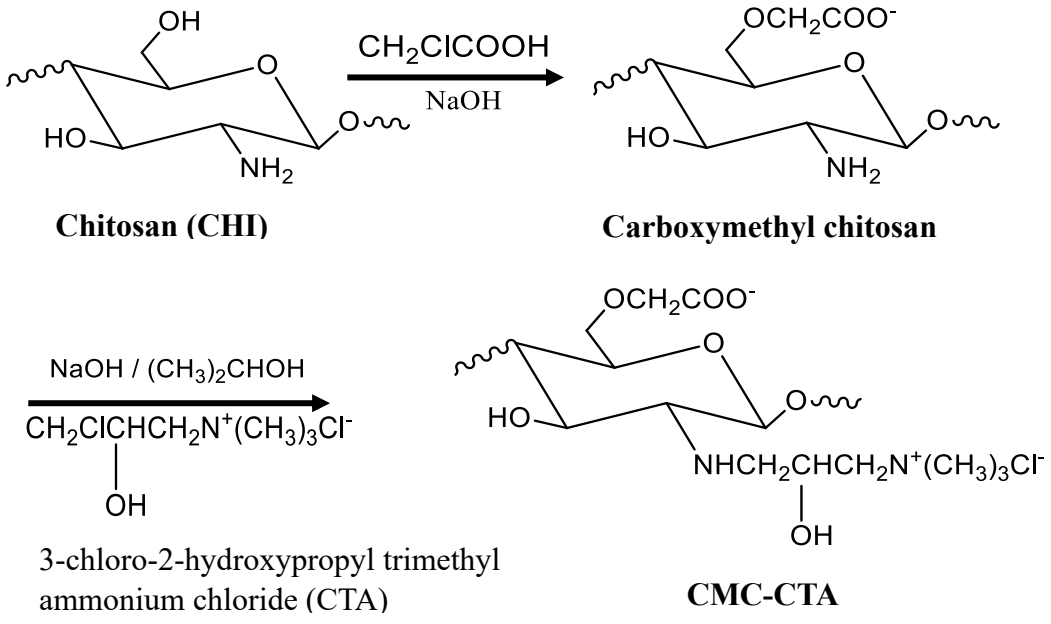

Scheme 5.1: Synthetic route of carboxymethyl chitosan (CMC) and 3-chloro-2-hydroxypropyl trimethylammonium chloride grafted onto CMC (CTA-CMC).

5.2.2 Characterization of flocculants

5.2.2.1 Preparation of CMC and CMC-CTA

The method for the synthesis of CMC and CTA was adopted from previous report and modified appropriately to suit the needs in this study.[40,41] Briefly, about 10 g of chitosan and 13.5 g of sodium hydroxide (NaOH) were added to 100 mL isopropanol. The mixture was stirred continuously until a uniform suspension was obtained and was allowed to be alkalized at 50 ^{o}C for 1 h afterward. Approximately 14.4 g of monochloroacetic acid was dissolved in 100 mL isopropanol and added dropwise. The reaction was allowed to take place for 4 h at 50 ^{o}C and quenched by adding 70% ethyl alcohol (200 mL). The solution was filtered, and the solid was rinsed with 70-90% ethyl alcohol to desalt and dewater the sample. The sample was dried in a vacuum at 25 ^{o}C. Thereafter, 1.0 g of the product was suspended in 80% ethyl alcohol aqueous solution, and then 37% HCl solution (10 ml) was added and stirred for 30 min. The suspension was filtered, and the solid was rinsed with 70–90% ethyl alcohol, followed by drying in a vacuum at 22 ^{o}C to constant weight.

In preparing the CMC-CTA, 8.0 g of CMC was added to a round-bottom flask. About 10 g of NaOH was dissolved in 75.0 mL of 2-propanol, and the solution was added to the CMC mixture in the flask. The mixture was heated up to 45 ^{o}C with constant stirring for 1.0 h until it became a viscous liquid. 3-chloro-2-hydroxypropyl trimethylammonium chloride (CTA) was added (24.0 mL) dropwise to the solution for 20 min where the temperature was fixed at 45 ^{o}C. Next, the temperature was increased to 60 ^{o}C, and the reaction was allowed to proceed for 10 h with constant mixing. The pH of the solution was adjusted to *ca* 7.0 using HCl (aq) and then filtered. The product was washed (3×) with 60 ml of methanol/water (85.0% w/w), then by 50.0 mL of ethanol (3×) and filtered, followed by drying at 80 °C. The synthetic strategy for CMC and CMC-CTA is shown in Scheme 5.1. The yields of the CMC (80.8%) and CMC-CTA (76.4%) are in good agreement with results obtained by Yang et al. for the independent synthesis of CMC-CTA.[40,41]

5.2.2.2 Degree of substitution of CMC

The degree of substitution (DS) was determined by a titrimetric method, as described by Ge et al.[42] In brief, CMC, (~0.2 g) was dissolved in 40 ml of water and the pH of the solution was adjusted to pH 2 by adding HCl. The CMC solution was then titrated with 0.1 M NaOH (aq) and the resultant pH of the solution after the addition of base was recorded. The amount of NaOH

required was determined by the second order differential method. The DS was estimated by equation (5.1).

$$DS = \frac{161 \cdot A}{m_{CMC} - 58 \cdot A} \tag{5.1}$$

$$A = V_{NaOH} \cdot c_{NaOH} \tag{5.2}$$

Here, V_{NaOH} and c_{NaOH} are the volume, at the equivalent point, and molar concentration of the aqueous NaOH, respectively, m_{CMC} is the mass of CMC (g), and 161 and 58 are the relative molecular weights (in g/mol) of glucosamine (chitosan monomer unit) and the carboxymethyl moiety.

5.2.2.3 FTIR spectroscopy

IR spectra of the materials were obtained using a Bio-RAD FTS-40 spectrophotometer. Powdered samples were mixed with pure spectroscopic grade KBr in a 1:10 (sample: KBr) weight ratio followed by grinding in a small mortar and pestle. The diffuse reflectance infrared Fourier transform (DRIFT) spectra were obtained in reflectance mode at 25 ^{o}C with a resolution of 4 cm^{-1} over the 400–4000 cm^{-1} spectral range. Multiple scans were recorded, and then background-corrected relative to pure KBr.

5.2.2.4 NMR Spectroscopy

The ^{1}H NMR spectra were recorded using a wide-bore (89 mm) 11.7 T Oxford superconducting magnet system (Bruker Bio Spin Corp; Billerica, MA, United States) equipped with a 5 mm PaTx1 probe. NMR acquisition parameters were controlled using a SSSC 500 console and workstation running X WIN-NMR 3.5. Standard pulse programs utilized were available from the TopSpin 1.3 software. The ^{13}C-NMR spectra were obtained using a Bruker AVANCE III HD spectrometer operating at 125.77 MHz (^{1}H frequency at 500.23 MHz) with a 4 mm DOTY CP-MAS probe. The ^{13}C CP/TOSS (Cross Polarization with Total Suppression of Spinning Sidebands) spectra were obtained with a spinning speed of 6 kHz with a ^{1}H 90˚ pulse of 3.5 μs, 1.0 ms contact time, and a ramp pulse on the ^{1}H channel. Acquisition of spectra utilized multiple scans (1024 - 2048) with a recycle delay of 2.0 s. All spectra were recorded using a 71 kHz SPINAL-64 decoupling sequence, where chemical shifts (δ) were referenced to adamantane (δ = 38.48 ppm).

5.2.2.5 Thermogravimetric analysis (TGA)

Thermogram profiles were obtained using a Q50 (TA instruments) with a heating rate of 5 $^{o}C \cdot min^{-1}$ to a maximum temperature of 500 ^{o}C, where nitrogen was the carrier gas. Thermal stability of the materials was shown using first derivative plots (DTG) of weight with temperature (%/^{o}C) against temperature (^{o}C) and weight (wt%) loss against temperature.

5.2.2.6 pH at the point of zero charge (pH_{pzc})

The determination of the pH at the point-of-zero-charge (pH_{pzc}) of the chitosan materials was adapted from the procedure reported by Singh et al.[43] After preparation of the NaCl solution (0.01M), 25 mL portions were added to six separate 125 ml Erlenmeyer flasks, where the pH of the solutions was adjusted between 2 and 12 with aqueous NaOH or HCl. Approximately 100 mg of the sample was added to each solution, where it was allowed to equilibrate for 48 h where the final pH was measured. The pH_{pzc} was determined as the point of intersection where the final pH and the initial pH of the solutions were plotted respectively.

5.2.3 Coagulation-flocculation process

Orthophosphate (P_i), ferric chloride and kaolinite stock solutions were prepared in deionized and distilled water. Standard solutions of CMC and CMC-CTA were prepared by dissolving in water. A standard chitosan solution was prepared with 0.01 M HCl (aq). A calibration curve of P_i was obtained using a vanadate molybdate colorimetric method at a wavelength of 420 nm, and pH 6.5.[44] The coagulation-flocculation process was carried out by an adapted procedure reported previously in Section 3.2.2 in Chapter 3. Approximately 1 L of an aqueous solution containing P_i was added to the jar tester, and 5.0 ml of the P_i solution was sampled for UV-Vis spectral analysis by adding 1.0 ml of vanadate molybdate reagent, where a yellow-colored complex formed after 20 min before recording the optical absorbance. A pre-determined volume of kaolinite solution was added to each jar solution to simulate colloidal particles in the P_i solution. The kaolinite dosage was maintained at 400 mg/L throughout, and the pH of the turbid P_i solutions was adjusted by using 0.1 M NaOH or HCl aqueous solutions, according to the conditions. A pre-determined amount of the coagulant ($FeCl_3$) was added to the solution, followed by rapid stirring for 3 min at 295 rpm. Thereafter, the stirring rate was reduced to 25 rpm for 20 min. During this period, the flocculant (chitosan, CMC or CMC-CTA) was added within the first 5 min. The stirring was stopped, and the solutions were allowed to settle for a given time before analysis. After the settling

time, a 10.0 ml solution aliquot was sampled from the top layer, and the transmittance (%T) was measured (λ= 800 nm). In addition, a 15 ml solution aliquot was sampled and centrifuged for 60 min, and then prepared for UV-Vis analysis to estimate P_i levels. The solution pH was measured after the appropriate settling period. The turbidity removal (%) and P_i removal (%) were calculated by equations (5.3) and (5.4), respectively.[44] Measurements were performed in triplicate and reported as the average value along with the standard deviation.

$$\%Turb_{removal} = \frac{T_c - T_o}{100 - T_o} \cdot 100\% \tag{5.3}$$

$$\%P_{i\,removal} = \frac{c_o - c_e}{c_o} \cdot 100\% \tag{5.4}$$

T_o and T_c are the transmittance (%T) of the turbid water before and after the CF process. The concentration values c_o and c_e refer to the P_i level before and after the CF process.

5.3 Results and Discussion

5.3.1 Characterization of flocculant materials

5.3.1.1 Degree of substitution

The degree of substitution (DS) of chitosan relates to the average number of substituted hydroxyl and amine groups per glucosamine unit. The DS value for CMC was determined using potentiometric titration because its operation is facile and reliable. Techniques such as ^{1}H-NMR and IR spectroscopy have been used for this same purpose; however, such methods require specialized sample preparation and excellent spectral resolution to achieve reliable results.[42,45] The DS value for CMC was estimated at 85.4% (Figure 5.1(a)), where the value of DS is comparable with other estimates[42,45], notwithstanding the different sources of chitosan. In determining the value of DS by equation (5.1), the mass of CMC was 0.2 g, where the molarity and volume of NaOH at the equivalent point were 0.1028 M and 32.5 ml, respectively.

5.3.1.2 FTIR spectroscopy

The IR spectra of chloroacetic acid, chitosan, CMC, and CMC-CTA are shown in Figure 5.1(b). The IR spectrum of chitosan has characteristic stretching bands at 3435 cm^{-1} for O-H, 2867 cm^{-1} for C-H, 1142 cm^{-1} for C-O-C, and 1109 cm^{-1} for C-O, and 1591 cm^{-1} for N-H bending. Similarly, the IR spectrum of CMC has O-H and C-H broad spectral bands between 2859 cm^{-1} and 3421

cm^{-1}, C-OH stretching at 1117 cm^{-1} and 1151, -COOH stretching at 1725 cm^{-1}, 1624 for an NR_4^+ group (R = H or alkyl substituent). The IR bands are characteristic of CMC, where the -COOH band at 1725 cm^{-1} supports the presence of a CM group grafted onto the chitosan backbone. The CMC-CTA spectrum has distinctive bands at 1599 cm^{-1} for –COO- group and 1471 cm^{-1} for $–CH_3$ of the quaternary ammonium group on the CTA structure, providing further support that CM and CTA groups are present in chitosan.

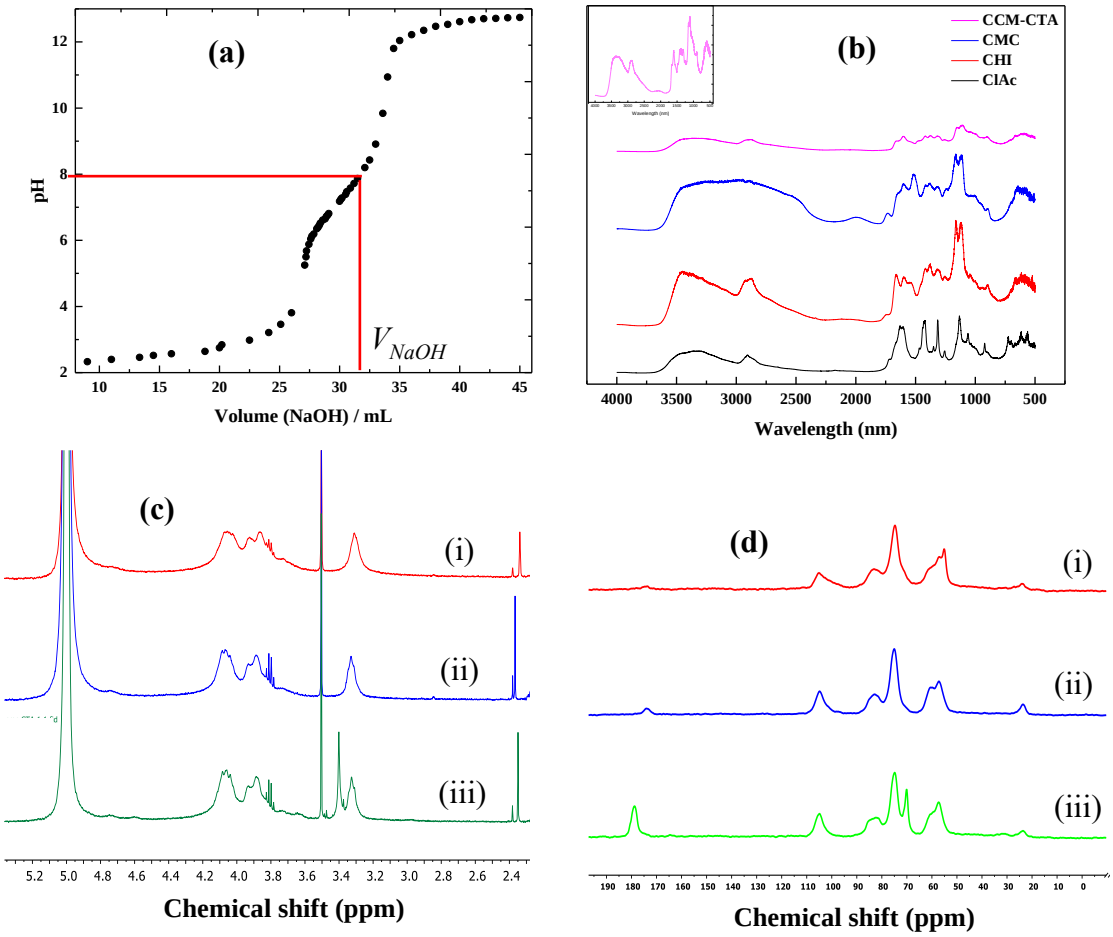

Figure 5.1: (a) Titration curve for estimation of the DS for CMC, where V_{NaOH} denotes the titrant volume of NaOH at the equivalent point (b) FT-IR spectra of chloroacetic acid (ClAc), Chitosan (CHI), CMC and CMC-CTA. The insert is an IR spectrum of CMC-CTA. (c) ^{1}H-NMR spectra of chitosan (i), carboxymethyl chitosan, CMC (ii), and CMC-CTA (iii). (d) ^{13}C-NMR of chitosan (i), carboxymethyl chitosan, CMC (ii), and CMC-CTA (iii).

5.3.1.3 NMR spectroscopy

Figure 5.1(c & d) illustrates the $^{1}H/^{13}C$-NMR spectra of CHI, CMC, and CMC-CTA. In Figure 5.1(c), chitosan showed characteristic peaks at 3.31 ppm (H2), 3.85 – 4.05 ppm (H2-H6), and 5.02 ppm (H1). The ^{1}H signatures at 3.40 and 3.94 ppm for CMC relate to methyl and CM groups, while the signature at 4.77 ppm is assigned as the H2' adjacent to the NR_4^+ group in Figure 5.1(c)iii. The signature at 2.94 ppm can be assigned to the NR_4^+ group. In the ^{13}C-NMR, signatures of chitosan at 173.4 ppm and 23.8 ppm were assigned to the carbonyl and methyl group of $COCH_3$ at C2. Signatures at 104.5, 57.0, 73.8, 82.4, 75.5, and 60.7 ppm were assigned to ^{13}C nuclei (C1-C6) of chitosan. In the spectrum of CMC, the spectral line at 177.2 ppm was assigned to –COOH. In addition, the signals at 48.2 ppm and 74.1 ppm in Figure. 1(d)iii relate to $N\text{-}CH_2$ and $–O\text{-}CH_2$, respectively. These features are indicative of carboxymethyl substitution at the hydroxyl and the amine groups of chitosan. The intense peak at 57.5 ppm in Figure 5.1(d)iii is due to the ^{13}C nuclei of the NR_4^+ group, and the signal at 74.1 ppm is attributed to the $-CH_2-$ of CM. Similar features are noted in for the $^{1}H/^{13}C$ NMR spectra for NMR for CHI, CMC, and CMC-CTA, in agreement with other reports.[36,40,41]

5.3.1.4 Thermogravimetric analysis (TGA)

TGA is a suitable method for studying the thermal stability and composition of structurally related materials, as shown for cross-linked polymers.[46] TGA provides a weight loss profile due to thermal decomposition, oxidation, or volatilization of materials, along with estimates of polymer composition when the thermal events can be resolved.[46] The TGA results herein are shown as the first derivative of mass with temperature (Figure 5.2a) and weight loss (Figure 5.2b) versus temperature, to characterize the trends for chitosan, CMC and CMC-CTA. In Figure 5.2a-b, two thermal events with weight loss profiles across the temperature range for CMC-CTA and CHI are shown, where the event below 100 ^{o}C relates to desorption of water and/or vapors, in accordance with their solvent affinity.[45] The thermal event between 200 ^{o}C and 500 ^{o}C relates to the volatilization of light hydrocarbon fragments and decomposition. In Figure 5.2(a & b), the thermal decomposition of CMC occurred at three stages: i) weight loss at *ca*. 35 ^{o}C to 240 ^{o}C due to the decomposition of the cyclic products containing cyclic olefin copolymer, ii) *ca*. 300 ^{o}C due to decarboxylation of the CMC, and iii) decomposition of $–NH_2$ groups in the form of NH_3 loss at *ca*. 305 ^{o}C to 500 ^{o}C. According to the TGA results in Figure 5.2(a & b), the onset of degradation occurs at ~296 ^{o}C, 202 ^{o}C, and 266 ^{o}C for CMC, CMC-CTA, and chitosan, respectively, in

agreement with TGA results reported elsewhere.[47] Abreu and Campana-Filho report that the thermal stability of CMC was lower than native chitosan.[36] Thermal decomposition of chitosan[32], and CMC[47] reveal that the presence of amine groups may lower the thermal stability, in agreement with Figure 5.2(a & b). This effect concurs with the reduced bond strength of heteroatom-C bonds versus C-C or C-H bonds and the role of chloride as an oxidizing agent during the thermal decomposition profile. The event for chitosan at 310 ^{o}C relates to the breakdown of the glucosamine unit, while the events at 270 ^{o}C and 410 ^{o}C relate to the decomposition of -COOH group and the glucopyranose unit of CMC.

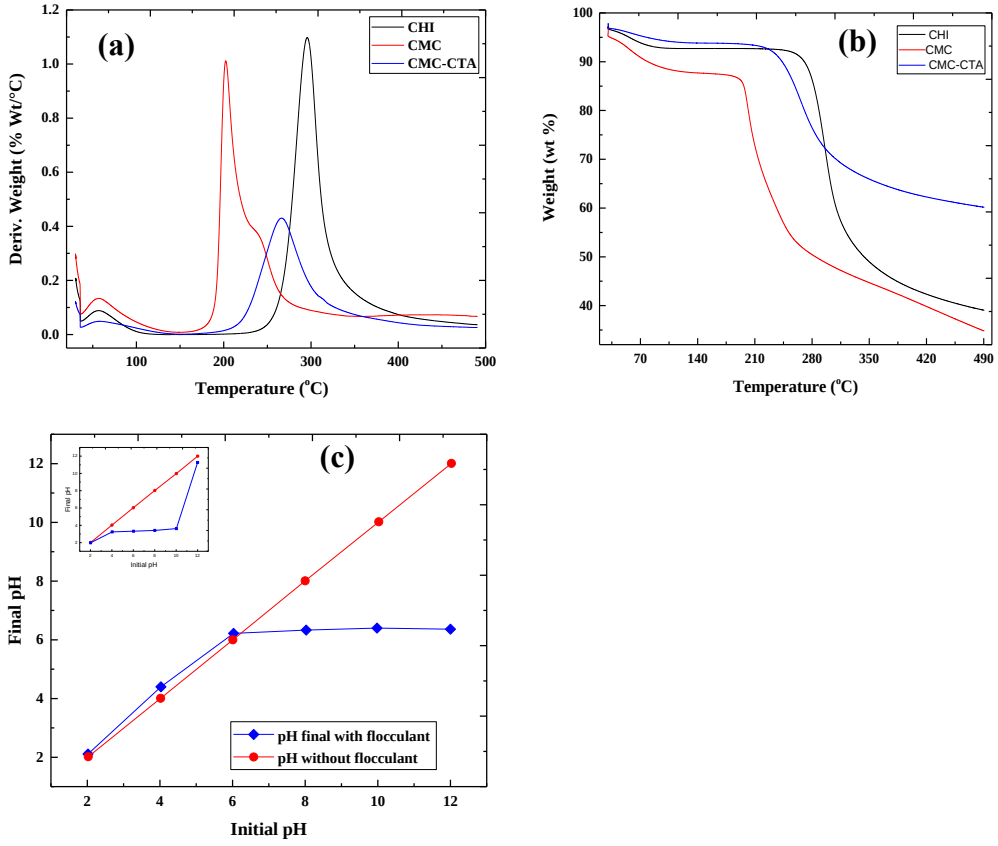

Figure 5.2: TGA profile of chitosan, carboxymethyl chitosan (CMC) and CMC-CTA: (a) First derivative of weight loss with temperature against temperature, and (b) weight loss with temperature. (c) PZC of CMC-CTA. The insert illustrates the PZC determination for CMC.

5.3.1.5 pH at the point-of-zero-charge (pH_{pzc})

The pH_{pzc} parameter indicates the pH where the net charge of a material is zero (pH_{pzc} = 0), and it provides insight on electrostatic interactions of a material surface with charged species. In the

case where pH lies below the pH_{pzc} (pH < pHp_{zc}), adsorption of OH^- ions and other anionic species occur because the ζ-potential of the sorbent is positive overall due to protonation at the surface, resulting in positively charged surface, as shown in Scheme 5.2. By contrast, the ζ-potential is negative when the solution pH > pH_{pzc}, where adsorption of cation species occurs due to deprotonation of the sorbent surface leading to negatively charged surface, as depicted in Scheme 5.2. The estimated value of pH_{pzc} (in parentheses) is listed for CMC-CTA (6.40) and CMC (3.30). Figure 5.2(c) reveals that CMC-CTA may be more suitable for the flocculation of anionic contaminants such as P_i species in wastewater, especially when pH < pH_{pcz}. In the case of CMC-CTA, the surface of the flocculant will have a positive charge when pH < 6.40. This condition favors the removal of anionic species since repulsive Coulombic effects are minimized at lower pH. In contrast, CMC has reduced flocculation at acidic pH due to greater electrostatic repulsions even though the carboxylic acid moiety is not ionized.

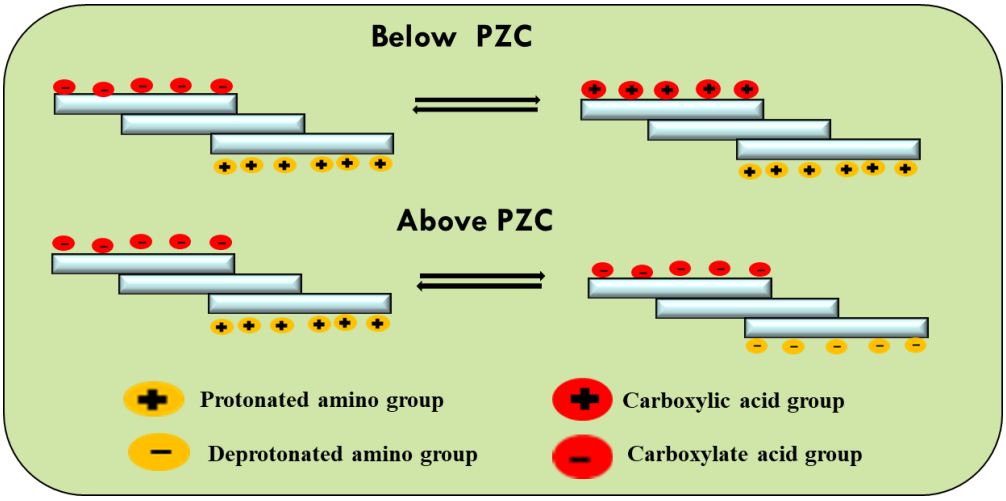

Scheme 5.2: Effect of pH on the PZC and surface charge of CMC-CTA flocculant.

5.3.2 Coagulation-flocculation

This study was aimed at a comparison of chitosan-based flocculants, with and without Fe(III) coagulant, for the co-removal of turbidity (colloidal kaolinite) and P_i species in wastewater. Estimates of the ζ-potential by Yang et al. reveal that kaolinite is negatively charged at alkaline and acidic pH.[40] Herein, the turbidity and P_i levels were addressed using ferric chloride and chitosan-based flocculant combinations in a binary and single-component systems. It will be

shown that the removal of T_i and P_i depends on several factors (flocculation dosage, initial pH, and settling time) in the following sections.

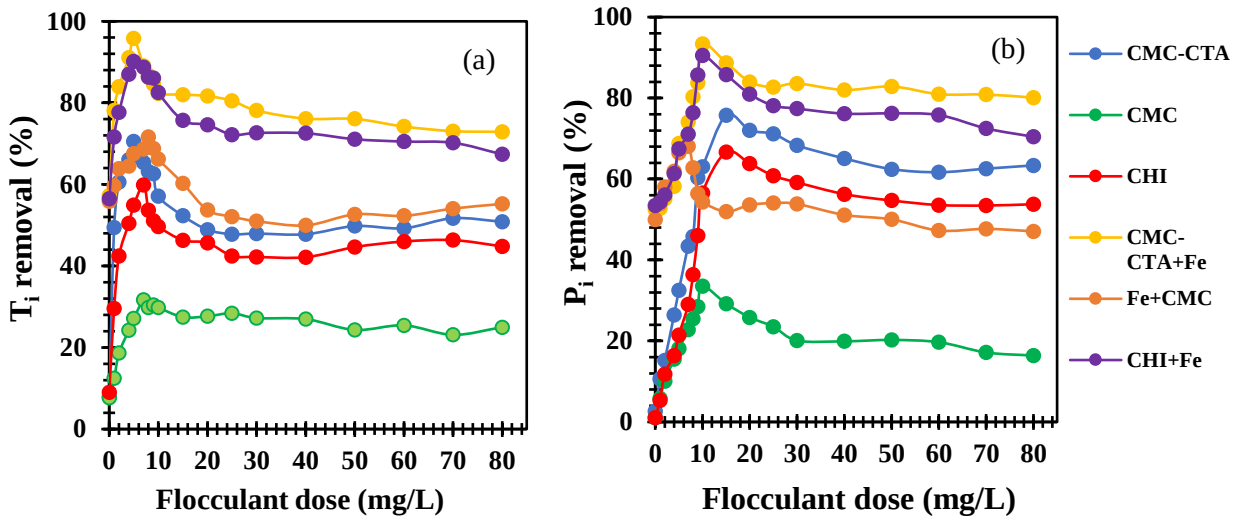

Figure 5.3: Effect of flocculant dosage with and without $FeCl_3$ coagulant for the removal of (a) turbidity and (b) phosphate. The initial concentration of kaolinite is 400 mg/L and P_i is 20 mg/L.

5.3.2.1 Effect of flocculant dosage

5.3.2.1.1 Turbidity removal

Figure 5.3(a) reports on the turbidity removal when the flocculants were used with and without $FeCl_3$ at constant pH. The solution pH was not altered and the results (Figure 5.3(a)) reveal T_i removal when the flocculants were used with and without $FeCl_3$. In the absence of ferric chloride, CMC-CTA had the highest removal (70.5%) with an optimum dosage of 5.0 mg/L. By comparison, chitosan (7.0 mg/L) and CMC (8.0 mg/L) had lower removal efficiency at 59.9% and 29.8%, respectively. The lower removal by CMC was expected since colloidal kaolinite and CMC possess a negative surface charge based on the pH_{pzc} results, contributing to electrostatic repulsion and restabilization of unbound colloidal kaolinite. The removal efficiency of the CMC (29.8%) relates to its polymer structure and flocculation properties via a bridging and ion-binding adsorption mechanism.[48] The ambient pH of the initial solution without pH adjustment ranged from 6.2 to 6.6, where protonation of CTA and CHI aided the removal of colloidal kaolinite through charge neutralization. In Figure 5.3(a), turbidity removal increased as the flocculant dosage increased up

to an optimal removal efficiency, where a decreased effect occurs at a higher dosage of each biopolymer. This trend follows an electrostatic charge neutralization mechanism since more cation species are present in the turbid water that undergo charge neutralization with negative colloidal particles as the flocculant dosage increases beyond the optimum value. Beyond the optimum flocculant dosage, precipitation of kaolinite occurs. However, the addition of excess cationic flocculant leads to restabilization due to charge reversal effects, where an excess positive charge on the aggregates and the flocs undergo repulsive interactions that lower turbidity removal.

Figure 5.3(a) illustrates the synergistic flocculation efficiency of CHI, CMC, and CMC-CTA, in combination with Fe(III), respectively. The results for CMC-CTA with $FeCl_3$ (Figure 5.3(a)) reveal the greatest turbidity removal, followed by CHI-$FeCl_3$ and CMC-$FeCl_3$ in descending order. As the flocculant dosage increases, the trend in T_i removal for the biopolymers increases up to an optimal value and decreases incrementally thereafter. The efficiency and optimal dosage of the flocculant in combination with $FeCl_3$ are given in parentheses: CMC-CTA (95.8%; 5 mg/L), CHI (88.8%; 7.0 mg/L) and CMC (68.8%; 9.0 mg/L). The presence of the Fe(III) species affect the removal efficiency of the process, where decreased turbidity removal (%) beyond the optimal dosage was attributed to the stabilization effects described above. Dey et al.[49] reported that flocculant dosage beyond the optimal level, where the density of the polymer flocculant increases in the colloidal suspension as repulsion occurs between the polymer branches. This leads to greater repulsive versus attractive interactions, where the suspended particles cannot interact favorably with groups on the flocculant, resulting in decreased T_i removal, referred to as de-flocculation.[49]

In addition, the removal efficiency of CMC-CTA was higher relative to CHI, even though protonation effects at pH 6.2 to 6.6 influence both flocculants. The presence of CTA and the carboxymethyl (CM) species on the chitosan backbone results in a size increase of the CMC-CTA flocculant and its hydrodynamic volume (V_{hyd}), in accordance with its intrinsic viscosity. The greater V_{hyd} of the biopolymer relates to its greater flocculation efficiency, in accordance with the flocculation model by Brostow et al.[50] When the polymer flocculant is added to a colloidal suspension, interaction with the colloidal particles occur and floc formation takes place by weak interaction with the polymer. The interaction between the polymer-colloidal particles will increase because of the greater V_{hyd} for CMC-CTA that leads to the rapid settling of the flocs. In addition, CMC bears a negative surface charge, where its T_i removal relates to an increase in the V_{hyd} of CMC due to the CM group and the presence of the Fe(III) species. This effect refers to an entropy-

driven process due to co-sphere overlap of hydration shells of the coagulant-flocculant-contaminant system, where desolvation provides the driving force for stabilization.

5.3.2.1.2 Phosphate removal

The presence of suspended solids influences the total P_i concentration due to surface interactions. In order to obtain low P_i residuals, the use of high coagulant dosage is often required since the P_i content associated with suspended solids is lowered. A large fraction of the precipitates formed using metal hydroxides occurs at a pH greater than 6.0. Hence, a combination of the inorganic coagulant and polymer flocculant requires a lower dosage of metal coagulant that reduces the amount of metal hydroxide formed. Figure 5.3(b) shows the effect of the flocculant dosage (with or without $FeCl_3$ coagulant) on the removal of P_i. In Figure 5.3(b), the presence of Fe^{3+} metal coagulant markedly improved the efficacy of the polymer flocculant for the removal of P_i, partly due to surface complexation mechanism. By contrast, the absence of $FeCl_3$ lowers the biopolymer removal efficiency according to the optimum flocculant dosage; CMC-CTA (75.8%, 15 mg/L), CMC (33.6%, 10 mg/L) and CHI (66.6%, 15 mg/L). The use of $FeCl_3$ in combination with the polymer flocculant led to a greater removal efficiency: 67.4% (5 mg/L CMC), 90.6% (10 mg/L CHI), and 93.4% (10 mg/L CMC-CTA). The presence of the metal coagulant led to a decrease in the optimum dosage of the polymer to achieve high P_i removal efficiency. The flocculants follow a similar trend where an increase in the removal level observed with greater biopolymer dosage until it reaches an optimum level. Thereafter, a decreased efficiency occurs that remains constant after further addition of the flocculant.

The decreasing trend in the removal efficiency (%) of P_i beyond the optimal dosage is shown in Figure 5.3(b). The effect was attributed to the stabilization of the P_i solution, in agreement with a parallel study.[51] As the $FeCl_3$ dosage increases, the pH shifts to an unfavorable range for P_i removal, leading to a decreased efficiency. The role of $FeCl_3$ and P_i in wastewater likely involves complex formation via surface complexation model and charge stabilization with an unclear flocculation mechanism proposed thus far in the literature. $FePO_4(s)$ is an insoluble product formed when $FeCl_3$ combines with P_i, equation (5.5), in agreement with a report by Jenkins et al.[52] Iron phosphate undergoes precipitation due to complex formation between Fe(III) and hydroxide species that is thermodynamically and kinetically favored.

$$Fe_3(PO_4)_2 \cdot (H_2O)_{14\,(aq)} + 2\ PO_4^{3-}{}_{(aq)} \rightarrow 3\ FePO_{4(s)} \downarrow + PO_4^{3-}{}_{(aq)} + 14\ H_2O_{(l)} \qquad (5.5)$$

Herein, the average dosage of coagulant ($FeCl_3$) at optimum condition was 12.5 mg/L with an initial P_i dose (25 mg/L). This level of $FeCl_3$ dosage is lower than other reported values. Mohammed and Shanshool[20] report an optimal dosage of $FeCl_3$ at 80 mg/L, Ebeling et al.[53] report 90 mg/L, and Banu et al.[54] report 80 mg/L, where further addition of the flocculant results in decreased P_i removal efficiency. As the dosage of the flocculant increased beyond the optimum dosage, precipitation of dissolved P_i occurred. The addition of excess flocculant led to re-stabilization of positively charged colloidal species with a corresponding reduction in P_i removal. An increase in the flocculant dosage beyond the optimal value leads to an increase in the amount of cationic charge species in the solution. A minimum level of cation species is required to neutralize the P_i anion species. The charge neutralization process may relate to the agglomeration of the P_i containing particulates by a bridging mechanism with eventual settling of the floc. However, a reverse effect occurs when excess cations are present. The excess positive charge stabilizes the neutral aggregates containing P_i while the macroflocs undergo repulsive interactions, resulting in a progressive decrease in the P_i removal efficiency. Similar results were reported elsewhere.[55,56]

Guibal et al. reported on the effectiveness of chitosan-based flocculants for the removal of suspended and dissolved substances in a homogeneous solution.[57] This relates to the greater accessibility of the amine groups for dissolved flocculant since it improves the solvent accessibility and kinetics of the process due to improved ionization and biopolymer hydration.[57] Homogeneous dissolution of species displays rapid kinetics of mixing (mass transfer) over solid flocculant forms. It is known that P_i and other structurally related oxyanions such as arsenate have favorable affinity to form complexes with chitosan and its modified forms.[14,15,24,28,29,58] The effect relates to the role of charge neutralization as a key step in coagulation and/or flocculation processes, followed by polymer bridging, in agreement with results obtained herein.

The influence of CMC dose on the removal of P_i, with and without $FeCl_3$ coagulant, is shown in Figure 5.3(b). The use of CMC alone showed poor P_i removal efficiency. CMC and P_i are anionic species at these conditions, where electrostatic repulsion and stabilization occurs with unbound P_i in solution. However, the polymer nature of CMC favors the removal of P_i by a bridging and ion-binding mechanism, especially in combination with a coagulant, as shown by the greater removal of P_i when CMC is used along with $FeCl_3$.

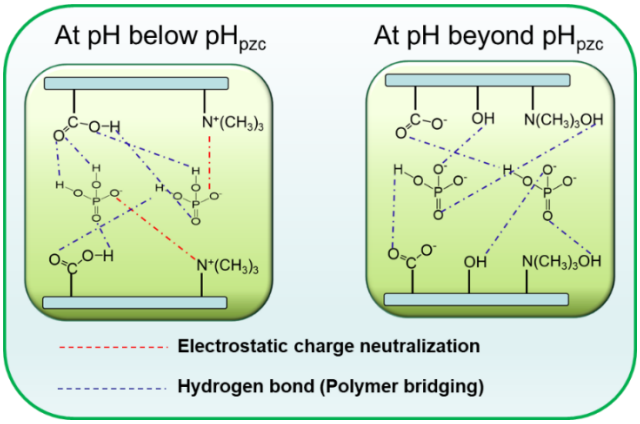

Scheme 5.3: Interaction between phosphate and CMC-CTA flocculant.

5.3.2.2 Effect of pH

5.3.2.2.1 Turbidity

Figure 5.4(a-c) illustrates the flocculation efficiency of CMC-CTA CHI and CMC for the removal of colloidal particles at variable pH and flocculant dosage. Chitosan-based flocculants were used in combination with $FeCl_3$ at a fixed dosage (12.5 mg/L), where the initial pH of the solutions was adjusted using 0.01M HCl or NaOH solutions. The results show that greater turbidity removal efficiency at pH values below 7, where optimum removal occurs at pH 6.0 for CMC and pH 4.0 for CHI and CMC-CTA, in accordance with the results obtained by Yang et al.[40,41] for amphoteric flocculants. At pH 4.0, the optimal T_i removal efficiency occurs for CHI (98.3%) and CMC-CTA (99.2%), while a maximum removal efficiency for CMC (70.3%) occurs at pH 6. Turbidity removal has a strong dependence on the relative dose of the flocculant due to its cationic nature. Above pH 6.0, the coagulant and flocculant properties of $FeCl_3$ decrease, in agreement with the critical role of charge neutralization in the T_i removal over the sweep mechanism.

Coagulation of the kaolinite colloidal species by charge neutralization may take place by adsorption of the Fe(III) species and its hydrolysis by-products, HFO, $Fe(OH)_2^+$ and $Fe(OH)^{2+}$. The desorption of neutral precipitates such as $Fe(OH)_3$ onto the negatively charged kaolinite surface contributes to lower repulsive interactions for the kaolinite suspension. At pH >7, the sweep coagulation mechanism is considered as a driving force to reduce the Gibbs energy of the system as there are no other cationic Fe-hydroxyl species present. As well, the surface charge of the $Fe(OH)_3$ lies very close to the isoelectric point or at even more negative values for these pH

conditions. In addition, the dissolution of $Fe(OH)_3$ precipitates results in the formation of complexes such as $[Fe(OH)_4]^-$ that contribute to increased colloidal stability of kaolinite. At this alkaline pH, CMC-CTA, CMC, and CHI undergo deprotonation and become negatively charged, leading to electrostatic repulsion with decreased T_i removal.[59] In Figure 5.4, the flocculation effect of CTA is notably greater than CHI at high pH (pH > 7) even though both undergo deprotonation at this condition. At pH 10, the maximum T_i removal efficiency of CMC-CTA and CHI is 72.7% and 34.3%, respectively. The offset in values relates to an increase in the polymer size and V_{hyd} since CTA is grafted onto the CMC backbone to form CMC-CTA. Previous studies have shown that the structure and charge state (cation, anion, or amphoteric) of a polymer flocculant in solution strongly influences its flocculation efficiency.[60]

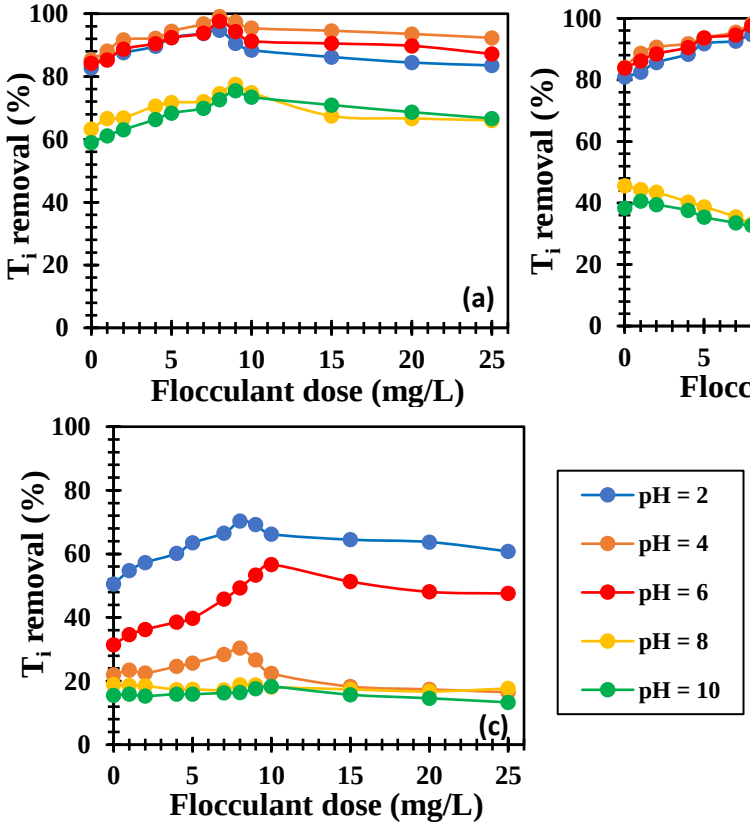

Figure 5.4: Turbidity removal efficiency at different pH values: (a) CMC-CTA (b) CHI and (c) CMC. The initial concentration of kaolinite was 400 mg/L.

5.3.2.2.2 Phosphate removal

Figure 5.5 depicts the effect of pH on the removal efficiency of P_i at variable biopolymer dosage and a fixed level of $FeCl_3$. As seen in Figure 5.5, improved P_i removal occurs at pH 4, where minimum removal occurs at pH 10. Optimal removal of P_i by Fe^{3+} occurs at an optimum pH of 4.0-5.5[61] since Fe(III) in phosphate solution results in $FePO_4$ formation at pH < 6.5. At pH > 6.5, iron converts to oxides and hydroxides. While $FePO_4$ has low solubility at the optimum pH obtained in this study, the P_i removal reaches a constant value *ca*. 30 min for all pH values (Figure 5.5a-c). The solubility of $FePO_4$ increases at greater pH[61]; whereas, P_i removal rose slightly above these high pH levels. $Fe(OH)_3$ and $Fe(OH)_4^-$ are present over this pH range since $[Fe(OH)_4]^-$ complexes have greater water solubility. It can be concluded that P_i removal occurs via complex formation of $FePO_4$ and $Fe(OH)_3$; however, $FePO_4$ formation is favored at lower pH.[1,2] At pH 10, $Fe(OH)_4^-$ is a major dissolved iron species, in agreement with the decreased removal observed.

At pH < pH_{PZC}, CMC-CTA and CHI are cationic species while CMC is anionic in nature, where precipitates of $FePO_4$ are formed in the presence of P_i solution and Fe(III). The polymer flocculants form cross-linked aggregates that enhance P_i removal via precipitation of $FePO_4$, along with related adsorption effects, as shown in Scheme 5.3. The influence of pH on the P_i removal follows a similar trend that is independent of the initial P_i dosage, where the efficiency increased from pH 2 to an optimum value near pH 4. Thereafter, the efficiency decreased as the alkalinity increased to pH 10. As $FeCl_3$ is added to the P_i-containing-water, where a fractional amount of $FeCl_3$ precipitates as the hydroxide form and H_3O^+ was released according to equation (5.6). The Fe^{3+} ions are soluble below pH 5.5 and do not precipitate during the dissolution process. In addition, iron phosphate ($FePO_4$) species are formed which are soluble at pH 6 to 7.[62] Above pH 7, the addition of $FeCl_3$ forms a soluble complex ($[Fe(OH)_4]^-$), lowering the efficiency of the coagulation-flocculation process.[63]

$$Fe^{3+}_{(aq)} + 3\ H_2O_{(l)} \rightarrow Fe(OH)_{3(s)} \downarrow + 3\ H^+_{(aq)} \qquad (5.6)$$

P_i removal has a strong dependence on the dosage of flocculant (CHI and CMC-CTA) due to its cationic nature. The amine groups of the chitosan-based flocculants are deprotonated at higher pH values, especially at conditions above pH 6.5 since the pK_a value of chitosan is *ca.* 6.2, as shown in Scheme 5.3. Chitosan does not associate favorably with phosphate via attractive ion-ion interactions at these conditions, however, through polymer bridging by forming several hydrogen

bonds between the hydroxyl groups of the phosphate and the flocculant. By contrast, attractive ion-ion interactions occur below pH 6.5 due to the association of chitosan/phosphate via Coulombic attraction, as illustrated in Scheme 5.3. Excess chitosan (cation form) in solution may result in colloidal stabilization at lower pH.

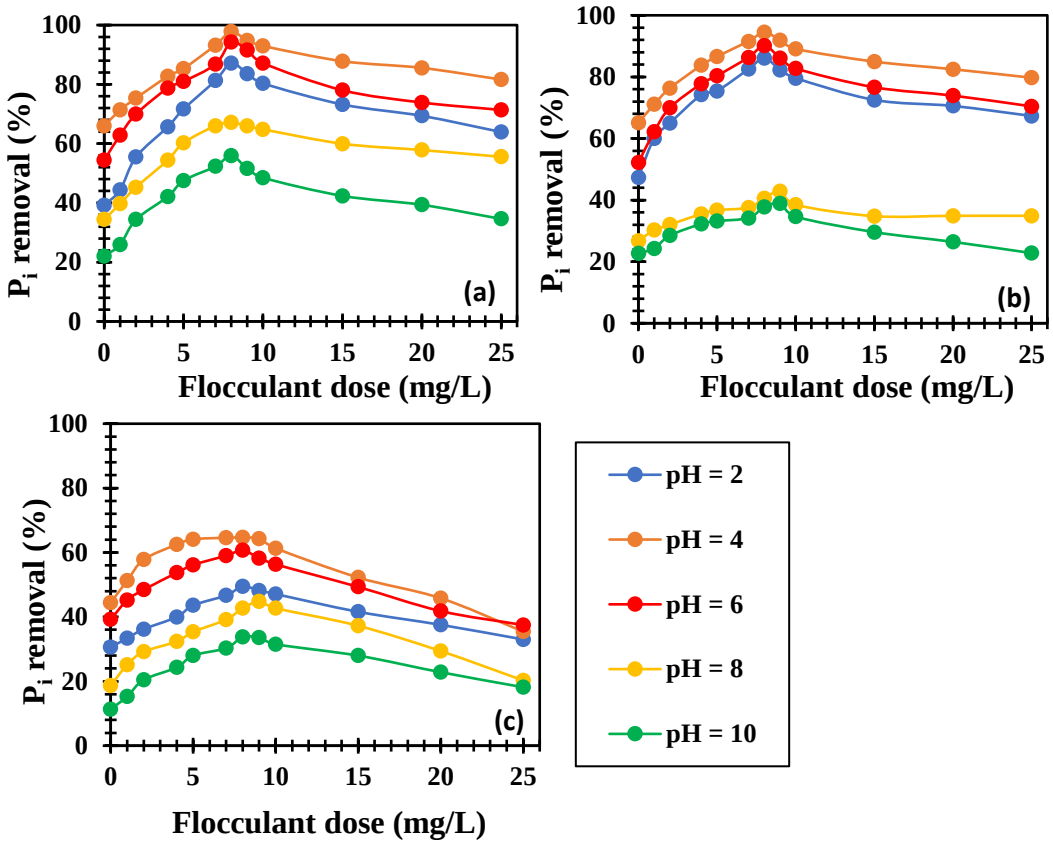

Figure 5.5: Effect of pH on the removal of P_i at variable flocculant dosage; (a) CMC-CTA (b) CHI and (c) CMC, where the initial concentration of P_i is 25 mg/L.

5.3.2.3 Effect of settling time

Coagulation uses rapid mixing that disperses coagulant in a wastewater solution to form microflocs, while flocculation involves slow mixing and addition of polymer flocculant to wastewater, aggregation of the microflocs form macroflocs which can be settled and filtered.[64,65] During the CF process, adequate time is needed to form flocs that are large enough to allow efficient removal by sedimentation in accordance with Stoke's law.[66] Figure 5.6 reveals the effect of settling time on the T_i and P_i removal efficiency using CMC, CHI and CMC-CTA at their optimal dosage values. The process was carried out using a variable time sequence: (i) fast mixing

at 295 rpm for 3 min after addition of the coagulant to the wastewater; (ii) slow mixing at 20 rpm for 25 min after addition of the polymer flocculant; and (iii) sedimentation at different times (1 to 60 min) to allow floc settling. After the desired settling time, an aliquot of the supernatant was sampled and prepared for T_i and P_i measurement by UV-Vis absorbance (λ = 800 nm). Figure 5.6 shows the effect of settling time on T_i and P_i removal, where the supernatant turbidity using the various flocculants show a decrease as settling time increases. In Figure 5.6, the flocs quickly settle out within the first 30 min with little or no change in the flocculation efficiency after the first 30 min and reveal that the flocculant properties do not improve for a settling time > 30 min. CTA and CHI show favorable removal due to the cationic amine group.

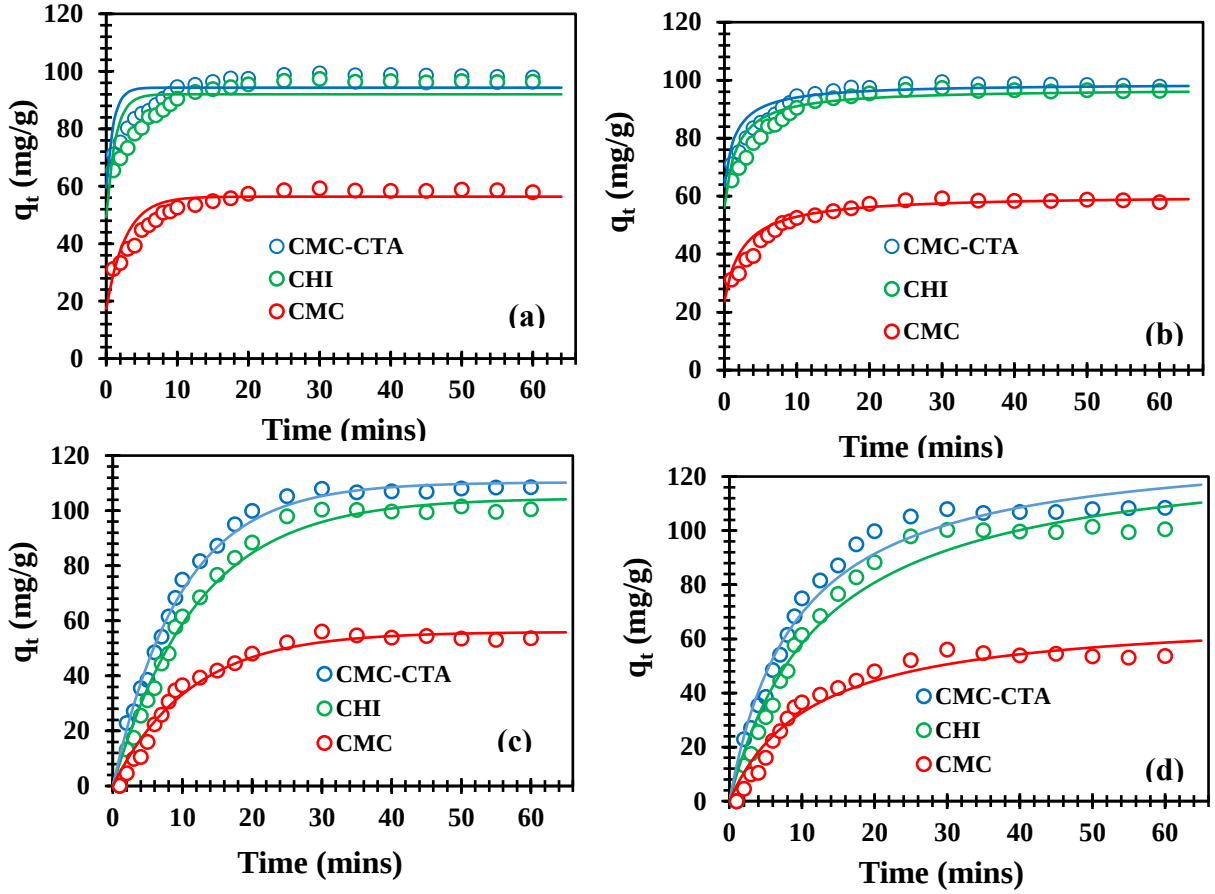

Figure 5.6: Flocculation kinetic profiles for turbidity and P_i removal at a variable time interval, where c_o for P_i is 25.0 mg/L, and T_i is 400 mg/L. Turbidity removal (a, b) and P_i removal (c, d) according to the PFO and PSO kinetic models, respectively.

The flocculation process is divided into three regions, according to Figure 5.6. In the first region, a rapid increase in flocculation occurs up to 15 min, where it increases steadily up to 30 min, where a dynamic equilibrium is reached beyond 30 min. The process in the first region occurs because of electrostatic interaction between the P_i or kaolinite particles with the Fe(III) species, leading to a charge neutralization process. P_i is negatively charged and becomes neutralized upon interaction with a Fe(III) cation. Fe(III) species may act as a cross-linker with the polymer via complex formation with functional groups of the polymer to form a gel phase leading to further adsorption of T_i and/or P_i.[67,68] In the second region, a gradual increase in the flocculation efficacy occurs because of a reduced effective cation charge on the floc surface. The third region illustrates that the dynamic equilibrium for the floc formation is 30 min. Similar effects for the removal of P_i using alginate-based flocculants were reported in Chapter 4.

The kinetics of the flocculation process was studied at the optimum conditions. The adsorption kinetics of P_i and T_i with the $FeCl_3$/flocculant system was investigated by the PFO and PSO models. The PSO model assumes that the sorption rate decreases linearly as the adsorption rate increases.[69] The PSO model assumes that the rate-limiting step involves interaction between the adsorbent (flocculant) and adsorbate (P_i or turbidity) that is often used to describe chemisorption.[70] The PFO and PSO models are described by equation (5.7) and (5.8), respectively.

$$q_t = q_e(1-e^{-k_1 t}) \tag{5.7}$$

$$q_t = \frac{k_2 q_e^{\,2} t}{1+k_2 q_e t} \tag{5.8}$$

Here, q_e and q_t are the levels of P_i or kaolinite particles adsorbed (mg/g) at dynamic equilibrium and at time t. k_1 and k_2 are the respective rate constants, where the parameters (k_1, k_2, and q_e) were estimated using non-linear regression fitting by equations (5.7) and (5.8). The "best fit" criterion between the experimental data and the kinetic models was determined by the minimization of the absolute sum of squares of errors (SSE) by equation (5.9).

$$SSE = \sum \sqrt{\frac{(q_{e,i} - q_{c,i})^2}{N}} \tag{5.9}$$

Here, $q_{e,i}$ is the experimental value and $q_{c,i}$ is the calculated or predicted value, according to the kinetic model, and N is the number of experimental data points.

Table 5.1: Pseudo-First-Order (PFO) and Pseudo-Second-Order (PSO) kinetic parameters for Turbidity and P_i removal at optimized flocculation conditions. c_o (Turb) = 400.0 mg/L and c_o (P_i) = 25.0 mg/L

Parameter	CMC	CHI	CMC-CTA
	PFO kinetic model (turbidity removal)		
$\mathbf{q_t\ (mg{\cdot}g^{-1})}$	56 ± 1	92 ± 2	94 ± 1
$\mathbf{k \cdot 10^3\ (min^{-1})}$	369 ± 7	767.9 ± 10	997 ± 13
$\mathbf{R^2}$	0.920	0.909	0.927
	PSO kinetic model (turbidity removal)		
$\mathbf{q_t\ (mg{\cdot}g^{-1})}$	60 ± 1	97 ± 1	99 ± 1
$\mathbf{k \cdot 10^3\ (g{\cdot}mg^{-1}{\cdot}min^{-1})}$	11 ± 1	14 ± 1	18 ± 2
$\mathbf{R^2}$	0.978	0.980	0.985
	PFO kinetic model (P_i removal)		
$\mathbf{q_t\ (mg{\cdot}g^{-1})}$	56 ± 1	104.6 ± 2	110 ± 1
$\mathbf{k \cdot 10^3\ (min^{-1})}$	90.3 ± 6.1	83 ± 4	103 ± 4
$\mathbf{R^2}$	0.974	0.987	0.990
	PSO kinetic model (P_i removal)		
$\mathbf{q_t\ (mg{\cdot}g^{-1})}$	70 ± 3	132 ± 2	134 ± 6
$\mathbf{k \cdot 10^3\ (g{\cdot}mg^{-1}{\cdot}min^{-1})}$	1 ± 0.2	0.6 ± 0.1	0.8 ± 0.1
$\mathbf{R^2}$	0.951	0.967	0.969

The results of the flocculation of P_i and turbidity by the $FeCl_3$/flocculant system are shown in Figure 5.6(a–d), where the lines represent the best-fit results for PFO and PSO models. Figure 5.6 (a, b) describe the flocculation kinetics for T_i removal, where Figure 5.6(c, d) represents the flocculation kinetics for P_i removal. In Figure 5.6, the T_i and P_i removal are well-described by each kinetic model, according to the values of the parameters listed in Table 5.1. In terms of the kinetics of the T_i removal, the results are in good agreement with the PSO model according to the best fit results in Table 5.1. However, in the case of the flocculation kinetics of P_i, the PFO model shows greater agreement over the PSO model (*cf.* Table 5.1). In addition, the predicted values of q_e determined by the PSO model agree well with experimental values, as compared with the PFO kinetic model for turbidity removal. However, the opposite was observed for P_i removal, where the best-fit values of q_e obtained from the PFO model agree more with the experimental values over the PSO model. The rate constant of the PFO (k_1) model is significantly greater than the PSO (k_2) model for the turbidity removal process, and the opposite is true for the P_i removal process. The PFO adsorption mechanism describes the flocculation of P_i by $FeCl_3$/flocculant system, according to the PFO model. This indicates that the P_i species are adsorbed by the flocculant system, where the rate decreases linearly as the adsorption rate increases. Similar results were

reported for the flocculation of anionic dyes and arsenates with polysaccharide-based flocculants.[71–73] The kinetic study herein showed that the PSO model described the flocculation process for turbidity removal. The analysis of kinetic parameters indicates the rate-limiting-step for the flocculation involves interaction between the flocculant and the anionic colloidal kaolinite, in accordance with a chemisorption-like process. The results herein show that there is favorable interaction between the outer surface sites of the flocculant system and P_i and/or kaolinite anion species due to the rapid equilibrium process at 30 min (Figure 5.6).

5.4 Conclusions

An amphoteric flocculant (CMC-CTA) was prepared from chitosan by grafting 3-chloro-2-hydroxypropyl trimethylammonium chloride (CTA) onto carboxymethyl chitosan (CMC). The structure of CMC-CTA was supported by various characterization methods. The dual removal of turbidity (T_i) and orthophosphate (P_i) by flocculation was studied using CMC-CTA, CHI, and CMC, with and without $FeCl_3$ coagulant. The removal efficiency of P_i and T_i using the flocculant with $FeCl_3$ in a binary system was much greater than in the absence of Fe(III) in a single-component system. CMC-CTA showed greater flocculation over CHI and CMC at all pH conditions, especially at the optimal pH 4, where the T_i (99.2%) and P_i (97.8%) removal was favored. Flocculation processes are governed by charge neutralization, followed by polymer bridging and adsorption mechanisms. The flocculation kinetics for P_i and T_i removal are well-described by the pseudo-first-order (PFO) and pseudo-second-order (PSO) models. The rate-limiting-step for T_i removal involves interactions between the flocculant and the kaolinite species, in agreement with a chemisorption-like process, while P_i removal is considered as a physisorption-like process. The CMC-CTA flocculant/Fe(III) system affords the use of acidic (pH 4) conditions for effective removal of T_i and P_i, where this study is anticipated to catalyzed future research and expand the scope of wastewater treatment using non-conventional conditions.

5.5 References

(1) Irdemez, S.; Demircio, N.; Yildiz, Y. S.; Bingul, Z. *Sep. Purif. Technol.* **2006**, *52*, 218–223.

(2) Irdemez, S.; Demircio, N.; Yildiz, Y. S. *J. Hazard. Mater.* **2006**, *137*, 1231–1235.

(3) Tran, N.; Drogui, P.; Blais, J.-F.; Mercier, G. *Sep. Purif. Technol.* **2012**, *95*, 16–25.

(4) Yeoman, S.; Stephenson, T.; Lester, J. N.; Perry, R. *Environ. Pollut.* **1988**, *49* (3), 183–233.

(5) Rybicki, S. *Phosphorus Removal From Wastewater - A Literature Review*; 1997.

(6) Némery, J.; Garnier, J. *Nat. Geosci.* **2016**, *9* (5), 343–344.

(7) Benyoucef, S.; Amrani, M. *Desalination* **2011**, *275* (1–3), 231–236.

(8) Attour, A.; Touati, M.; Tlili, M.; Amor, M. Ben; Lapicque, F.; Leclerc, J. *Sep. Purif. Technol.* **2014**, *123*, 124–129.

(9) Golder, A. K.; Samanta, A. N.; Ray, S. *Sep. Purif. Technol.* **2006**, *52*, 102–109.

(10) Tanada, S.; Kabayama, M.; Kawasaki, N.; Sakiyama, T.; Nakamura, T.; Araki, M.; Tamura, T. *J. Colloid Interface Sci.* **2003**, *257* (1), 135–140.

(11) Vasudevan, S.; Lakshmi, J.; Jayaraj, J.; Sozhan, G. **2009**, *164*, 1480–1486.

(12) Filipkowska, U.; Jóźwiak, T.; Szymczyk, P. *Prog. Chem. Appl. Chitin its Deriv.* **2014**, *19* (1), 5–14.

(13) Mahaninia, M. H.; Wilson, L. D. *J. Colloid Interface Sci.* **2017**, *485*, 201–212.

(14) Mahaninia, M. H.; Wilson, L. D. *Ind. Eng. Chem. Res.* **2017**, *56* (7), 1704–1712.

(15) Mahaninia, M. H.; Wilson, L. D. *Ind. Eng. Chem. Res.* **2016**, *55* (45), 11706–11715.

(16) Sathasivan, A. In *Encyclopedia of life support systems*; McGraw Hill Professional, 2010; pp 1–16.

(17) Gautam, R. K.; Banerjee, S.; Gautam, P. K.; Chattopadhyaya, M. C. *Adv. Environ. Res.* **2014**, *36*, 1–23.

(18) Peleka, E. N.; Mavros, P. P.; Zamboulis, D.; Matis, K. a. *Desalination* **2006**, *198* (1–3), 198–207.

(19) Dunets, C. S.; Zheng, Y. *Hortscience* **2015**, *50* (6), 921–926.

(20) Mohammed, S. A. M.; Shanshool, H. A. *Iraqi J. Chem. Pet. Eng.* **2009**, *10* (2), 35–42.

(21) Quinlan, P. J.; Tanvir, A.; Tam, K. C. *Carbohydr. Polym.* **2015**, *133*, 80–89.

(22) Tripathy, T.; De, B. R. *J. Phys. Sci.* **2006**, *10*, 93–127.

(23) Yuan, B.; Shang, Y.; Lu, Y.; Qin, Z.; Jiang, Y.; Chen, A.; Qian, X.; Wang, G.; Yang, H.; Cheng, R. *J. Appl. Polym. Sci.* **2010**, *117* (I), 1876–1882.

(24) Renault, F.; Sancey, B.; Badot, P. M.; Crini, G. *Eur. Polym. J.* **2009**, *45* (5), 1337–1348.

(25) Tzoupanos, N. D.; Zouboulis, A. I. *6th IASME/WSEAS Int. Conf. HEAT Transf. Therm. Eng. Environ.* **2008**, 309–317.

(26) Sharma, B. R.; Dhuldhoya, N. C.; Merchant, U. C. *J. Polym. Environ.* **2006**, *14* (2), 195–202.

(27) Zemmouri, H.; Drouiche, M.; Sayeh, A.; Lounici, H.; Mameri, N. *Energy Procedia* **2013**,

36, 558–564.

(28) Asere, T. G.; Mincke, S.; De Clercq, J.; Verbeken, K.; Tessema, D. A.; Fufa, F.; Stevens, C. V.; Du Laing, G. *Int. J. Environ. Res. Public Health* **2017**, *14* (8), 1–19.

(29) Mahaninia, M. H.; Wilson, L. D. *J. Colloid Interface Sci.* **2017**, *485*, 201–212.

(30) Bratskaya, S. Y.; Pestov, A. V; Yatluk, Y. G.; Avramenko, V. A. *Colloids Surfaces A Physicochem. Eng. Asp.* **2009**, *339*, 140–144.

(31) Fortin–Chevalier, T.; Leduc, R. *Int. J. Environ. Waste Manag.* **2014**, *14* (4), 358–375.

(32) Holme, H. K.; Foros, H.; Pettersen, H.; Dornish, M.; Smidsrùd, O. *Carbohydr. Polym.* **2001**, *46*, 278–294.

(33) Rojas-Reyna, R.; Schwarz, S.; Heinrich, G.; Petzold, G.; Schutze, S.; Bohrisch, J. *Carbohydr. Polym.* **2010**, *81* (2), 317–322.

(34) Zhang, W.; Shang, Y.; Yuan, B.; Jiang, Y.; Lu, Y.; Qin, Z.; Chen, A.; Qian, X.; Yang, H.; Cheng, R. *J. Appl. Polym. Sci.* **2010**, *117*, 2016–2024.

(35) Wang, J.; Chen, Y.; Yuan, S.; Sheng, G.; Yu, H. *Water Res.* **2009**, *43* (20), 5267–5275.

(36) Abreu, F. R. De; Campana-Filho, S. P. *Carbohydr. Polym.* **2009**, *75* (2), 214–221.

(37) Ali, S. A.; Singh, R. P. *Macromol. Symp.* **2009**, *277*, 1–7.

(38) Cai, Z.; Song, Z.; Shang, S.; Yang, C. *Polym. Bull.* **2007**, *59*, 655–665.

(39) Li, S.; Zhou, P.; Yao, P.; Wei, Y.; Zhang, Y.; Yue, W. *J. Applied Polymer Sci.* **2010**, *116*, 2742–2748.

(40) Yang, Z.; Shang, Y.; Huang, X.; Chen, Y.; Lu, Y.; Chen, A.; Jiang, Y.; Gu, W.; Qian, X.; Yang, H.; Cheng, R. *J. Environ. Sci. (China)* **2012**, *24* (8), 1378–1385.

(41) Yang, Z.; Shang, Y.; Lu, Y.; Chen, Y.; Huang, X.; Chen, A.; Jiang, Y.; Gu, W.; Qian, X.; Yang, H.; Cheng, R. *Chem. Eng. J.* **2011**, *172*, 287–295.

(42) Ge, H. C.; Luo, D. K. *Carbohydr. Res.* **2005**, *340* (7), 1351–1356.

(43) Singh, J.; Mishra, N. S.; Uma; Banerjee, S.; Sharma, Y. C. *BioResources* **2011**, *6* (3), 2732–2743.

(44) Patel, H.; Vashi, R. T. *J. Saudi Chem. Soc.* **2012**, *16* (2), 131–136.

(45) Bidgoli, H.; Zamani, A.; Taherzadeh, M. J. *Carbohydr. Res.* **2010**, *345* (18), 2683–2689.

(46) Mohamed, M. H.; Wilson, L. D.; Headley, J. V. *Carbohydr. Res.* **2011**, *346* (2), 219–229.

(47) Kittur, F. S.; Prashanth, K. V. H.; Sankar, K. U.; Tharanathan, R. N. *Carbohydr. Polym.* **2002**, *49*, 185–193.

(48) Bhalkaran, S.; Wilson, L. D. *Int. J. Mol. Sci.* **2016**, *17* (10), 1662–1881.

(49) Dey, K. P.; Mishra, S.; Sen, G. *J. Water Process Eng.* **2017**, *18*, 113–125.

(50) Brostow, W.; Pal, S.; Singh, R. P. *Mater. Lett.* **2007**, *61*, 4381–4384.

(51) Ahmad, A. L.; Sumathi, S.; Hameed, B. H. *Chem. Eng. J.* **2006**, *118* (1–2), 99–105.

(52) Jenkins, D.; Ferguson, J.; Menar, A. *Water Res.* **1971**, *5*, 369–389.

(53) Ebeling, J. M.; Sibrell, P. L.; Ogden, S. R.; Summerfelt, S. T. *Aquac. Eng.* **2003**, *29* (1–2), 23–42.

(54) Banu, R. J.; Do, K. U.; Yeom, I. T. *Int. J. Environ. Sci. Technol.* **2007**, *5* (1), 93–98.

(55) Roussy, J.; Van Vooren, M.; Guibal, E. *J. Dispers. Sci. Technol.* **2005**, *25* (5), 663–677.

(56) Huang, C.; Chen, Y. *J. Chem. Technol. Biotechnol.* **1996**, *66* (3), 227–232.

(57) Guibal, E.; Van Vooren, M.; Dempsey, B. A.; Roussy, J. *Sep. Sci. Technol.* **2006**, *41* (11), 2487–2514.

(58) Bhalkaran, S.; Wilson, L. D. *Int. J. Mol. Sci.* **2016**, *17* (10).

(59) Ersoy, B.; Tosun, I.; Gunay, A.; Dikmen, S. *Clean* **2009**, *37* (3), 225–232.

(60) Qian, J. W.; Xiang, X. J.; Yang, W. Y.; Wang, M.; Zheng, B. Q. *Eur. Polym. J.* **2004**, *40*, 1699–1704.

(61) Eilbeck, W. J.; Mattock, G. *Chemical Processes in Waste Water Treatment*; John-Wiley and Sons: West Sussex, 1987.

(62) Sedlak, R. I. *Phosphorus and nitrogen removal from municipal wastewater*, Second.; Lewis Publishers: New York, USA, 1991.

(63) Teh, C. Y.; Wu, T. Y.; Juan, J. C. *Ind. Crops Prod.* **2014**, *56*, 17–26.

(64) Hameed, Y. T.; Idris, A.; Aslina, S. *J. Environ. Manage.* **2016**, *184*, 494–503.

(65) Rajasulochana, P. *Resour. Technol.* **2016**, *2* (4), 175–184.

(66) Jadhav, M. V.; Mahajan, Y. S. *KSCE J. Civ. Eng.* **2013**, *17* (2), 328–334.

(67) Rezende, R.; Bártolo, P.; Mendes, A.; Filho, R. *8th Int. Conf. Chem. Process Eng.* **2007**, *11*, 509–514.

(68) Simpson, N. E.; Stabler, C. L.; Simpson, C. P.; Sambanis, A.; Constantinidis, I. *Biomaterials* **2004**, *25* (13), 2603–2610.

(69) Lagergren, S. *K. Sven. Vetensk. Sakademiens Handl.* **1898**, *24* (1–39), 2474–2479.

(70) Ho, Y. S.; McKay, G. *Process Biochem.* **1999**, *34* (5), 451–465.

(71) Kwok, K. C. M.; Koong, L. F.; Chen, G.; McKay, G. *J. Colloid Interface Sci.* **2014**, *416*, 1–10.

(72) Lin, Q.; Qian, S.; Li, C.; Pan, H.; Wu, Z.; Liu, G. *Carbohydr. Polym.* **2012**, *90* (1), 275–283.

(73) Singh, R. P.; Pal, S.; Rana, V. K.; Ghorai, S. *Carbohydr. Polym.* **2013**, *91* (1), 294–299.

CHAPTER 6

6 Optimization of orthophosphate and turbidity removal using an amphoteric chitosan-based flocculant-ferric chloride coagulant system[4]

Description

This chapter is focused on the optimization of the amphoteric flocculant, CMC-CTA (which was prepared in Chapter 5) with $FeCl_3$ coagulant in a binary system for the dual removal of turbidity (T_i) and phosphate (P_i) using the Box-Behnken RSM. Optimal conditions for pH, flocculant dosage, coagulant dosage and settling time were obtained for the removal of P_i and T_i, which showed significant improvement over the use of native polymer materials combined with $FeCl_3$ in a binary system. Greater removal of P_i and T_i were observed for both predicted and experimental data at the optimal conditions. The Fe(III)-CMC-CTA flocculant system showed optimum adsorption properties towards P_i and T_i with increased adsorption capacity.

Author's contribution

Lee D. Wilson and I conceived the project. I performed all the experimental work, data processing and analysis, and wrote the first draft of the manuscript as well as making further revisions where and when necessary on subsequent drafts. Dr. L.D. Wilson was responsible for the supervision of the project, editorial guidance for revision of the manuscript drafts, and corresponding author. Permission was obtained from all contributing authors before the inclusion of the manuscript in this thesis.

Relation of Manuscript 4 to Overall Objective of this Project

This chapter is a continuation of Chapter 5, where an amphoteric chitosan-based flocculant material was prepared and characterized using physicochemical methods related to flocculation properties. This study discusses the optimization of the factors affecting the CF process using Box-Behnken response surface methodology to obtain an optimal condition for efficient P_i and T_i

[4] Reproduced with permission from Agbovi, H. K.; Wilson, L. D. *Environ. Chem*. 2019, 16 (8), 599–612. Copyright 2019 CSIRO.

removal. The study reported herein relates to the second theme (synthesis, characterization and flocculation properties of high molecular chitosan-based amphoteric flocculant for P_i and T_i removal in a single-component and binary systems) of the thesis research. The second, fourth, fifth and sixth hypotheses discussed in the Chapter 1 have been addressed in this chapter. An optimal condition was generated using the BBD-RSM for the removal of P_i and T_i, in which the experimental and predicted removal efficiencies were comparable.

6.1 Introduction

Phosphorus is an essential plant nutrient for growth and development, where it exists in aquatic systems as inorganic (ortho- and poly-phosphates) and organic forms (e.g., detergents). Phosphate present in water and wastewater originates from human, domestic and industrial waste, as well as fertilizer effluent run-off from agricultural activities.[1] Despite the importance of phosphate as an essential micronutrient in water, elevated levels lead to eutrophication and excessive algae growth.[2] Excess phosphate disturbs the balance of organisms present in water by affecting water quality through the depletion of oxygen as algae decay. In general, phosphate effluent is regulated to levels below 0.5 mg/L[3], where discharge limits (mg/L) are controlled, as follows: USA (0.5 – 1.0), India (5.0), France (1.0 – 2.0) , Tunisia (10.0), Canada (0.1), Ghana (2.0), and Japan (16.0) mg/L.[3–8] The removal of orthophosphate (P_i) in wastewater has been tested by different methods: adsorption[9–12], biological removal[13,14], electro-coagulation[15], membrane processes[16] and chemical precipitation.[17,18] Coagulation-flocculation (CF) has been used widely for wastewater and water treatment in both the past and present due to its facile operation and efficiency. CF has been applied directly or indirectly to control particulates, microorganisms, natural organic matter (NOM), synthetic organic carbon, precursors of disinfection by-products (DBPs), metals, and some inorganic ions to control drinking water quality.[19] The efficiency of CF is influenced by several factors such as temperature, mixing speed and time, flocculant/coagulant dosage, pH, retention time and initial contaminant concentration of the water or wastewater.[20] The CF process attains maximum efficiency when these factors are optimized.

Optimizing the key parameters in the CF process through the classical method, known as one-variable-at-a-time, involves fixing all other variables constant while varying one variable sequentially to obtain the optimal conditions. This is a time-consuming, expensive, and complicated process for a multi-variable system that often fails to resolve the multi-variable inter-

relationships. To overcome these challenges, statistical experimental design techniques using the response surface methodology (RSM) has been designed for the optimization of a multi-variable experiment. RSM is a collection of statistical and mathematical methods that are useful for designing experiments, building models, evaluating the effects of several factors in order to achieve optimum conditions for desirable responses with a limited number of experiments.[21] The RSM has been widely used in various fields such as optimizing fermentation conditions[22,23], and optimizing self-nanoemulsified capsule dosage form (SNCDF) of a highly lipophilic model compound, Coenzyme Q10.[24] In the field of water treatment, applying RSM to optimize the CF process for the treatment of wastewater was reported in many studies.[19,20,25–28] However, regarding the use of RSM for designing an experimental protocol to obtain optimal conditions for the simultaneous CF of phosphate and turbidity using chitosan-based amphoteric flocculant, no study has been reported yet.

Chitosan is a linear polysaccharide copolymer that consists of N-acetyl-D-glucosamine with variable deacetylation based on its preparation.[29] The relative solubility of chitosan relates to its efficiency as a flocculant, especially at lower pH since it is relatively water insoluble above its pK_a and in most organic solvents. Modified chitosan materials may have wider application[30–34], especially amphoteric forms that contain quaternary ammonium groups. Synthetic modification of chitosan with 3-chloro-2-hydroxypropyl trimethylammonium chloride (CTA) and carboxymethyl groups to improve water solubility over wider pH conditions. Amphoteric materials possess favorable charge neutralization of negatively charged species and colloidal suspensions.[35–39] As reported in Chapter 5 and elsewhere [40,41], CTA-chitosan has been shown to be more effective in turbidity removal compared to native chitosan. By contrast, amphoteric chitosan-based flocculants have not been reported for turbidity removal and dissolved solids such as phosphate in wastewater at the time of this report.

This study aims to optimize the CF potential of grafted 3-chloro-2-hydroxypropyl trimethylammonium chloride CMC (CMC-CTA) in conjunction with ferric chloride for the simultaneous removal of P_i and T_i along with the Box-Behnken Design (BBD) and the response surface methodology (RSM). The coagulant-flocculant system studied herein utilizes a coagulant (ferric chloride) and a biopolymer flocculant (CMC-CTA). This study contributes to binary-flocculant systems with improved efficiency and sustainability by reduction of coagulant and flocculant dosage, enhancement of the flocculation activity, and sustainability by reducing

secondary pollution, as compared with conventional synthetic flocculant systems (aluminium sulphate, ferric sulphate, polyaluminium chloride and ferrous sulphate).

6.2 Materials and methods

6.2.1 Materials

All chemicals were of analytical reagent (AR) grade. Kaolinite, hydrated ferric chloride ($FeCl_3 \cdot 6H_2O$), anhydrous monobasic potassium phosphate (KH_2PO_4), NaOH (aq), HCl (aq), vanadate molybdate reagent, chitosan (medium molecular weight, 85% deacetylation), monochloroacetic acid, ethyl alcohol, isopropanol, 3-chloro-2-hydroxypropyl trimethylammonium chloride (CTA) and spectroscopic grade potassium bromide (KBr) were purchased from Sigma-Aldrich, Oakville, Ontario, Canada. All materials were used as received unless specified otherwise.

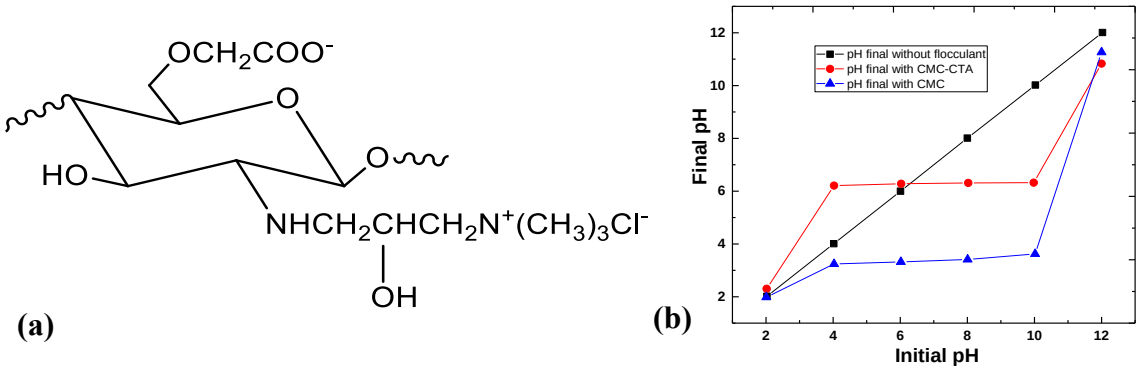

Figure 6.1: (a) Molecular structure of the synthesized amphoteric CMC-CTA flocculant. (b) Point of zero charge of CMC-CTA and CMC.

6.2.2 Synthesis and characterization of CMC-CTA

A two-step route described in detail in Chapter 5 was adopted to synthesize the CMC-CTA flocculant, as shown in Scheme A9.1 (Appendix A). In the first step, carboxymethyl chitosan (CMC) was synthesized from chitosan and monochloroacetic acid by etherification. In the second step, CMC-CTA was synthesized by grafting CTA branches onto CMC backbone by adding a suitable amount of CTA monomer. The structure of the CMC-CTA flocculant is presented in Figure 6.1a. The yields of the CMC (80.8%) and CMC-CTA (76.4%) are in good agreement with the results obtained by Yang et al. for the independent synthesis of CMC-CTA[41,42]. The estimated

value of the point of zero charge, pH_{pzc} (in parentheses), is listed for CMC-CTA (~6.40) and CMC (~3.30), as illustrated in Figure 6.1b. Potentiometric titration was used as an alternate method for estimating the degree of substitution (DS) due to its facile operation and low cost. The cationic DS for CMC-CTA was estimated at 85.4%, where the value of DS is comparable with other estimates[43,44], notwithstanding the different sources of chitosan. CMC-CTA flocculant was characterized by several techniques such FT-IR, ^{1}H-NMR, ^{13}C-NMR (solid state), potentiometry, point of zero charge and TGA, and the results are presented in Appendix A (Figures A9.3 & A9.4).

Table 6.1: Levels of each factor for the Box-Behnken experimental design

Independent variable	Unit	Symbol	Coded level		
			Low (-1)	Middle (0)	High (+1)
CMC-CTA dose	mg/L	*A*	1	3	5
$FeCl_3$ dose	mg/L	*B*	5	10	15
Initial pH		*C*	2	7	12
Settling time	min	*D*	10	35	60

6.2.3 Coagulation-flocculation experiment

Standard orthophosphate (P_i), ferric chloride and CMC-CTA aqueous stock solutions were prepared by dissolving in deionized and distilled water. A calibration curve of P_i was obtained using a vanadate molybdate colorimetric method at a wavelength of 420 nm at pH 6.5 as described in Section A9.2.1 (Appendix A). The CF process was performed, based on the experimental design matrix obtained from the BBD and the RSM, using a program-controlled conventional jar test apparatus with six-2 L jars and stirrers. Approximately 1 L of an aqueous solution containing P_i was added to the jar tester and 5.0 ml of the P_i solution was sampled for UV-Vis spectral analysis by adding 1.0 ml of vanadate molybdate reagent, where a yellow-colored complex formed after 20 min before recording the optical absorbance. A pre-determined volume of kaolinite solution was added to each jar solution to simulate colloidal particles in the P_i solution. The kaolinite dosage was maintained at 400 mg/L throughout while the initial P_i concentration was kept at 30 mg/L. The pH of the turbid P_i solutions was adjusted by using 0.1 M NaOH or HCl, according to the conditions. A pre-determined amount of the coagulant (ferric chloride) was added to the solution,

followed by rapid stirring for 3 min at 295 rpm, which is considered as the coagulation stage. Thereafter, the flocculation stage was initiated, whereby the stirring rate was reduced to 25 rpm for 20 min. During this period, the flocculant (CMC-CTA) was added within the first 5 min after the coagulation stage. The stirring was stopped, and the solutions were allowed to settle for a given time (10 – 60 min) before analysis. After the settling time, a 10.0 ml solution aliquot was sampled from the top layer and the transmittance (%T) was measured (λ= 800 nm). In addition, a 15 ml solution aliquot was sampled and centrifuged for 60 min at 1550 rpm, and then prepared for UV-Vis analysis to estimate P_i. The solution pH was measured after the appropriate settling period. The turbidity removal (%) and P_i removal (%) was calculated by equations. (6.1) and (6.2).

$$\%T_{i\ removal} = \frac{T_c - T_o}{100 - T_o} \cdot 100\% \tag{6.1}$$

$$\%\mathrm{P}_{i\ removal} = \frac{c_o - c_e}{c_o} \cdot 100\% \tag{6.2}$$

Here, c_0 and c_e are the initial and equilibrium concentrations of P_i in solution (mg/L) and T_o and T_c are the transmittance (%T) of the turbid water before and after the CF process. Measurements were performed in triplicate and reported as the average value along with the standard deviation. Details on the statistical experimental design using the Box-Behnken design (BBD) and the response surface method (RSM) are discussed in Section 9.1.4.1 in Appendix A.

6.3 Results and discussion

6.3.1 Box-Behnken Statistical Analysis

A preliminary study in Chapter 5 on the effect of coagulant dosage, flocculant dosage, type of flocculant, pH, mixing speed and time, temperature, and retention time on the CF process for the removal of T_i and P_i was carried out in order to determine the most critical factors and their region of interest. The most significant factors affecting the CF process were selected to be pH, coagulant and flocculant dosages and settling time and were employed herein. The Box-Behnken response surface methodology was employed to evaluate the relationship between the flocculation responses (T_i and P_i removal) with the most important independent variables ($FeCl_3$ dosage, CMC-CTA dosage, pH and settling time). A total of twenty-nine experiments was conducted and the results are listed in Table 6.2. Several response models, such as linear, interactive, quadratic and cubic models, can be correlated with the experimental data. However, a suitable selection of the best

model is required since it must best correlate with the experimental data depending on its adequacy. Because the quadratic equation contains fewer coefficients, it was selected to represent the correlation between the experimental data and the responses.

Table 6.2: Box-Behnken experimental design matrix of four variables along with the experimental and calculated response for P_i and T_i removal efficiency

Run	CMC-CTA dose (*A*)	$FeCl_3$ dose (*B*)	pH (*C*)	Settling time (*D*)	Expt P_i removal (%)	Expt T_i removal (%)	Calc. P_i removal (%)	Calc. T_i removal (%)
1	1	5	7	35	70.2±0.4	90.6±0.1	70.4	90.2
2	1	15	7	35	59.0±0.3	90.7±1.0	59.1	90.4
3	5	5	7	35	63.4±0.2	76.0±0.8	63.6	75.7
4	5	15	7	35	75.0±0.6	76.9±0.1	75.1	76.6
5	3	10	2	10	97.4±1.8	80.5±0.1	97.0	80.5
6	3	10	2	60	89.5±0.8	76.8±0.2	89.4	76.7
7	3	10	12	10	88.3±0.4	91.9±1.1	88.6	91.4
8	3	10	12	60	82.0±0.3	95.8±0.2	82.6	95.2
9	1	10	7	10	68.5±0.4	99.1±0.4	68.2	99.1
10	1	10	7	60	62.0±1.0	99.1±0.3	63.6	101.4
11	5	10	7	10	72.9±0.5	84.3±1.0	72.8	84.8
12	5	10	7	60	66.4±0.4	84.6±0.3	66.1	85.0
13	3	5	2	35	93.1±0.2	70.0±0.8	92.7	69.7
14	3	5	12	35	86.3±1.4	84.2±0.4	85.7	84.1
15	3	15	2	35	93.6±1.1	69.6±0.2	93.5	70.0
16	3	15	12	35	85.4±0.7	84.3±0.3	85.2	84.9
17	1	10	2	35	67.9±0.6	85.2±1.1	68.6	85.5
18	1	10	12	35	60.9±1.1	98.9±1.1	60.9	99.5
19	5	10	2	35	72.8±0.9	70.9±0.2	73.2	70.7
20	5	10	12	35	65.9±0.1	86.10.3	65.6	86.1
21	3	5	7	10	92.2±0.3	82.8±0.1	92.5	83.2
22	3	5	7	60	85.8±0.3	83.0±0.1	86.1	83.7
23	3	15	7	10	92.8±0.4	84.6±0.2	92.9	84.2
24	3	15	7	60	85.8±0.5	83.9±1.6	85.8	83.8
25	3	10	7	35	95.8±0.5	96.3±2.8	96.4	96.7
26	3	10	7	35	95.6±0.4	96.1±1.8	96.4	96.7
27	3	10	7	35	96.6±0.1	96.8±2.6	96.4	96.7
28	3	10	7	35	96.1±0.4	97.2±2.9	96.4	96.7
29	3	10	7	35	97.5±0.1	96.9±2.2	96.4	96.7

The BBD for statistical analysis and the RSM was employed to investigate the effects of the four independent variables on the response functions, and the evaluation of the optimal conditions to maximize P_i and T_i removal (%). The independent variables were CMC-CTA dosage (*A*), $FeCl_3$

dosage (*B*), pH (*C*) and settling time (*D*). The experimental design consisted of four variables (*A, B, C, and D),* each at three levels, coded as -1, 0 and +1, for low, middle and high values (*cf.* Table 6.1). The optimization procedure involved study of the response of the statistically designed combinations, estimating the coefficients by fitting the experimental data to the response functions, predicting the response of the fitted model and *goodness-of-fit* of the model.[45,46] The results for the P_i and T_i removal (%) are listed in Table 6.2. The coefficients of the response function for the independent variables were determined by correlating the experimental data with the response functions using Quantum XL Sigmazone DOE regression program. Different response functions and the respective coefficients are described by equations (6.3 and 6.4). The following regression equations are the empirical models in terms of coded factors for P_i and T_i removal by equations (6.3) and (6.4), respectively.

$$Y_{P_i} = 96.37 + 2.31A + 0.056B - 3.814C - 3.380D + 5.704AB + 0.029AC - 0.0066AD - 0.344BC - 0.167BD + 0.389CD - 25.77A^2 - 3.579B^2 - 3.521C^2 - 3.456D^2 \quad (6.3)$$

$$Y_{T_i} = 96.68 - 7.068A + 0.274B + 7.341C - 0.0047D + 0.180AB + 0.349AC + 0.085AD + 0.127BC - .0226BD + 1.877CD - 2.600A^2 - 10.839B^2 - 8.638C^2 - 2.099D^2 \quad (6.4)$$

Statistical testing of the model was performed with the Fisher's statistical test for analysis of variance (ANOVA). The ANOVA test for the P_i removal is presented in Table 6.3. The ANOVA test estimates the suitability of the response functions and the significance of the effects of the independent variables. The student's *t*-test and *p*-values were checked to determine the statistical significance of the BBD-RSM variables and their interactions at variable probability values.[47] The $F_{statistic}$ (the ratio of mean square due to regression to mean square to real error) of 1281 for P_i removal and 248.6 for T_i removal was greater than $F_{statistic}$ (4.94). According to ANOVA test, a large value of F indicates that most of the variables in the response can be described by the regression equation, and probability value (*p* values) less than 0.05 are considered to be statistically significant. The ANOVA results indicate that the second order polynomial equation adequately represents the actual relationship between the T_i and P_i removal (%) and the independent variables ($FeCl_3$ dose, CMC-CTA dose, pH and setting time).

Table 6.3: ANOVA table for P_i removal (%), and T_i removal (%) responses

Source	Seq SS	Adj SS	DF	Adj MS	F	*p*	Remarks
P_i removal (%)							
CMC-CTA dose (*A*)	128.2	128.2	1	128.2	237.4	0.000	Y
$FeCl_3$ dose (*B*)	0.075	0.075	1	0.075	0.139	0.711	N
pH (*C*)	349.1	349.1	1	349.1	646.6	0.000	Y
Settling time (*D*)	274.2	274.2	1	274.2	508.0	0.000	Y
AB	260.3	260.3	1	260.3	482.1	0.000	Y
AC	0.007	0.007	1	0.007	0.012	0.912	N
AD	0.000	0.000	1	0.000	0.001	0.980	N
BC	0.946	0.946	1	0.946	1.752	0.193	N
BD	0.223	0.223	1	0.223	0.414	0.523	N
CD	1.212	1.212	1	1.212	2.246	0.141	N
AA	8,323	8,616	1	8,616	15,960	0.000	Y
BB	84.12	166.1	1	166.1	307.7	0.000	Y
CC	110.6	160.8	1	160.8	297.9	0.000	Y
DD	155.0	155.0	1	155.0	287.0	0.000	Y
Error	23.21	23.21	43	0.540			
Error pure	18.23	18.23	33	0.552			
Error lof	4.986	4.986	10	0.499			
Total	9,710		57				
T_i removal (%)							
CMC-CTA dose (*A*)	1,199	1,199	1	1,199	1,028	0.000	Y
$FeCl_3$ dose (*B*)	1.799	1.799	1	1.799	1.543	0.221	N
pH (*C*)	1,293	1,293	1	1,293	1,109	0.000	Y
Settling time (*D*)	0.001	0.001	1	0.001	0.000	0.983	N
AB	0.259	0.259	1	0.259	0.222	0.640	N
AC	0.975	0.975	1	0.975	0.836	0.366	N
AD	0.058	0.058	1	0.058	0.050	0.825	N
BC	0.129	0.129	1	0.129	0.111	0.741	N
BD	0.409	0.409	1	0.409	0.351	0.557	N
CD	28.18	28.18	1	28.18	24.16	0.000	Y
AA	1.840	87.69	1	87.69	75.18	0.000	Y
BB	1,151	1,524	1	1,524	1,307	0.000	Y
CC	913.8	968.1	1	968.1	829.9	0.000	Y
DD	57.20	57.20	1	57.20	49.03	0.000	Y
Error	50.16	50.16	43	1.166			
Error pure	43.14	43.14	33	1.307			
Error lof	7.017	7.017	10	0.702			
Total	4,698		57				

Note: 'Remarks' means whether the variable under consideration has any significant contribution to the P_i or T_i removal efficiency, where Y and N represent statistically significant and insignificant variables, respectively.

Figure 6.2 is a Pareto plot for the T_i and P_i removal that depicts the standardized effect variables based on the *t* values of the independent variables, along with quadratic and interaction effects.

The length of each bar in Figure 6.2 represents the standardized effect of that variable on the response functions (P_i and T_i removal), and the alpha level (α) of 0.05 was employed to evaluate the statistical significance. Values of *p* less than 0.05 indicate a statistically significant variable effect. If the *p*-value is greater than 0.05, the variable effect was considered to be statistically insignificant. The Pareto plots in Figure 6.2 can be used to understand the impact of each variable on the final response of the P_i and the T_i removal. Pareto graphics have positive and negative bars. The positive bars suggest that by varying the factor, the response function increases, while the negative bars indicate the opposite.

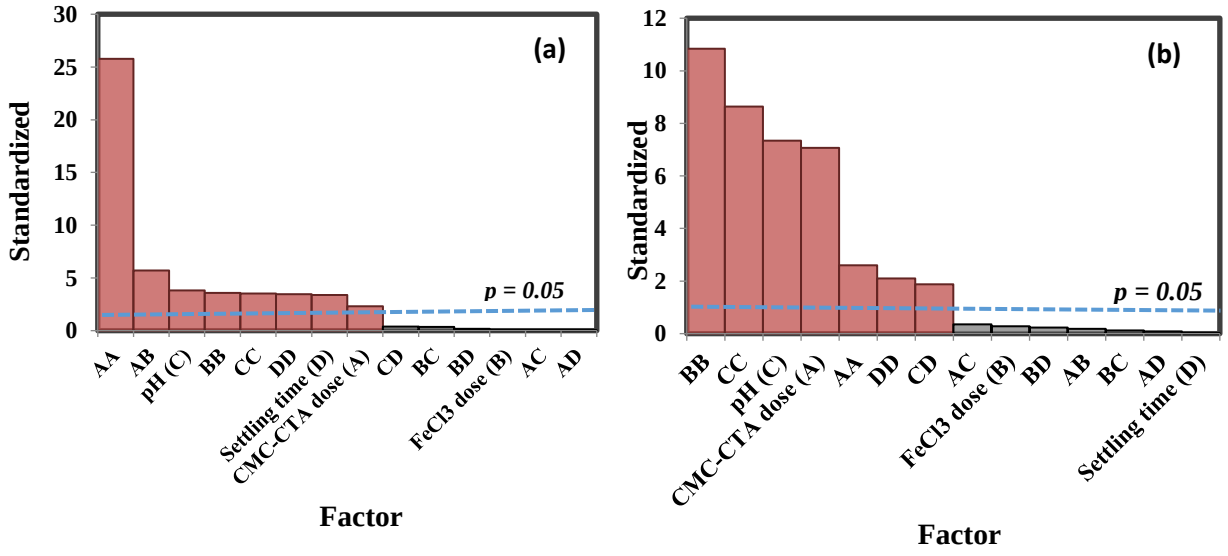

Figure 6.2: Pareto chart showing the standardized effects of variables on (a) phosphate (P_i) and (b) Turbidity removal efficiency.

For the P_i removal efficiency, the selected 1st-order and 2nd-order variables were shown to be statistically significant except $FeCl_3$ (*B*), according to the Pareto plot in Figure 6.2 and Table 6.3, indicating that the CF process largely depends on the CMC-CTA dosage and pH of the medium. In addition, for the interactive variables, *AC, AD, BC, BD and CD* were found to be statistically insignificant. Similarly, for the T_i removal efficiency, the selected 1st-order and 2nd-order variables were shown to be statistically significant, except $FeCl_3$ (*B*) and settling time (*D*). Also, for the interactive variables *AB*, *AC*, *AD*, *BC* and *BD* were found to be insignificant except *CD*, according to the Pareto plot in Figure 6.2 and the values listed in Table 6.3. The insignificant variables were identified because the Pareto bars for these variables are below the reference line, as shown in Figure 6.2, and their *p* values are relatively high ($p > 0.05$), as listed in Table 6.3. The significant

component of the regression model is in the order *AA* > *AB* > *C* > *BB* > *CC* > *D* > *A* for the present application for the P_i removal efficiency. On the other hand, for the removal of T_i, the most significant components of the quadratic terms are in the order *BB* > *CC* > *C* > *A* > *AA* > *DD* > *CD*. This indicates that the CF process for the P_i removal is strongly dependent on the CMC-CTA dosage, pH and combined interaction of the flocculant and the coagulant dosages. In addition, the CF process for the T_i removal is dependent on the $FeCl_3$ dosage and pH, and the flocculant dosage. The settling time was found to have insignificant effect on the removal of both P_i and T_i.

The quality *(goodness-of-fit)* of the regression model was determined by coefficients of R^2, adjusted R^2 and standard error of estimate (SEE). The value of the R^2 coefficient indicates the ratio of the sum of squares due to regression (SSR) to the total sum of squares (SST), where R^2 corresponds to the proportion of the total variation in the response predicted by the model. A value of R^2 close to unity is appropriate and a rational agreement with adjusted R^2 is important.[28] A high R^2 coefficient ensures a satisfactory adjustment of the quadratic model to the experimental data. The R^2 statistic indicates that the models account for 99.76% of the variable P_i and 98.93% for the variable T_i removal efficiency. This suggests that only 0.24% (for P_i) and 1.07% (for T_i) of the total variation could not be explained by the empirical model. The adjusted R^2 statistic (99.68% and 98.56%) for P_i and T_i removal, respectively, is more suitable for comparing models with a range of independent variables. The SSE shows the standard deviation of the residuals to be 0.735 and 1.08 for P_i and T_i removal, respectively. The accuracy of the regression model was verified by the parity and residual plots in Figure 6.3. Figures 6.3 (a & c) illustrate the plots of the predicted P_i and T_i removal (%) versus measured values. Most of the data are distributed near the straight line, where the measured and predicted values are similar, indicating that the regression model is predictive. These plots provide information on the fit criteria contained in the residuals. In Figures 6.3(b & d), the maximum deviation between the predicted and the measured P_i and T_i removal efficiencies is below 4.0% and reveals a good correlation between the predicted and the measured values.

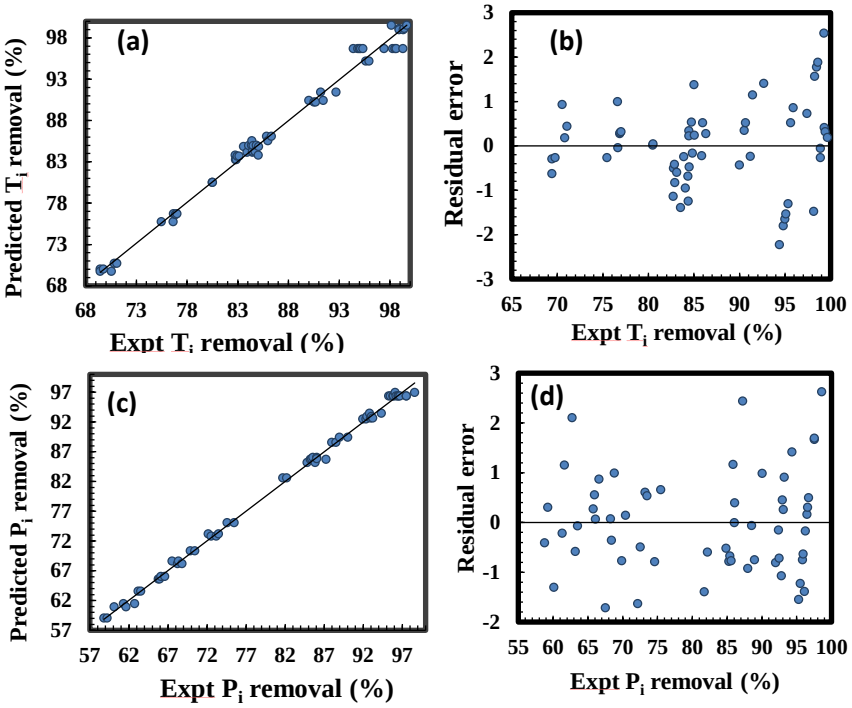

Figure 6.3: Parity plot showing the correlation between the predicted and experimental values of (a) turbidity and (c) phosphate removal efficiency. Residual error as a function of experimental data of (b) turbidity and (d) phosphate removal.

6.3.2 Main effects of the independent variables on the response functions

Figure 6.4 is a plot depicting the main effects of the CF factors on T_i and P_i removal efficiency. Figure 6.4 appropriately illustrates essential factors that are at two or more levels in a designed experiment, enabling an in-depth analysis of the effects of factors considered in the coagulation-flocculation process.[26] These plots provide a preliminary conclusion about the effects of the CF independent variables; pH, $FeCl_3$ dose, alginate dose, and settling time on the response functions (P_i and T_i removal efficiency) shown in Figure 6.4. In Figure 6.4a, the P_i removal (%) decreased as the CMC-CTA dosage increases, indicating less flocculant dosage is required to obtain optimal removal. The P_i removal (%) increased as the $FeCl_3$ dosage increased until it reached an optimum value (90.4%), where a decrease occurred with an increase in the coagulant dosage. In addition, as the pH is increased, there is a sharp increase in the P_i removal (%) until a value of 89.4 %, which then increased again steadily as the pH further increased. The settling time appears to have an independent effect on the P_i removal (%) since an increase in the settling time of the flocs did not

significantly affect the P_i removal efficiency. In the case of the T_i removal (%) (*cf*. Figure 6.4(b)), the removal efficiency reached an optimal value (91.4%) as the CMC-CTA dosage increased, and then decreased sharply with increasing CMC-CTA dosage. An increase in the $FeCl_3$ dosage had an independent effect on the T_i removal efficiency since increasing the $FeCl_3$ dosage (5.0 mg/L to 15 mg/L) had a negligible effect on the T_i removal efficiency. In addition, as the pH increases from 2 to 12, the T_i removal efficiency increased slightly (85.7% to 87.1%), where a similar effect was noted for settling time on the T_i removal efficiency in Figure 6.4b(iv). Determination of the role of the main effects to evaluate the response function is challenging because it does not account for interaction effects between different independent factors on the response variables. Hence, the effects of the interaction variables on P_i and T_i removal efficiency are discussed in the next section.

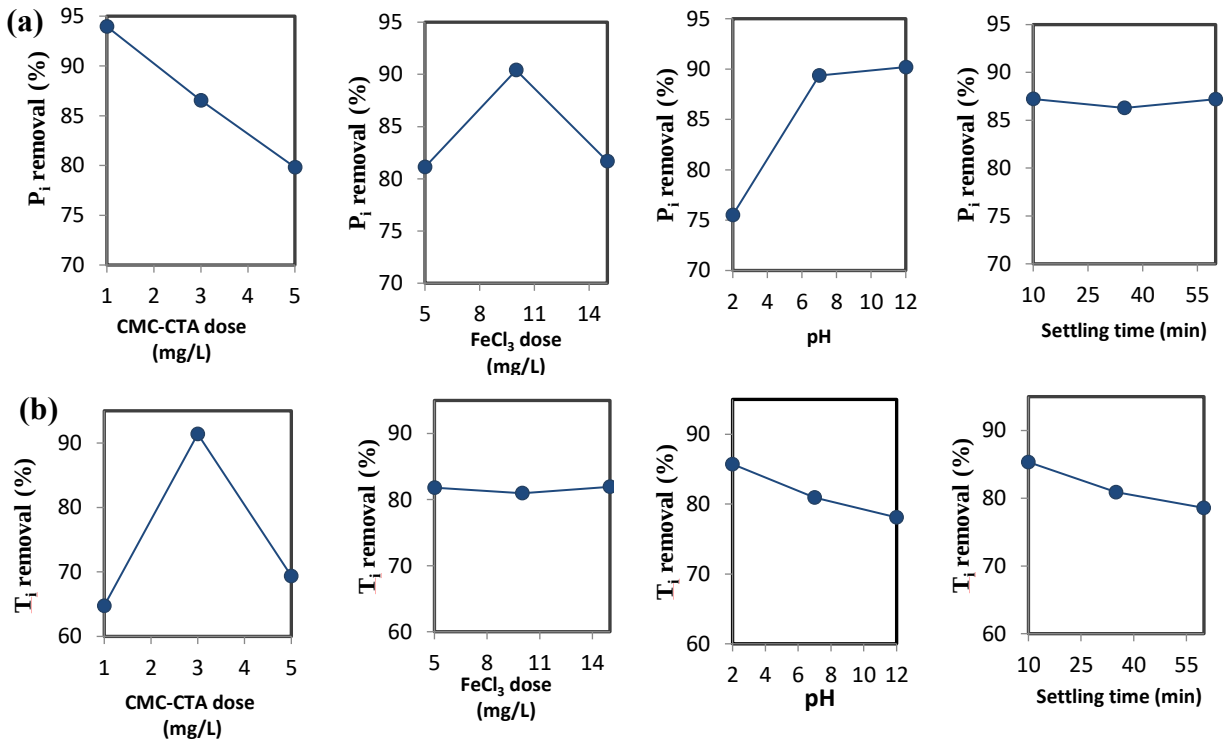

Figure 6.4: Main effects plot of (i) CMC-CTA dose, (ii) $FeCl_3$ dose (iii) initial pH alginate dose and (iv) settling time on (a) phosphate and (b) turbidity removal efficiency.

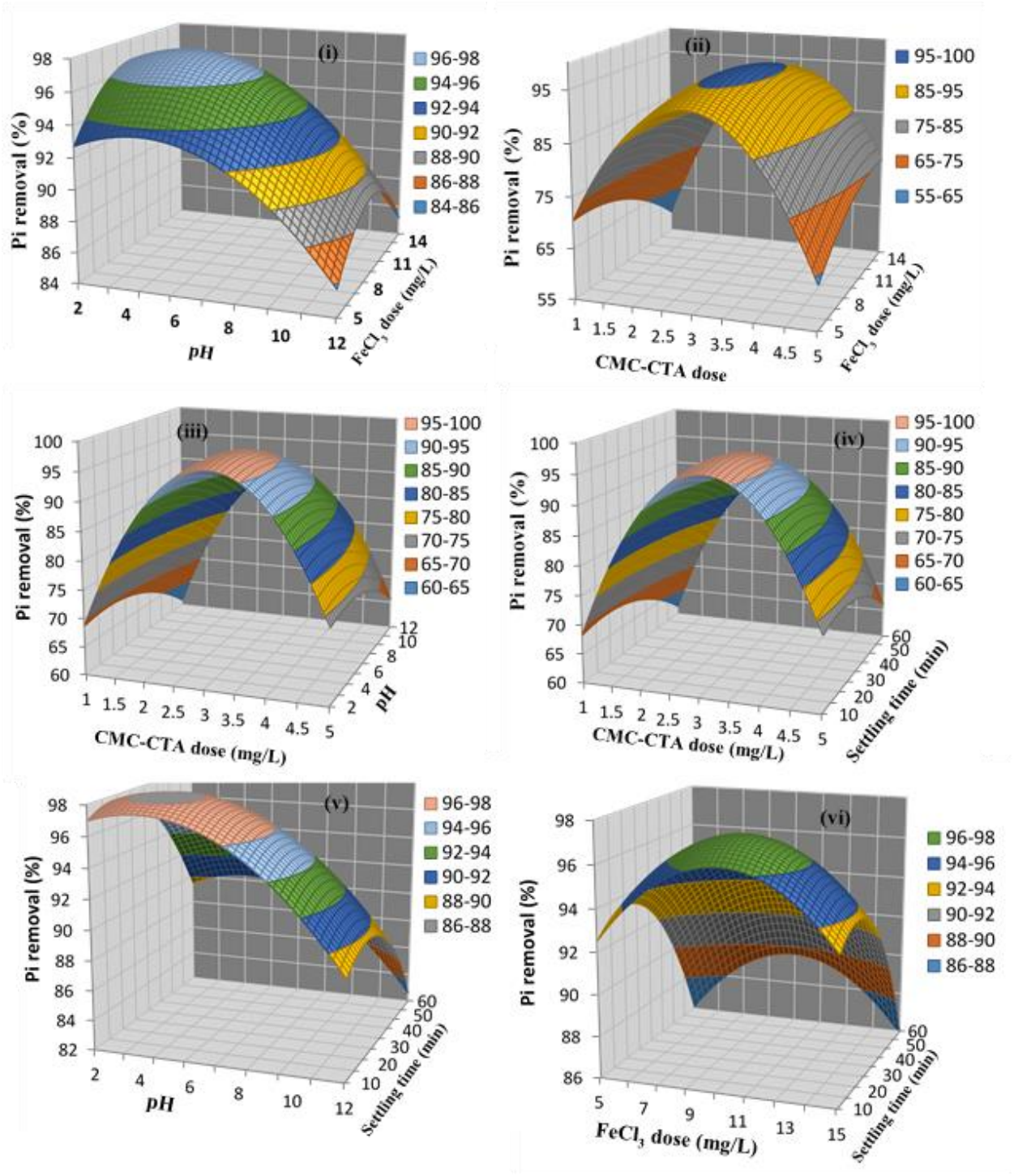

Figure 6.5: Three-dimensional Box-Behnken response surface plots of P_i removal (%) as a function of (i) pH and $FeCl_3$; (ii) CMC-CTA dose and $FeCl_3$ dose; (iii) CMC-CTA dose and pH; (iv) CMC-CTA dose and setting time; (v) pH and settling time; and (vi) $FeCl_3$ dosage and settling time.

6.3.3 The interactive effects of variables on phosphate flocculation

The three-dimensional (3D) response surface plots (Figure 6.5) and 2D contour plots in Figure A9.5 (Appendix A) were obtained from the model-predicted response by changing two independent variables within the experimental conditions while keeping the other two terms constant at the optimal level. The response surface is a graphical representation of the regression equation for the visualization of the relationship between the response and experimental levels of each variable.[48] These plots are useful to assess the interactive relationship between the independent variables and the response functions. The elliptical contour plots in Figure A9.6 show significant interactive effects on P_i removal (%) between any two variables. In other words, there are significant interactive effects on the response variable between $FeCl_3$ and alginate dosage, $FeCl_3$ dosage and pH, $FeCl_3$ dosage and settling time, CMC-CTA dosage and settling time, pH and settling time, as well as alginate dosage and pH. In addition, the obvious peak in the 3D response surface plots for the P_i and T_i removal (%) confirms that the optimal conditions were exactly located inside the design boundary. The contribution of interactive effects between different variables is discussed below.

Figure 6.5(i) shows the response surface plot and Figure A9.5(i) shows the contour plots for the interaction between pH and $FeCl_3$ dose at the optimal levels of CMC-CTA dose and settling time. Between pH 2.0 to 4, the P_i removal increased from 93.2% to 98.6%, while a decrease to 86.6% occurs as the pH increases further. At pH 10 and $FeCl_3$ dosage of 15.0 mg/L, the P_i removal is 88.6%, however, at pH 2 and $FeCl_3$ dose of 12 mg/L, the P_i removal was 90.0%. This indicates that as the pH and $FeCl_3$ dosage increase, the P_i removal (%) increases until it reaches an optimal value and then decreases as these variables (pH/ $FeCl_3$ dosage) increase. The results obtained herein are expected because pH has a remarkable influence on the CF process. The pH of the medium controls charge neutralization process on hydrolysis products and the precipitation of Fe(III) hydroxides. Phosphate has an anionic surface charge in its ionized state, where hydrolysis products of $FeCl_3$ can neutralize the charge of P_i. Therefore, charge neutralization is a likely mechanism for P_i removal, where adsorption and sweeping may be considered as possible removal mechanisms due to the presence of CMC-CTA. In acidic media at low pH, protonation may occur, resulting in reduced charge density, which leads to self-assembly of P_i where less coagulant is required. For instance, at a fixed pH, an increase of the $FeCl_3$ dose leads to greater P_i removal until an optimum dose of 10.4 mg/L, which decreases gradually as the $FeCl_3$ dose further increases.

Figure 6.5(ii) represents the response surface plot and Figure A9.5(ii) represents the contour plot for P_i removal at optimal levels of pH and settling time, and variable CMC-CTA and $FeCl_3$ dosages within the experimental design. The 3D surface plot provides evidence that an interaction occurs between the dosage of $FeCl_3$ and CMC-CTA with the level of P_i removal. This relates to a peak in the response surface plot within the experimental boundary. At greater CMC-CTA and $FeCl_3$ dosages, the P_i removal (%) also increased until an optimal value (99.2%) was obtained at 3.2 mg/L and 10.4 mg/L for CMC-CTA and $FeCl_3$, respectively. Beyond the optimum dosage of the coagulant and the flocculant, there is an excess of these materials in the solution, which causes restabilization, and dispersion of the flocs formed which lowers the removal efficiency. Greater removal (> 92%) was obtained at all conditions. At the optimum pH, hydroxide of the Fe(III) neutralizes the phosphate through charge neutralization and surface complexation mechanisms. The $FePO_4$ precipitate is swept and then adsorbs the CMC-CTA polyelectrolyte species by polymer bridging and adsorption mechanisms.[49]

P_i removal was studied as a function of CMC-CTA dosage and pH and the results are presented in Figure 6.5(iii) as 3D surface and Figure A9.5(iii) as 2D contour plots. The plots indicate that the optimal regions for the two interacting variables are located within the design boundary. At a constant CMC-CTA dosage such as 1.0 mg/L, the P_i removal (%) increases until an optimum pH condition is obtained at 4.2. As the pH increases beyond the optimum level, the P_i removal decreases notably. By comparison, the CMC-CTA dose increased at constant pH where the P_i removal increases steadily at an optimum dose of 3.1 mg/L and decreases as the CMC-CTA dose increases beyond the optimal value. As the pH and CMC-CTA dose was increased, the P_i removal (%) increased, while the opposite occurs as the pH and CMC-CTA dosage increase beyond their optimal values. Figure 6.5(iv) depicts the response surface plot and Figure A9.5(iv) illustrates a contour plot for P_i removal at optimal levels of pH and $FeCl_3$ dose at variable CMC-CTA dose and settling time. From Figure 6.5(iv), at constant CMC-CTA dose, the P_i removal (%) increased from 10 to 21.9 min. Beyond the optimal settling time, the removal (%) decreased. In addition, the P_i removal (%) increased with greater CMC-CTA dosage at a fixed settling time. However, beyond this optimal value, the removal (%) decreased. This implies that the interaction between settling time and CMC-CTA dosage within the specified range has a significant impact on P_i removal. Similar results were observed for the variation between settling time and $FeCl_3$ dose, as shown in Figure 6.5(vi). Figure 6.5(vi) shows the effect of variable pH and settling time at the optimal levels

of $FeCl_3$ and CMC-CTA dosage on the P_i removal. An increase in pH at constant settling time yielded greater P_i removal, where the response variable decreased as the pH increased beyond the optimal level. On the other hand, at constant pH, greater efficiency was obtained with a longer settling time until it reached an optimal value at 39.2 min, with a gradual decrease as the settling time increased. During the long contact time, the P_i species were destabilized, which led to the formation of large flocs with excellent settling ability. However, beyond the optimal settling time, restabilization of the flocs occurred that resulted in lower removal efficiency. As the pH and settling time decreased or increased beyond their optimal level, the P_i removal was lower than the optimal conditions.

6.3.4 The interactive effects of variables on turbidity flocculation

Figure 6.6 shows 3D response surface plots and Figure A9.6 depicts 2D contour plots of the quadratic model for turbidity flocculation. Similar to the P_i removal discussed in Section 6.3.3, the elliptical contour plots show significant interactive effects on T_i removal (%) between any two variables. Figure 6.6(i) depicts the 3D surface plots for the interaction between pH and $FeCl_3$ dosage at fixed optimal conditions of CMC-CTA dosage and settling time. Increased T_i removal was observed with increasing $FeCl_3$ dose and pH values, with maximum removal of 98.6% at pH 9.1 and $FeCl_3$ dose of 10.0 mg/L. However, an increase in both $FeCl_3$ dose and pH beyond the optimum region resulted in a decrease in the T_i removal (%). At $FeCl_3$ doses higher than 10.0 mg/L, the removal efficiency began to decrease at all the coagulation pH values. This indicates that $FeCl_3$ overdosing occurred in the reaction solution. Overdosing deteriorated the supernatant quality, resulting in restabilization of the colloidal particles, limiting the coagulation efficiency. At the optimum $FeCl_3$ dosage, coagulation occurs generally between pH 6 and 9.5. At such conditions, the $FeCl_3$ coagulant requires sufficient alkalinity for proper hydrolysis to take place, where the formation of insoluble hydroxides leads to a reduction in turbidity.[50] At pH 6-9.5, the sweep-floc mechanism leads to the rapid formation of amorphous solid-phase $Fe(OH)_3(s)$, further supporting the results obtained herein. Hence the removal of turbidity occurred by adsorption on the $Fe(OH)_3(s)$.[51]

Figure 6.6(ii) depicts the response surface and contour plot (Figure S6.4(ii)) for T_i removal (%) at optimal levels of pH and settling time, with variable CMC-CTA and $FeCl_3$ dosages for the experimental design. Figure 6.6(ii) shows that a maximum T_i removal of more than 95% occurs at

CMC-CTA and $FeCl_3$ dosages of 1.0 mg/L and 10.0 mg/L, respectively. This maximum removal occurs because the coagulant ($FeCl_3$) becomes ionized, and the ionized Fe^{3+} can easily neutralize the residual charge on particles and expand the chain on the bridge of polymer flocculant. Beyond a dosage of 1.0 mg/L for CMC-CTA, excess flocculant in the colloidal suspension may lead to restabilization of the flocs, which causes a reduction in the T_i removal efficiency. In Figure 6.6(ii), the turbidity removal increased as the coagulant and flocculant dosages increased up to the optimal removal level, where a decreased effect occurs thereafter. This trend follows an electrostatic charge neutralization mechanism since more cation species are present in the turbid water that undergo charge neutralization with the negatively charged colloidal particles as the flocculant dosage increases below the optimum value. Beyond the optimum flocculant dosage, precipitation of kaolinite occurs. However, the addition of excess cationic flocculant leads to re-stabilization, where an excess positive charge on the aggregates and macroflocs undergo repulsive interactions that reduce turbidity removal. Dey et al.[52] reported that flocculant dosage beyond the optimal level led to a greater polymer flocculant density in the colloidal suspension as intermolecular repulsion occurs between the polymer branches. The greater repulsive over attractive interactions contribute to suspended particles with lesser interactions with the flocculant functional groups, resulting in decreased turbidity removal known as de-flocculation.[52] The interaction between the flocculant dosage and the pH is illustrated in Figure 6.6(iii) and Figure A9.6(iii). The symmetrical elliptical shape contour with the maximum response at the central contour plot indicates that there was a significant interaction between flocculant dosage and pH for turbidity removal. The T_i removal (%) increased with greater CMC-CTA dosage and pH until a maximum value is obtained (99.1%) at optimal values of 1.0 mg/L of CMC-CTA and pH 9.1. However, a decrease in the removal (%) occurs outside the optimal condition due to excess positively charged ions in the colloidal suspension that leads to stabilization of the flocs, as discussed above. This phenomenon can be explained as follows: within an optimum pH, the hybrid copolymer can neutralize the residual charge on the particles for that range by expanding the chain of polymer bridging.

The response surface and contour plots for T_i at optimal levels of pH and $FeCl_3$ dose, while varying CMC-CTA dose and settling time for the experimental design is illustrated in Figures 6.6(iv) and A9.6(iv). From Figure 6.6(iv), at a fixed dosage of CMC-CTA, the T_i removal (%) increases from 10 to 39.3 min. However, beyond the optimal settling time, the removal level remains virtually constant. Greater removal (84 -100%) was obtained at all working conditions.

This implies that the interaction between settling and CMC-CTA dosage within the specified range does not significantly impact T_i removal. According to Figure 6.6(v), the interaction between pH and settling time indicates that the optimal pH and settling time values are 9.1 and 39.3 min. A sharp feature is observed in the response surface plot showing the interaction between $FeCl_3$ dosage and settling time, as illustrated in Figure 6.6(vi). The apparent peak in the response surfaces for the T_i removal (%) confirms that the optimal conditions were exactly within the design boundary.

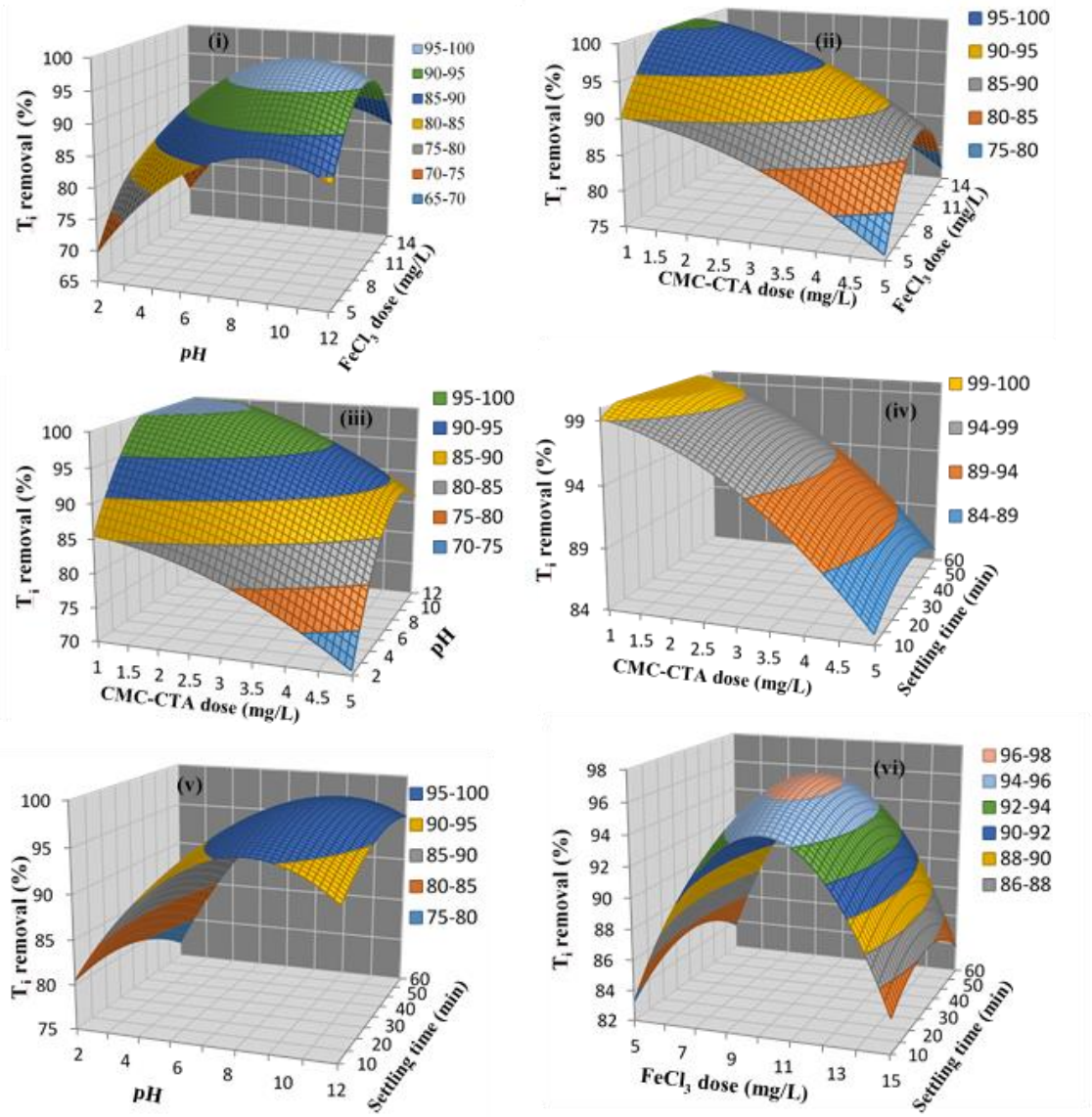

Figure 6.6: Three-dimensional Box-Behnken response surface plots of T_i removal (%) as a function of (i) pH and $FeCl_3$; (ii) CMC-CTA dose and $FeCl_3$ dose; (iii) CMC-CTA dose and pH; (iv) CMC-CTA dose and setting time; (v) pH and settling time; and (vi) $FeCl_3$ dosage and settling time.

Table 6.4: Results of validation experiments under optimized conditions

Test	Independent variable				P_i Removal (%)		T_i Removal (%)	
	CMC-CTA dose (mg/L)	$FeCl_3$ dose (mg/L)	pH	Settling time (min)	Expt value	Calc. value	Expt value	Calc. value
1	3.0	10	6.8	28	97.7 ± 0.7	96.4	96.4 ± 0.5	96.7
2	1.5	5.0	2.0	25	80.4 ± 0.9	81.6	74.4 ± 0.2	74.3
3	5.0	7.5	4.5	22.5	70.5 ± 1.1	70.9	78.5 ± 0.8	77.9
4	4.0	12.5	9.5	47.5	87.1 ± 0. 5	86.3	90.9 ± 0.6	91.5
5	5.0	15	12	55	61.9 ± 0.5	62.7	75.1 ± 0.7	75.8
6	3.0	8.0	6.0	10	96.3 ± 0.4	96.3	92.0 ± 0.7	91.2

6.3.5 Optimization conditions and verification

The optimization for individual removal of phosphate and turbidity achieved under different optimal conditions is a major challenge in wastewater treatment. Therefore, it is important to take into account the comprehensive removal of these contaminants for practical applications. Removal of phosphate and turbidity are two individual responses, where the optimization was achieved under different optimal conditions. Figure 6.7 shows the T_i vs. P_i removal for the coagulant-flocculant system studied herein. Accordingly, there is no obvious correlation between the two responses. Thus, the removal mechanisms of turbidity and phosphate are likely different and the optimum conditions for the removal of each substance differ. Therefore, a compromise among the conditions for the two responses is desirable. The optimal conditions for maximum P_i and T_i removal were determined by the response models by the experimental data. The optimal conditions calculated from the regression equations in equations 6.5 and 6.6 are as follows: CMC-CTA dosage of 3.1 mg/L; 10.4 mg/L for $FeCl_3$ dosage; pH of 4.12 and settling time of 21.9 min for phosphate removal, and CMC-CTA dosage of 1.0 mg/L; 10.0 mg/L for $FeCl_3$ dosage; pH of 9.1 and settling time of 39.2 min for T_i removal. The corresponding removal of P_i and T_i for these optimal conditions is 98.4% and 99.8%, respectively. The optimized condition indicates acidic condition, shorter settling time and relatively minimal dose of CMC-CTA is required to achieve optimal P_i removal. However, longer settling time, alkaline condition and lesser flocculant are required to maximize the T_i removal efficiency. Since both responses have different optimal condition, a compromise among the conditions for the two responses is desired. The desirability function approach was employed to achieve such a goal. The compromised optimal conditions calculated from the regression equation were as follows: CMC-CTA dosage of 3.0 mg/L, $FeCl_3$

dosage of 10.1 mg/L, pH 6.8 and settling time of 28.0 min, respectively. The corresponding removal is 96.4% and 96.7%, for P_i and T_i removal.

The validity of the statistical methodology and the experiment was confirmed by performing additional experiments in triplicate at the compromised optimized conditions, and five other conditions within the range of the experimental design. The selected conditions for the CMC-CTA dosage, $FeCl_3$ dosage, pH and settling time are listed in Table 6.4, along with the predicted and the experimental results for phosphate and turbidity removal efficiency. The P_i removal by experiment was 97.7 ± 0.7%, and T_i removal was 96.4 ± 0.5, in good agreement with the predicted optimal P_i (96.4%) and T_i (96.7%) removal efficiencies. As shown in Table 6.4, the measured and the estimated values of P_i and T_i removal (%) obtained from the RSM are close to each other. The result verifies that the RSM approach is useful for optimizing the operational conditions of the coagulation-flocculation process. As well, the RSM enables the prediction of an empirical relationship between the response factors (P_i and T_i) and the independent variables. Table A9.9 (Appendix A) represents a comparison between the removal of P_i using different coagulants and/or flocculant systems. The results show that the P_i removal at the optimized conditions herein for the binary Fe(III)-CMC-CTA coagulant-flocculant system is significantly greater when compared with other coagulant-flocculant systems. Herein, slower dosages of $FeCl_3$ and CMC-CTA, as well as acidic to neutral pH conditions are required for efficient dual-removal of T_i and P_i.

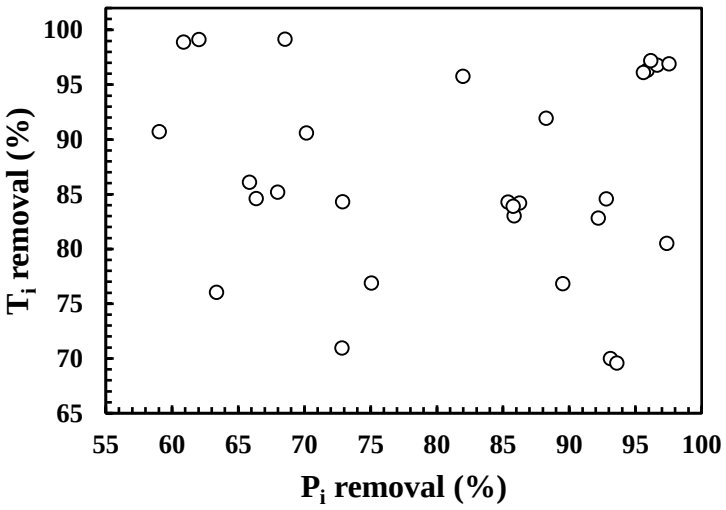

Figure 6.7: Turbidity removal (%) as a function of phosphate removal (%) using the coagulant-flocculant system.

6.3.6 Flocculation kinetics

During the CF process, a rapid stirring is required to uniformly disperse coagulant in a wastewater solution to form microflocs, followed by slow mixing upon addition of the polymer flocculant to the wastewater, leading to agglomeration of the microflocs to form macroflocs.[53,54] The properties of the macroflocs depend on the contact time between the flocculant and the microflocs. Adequate contact time is important to form large, dense and compact flocs that have greater settling properties.[55] Figure 6.8(a & b) illustrates the effect of settling time on the T_i and P_i removal efficiency using Fe(III)-CMC-CTA at the optimal conditions. The process was carried out using a variable time sequence, as discussed in Section 5.3.2.3 (in Chapter 5): (i) fast mixing at 295 rpm for 3 min after addition of the coagulant to the wastewater; (ii) slow mixing at 20 rpm for 25 min after addition of the polymer flocculant; and (iii) sedimentation at different times (1 to 90 min) to allow floc settling. After the desired settling time, an aliquot of the supernatant was sampled and prepared for turbidity and P_i measurement by UV-Vis absorbance. The kinetics of the CF process for P_i and T_i removal at the optimum conditions are depicted in Figure 6.8(a & b). The results show that the flocs quickly settle out within the first 20 min with little or no change in the flocculation efficiency after the first 25 min and reveal that the flocculant properties do not improve for a settling time beyond 20 min.

The PFO and PSO kinetic models were used to evaluate the adsorption kinetics of P_i and kaolinite colloidal species with the Fe(III)-CMC-CTA flocculant system. The PSO model is based on the assumption that the rate-limiting step involves interaction between the adsorbent (flocculant) and adsorbate that is often used to describe a chemisorption process[56]; however, the PSO model suggests that the sorption rate decreases linearly as the adsorption rate increases.[57] The PFO and PSO models are described by equation (6.5) and (6.6), respectively.

$$q_t = q_e(1-e^{-k_1 t}) \tag{6.5}$$

$$q_t = \frac{k_2 q_e^{\,2} t}{1+k_2 q_e t} \tag{6.6}$$

Here, q_e and q_t are the level of P_i or kaolinite particles adsorbed (mg/g) at dynamic equilibrium and at time t. k_1 and k_2 are the respective rate constants, where the parameters (k_1, k_2 and q_e) were estimated using non-linear regression fitting by equations (6.5) and (6.6).

Table 6.5: Pseudo-First-Order (PFO) and Pseudo-Second-Order (PSO) kinetic parameters for T_i and P_i removal at optimized flocculation conditions. c_o (T_i) = 400.0 mg/L and c_o (P_i) = 35.0 mg/L

Parameter	Kinetic models	
	PFO: P_i removal	**PSO: T_i removal**
q_t ($mg \cdot g^{-1}$)	165 ± 1	114 ± 1
$k \cdot 10^3$ (min^{-1})	131 ± 5	1.9 ± 0.1
R. Chi^2	16	7
R^2	0.991	0.987
	PSO: P_i removal	**PSO: T_i removal**
q_t ($mg \cdot g^{-1}$)	185 ± 3	103 ± 2
$k \cdot 10^3$ ($g \cdot mg^{-1} \cdot min^{-1}$)	1.0 ± 0.1	146 ± 10
R. Chi^2	38	21
R^2	0.977	0.959

The results of the flocculation of P_i and T_i by the $FeCl_3$/flocculant system are shown in Figure 6.8(a & b), where the lines represent the best-fit results for PFO and PSO models. Values of k_1, k_2, q_e and R^2 obtained from the regression analysis are listed in Table 6.5. Figure 6.8(a, b) describes the flocculation kinetics for P_i and T_i removal, respectively. The results in Figure 6.8 and the parameters in Table 6.5 show that T_i and P_i removal is well-described by each kinetic model. The flocculation kinetics of P_i are in good agreement with the PFO model whereas the kinetics of the T_i removal agrees with the PSO model according to the best fit results in Table 6.5. In addition, the predicted values of q_e determined by the PFO model agree well with experimental values, as compared with the PSO kinetic model for P_i removal. But the reverse was observed for T_i removal, where the best-fit values of q_e obtained from the PSO model agree more with the experimental values over the PFO model. The rate constant of the PSO (k_2) model is significantly greater than the PFO (k_2) model for the P_i removal process, however, for the T_i removal, values of k_1 are remarkably greater than k_2 values as depicted in Table 6.5. The kinetic study herein showed that the PSO model described the flocculation process for T_i removal. The analysis of kinetic parameters indicates the rate-limiting-step for flocculation involves interaction between the Fe(III)-CMC-CTA flocculant system and the anionic colloidal kaolinite, following a chemisorption-like process, where the flocculation process could be considered as irreversible. Also, the PFO adsorption mechanism describes the flocculation of P_i by Fe(III)-CMC-CTA flocculant system, per the PFO model. This shows that the P_i species are adsorbed by the flocculant system, where the rate decreases linearly as the adsorption rate increases. The results presented

herein are comparable to those obtained in Chapter 4 and other previous reports where phosphate, arsenate and anionic dyes were flocculated with polysaccharide-based flocculants.[58–60] The rapid equilibrium process at 22 min (Figure 6.8(a & b)) indicates that P_i and/or kaolinite anion species interact well with the outer surface sites of the flocculant system.

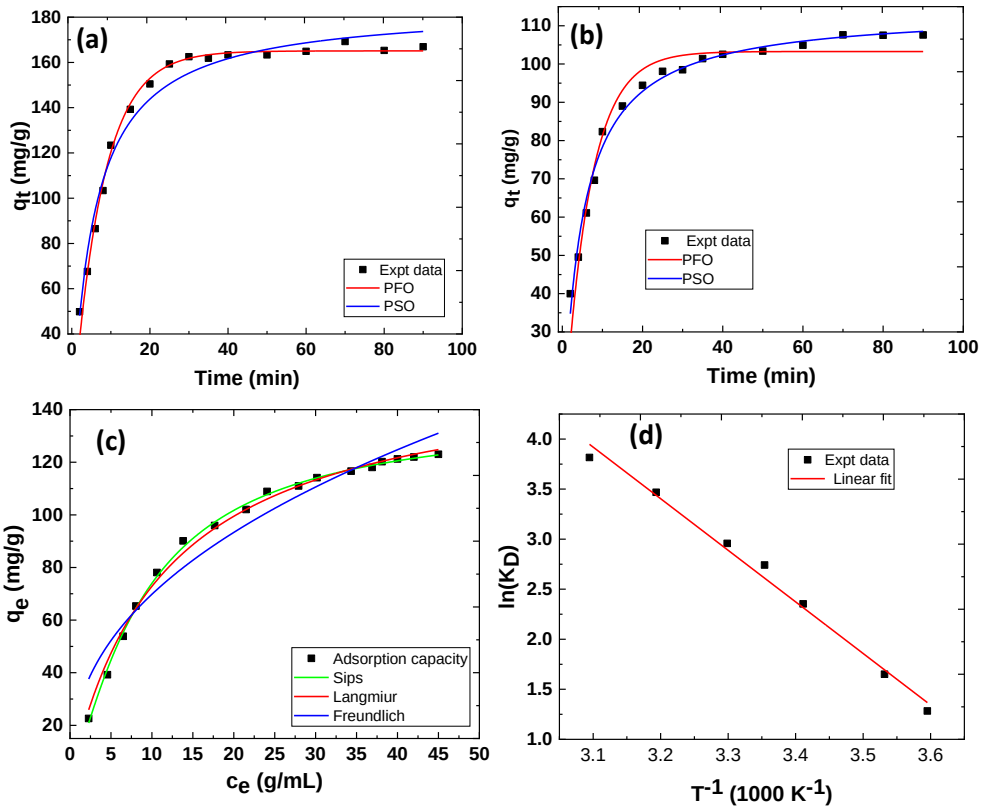

Figure 6.8: Flocculation kinetics of (a) P_i and (b) T_i removal in aqueous solution at variable time intervals. (c) The adsorption isotherm of P_i by combined $FeCl_3$ and CMC-CTA at optimized flocculation condition. (d) van't Hoff plot of ln(K_s) vs 1/T for P_i adsorption on CMC-CTA-$FeCl_3$ flocculants.

6.3.7 Flocculation adsorption

Initial contraction of the contaminant in wastewater is known to affect the CF performance significantly. Hence, the effect of the initial concentration of P_i on the CF removal efficiency was investigated through adsorption studies. Understanding of the interaction between adsorbates and adsorbents and the optimization conditions can be obtained from the adsorption isotherms.[61] In this study, the adsorption isotherm models were used to understand the adsorption processes to elucidate the flocculation mechanism. The experimental results were fitted by Langmuir, Sips and

Freundlich adsorption isotherms. The equations for the Langmuir,[62] Freundlich,[63] and Sips[64] isotherm models are given below from equation (6.7 to 6.9). The assumptions of each model have been discussed in Section 2.8.2. In this study, the adsorption isotherm models were used to understand the adsorption processes to understand the flocculation mechanism.

$$q_e = \frac{K_l q_m c_e}{1 + K_l c_e} \tag{6.7}$$

$$q_e = K_f c_e^{1/n} \tag{6.8}$$

$$q_e = \frac{K_s q_m c_e^{n_s}}{1 + K_s c_e^{n_s}} \tag{6.9}$$

Herein, q_m (mg·g^{-1}) is the monolayer adsorption of P_i per unit mass of Fe(III)-CMC-CTA adsorbent and q_e is the amount of adsorbed P_i (mg·g^{-1}). K_l (Lg^{-1}) K_f and K_s (Lg^{-1}) are the equilibrium adsorption constants for Langmuir, Freundlich and Sips models, respectively, which are related to the affinity of the binding sites. In the Freundlich model, the empirical exponent variable (n) gives useful information on the shape of the isotherm, where the adsorption process may be classified as unfavorable ($1/n > 1$), favorable ($1/n < 1$), and irreversible ($1/n = 0$). In the Sips model, at low adsorbate concentrations, it converges to a Freundlich isotherm. At high adsorbate concentration (or $n_s = 1$), the model reduces to a Langmuir isotherm.[65]

Figure 6.8c is the adsorption isotherm for the removal of P_i by Fe(III)-CMC-CTA flocculant system. The fitted lines through the data represent the *goodness-of-fit* of the isotherm models employed herein, where the variables are listed in Table 6.6. According to the results in Figure 6.8c and Table 6.6, the dimensionless constant, n^{-1} in the Freundlich model exceeds unity (2.4 ± 0.2) and suggests that the adsorption process is not favorable and does not follow a heterogeneous process. Additionally, the removal of P_i by the Fe(III)-CMC-CTA flocculant system is well-described by the Langmuir and Sips models. The value of n_s (1.1 ± 0.1), according to Sips model, is near unity, which implies that the Sips isotherm converges with the Langmuir model when n_s=1 and indicates favorable adsorption of phosphate. Hence, it can be inferred that the flocculation of P_i by Fe(III)-CMC-CTA follows a homogeneous mechanism based on the charge neutralization reaction between the anionic P_i and the ferric cation and cationic CMC-CTA flocculant under acid and neutral conditions. Moreover, the monolayer adsorption capacity (q_m; mg/g) for P_i, given in parentheses at the optimized conditions, are greater for the Langmuir isotherm (157 ± 3) relative

to the Sips isotherm (139 ± 3). Herein, the Langmuir model is considered more reliable due to n_s value (from Sips model) being near-unity as well as the relative simplicity and favorable *goodness-of-fit* for the Fe(III)-CMC-CTA flocculant system for the Langmuir model. The Langmuir adsorption constant, K_l is 0.09 ± 0.01 L/g, where this describes the adsorption process of P_i adsorbed on Fe(III)-CMC-CTA. This shows that there a strong affinity between P_i with Fe(III)-CMC-CTA to form large, dense and stable flocs in solution. The flocculation isotherm would have been described by the Freundlich model if other interactions occur besides electrostatic processes during flocculation. The Freundlich isotherm model is often used to describe heterogeneous adsorption systems.[66]

Table 6.6: Langmuir, Sips and Freundlich adsorption isotherm coefficients and thermodynamic parameters for adsorption of P_i by CMC-CTA-$FeCl_3$ flocculant system at pH 6.5

Parameter	**Adsorption isotherm model**			**T (K)**	**ΔG° (kJ/mol)**	**ΔH° (kJ/mol)**	**ΔS° (J/K mol)**
	Langmuir	**Sips**	**Freundlich**	283	-3.9		
Q_m (mg/g)	157 ± 3	139 ± 2		293	-5.7		
***K* x 10^{-3}**	87 ± 5	63 ± 5	27 ± 3	298	-6.8	43 ± 2	165 ± 6
n		1.1 ± 0.1	2.4 ± 0.8	303	-7.5		
R. Chi^2	6	2	54	313	-9.0		
R^2	0.994	0.998	0.949	323	-10		

6.3.8 Flocculation thermodynamics

The effect of temperature on the coagulation-flocculation of P_i by the Fe(III)-CMC-CTA flocculant system was investigated via thermodynamic studies. Values of the thermodynamic parameters such as the change in standard Gibbs free energy (ΔG^o) at equilibrium, standard enthalpy (ΔH^o) and standard entropy (ΔS^o) were calculated according to the equations below. These parameters were obtained by performing the flocculation process at variable temperatures.

$$\Delta G^\circ = -RT \ln K_D \tag{6.10}$$

$$\Delta G^\circ = \Delta H^\circ - T\Delta S^\circ \tag{6.11}$$

$$\ln K_D = \frac{\Delta S^\circ}{R} - \frac{\Delta H^\circ}{RT} \tag{6.12}$$

Here, R is the universal gas constant (8.314 J·mol^{-1}·K^{-1}), T is the absolute temperature and K_D is the adsorption equilibrium constant from the Langmuir, which is given according to equation (6.13).[67]

$$K_D = \frac{q_e}{c_e} \tag{6.13}$$

Values of ΔG^o were calculated at different temperatures using equation (2.13) and they are listed in Table 6.6. Also, the values of ΔH^o and ΔS^o were obtained by a linear fitting following equation (6.12) when $\ln K_D$ was plotted as a function of T^{-1}, and the results are presented in Figure 6.8d and Table 6.6. The flocculation-adsorption process is spontaneous due the negative values of ΔG^o for the P_i adsorption. As the temperature increases, the values of ΔG^o increase negatively, suggesting that the flocculation of P_i is energetically favorable at all temperatures. The positive values of ΔH^o obtained herein confirms that the flocculation process is endothermic and the product (flocs) is thermodynamically stable. Since ΔH^o is less than 40 kJ/mol, hence, it can be asserted that the flocculation process involves physical interaction (physisorption) between the P_i and the Fe(III)-CMC-CTA flocculant. The value of ΔS^o is positive, suggesting increased randomness and spontaneity at the liquid-liquid interface during the flocculation-adsorption process and the value reflects the strong adhesion of the Fe(III)-CMC-CTA flocculants towards the P_i. Also, the positive nature of ΔS^o implies that the spontaneity of the flocculation process is entropy driven. The results obtained herein are comparable to previous reports.[67–70]

6.3.9 Coagulation-flocculation mechanism

When $FeCl_3$ coagulant is added to turbid phosphate wastewater, the contaminants are predominantly coagulated by charge neutralization. In this case, the positive charge on the metal ion neutralizes the negatively charged sites of the contaminant particles. The addition of the polymer flocculant (CMC-CTA) acts as a destabilizing agent through charge neutralization and precipitation mechanism due to the electrostatic attraction between the positive charge on the polyelectrolyte and the negative charge on the contaminants. In the charge neutralization mechanism, flocculation may take place due to the reduced surface charge of the particles (reduction of zeta potential). As well, a decreased electrical repulsion between colloidal particles favors van der Waals attraction that results in initial aggregation of colloidal and fine suspended materials to form microfloc.[71] Hence, growth of microflocs to macroflocs occurs through flocculation due to the reduced surface charge of the particles and the decreased electrical repulsion

between them owing to the depression of the electrical double layer, leading to destabilization of the colloidal particles.[72] When the CMC-CTA dosage is low, electrostatic charge repulsion is another mechanism that may occur[73,74] because the particle surface is not fully covered as for the initial stages of adsorption. This is known as electrostatic patching, as discussed in Section 2.7.1 in Chapter 2, and occurs when a highly charged cationic polyelectrolyte adsorbs on a negatively charged surface to give overall neutrality. This happens because the average distance between surface sites is greater than that between charged segments along the polymer chain; hence, it is not possible for each surface charged site to be neutralized by a cationic polyelectrolyte unit.[75] Flocculation occurs due to electrostatic interaction between the positive patches and the negative area, which leads to particle attachment as particles come closely together.[76]

Another flocculation mechanism relates to polymer bridging that involves the formation of macroflocs from microflocs produced by coagulation with $FeCl_3$ through a flocculation process upon the addition of CMC-CTA. In this process, electrolyte bound to floc particle has loops and dangling/tailing chains that can attach to nearby particles.[71] The mechanism is favored when long-chain polymers without a high level of charge are used.[77] In this process, electrostatic and non-electrostatic forces cause one polymer chain to be adsorbed on two or more flocs. This occurs when the surface is partly covered, especially at the initial stages of the process, or when the polymer dosage is low and occurs immediately at the point of the addition of the polymer according to the mixing conditions.[78] At acidic condition, there is an affinity between the positively charged CMC-CTA and negatively charged colloidal suspensions (kaolinite-induced turbidity) and dissolved materials (P_i); hence, adsorption of polymer chains may occur. Due to the numerous points of attachment, the affinity between the polymer segment and the surface sites of the contaminants is low. In addition, the adsorption affinity should be appreciable to overcome the loss of entropy associated with polymer adsorption because an adsorbed chain will have a more restricted configuration than a random coil in free solution.[75] According to Napper[79], polymer adsorption usually follows three categories; (i) attached the surface in trains; (ii) projecting of polymer into the solution as tails; and (iii) the formation of loops, between trains. Adsorption of polymer segments onto contaminant surface sites may occur via electrostatic interactions, hydrogen bonding or ionic bonding. Electrostatic interaction between polyelectrolytes with opposite charges to that of the surface site are strongly adsorbed. Adsorption occurs because of the

interaction between oppositely charged ionic species. Scheme 1 is a general illustration of the coagulation-flocculation process described herein.

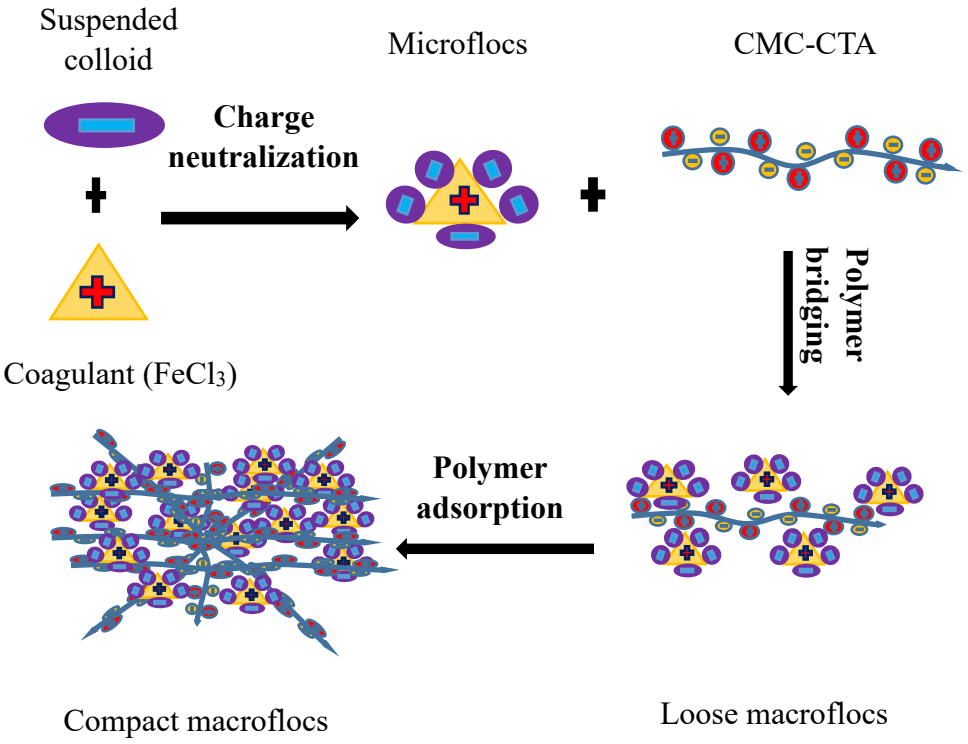

Scheme 6.1: Schematic illustration of the proposed coagulation-flocculation mechanism.

6.4 Conclusion

In Chapter 5, an amphoteric chitosan-based flocculant was synthesized by grafting 3-chloro-2-hydroxypropyl trimethylammonium chloride onto a carboxymethyl chitosan backbone denoted as CM-CTA. Herein, a jar test system was used to investigate the optimization of the coagulation-flocculation system for phosphate and turbidity removal in an aqueous medium. The Box-Behnken method was used to design the order of the experimental runs and to statistically analyze the experimental data in order to optimize the conditions for maximum P_i and T_i removal. The CMC-CTA and $FeCl_3$ dosage, together with pH and settling time, were determined as significant factors to yield optimal P_i and turbidity removal. By employing the BBD, on the basis of RSM, it was proven that combination of CMC-CTA dosage, $FeCl_3$ dosage, pH and settling time has a considerable effect on removal of the selected response functions. The predicted quadratic

polynomial models by the RSM method was used to estimate the P_i and T_i removal over the range of experimental design. Optimal conditions for the CF process occurred at pH 4.1, $FeCl_3$ (10.4 mg/L), CMC-CTA dosage (3.1 mg/L) and settling time (21.9 min) for P_i removal, and pH 9.4, $FeCl_3$ (10.2 mg/L), CMC-CTA dosage (1.0 mg/L) and settling time (39.8 min) for T_i removal with a high removal efficiency for P_i (98.4%) and T_i (99.8%). The compromised optimal conditions calculated from the regression equation were as follows: CMC-CTA dosage (3.0 mg/L), $FeCl_3$ dosage (10.1 mg/L), pH 6.8 and settling time of 35.0 min. The corresponding removal was 96.4% and 96.7%, for P_i and T_i. The validation results showed good agreement between experimental results and the RSM predictions, further illustrating that RSM can be used to model and optimize CF processes for phosphate and turbidity removal for demanding water treatment and technology applications. The flocculation process occurred via physisorption interaction between the colloidal species and the Fe(III)-CMC-CTA flocculant system and the process was spontaneous and driven by entropic forces relative to enthalpic forces.

6.5 References

(1) Yeoman, S.; Stephenson, T.; Lester, J. N.; Perry, R. *Environ. Pollut.* **1988**, *49* (3), 183–233.

(2) Hudson, J. J.; Taylor, W. D.; Schindler, D. W. *Nature* **2000**, *406* (6791), 54–56.

(3) Benyoucef, S.; Amrani, M. *Desalination* **2011**, *275* (1–3), 231–236.

(4) Apau, J.; Agbovi, H. K.; Wemegah, D. D. *J. Sci. Technol.* **2013**, *33* (3), 89–97.

(5) Attour, A.; Touati, M.; Tlili, M.; Amor, M. Ben; Lapicque, F.; Leclerc, J. *Sep. Purif. Technol.* **2014**, *123*, 124–129.

(6) Golder, A. K.; Samanta, A. N.; Ray, S. *Sep. Purif. Technol.* **2006**, *52*, 102–109.

(7) Vasudevan, S.; Lakshmi, J.; Jayaraj, J.; Sozhan, G. **2009**, *164*, 1480–1486.

(8) Tanada, S.; Kabayama, M.; Kawasaki, N.; Sakiyama, T.; Nakamura, T.; Araki, M.; Tamura, T. *J. Colloid Interface Sci.* **2003**, *257* (1), 135–140.

(9) Mahaninia, M. H.; Wilson, L. D. *J. Appl. Polym. Sci.* **2016**, *133* (5), 1–10.

(10) Filipkowska, U.; Jóźwiak, T.; Szymczyk, P. *Prog. Chem. Appl. Chitin its Deriv.* **2014**, *19* (1), 5–14.

(11) Sø, H. U.; Postma, D.; Jakobsen, R.; Larsen, F. *Geochim. Cosmochim. Acta* **2011**, *75* (10), 2911–2923.

(12) Yan, L. G.; Xu, Y. Y.; Yu, H. Q.; Xin, X. D.; Wei, Q.; Du, B. *J. Hazard. Mater.* **2010**, *179* (1–3), 244–250.

(13) Sathasivan, A. In *encyclopedia of life support systems*; McGraw Hill Professional, 2010; pp 1–16.

(14) Gautam, R. K.; Banerjee, S.; Gautam, P. K.; Chattopadhyaya, M. C. *Adv. Environ. Res.* **2014**, *36*, 1–23.

(15) Inan, H.; Alaydın, E. *Desalin. Water Treat.* **2014**, *52* (7–9), 1396–1403.

(16) Peleka, E. N.; Mavros, P. P.; Zamboulis, D.; Matis, K. a. *Desalination* **2006**, *198* (1–3), 198–207.

(17) Dunets, C. S.; Zheng, Y. *Hortscience* **2015**, *50* (6), 921–926.

(18) Mohammed, S. A. M.; Shanshool, H. A. *Iraqi J. Chem. Pet. Eng.* **2009**, *10* (2), 35–42.

(19) Trinh, T. K.; Kang, L. S. *Chem. Eng. Res. Des.* **2011**, *89* (7), 1126–1135.

(20) Kumar, S. S.; Bishnoi, N. R. *Appl. Water Sci.* **2017**, *7* (4), 1943–1953.

(21) Montgomery, D. C. *Design and analysis of experiments*, 9th ed.; Wiley: Hoboken, New Jersey, 2017.

(22) Murthy, M. S. R. C.; Swaminathan, T.; Rakshit, S. K.; Kosugi, Y. *Bioprocess Eng.* **2000**, *22*, 35–39.

(23) Li, Y.; Liu, Z.; Zhao, H.; Xu, Y.; Cui, F. *Biochem. Eng. J.* **2007**, *34* (1), 82–86.

(24) Palamakula, A; Nutan, M. T. H.; Khan, M. A. *AAPS PharmSciTech* **2004**, *5* (4), 114–121.

(25) Dawood, A. S.; Li, Y. *Polish J. Environ. Stud.* **2014**, *23* (1), 43–50.

(26) Ghafari, S.; Aziz, H. A.; Isa, M. H.; Zinatizadeh, A. A. *J. Hazard. Mater.* **2009**, *163* (2–3), 650–656.

(27) Singh, A.; Srivastava, A.; Tripathi, A.; Dutt, N. N. **2016**, *4* (2), 23–29.

(28) Li, N.; Hu, Y.; Lu, Y.-Z.; Zeng, R. J.; Sheng, G.-P. *Sci. Rep.* **2016**, *6*, 26115.

(29) Zemmouri, H.; Drouiche, M.; Sayeh, A.; Lounici, H.; Mameri, N. *Energy Procedia* **2013**, *36*, 558–564.

(30) Holme, H. K.; Foros, H.; Pettersen, H.; Dornish, M.; Smidsrùd, O. *Carbohydr. Polym.* **2001**, *46*, 278–294.

(31) Rojas-Reyna, R.; Schwarz, S.; Heinrich, G.; Petzold, G.; Schutze, S.; Bohrisch, J. *Carbohydr. Polym.* **2010**, *81* (2), 317–322.

(32) Wang, J.; Chen, Y.; Yuan, S.; Sheng, G.; Yu, H. *Water Res.* **2009**, *43* (20), 5267–5275.

(33) Yuan, B.; Shang, Y.; Lu, Y.; Qin, Z.; Jiang, Y.; Chen, A.; Qian, X.; Wang, G.; Yang, H.; Cheng, R. *J. Appl. Polym. Sci.* **2010**, *117* (I), 1876–1882.

(34) Zhang, W.; Shang, Y.; Yuan, B.; Jiang, Y.; Lu, Y.; Qin, Z.; Chen, A.; Qian, X.; Yang, H.; Cheng, R. *J. Appl. Polym. Sci.* **2010**, *117*, 2016–2024.

(35) Abreu, F. R. De; Campana-filho, S. P. *Carbohydr. Polym.* **2009**, *75* (2), 214–221.

(36) Ali, S. A.; Singh, R. P. *Macromol. Symp.* **2009**, *277*, 1–7.

(37) Bratskaya, S. Y.; Pestov, A. V; Yatluk, Y. G.; Avramenko, V. A. *Colloids Surfaces A Physicochem. Eng. Asp.* **2009**, *339*, 140–144.

(38) Cai, Z.; Song, Z.; Shang, S.; Yang, C. *Polym. Bull.* **2007**, *59*, 655–665.

(39) Li, S.; Zhou, P.; Yao, P.; Wei, Y.; Zhang, Y.; Yue, W. *J. Applied Polymer Sci.* **2010**, *116*, 2742–2748.

(40) Yang, J. S.; Xie, Y. J.; He, W. *Carbohydr. Polym.* **2011**, *84* (1), 33–39.

(41) Yang, Z.; Shang, Y.; Huang, X.; Chen, Y.; Lu, Y.; Chen, A.; Jiang, Y.; Gu, W.; Qian, X.; Yang, H.; Cheng, R. *J. Environ. Sci. (China)* **2012**, *24* (8), 1378–1385.

(42) Yang, Z.; Shang, Y.; Lu, Y.; Chen, Y.; Huang, X.; Chen, A.; Jiang, Y.; Gu, W.; Qian, X.; Yang, H.; Cheng, R. *Chem. Eng. J.* **2011**, *172*, 287–295.

(43) Ge, H. C.; Luo, D. K. *Carbohydr. Res.* **2005**, *340* (7), 1351–1356.

(44) Bidgoli, H.; Zamani, A.; Taherzadeh, M. J. *Carbohydr. Res.* **2010**, *345* (18), 2683–2689.

(45) Usharani, K.; Lakshmanaperumalsamy, P. *J. Microbiol. Biotechnol. Food Sci.* **2016**, *05* (06), 534–547.

(46) Usharani, K.; Muthukumar, M. *Int. J. Environ. Sci. Technol.* **2013**, *10* (3), 591–606.

(47) Yetilmezsoy, K.; Demirel, S.; Vanderbei, R. J. *J. Hazard. Mater.* **2009**, *171* (1–3), 551–562.

(48) Trinh, T. K.; Kang, L.-S. *Environ. Eng. Res.* **2010**, *15* (2), 63–70.

(49) Bratby, J. *Coagulation and Flocculation in Water and Wastewater Treatment*, IWA Publishing: London, 2006.

(50) Bhatia, S.; Othman, Z.; Ahmad, A. L. *Chem. Eng. J.* **2007**, *133* (1–3), 205–212.

(51) Lee, J. D.; Lee, S. H.; Jo, M. H.; Park, P. K.; Lee, C. H.; Kwak, J. W. *Environ. Sci. Technol.* **2000**, *34* (17), 3780–3788.

(52) Dey, K. P.; Mishra, S.; Sen, G. *J. Water Process Eng.* **2017**, *18*, 113–125.

(53) Hameed, Y. T.; Idris, A.; Aslina, S. *J. Environ. Manage.* **2016**, *184*, 494–503.

(54) Rajasulochana, P. *Resour. Technol.* **2016**, *2* (4), 175–184.

(55) Jadhav, M. V.; Mahajan, Y. S. *KSCE J. Civ. Eng.* **2013**, *17* (2), 328–334.

(56) Ho, Y. S.; McKay, G. *Process Biochem.* **1999**, *34* (5), 451–465.

(57) Lagergren, S. *K. Sven. Vetensk. Sakademiens Handl.* **1898**, *24* (1–39), 2474–2479.

(58) Kwok, K. C. M.; Koong, L. F.; Chen, G.; McKay, G. *J. Colloid Interface Sci.* **2014**, *416*, 1–10.

(59) Lin, Q.; Qian, S.; Li, C.; Pan, H.; Wu, Z.; Liu, G. *Carbohydr. Polym.* **2012**, *90* (1), 275–

283.

(60) Singh, R. P.; Pal, S.; Rana, V. K.; Ghorai, S. *Carbohydr. Polym.* **2013**, *91* (1), 294–299.

(61) Kono, H.; Kusumoto, R. *J. Water Process Eng.* **2015**, *7*, 83–93.

(62) Langmuir, I. *J. Am. Chem. Soc.* **1916**, *252*, 2221–2295.

(63) Freundlich, H. M. F. *Z. Phys. Chem.* **1909**, *57*, 385–470.

(64) Sips, R. *J. Chem. Phys.* **1948**, *18* (5), 490–495.

(65) Ho, Y. S.; Porter, J. F.; Mckay, G. *Water, Air, Soil Pollut.* **2002**, *141* (1–4), 1–33.

(66) Crini, G. *Dye. Pigment.* **2008**, *77* (2), 415–426.

(67) Karunanayake, A. G.; Navarathna, C. M.; Gunatilake, S. R.; Crowley, M.; Anderson, R.; Mohan, D.; Perez, F.; Pittman, C. U.; Mlsna, T. *ACS Appl. Nano Mater.* **2019**, *2* (6), 3467–3479.

(68) Xie, F.; Dai, Z.; Zhu, Y.; Li, G.; Li, H.; He, Z.; Geng, S.; Wu, F. *Colloids Surfaces A Physicochem. Eng. Asp.* **2019**, *562*, 16–25.

(69) Hena, S.; Atikah, S.; Ahmad, H. *Int. J. Eng. Sci.* **2015**, *4* (1), 51–62.

(70) Lin, J.; He, S.; Wang, X.; Zhang, H.; Zhan, Y. *Colloids Surfaces A Physicochem. Eng. Asp.* **2019**, *561*, 301–314.

(71) Lee, C. S.; Robinson, J.; Chong, M. F. *Process Saf. Environ. Prot.* **2014**, *92* (6), 489–508.

(72) Kleimann, J.; Gehin-Delval, C.; Auweter, H.; Borkovec, M. *Langmuir* **2005**, *21* (8), 3688–3698.

(73) Kasper, D. R. Theoretical and experimental investigations of the flocculation of charged particles in aqueous solutions by polyelectrolytes of opposite charge, Ph.D. Thesis, California Institute of Technology, Pasadena, California 1971. https://resolver.caltech.edu/CaltechTHESIS:04232014-095415213.

(74) Gregory, J. *J. Colloid Interface Sci.* **1973**, *42* (2), 448–456.

(75) Bolto, B.; Gregory, J. *Water Res.* **2007**, *41*, 2301–2324.

(76) Sher, F.; Malik, A.; Liu, H. *J. Environ. Chem. Eng.* **2013**, *1* (4), 684–689.

(77) Razali, M. A. A.; Ahmad, Z.; Ahmad, M. S. B.; Ariffin, A. *Chem. Eng. J.* **2011**, *166* (2), 529–535.

(78) Hoogeveen, N. G.; Cohen Stuart, M. A.; Fleer, G. J. *Colloids Surfaces A Physicochem. Eng. Asp.* **1996**, *117* (1–2), 77–88.

(79) Napper, D. H. *Polymeric stabilization of colloidal dispersions*; Academic Press Inc.: New York, 1983.

CHAPTER 7

7 Flocculation properties of cationic chitosan-based flocculant for phosphate and turbidity remediation

Description

This study reports on the design of a series of a single-component, high molecular weight, and mechanically stable cationic bioflocculants for efficient removal of phosphate and colloidal suspended particles (turbidity), without the need to employ inorganic coagulants. The bioflocculants were characterized by several techniques to confirm the structure of the modified biopolymer materials. The flocculation properties of the modified materials were investigated, where the effects of several external conditions (pH, flocculant dosage, settling time, and temperature) were examined. Also, flocculation kinetics, adsorption, and equilibrium thermodynamics were studied, and the flocs were characterized by several techniques.

Author's contribution

Lee D. Wilson and I conceived the project. I performed all the experimental work, data processing and analysis, and wrote the first draft of the manuscript as well as making further revisions where and when necessary on subsequent drafts. Dr. L.D. Wilson was responsible for the supervision of the project, editorial guidance for revision of the manuscript drafts, and corresponding author. Permission was obtained from all contributing authors before the inclusion of the manuscript in this thesis.

Relation of Chapter 7 to Overall Objective of this Project

This chapter discusses the modification of chitosan to form a single-component flocculant system for enhanced removal of phosphate and turbidity. It addresses the third research theme that focuses on the synthesis, characterization and flocculation performance and floc structural properties of high molecular weight cationic chitosan-based flocculant. In addition, this study supported hypotheses 1, 2, 3, and 6 introduced in Section 1.4 of Chapter 1. Herein, it was observed that modification of native chitosan improved its flocculation performance in a single-component system without the addition of metal ion coagulant. Also, external factors such as pH, temperature, settling time, and flocculant dosage had a significant effect on the removal efficiency, where an

optimum set of conditions is required to obtain maximum removal. Moreover, the modified biopolymer resulted in improving the properties of the flocs. Entropy effects were concluded from a thermodynamic study of the flocculation process at variable temperature.

7.1 Introduction

Conventional coagulation-flocculation (CF) involves the use of chemical reagents to promote the removal of colloidal suspended particles and dissolved nutrients in wastewater. Accordingly, CF-based wastewater treatment occurs in two successive stages; destabilization of stable colloidal particles followed by aggregation. For a typical coagulation process, a metal ion such as aluminium sulphate, ferric chloride, ferric sulphate or polyaluminium sulphate (or chloride) is added to the wastewater as a coagulant, which results in destabilization of the colloidal particles. However, mineral salts of this form possess several disadvantages such as pH dependence for efficient performance due to charge neutralization, large dosage requirements, ineffectiveness at low temperatures, large sludge volume production, secondary pollution in the sludge disposal and health concerns due to the amount of residual aluminium remaining in the water. To address these limitations, metal salt coagulants have been combined with synthetic polymers for efficient removal of suspended solids.[1,2] However, it is known that residual synthetic polymers, such as polyacrylate, polystyrene sulphonate, polyethylene oxide, and poly(diallyldimethyl) ammonium chloride in water may cause neurological disorders in human.[2,3] Therefore, the use of biopolymer materials as flocculants have attracted greater attention as alternative materials for wastewater treatment. Biopolymer flocculants are biodegradable, biocompatible and cost efficient, and have reduced toxicity, and typically form larger and denser flocs with less sludge volume.[4] One such polymer is chitosan, which is the second most abundant polysaccharide after cellulose, where it is obtained from the deacetylation of chitin biopolymers. In the last two decades, chitosan has attracted considerable attention as a bioflocculant due to its biodegradability and biocompatibility[5,6], as well as its CF potential towards different contaminants in wastewater, such as dissolved nutrient (phosphate, nitrate, etc.), bacterial suspension, colloidal suspension (suspended solids), metal ions, dyes, milk processing plants and oily wastewater.[7,8] Even though chitosan has attracted a large interest in wastewater treatment, it has a lower molecular weight and semi-crystalline structure that is generally insoluble in water at alkaline and neutral pH conditions. This is due to its strong intermolecular and intramolecular hydrogen bonding, which limits its

application in wastewater treatment at a wider pH range.[9] Therefore, it is necessary to modify the structure and morphology of chitosan to improve its water solubility over a wide range of pH and increase its level of functionalization. Chitosan has many free amine and hydroxyl groups along its chain, which can be used to modify it through graft polymerization. During graft polymerization of chitosan, synthetic functional polymers such polyacrylamide (PAM) or polyacrylic acid are introduced as side chains to the backbone of the chitosan. Grafting of PAM onto chitosan leads to the development of efficient flocculants with controlled biodegradation, shear ability, amorphous structure and improved functional properties.[10] Lu et al[11], have shown that grafting of PAM onto chitosan significantly increased solubility due to the breaking of the semi-crystalline network structure in chitosan by the grafting. However, graft modification of chitosan with PAM has limitations such as lower charge density, poor thermal stability, lower hydrodynamic volume and radius. Hence, quaternization of the Chi-*g*-PAM polymer flocculant with CTA to obtain a cationic flocculant will improve these properties and enhance the flocculation efficiency of these polymer flocculants. The presence of fine clay minerals such as kaolinite has been problematic for tailings in several industries such as phosphate and oil sand processing industries.[12] Previous reports[13,14] on the surface charge properties of kaolinite clay have shown that the surfaces (alumina face, silica face, and edge face) are all negatively charged in both acidic and alkaline conditions. Therefore, the introduction of positively charged materials such as a cationic polymer flocculant into kaolinite dispersion will improve aggregation between these fine clay particles, resulting in the formation of kaolinite clusters (flocs). Another major pollutant in wastewater is phosphorus, which is an essential plant nutrient for growth and development, where it exists in aquatic systems as orthophosphate, polyphosphate, phosphonate or organophosphate. However, excess phosphorous in water bodies lead to eutrophication and excessive algae growth in lakes and rivers, which raises concerns for aquatic life.[15–17] At different pH conditions, phosphorus may exist as H_3PO_4 (pH < 2) $H_2PO_4^-$ (pH 2.0 – 6.8), HPO_4^{2-} (pH 6.8 – 11) and PO_4^{3-} (pH > 11). Hence, at pH > 2, all the species are negatively charged and are expected to undergo electrostatic attractive interaction with cationic flocculants.

This work is aimed at designing single-component CF materials for improved removal of kaolinite colloidal dispersion and dissolved orthophosphate. Herein, a non-toxic quaternary ammonium reagent, CTA was introduced onto Chi-*g*-PAM chains via quaternization process and a series of strong cationic flocculants (CTA-Chi-*g*-PAM) were obtained. The functional and

flocculation properties of these materials were investigated in the presence of a kaolinite clay suspension and phosphate, where the effects of pH, flocculant dosage, and settling time were tested. An evaluation of the flocculation kinetics (time dependent) and thermodynamic (temperature dependent) properties of the flocculation process are discussed herein. The cationic flocculants are anticipated to outperform other coagulant and flocculant materials reported in Table 7.1, in terms of dosage required for optimal removal, pH and temperature dependence for effective performance, settling properties of flocs, flocs size and morphology, and total elimination of mineral salts as coagulants.

Table 7.1: Comparison of the removal of phosphate in wastewater using different coagulant-flocculant systems

Water Source	Flocculant	Optimum dosage (mg/L)	Optimum pH	Efficiency (%)	Reference
SW	Fe(III) + CMC-CTA	10, 3.0	6.5	96.4	This thesis**
SW	Chitosan	20	6.2 - 7.0	78 ± 0.1	This thesis*
SW	Chitosan + Alum	49	5.8 - 7.0	88 ± 0.8	This thesis*
Struvite	Chitosan and Alginate	10, 20	N/A	80	Latifian et al.[18]
MW	Chitosan	60	9.5	89	Dunets and Zheng[19]
SW	Chitosan + PAC	67.9; 20.05	7.5	99.4	Li et al.[20]
SW	Zr^{4+}-chitosan	50	4	60.6	Liu and Zhang[21]
AW	HMW Chitosan	12	7.2	99.1	Chung et al.[22]
MW	Chitosan	10	7	98	Turunen et al.[23]
SW	CMC-CTA	5	6.5	70.5	This thesis**
SW	CMC	8	6.5	29.8	This thesis**

SW: Synthetic wastewater; MW: Municipal wastewater; AW: Agricultural wastewater.

This thesis* (Results from Chapter 3) and This thesis** (Results from Chapter 5).

7.2 Materials and methods

7.2.1 Materials and Chemicals

All chemicals were of analytical reagent (AR) grade. Anhydrous monobasic potassium phosphate (KH_2PO_4), NaOH (aq), HCl (aq), vanadate molybdate reagent, chitosan (medium molecular weight, 85% deacetylation), ethyl alcohol, isopropanol, 3-chloro-2-hydroxypropyl trimethylammonium chloride (CTA), acrylamide, potassium persulfate, acetone and spectroscopic grade potassium bromide (KBr) were purchased from Sigma-Aldrich, Oakville, Ontario, Canada. All materials were used as received unless specified otherwise.

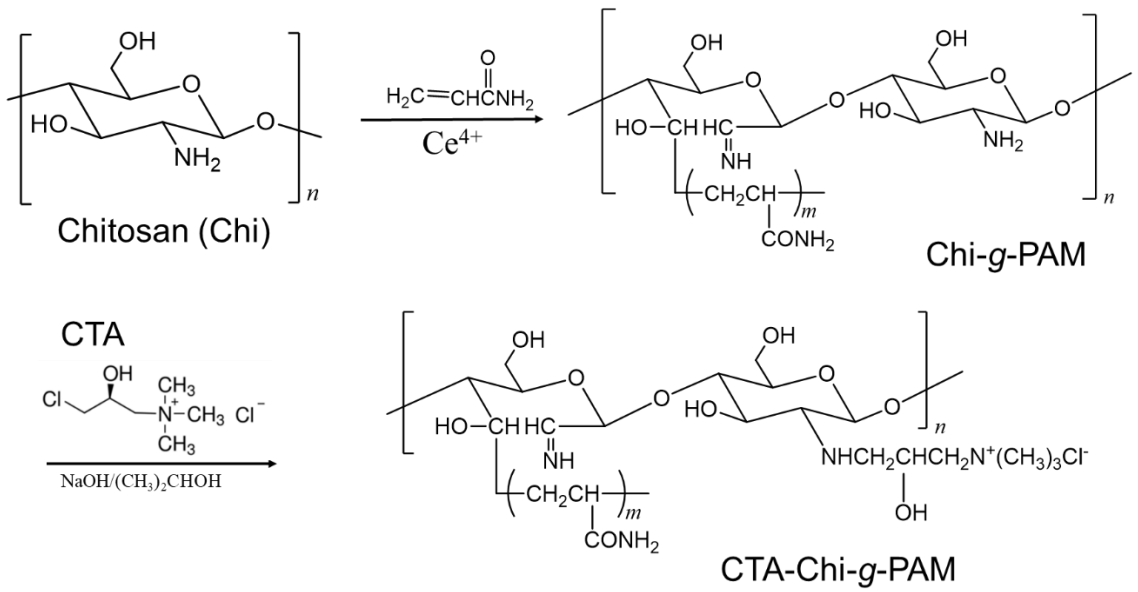

Scheme 7.1: Synthetic routes of chitosan-grafted-polyacrylamide (Chi-*g*-PAM) and 3-chloro-2-hydroxypropyl trimethylammonium chloride (CTA) quaternized onto Chi-*g*-PAM to form cationic flocculant (CTA-Chi-*g*-PAM).

7.2.2 Preparation of CMC and CMC-CTA

The method for the synthesis of CMC and CTA was adopted from a previous report[11], where it was slightly modified for this study. Briefly, about 1.0 g of chitosan was dissolved in a 1% (v/v) acetic acid aqueous solution (50 mL) via agitation. After 30 min of stirring under N_2, 5 mL potassium persulfate solution (0.28 wt%) initiator and an acrylamide monomer (5 g) were added to the solution with continuous stirring at 23 ^{o}C. The polymerization was stopped after 3 h, and the grafted chitosan-*g*-PAM copolymer was precipitated in acetone. The product was purified four times by repeated dissolving-precipitating treatment, and then further purified by Soxhlet extraction over 72 h using acetone as solvent. The Chi-*g*-PAM was dried in a vacuum oven at 50 ^{o}C for 48 h to a constant weight. The grafting ratio (G) was calculated using equation (7.1), where w_1 and w_2 are the weights of the original and grafted samples, respectively.

$$G = \frac{(w_2 - w_1)}{w_1} * 100\% \tag{7.1}$$

In the synthesis of the quaternized flocculant, a desired amount of Chi-*g*-PAM was added into isopropanol and a 10 wt % NaOH blending aqueous solution. The mixture was heated at 45 ^{o}C in an oil bath under continuous stirring (75 rpm) and alkalized for 1 h until the solution became a

thick liquid. A required amount of aqueous CTA was added into the mixture and the reaction was kept at 60 ^{o}C for 10 h under agitation. The solid product was filtered and rinsed in 90% ethanol for removal of salt and water, then by Soxhlet extraction using acetone as a solvent for 48 h for further treatment and was then dried at room temperature. The amount of chitosan-*g*-PAM was kept constant, while varying the amount of CTA for each synthesis trial, in order to prepare a series of CTA-Chi-*g*-PAM flocculant samples with various degrees of substitution (DS) of CTA. The mass ratios of Chi-g-PAM to CTA were 2:1, 2:2, 2:3, 2:4 and 2:5, and are denoted as CTA-Chi-*g*-PAM-1, CTA-Chi-*g*-PAM-2, CTA-Chi-*g*-PAM-3, CTA-Chi-*g*-PAM-4, CTA-Chi-*g*-PAM-5, respectively. Scheme 7.1 represents the synthetic routes for Chi-*g*-PAM and CTA-Chi-*g*-PAM.

7.2.3 Flocculant characterization

7.2.3.1 Degree of substitution of CTA-Chi-*g*-PAM

The degree of substitution (DS) of the quaternized copolymer flocculant was evaluated using both potentiometric and spectroscopic ^{1}H-NMR measurements. The DS was determined by conductivity titration apparatus with aqueous $AgNO_3$, in which a silver and calomel electrodes were used as the measurement and reference electrodes, respectively. The degree of quaternization was determined by titrating the chloride ion in the CTA with aqueous $AgNO_3$ and the DS was calculated according to equation (7.2).[66]

$$DS = \frac{V * c}{V \cdot c + \frac{(m - V \cdot c \cdot 420)}{162}} \cdot \frac{1}{DD} \cdot 100\% \qquad (7.2)$$

Here, c (mol/L) and V (L) are the molar concentration and volume of the $AgNO_3$ solution at the equivalence point, m (g) is the mass of the quaternized flocculant. Values of 421 and 162 represent the molar mass (g/mol) of the repeated units of the quaternized copolymer flocculant and glucosamine units in chitosan, respectively. DD is the degree of deacetylation of chitosan, which was 85% in this study.

The degree of substitution of the quaternized flocculants was also calculated using the ^{1}H-NMR in Figure A9.7 (in Appendix A). Using the signals at 4.66 ppm (H1) and 4.16 ppm (H2') from the CTA-Chi-*g*-PAM spectra, the values of DS were calculated using equation (7.3), where $A_{H2'}$ and A_{H1} are the NMR peak areas corresponding to protons of H2' and H1, respectively.

$$DS = \frac{A_{H2'}}{A_{H1}} \cdot 100\% \quad (7.3)$$

7.2.3.2 FT-IR spectroscopy

IR spectra of the materials were obtained using a Bio-RAD FTS-40 spectrophotometer. Powdered samples were mixed with pure spectroscopic grade KBr in a 1:7 (sample: KBr) weight ratio followed by grinding in a small mortar and pestle. The diffuse reflectance infrared Fourier transform (DRIFT) spectra were obtained in reflectance mode at 25 ^{o}C with a resolution of 4 cm^{-1} over the 400–4000 cm^{-1} spectral range. Multiple scans were recorded and then background corrected relative to pure KBr.

7.2.3.3 NMR Spectroscopy

The ^{1}H NMR spectra were recorded using a wide-bore (89 mm) 11.7 T Oxford superconducting magnet system (Bruker Bio Spin Corp; Billerica, MA, United States) equipped with a 5 mm PaTx1 probe. NMR acquisition parameters were controlled using a SSSC 500 console and workstation running X WIN-NMR 3.5. Standard pulse programs utilized were available from the TopSpin 1.3 software. In here, D_2O was used as the solvent. The ^{13}C-NMR spectra were obtained using a Bruker AVANCE III HD spectrometer operating at 125.77 MHz (^{1}H frequency at 500.23 MHz) with a 4 mm DOTY CP-MAS probe. The ^{13}C CP/TOSS (Cross Polarization with Total Suppression of Spinning Sidebands) spectra were obtained with a spinning speed of 6 kHz with a ^{1}H 90˚ pulse of 3.5 µs, 1.0 ms contact time, and a ramp pulse on the ^{1}H channel. Acquisition of spectra utilized multiple scans (1024 - 2048) with a recycle delay of 2.0 s. All spectra were recorded using a 71 kHz SPINAL-64 decoupling sequence, where chemical shifts (δ) were referenced to adamantane (δ=38.48 ppm).

7.2.3.4 Thermogravimetric analysis (TGA)

Thermogram profiles were obtained using a Q50 (TA instruments) with a heating rate of 5 ^{o}C·min^{-1} to a maximum temperature of 500 ^{o}C, where nitrogen was the carrier gas. The thermal stability of the materials was shown using first derivative plots (DTG) of weight with temperature (%/^{o}C) against temperature (^{o}C) and weight (wt%) loss against temperature.

7.2.3.5 pH at the point of zero charge (pH_{pzc})

The determination of the pH at the point-of-zero-charge (pH_{pzc}) of the flocculant was adapted from the procedure reported by Singh et al.[67] After the preparation of the NaCl solution (0.01 M), 25 ml portions were added to six separate 125 ml Erlenmeyer flasks. The pH of the solutions was then adjusted between 2 and 12 with aqueous NaOH or HCl. Approximately 100 mg of the sample was added to each solution and it was allowed to equilibrate for 48 h where the final pH was measured. The difference between the final and initial pHs (ΔpH) was plotted as a function of the initial pH, where the pH_{pzc} was determined as the point of intersection between ΔpH and the initial pH.

7.2.3.6 SEM imaging

Scanning electron microscopy (SEM; Model SU8000, HI-0867-0003) was used to study the surface morphology of chitosan, chi-*g*-PAM and CTA-Chi-*g*-PAM flocculant materials. Images of gold-coated samples were collected under the following instrument conditions; accelerating voltage-10 kV, 9 mm working distance (WD), magnification-2000× and a sample spot size-50 at room temperature.

7.2.3.7 X-ray Diffraction (pXRD)

The X-ray diffraction patterns of chitosan, chi-g-PAM and CTA-Chi-*g*-PAM flocculant materials were obtained using a PANalytical Empyrean powder X-ray diffractometer. A monochromatic Co−Kα1 radiation was used in which the current and the applied voltage were set to 45 mA and 40 kV, respectively. The samples were mounted in a horizontal configuration after evaporation of methanol films. The pXRD patterns were measured in continuous mode over a 2θ range, where 2θ = 1−70° with a scan rate of 3.2° min^{-1}.

7.2.3.8 Zeta potential

The zeta potential (ζ) of the polymer flocculant materials was determined using a Zetasizer Nano-ZS90 instrument (Malvern Instruments, Westborough, MA, USA) by measuring the electrophoretic mobility (U_E) of the polymer solution (0.05% w/w, at pH 7.0), and utilizing Henry's equation (7.4) to calculate the zeta potential:[68]

$$U_E = \frac{2\varepsilon \cdot \zeta \cdot f(\kappa\alpha)}{3\eta} \tag{7.4}$$

Here, ε (Farad/m) is the permittivity, $f(\kappa\alpha)$ is a function related to the ratio of particle radius (α, nm) and the Debye length (κ, nm^{-1}), and η (mPa·s) is the dispersion viscosity. The Smoluchowski approximation f ($\kappa\alpha$) equaled to 1.5, as folded capillary cells were used with point scatters larger than 200 nm in a dispersant with electrolyte concentrations of > 1 mmol/L.[69]

7.2.4 Floc size distribution and properties analysis

At the end of the coagulation-flocculation process, samples of the flocs were taken for floc size distribution measurement. The particle size distribution and floc size of kaolinite particles and flocs were measured by a laser particle size analyzer, MasterSizer 2000 (Malvern Instruments) equipped with a wet dispersion cell of the Mastersizer 2000 (Hydro 2000^{SM}) at a wavelength of 633 nm. Chemical properties of the flocs were evaluated using FT-IR and their surface charge was determined via zeta potential measurement using Melvin Zetasizer at varying pH. In addition, the surface morphology of the flocs was studied by SEM, under the same condition discussed earlier.

7.2.5 Coagulation-flocculation process

Standard stock solutions of orthophosphate (5000 mg/L), Chi-*g*-PAM (2000 mg/L) and CTA-Chi-*g*-PAM (2000 mg/L) were prepared by dissolving the solutes in doubly deionized Millipore water and further diluted to the desired concentrations. The CF process was carried out by an adapted procedure reported in Section 3.2.2 (Chapter 3). Approximately 1 L of an aqueous solution containing P_i was added to the jar tester, and 5.0 ml of the P_i solution was sampled for analysis. A pre-determined volume of kaolinite dispersion was added to each jar solution to simulate colloidal particles in the P_i solution. The kaolinite dosage was maintained at 400 mg/L throughout and the pH of the turbid P_i solutions was adjusted by using 0.1 M NaOH or HCl, if necessary. A pre-determined amount of the flocculant (Chi-*g*-PAM and CTA-Chi-*g*-PAM) was added to the solution, followed by rapid stirring for 3 min and slow mixing for 20 min at 295 rpm and 25 rpm, respectively, without the addition of any metal coagulant. The stirring was stopped, and the flocs were allowed to undergo sedimentation. Once the flocs have settled, a 10.0 ml solution aliquot was sampled from the top layer and the transmittance (%T) was measured (λ= 800 nm). In addition, a 15 ml solution aliquot was sampled and centrifuged when necessary for 60 min, and then prepared for UV-Vis analysis to estimate P_i levels in the treated samples. P_i concentration before and after the flocculation process was evaluated using colorimetric determination with vanadate molybdate as a complexing agent to form a colored complex solution with P_i. With the aid of a calibration

curve, the P_i concentration was measured with a double beam UV-Vis spectrophotometer where the absorbance was measured at λ_{max} = 420 nm. The T_i removal (%), P_i removal (%) and removal capacity ($mg \cdot g^{-1}$) were calculated by equations (7.5 - 7.7), respectively. Measurements were performed in triplicate and reported as the average value along with the standard deviation.

$$\%Turb_{removal} = \frac{T_c - T_o}{100 - T_o} \cdot 100\% \tag{7.5}$$

$$\%P_{i\,removal} = \frac{c_o - c_e}{c_o} \cdot 100\% \tag{7.6}$$

$$q_e = \frac{(c_0 - c_e) \cdot V}{m} \tag{7.7}$$

Here, T_o and T_c are the transmittance (%T) of the turbid water before and after the flocculation process. c_o and c_e are the initial and equilibrium concentrations of P_i in the solution (mg/L), V is the volume (L) of the solution and m (g) is the mass of the adsorbent (flocculant).

7.3 Results and Discussion

7.3.1 Characterization of flocculants

7.3.1.1 Degree of substitution

The degree of substitution (DS) of CTA onto the copolymer flocculant has a significant impact on their physical and chemical properties as well as their reactivity. Higher DS of CTA is expected to increase the solubility of the cationic quaternized flocculants over a wide range of pH. The DS of such cationic flocculants relates to the average number of substituted $–NH_2$ and/or –OH groups per glucosamine unit in the structure of chitosan. As expected, the DS increased with an increasing CTA weight ratio in the cationic polymer, as reported in Table 7.2. This indicates that as the CTA weight ratio increased, more quaternary ammonium ion groups are introduced to the grafted copolymer, making them more cationic and subsequently enhancing their solubility in water at a wider pH range, which positively affects the flocculation efficiency. The results obtained herein are comparable to previous reports.[24,25]

Table 7.2: Degree of substitution (DS) and solubility of cationic chitosan-based flocculants

Sample	(DS; %)	Solubility in water at different pH values										
		2	**3**	**4**	**5**	**6**	**7**	**8**	**9**	**10**	**11**	**12**
Chitosan		S	S	S	S	SS	N	N	N	N	N	N
Chi-*g*-PAM	67.3*	S	S	S	S	S	S	S	S	SS	SS	SS
CTA-Chi-*g*-PAM-1	39.0	S	S	S	S	S	S	S	S	S	SS	SS
CTA-Chi-*g*-PAM-2	47.9	S	S	S	S	S	S	S	S	S	S	SS
CTA-Chi-*g*-PAM-3	56.4	S	S	S	S	S	S	S	S	S	S	S
CTA-Chi-*g*-PAM-4	66.5	S	S	S	S	S	S	S	S	S	S	S
CTA-Chi-*g*-PAM-5	76.0	S	S	S	S	S	S	S	S	S	S	S

S = soluble; SS = sparingly soluble; NS = insoluble. * = % grafting of PAM onto chitosan

7.3.1.2 ^{1}H- and ^{13}C-NMR spectroscopy

Evidence of the modification of the native chitosan was confirmed by signatures in the ^{1}H-NMR spectra in Figure 7.1a. The ^{1}H-NMR spectra of the acrylamide monomer (PAM), chitosan, Chi-*g*-PAM and CTA-Chi-*g*-PAM are shown for comparison. The spectrum for PAM shows characteristic spectral lines of characteristic groups at 6.09 ppm (=CH-N) and 5.69-5.72 ppm (=CH_2). The chitosan spectrum reveals characteristic signatures (ppm) at 4.45 (H1), 3.57-3.77 (H4-H6), 3.01 (H2) and 3.44 (H3). By comparison, the spectrum of Chi-*g*-PAM, strong resonance lines at 1.55 ppm and 2.11 ppm that represent –CH_2- and –CH- groups, which are characteristic of polyacrylamide[24,26], supporting that PAM was grafted onto the chitosan backbone. In the case of the quaternized cationic flocculants, the resonance line at 3.13 ppm, depicting methyl ((CH_3)$_3^+$N-)) groups in the quaternary ammonium ion, identified the presence of CTA. Also, additional spectral lines (ppm) at 2.43, 4.21 and 3.32 represent several CTA groups (H10, H11 and H12).[11,24] This supports the introduction of the CTA onto the grafted copolymer to make it cationic. According to Figure A9.7 (*cf.* Appendix A), the intensity of the peak at 3.13 ppm increased as the weight ratio of the CTA in the quaternized flocculant increased, indicating a significant increase in the DS of the flocculant materials from CTA-Chi-*g*-PAM-1 to CTA-Chi-*g*-PAM-5.

The solid state ^{13}C-NMR spectra of PAM, chitosan, Chi-*g*-PAM and CTA-Chi-*g*-PAM are presented in Figure 7.1b. The spectrum of PAM shows signature peaks at 169 ppm, 130 ppm and 128 ppm for C=O, -CH= and –CH- nuclei in the acrylamide structure. Chitosan showed characteristic peaks (ppm) at 104.8, 57.3, 74.7 and 83.1, which are assigned to C1, C2 and C6, C3 and C5 and C4, respectively. Also, as a result of the incomplete deacetylation of the chitosan, it showed peaks at 24.1 ppm and 179 ppm, which are assigned to methyl-C and -C=O of the

acetamido groups in the chitosan. In the spectrum of the grafted chitosan (Chi-*g*-PAM), the presence of -$CONH_2$ group in the grafted flocculant is evident due to the strong and intense ^{13}C line (C=O) at 173.9 ppm.[27,28] In the spectrum of the cationic flocculant, the presence of CTA on the grafted copolymer is confirmed by the strong signature at 54.8 ppm, which is ascribed to the -CH_3 moieties of the quaternary ammonium ion group.[11,27,28] The presence of the methyl carbon shows a successful synthesis of the cationic flocculants. According to Figure A9.8, the intensity of the ^{13}C nuclei at 54.8 ppm increased from CTA-Chi-*g*-PAM-1 to CTA-Chi-*g*-PAM-5, indicating that the cationic content in the flocculant increases as the DS of CTA increases.

7.3.1.3 FT-IR spectroscopy

FT-IR spectral studies on the flocculant materials were conducted to provide complementary support of chemical modification of the native chitosan. The IR spectra of PAM, chitosan, Chi-*g*-PAM and CTA-Chi-*g*-PAM are depicted in Figure 7.1c. The spectrum of chitosan showed O-H and C-H vibration stretching at 3452 cm^{-1} and 2868 cm^{-1}, respectively, in agreement with related reports.[29,30] The IR wavenumbers (in cm^{-1}) at 1656, 3452 and 1320 are the characteristic absorption bands of the amine groups of chitosan. In addition, other bands (in cm^{-1}) at 1589, 1034, 1050 and 1150 represent N-H bending, C6-OH, C3-OH stretching and C-O-C bonds stretching, respectively. Comparing the spectra between chitosan and Chi-*g*-PAM, there is a sharp absorption band at 1666 cm^{-1} and a small peak at 1603 cm^{-1}, which signifies C=O and N-H stretching in the amide of the PAM. The new peak at 1449 cm^{-1} shows C-N stretching in the amide, whereas the peak at 1410 cm^{-1} shows $–COO^-$ stretching.[27] These IR bands are signatures of the PAM, which support the grafting of the PAM onto chitosan. The presence of the cationic CTA group on the Chi-*g*-PAM was confirmed by the peak at 1473 cm^{-1}, which relates to the methyl groups in the quaternary ammonium ion of CTA.[29,31] According to Figure A9.9, which represents the IR spectra of the CTA-Chi-*g*-PAM flocculants with different DS for CTA, it shows identical spectra with the absorption band at 1473 cm^{-1} increasing in intensity as the DS increases for CTA. An interesting insight observed in Figure 7.1c and Figure A9.9 is that the N-H stretching band at 1589 cm^{-1} disappeared in the spectra of the cationic flocculants and the C6-OH peak shifted from 1034 cm^{-1} to 1024 cm^{-1}, which shows that quaternization of Chi-*g*-PAM with the CTA group mostly took place at C6. This depicts that the intermolecular and intramolecular hydrogen bonds were broken in the preparation of the quaternized chitosan-based flocculants.

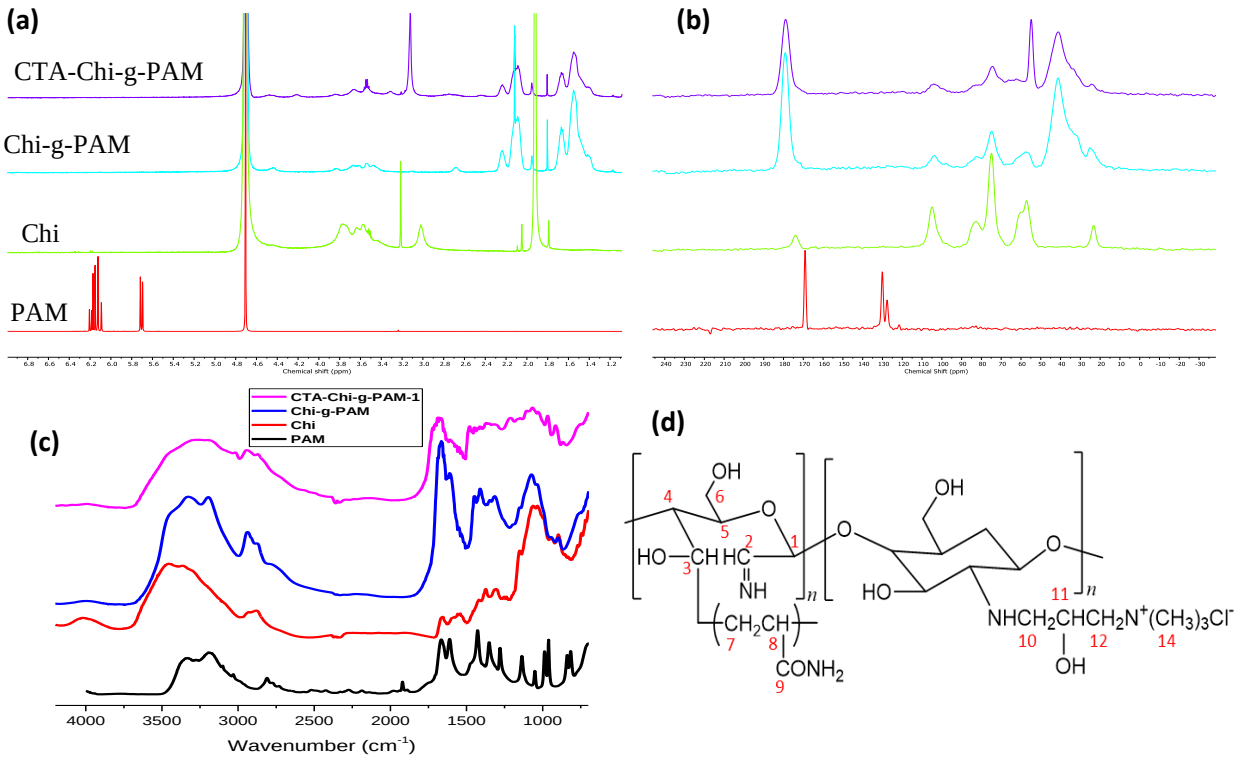

Figure 7.1:(a) ^{1}H-NMR, (b) ^{13}C-NMR and (c) FT-IR spectra of acrylamide monomer (PAM), chitosan (Chi), grafted copolymer (Chi-*g*-PAM) and cationic quaternized flocculant (CTA-Chi-*g*-PAM). (d) Chemical structure of CTA-Chi-*g*-PAM.

7.3.1.4 TGA

Structural composition and thermal stability of related materials such as cross-linked and grafted polymers have been investigated using TGA.[32–34] Information such as weight loss profiles due to thermal decomposition, as well as estimation of polymer composition relating to the presence of resolved thermal events, can be inferred from TGA profiles. In this report, the TGA results are presented as the first derivative weight with temperature (DTA) (Figure 7.2a) and the weight loss (Figure 7.2b) as a function of temperature for various systems: PAM, chitosan, Chi-*g*-PAM and CTA-Chi-*g*-PAM flocculant materials. The TGA profiles of the other cationic flocculants with different DS of CTA are shown in Figure A9.11. According to the results presented herein, PAM has three thermal events with a weight loss profile across a range from 22 ^{o}C to 500 ^{o}C. The first thermal event occurred between 22-152 ^{o}C with a solvent desorption process at 139 ^{o}C due to loss of water bound molecules. The second and third weight loss event occurred at 254 ^{o}C and 343 ^{o}C, respectively, due to the loss of imide groups. At this temperature, one

ammonia molecule is liberated for every two amide groups, leading to the formation of imide. Subsequently, the thermal degradation of the imides occurs at these stages (254 ^{o}C and 343 ^{o}C).[35,36] Chitosan showed two thermal events. In the first thermal event, weight loss occurred at a temperature below 100 ^{o}C, and it is due to the loss of moisture and other volatile constituents, with maximum weight loss occurring at 57 ^{o}C. As reported in Section 5.3.1.4 in Chapter 5, the second weight loss occurred at 296 ^{o}C, which is assigned to the decomposition of the chitosan structure, which relates to the breakdown of the glucosamine units of the biopolymer. The grafted copolymer and quaternized flocculants showed three thermal events, which differ from chitosan, according to Figure 7.2a. Chi-*g*-PAM has thermal decompositions at 52 ^{o}C, 285 ^{o}C and 386 ^{o}C, while that of CTA-Chi-*g*-PAM appeared at 66 ^{o}C, 268 ^{o}C and 397 ^{o}C. The decomposition at 285 ^{o}C (for Chi-*g*-PAM) and 268 ^{o}C (for CTA-Chi-*g*-PAM) is due to the degradation of the glucosamine units in the chitosan backbone. The values are less than that of chitosan since, during the grafting modification, part of the –C-C- linkage between the amine and the hydroxyl groups between biopolymer units of chitosan became interrupted due to steric effects, thereby attenuating the intramolecular and intermolecular hydrogen bonding.[37,38] Also, the decomposition temperature of the glucosamine units in the cationic flocculant was less than that in the grafted copolymer because it shows the presence of amine groups, which may lower the thermal stability of the CTA-Chi-*g*-PAM. This effect is in accordance with the reduced bond strength of heteroatom-C bonds vs C-C or C-H bonds and the role of chloride ion as an oxidizing agent during the thermal decomposition profile, as discussed in Section 5.3.1.4 in Chapter 5. The thermal events at 386 ^{o}C and 397 ^{o}C are due to the decomposition of the PAM grafted chains. However, in the case of the CTA-Chi-*g*-PAM flocculants, the decomposition temperature was higher because of the presence of the cationic quaternary ammonium group.

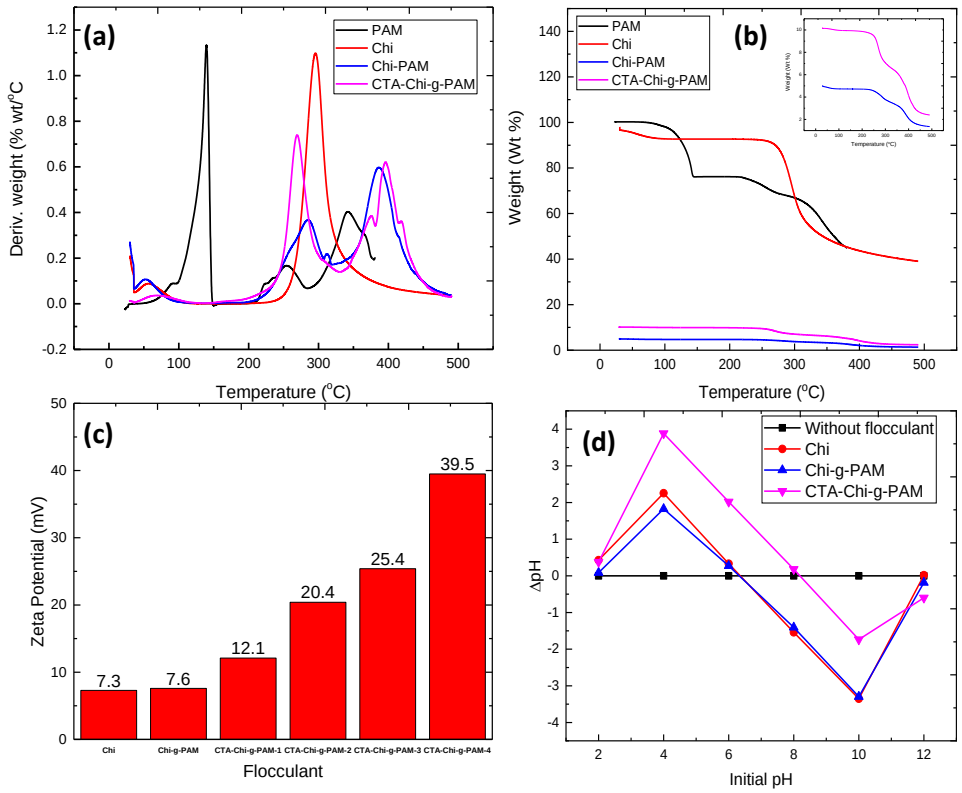

Figure 7.2: TGA profile of PAM, Chi, Chi-*g*-PAM, CTA-Chi-*g*-PAM: (a) First derivative of weight loss with temperature against temperature, and (b) weight loss with temperature. Zeta potential and point-of-zero-charge (d) of the polymer flocculant. The inset in (b) represents the TGA of Chi-*g*-PAM and CTA-Chi-*g*-PAM.

7.3.1.5 Zeta potential (ζ-potential) and point-of-zero-charge (pH_{pzc})

Kaolinite colloidal particles have a negative surface charge due to electrical double layer effects, which causes enhanced stability of a colloidal dispersion.[13,14] Hence, the surface charge properties of the flocculant materials will significantly alter their flocculation properties. Figure 7.2c shows the zeta potential of the various flocculants at ambient pH (7). According to Figure 7.2c, chitosan and Chi-*g*-PAM had relatively ζ-potential values of +7.3 mV and +7.6 mV, respectively. The positive ζ-potential of chitosan is due to the protonation of the amine group near or at pH values below the pK_a of chitosan, where the pK_a value (~6.2) depending on the source of the material.[39] An interesting insight is that the non-ionic nature of PAM did not alter the surface charge of the chitosan, as confirmed in the zeta potential measurements, in agreement with a previous report.[29] The incorporation of CTA cationic groups onto the copolymer was evident by

the increased positive ζ-potential of the CTA-Chi-*g*-PAM flocculants. As expected, increasing the DS of CTA in the polymer flocculant significantly increased the ζ-potential of the polymer solutions.[40,41] For instance, CTA-Chi-*g*-PAM-1 and CTA-Chi-*g*-PAM-5, which respectively had the low and high CTA DS, had ζ-potential values of +12.1 mV and +39.5 mV. Addition of CTA to the Chi-*g*-PAM polymer enhanced the positive surface charge of the flocculant, which is essential for effective flocculation of anionic species such as phosphate, sulphate, nitrate and arsenate. A complementary result to the zeta potential is the point-of-zero-charge, which represents the pH value at which the net charge of a material is zero. It gives insights on electrostatic interaction of a material surface with charged species, as discussed in Section 2.2.3 in Chapter 2. At pH < pH_{pzc}, where the pH is greater than the pK_a of the material, adsorption of negatively charged species occurs due to protonation of the surface of the sorbent material. However, at pH > pH_{pzc}, adsorption of positive charged species such as metal ions occur owing to deprotonation of the sorbent surface. The pH_{pzc} results are in good agreement with that of the zeta potential. According to Figure 7.2d, the pH_{pzc} of chitosan and Chi-*g*-PAM are 6.39 and 6.34, respectively, indicating that the non-ionic PAM did not have any impact on the surface charge of the grafted copolymer. The isoelectronic point (IEP), where pH = zero, for the cationic flocculant ranges from 6.45 to 8.21, as depicted in Figure A9.10 (Appendix A), which shows that the pH_{pzc} of these materials are from acidic to alkaline region. The results suggest that the cationic flocculants will be protonated in both acidic and near-alkaline medium, which will enhance their solubility in water over a wide pH range and consequently improve flocculation of the colloidal and dissolved anionic contaminants since repulsive Coulombic effects will be minimized at this pH range.

7.3.1.6 pXRD

pXRD patterns of the various synthesized flocculant materials were investigated to evaluate their structural or relative crystallinity, as compared to the pristine biopolymer material (chitosan). Figure 7.3a illustrates the X-ray diffraction profiles of chitosan, Chi-*g*-PAM and different cationic quaternized flocculants (CTA-Chi-*g*-PAM). The pXRD patterns of chitosan showed one intense characteristic peak at 2θ-value of 20^o and two minor peaks at 10^o and 35^o. The two minor peaks are due to the strong hydrogen bonding of chitosan, suggesting the semi-crystalline nature of chitosan molecules and its poor solubility in water.[42] They also represent hydrated crystals of low crystallinity and correspond to form I. The reflection at 2θ of 20 ^{o} is identified as a representative of the equivalent of form II.[43,44] The grafting of chitosan with PAM results in a more disordered

structure, as evidenced by a single, less intense and broad peak that is observed at 20 ^{o} in the pXRD pattern of the Chi-*g*-PAM. This behavior suggests that the grafted copolymer possessed more amorphous character, as compared with chitosan. Also, the disappearance of the two minor peaks at 10^{o} and 35^{o} indicates the breaking of hydrogen bonds in the grafted flocculant, leading to a more disordered amorphous structure.[27,44,45] Considering the pXRD patterns of the cationic flocculants, the signal at 2θ value at 20^{o} becomes broader and disappears as the cationic (CTA) content increases. This is evidenced by the results for CTA-Chi-*g*-PAM-5 that has the most amount of CTA, where there is no pXRD signature at 2θ = 20^{o}. This shows that the quaternization of the grafted flocculant remarkably changed the morphology of the polymer from crystalline to amorphous on account of the decreased number of free hydroxyl and amine groups compared to the native chitosan, resulting in a reduction in intra- and inter-molecular hydrogen bonding between the molecules. Functionalization of chitosan with CTA resulted in a reduction of the well-ordered directional interactions between biopolymer chains of chitosan. In turn, this results in a reduction of its relative crystallinity, for a reason stated previously, and subsequently increased its solubility in water, which further enhanced its flocculation ability.[43]

7.3.1.7 SEM

To understand further the morphology and porous nature of the grafted biopolymer flocculant materials, SEM micrographs of the samples were obtained. Figure 7.3b displays SEM images of PAM, Chitosan, Chi-*g*-PAM and CTA-Chi-*g*-PAM. The SEM images of the acrylamide monomer (Figure 7.3b(i)) have rough, fibrous and network-like morphology.[46] Differences can be observed among the flocculant materials. Graft polymerization and cationic quaternization of the chitosan resulted in modified surface morphology, porosity as well as physical and chemical properties of the chitosan, as shown in Figure 7.3(b). It is obvious that chitosan had a relatively flat and smooth surface without any pore-like structures, which is in agreement with the highly ordered nature of chitosan, according to the results related to its relative crystallinity from pXRD studies.[47,48] Grafting of PAM onto chitosan changed its conformation and the morphology. According to Figure 7.3b (iii), the SEM micrograph of Chi-*g*-PAM has a rough surface and loose structures with micropores. The micrograph also shows that there is an absence of phase separation between chitosan and PAM. The introduction of PAM grafts onto chitosan led to the disruption of the semi-crystalline structure since the intra- and inter-molecular hydrogen bonding interactions were reduced. SEM images of the CTA quaternized flocculant had a rough, irregular, loosened and

porous network surface morphology. According to an independent study, the introduction of the cationic groups to the grafted copolymer backbone weakened and destroyed the original relatively ordered crystals of the chitosan.[47,49] According to the SEM images in Figures A9.12 and A9.13 in Appendix A for the cationic quaternized flocculants, CTA-Chi-*g*-PAM-5 exhibited the most porous, rough and network-like structure, which is attributed to the greater DS of CTA in the polymer flocculant. The porous morphology of these flocculants is anticipated to be beneficial for the flocculation process since more pores are efficient for adsorbing and flocculating contaminants in wastewater.

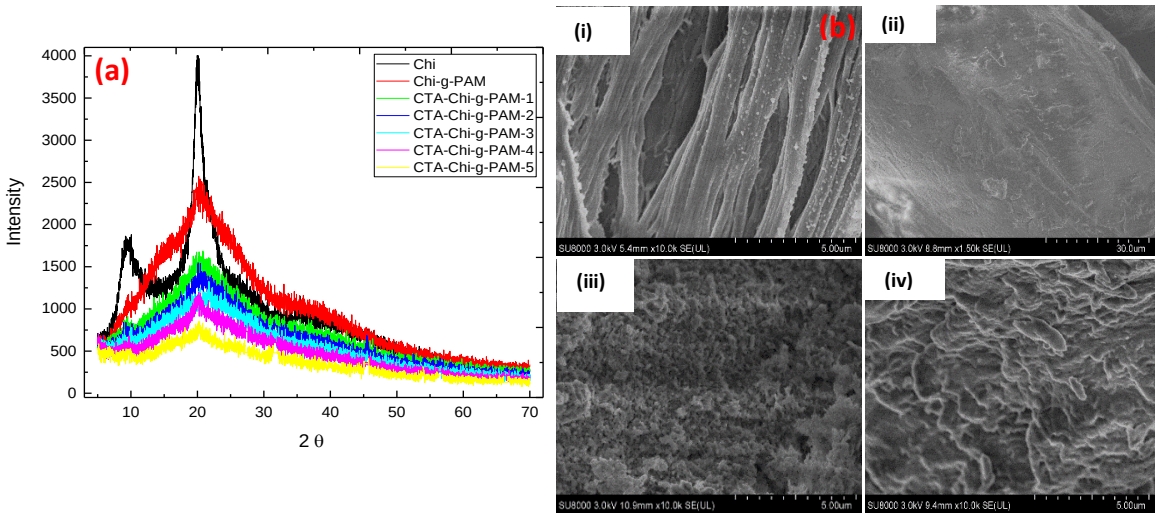

Figure 7.3: (a) pXRD patterns and (b) SEM micrograph of the polymer flocculants, where (i) PAM, (ii) Chi, (iii) Chi-*g*-PAM and (iv) CTA-Chi-*g*-PAM.

7.3.1.8 Solubility in water

Water solubility is one of the most important characteristics of an efficient flocculant in wastewater treatment.[50] Even though chitosan has been used as coagulant aid and/or flocculant, its poor solubility in water at pH > 6.2 limits its applicability over a wide range of pH.[41] Hence, flocculant solubility in both acidic and alkaline media is favorable to a wide range of applications. Table 7.2 reports the aqueous solubility of chitosan, Chi-*g*-PAM and CTA-Chi-*g*-PAM over a wide range of pH. As expected, chitosan is soluble in acidic region (pH < 6) but insoluble at alkaline conditions. Grafting of PAM onto the chitosan backbone increased its solubility up to pH 9 and showed evidence of partial solubility at pH > 9. As discussed in the pXRD results, the increased

solubility in the grafted copolymer is attributed to the destruction of the highly ordered crystalline structure in the chitosan and due to the breaking of inter- and intra-molecular hydrogen bonds that maintain a noncovalent network of chitosan.[51] Compared with chitosan and Chi-*g*-PAM, the cationic flocculants showed remarkably improved aqueous solubility over a wide pH range. The excellent solubility of the CTA-Chi-*g*-PAM flocculants could be owing to the ionic nature of the cationic quaternary ammonium ion group in the CTA, leading to more favorable ion-dipole interactions. Also, the polymer-polymer interactions were lessened, and the polymer-solvent interactions were enhanced due to the inhibition of hydrogen bonding interactions due to functionalization of CTA onto Chi-*g*-PAM. The solubility of the quaternized flocculants increased with increasing DS of the CTA. For instance, CTA-Chi-*g*-PAM-5 was completely soluble in water in both acidic and basic media; however, CTA-Chi-*g*-PAM-1 with the lowest CTA DS was soluble up to pH 10 but sparingly soluble beyond that pH condition.

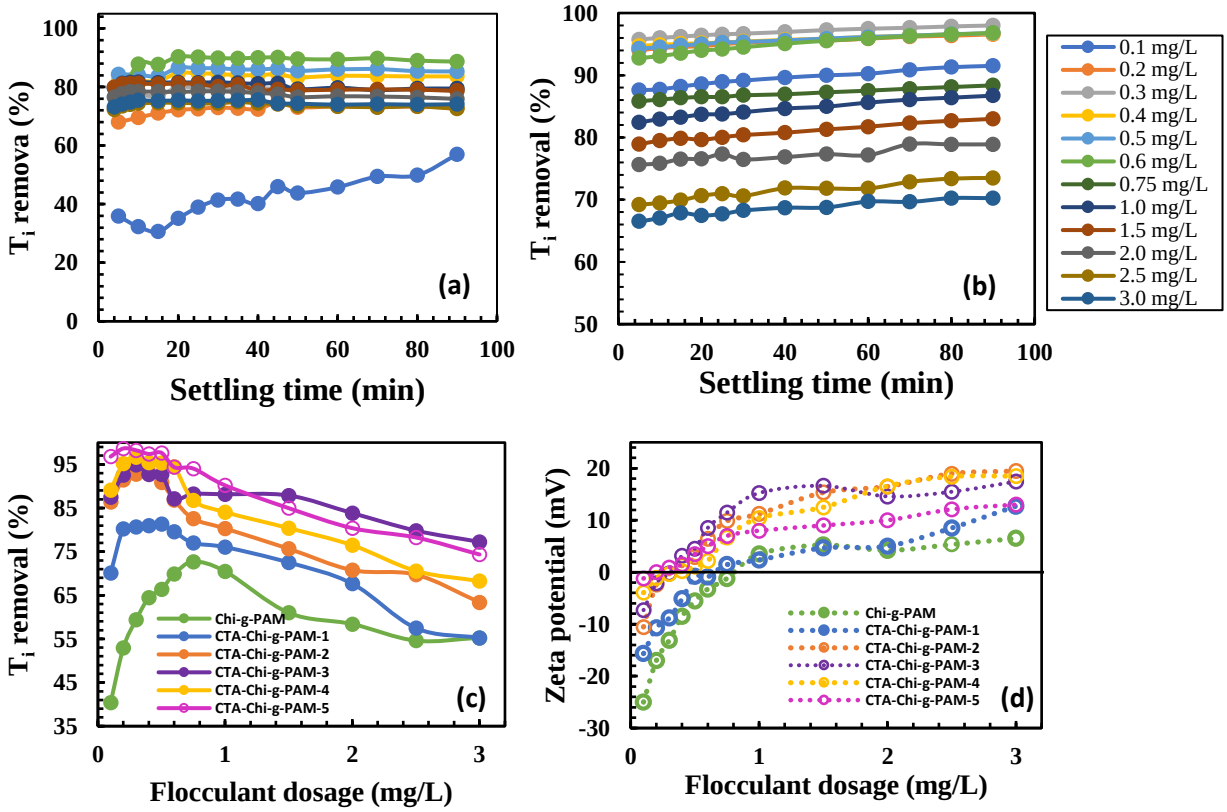

Figure 7.4: Effects of settling time on the removal turbidity with (a) Chi-*g*-PAM and (b) CTA-Chi-*g*-PAM-4. Effects of flocculant dosage on (a) turbidity removal and (b) zeta potential.

7.3.2 Coagulation-flocculation

7.3.2.1 Effect of settling time

Naturally, colloidal particles are poorly sedimented by conventional gravitational settling and may take a long period for this to occur, if not impossible, due to the stable nature of colloidal suspension owing to electrostatic repulsions relating to the electric double layer, as discussed in Section 2.2.2 (Chapter 2). Addition of coagulants to the colloidal dispersion causes destabilization of the colloidal particles and further addition of flocculant leads to aggregation of the destabilized particles to form macroflocs, which improves their settling ability over a short period.[52] Figure 7.4 (a & b) shows the effect of settling time on turbidity removal efficiency of the simulated kaolinite colloidal suspension using Chi-*g*-PAM and the CTA-Chi-*g*-PAM-4 flocculants, whereas the other flocculants are reported in Figure A9.14 in Appendix A. In here, there was no addition of metal ion coagulants. The quaternary ammonium ion group in the CTA acted as a coagulant to destabilize the colloidal system through the breaking of the electric double layer, which reduced the electrostatic repulsion between the colloidal particles, then led to electrostatic charge neutralization. Thereafter, the polymer component of the flocculants brought about aggregation of the destabilized colloidal particles. This resulted in the formation of larger, denser and compact flocs with great settling ability. According to Figure 7.4a, the T_i removal efficiency increased steadily with greater settling time up to 90 min, especially at a low flocculant dosage (0.1 mg/L). As the flocculant dosage increased, settling time did not have any significant influence on the removal efficiency. For instance, for Chi-*g*-PAM, the T_i removal after 5 min and 90 min of settling are 87.8% and 88.6%, respectively, at a dosage of 0.75 mg/L. Similarly, T_i removal after the same settling time for CTA-Chi-*g*-PAM-1 and CTA-Chi-*g*-PAM-4 are 91.0% and 92.0% as well as 94.7% and 96.8% at respective dosage values of 0.5 mg/L and 0.3 mg/L. At the low flocculant dosage, there are insufficient cationic sites on the polymer flocculants to destabilize the suspended colloidal particles; hence, aggregation of the particles occurs over time during the flocculation stage via polymer bridging. However, sufficient levels of flocculant result in adequate cationic quaternary ammonium groups to destroy the stability of the colloidal particles via electrical double layer depression and charge neutralization in relation to orthokinetic flocculation process. Thus, the particles are able to aggregate over a short period and settle rapidly. In addition, for all the flocculants, at high dosage, the T_i removal increased steadily with greater settling time. This could be due to the presence of excess flocculants at high dosage, which causes restabilization of the

flocs due to charge reversal effects. These results show that when adequate flocculant dosage is used, settling time can be as fast as 5 min, which is beneficial for wastewater treatment. The faster settling ability of the flocs at sufficient flocculant dosage could be due to the formation of aggregates with adequate size, which was able to settle rapidly with no challenges. The larger and denser flocs obtained at these dosages were attributed to the adsorption of higher molecular weight cationic chitosan-based flocculant onto the microflocs obtained from the destabilization of the colloidal particles that promote rapid rates of settling.[53]

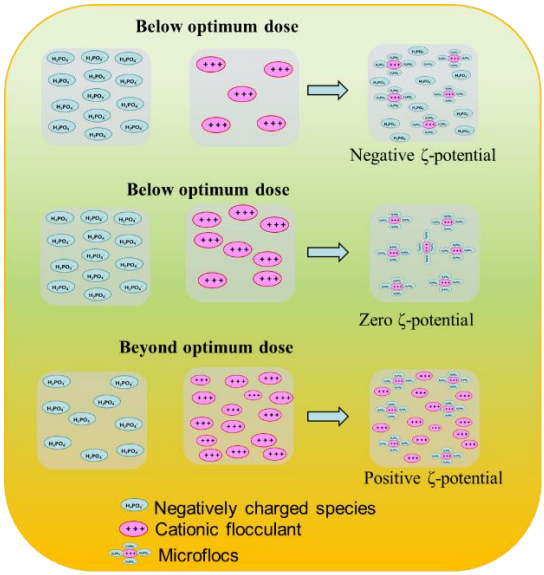

Scheme 7.2: Illustration of the coagulation of negatively charged species (kaolinite or phosphate) with cationic flocculants via charge neutralization at different flocculant dosage.

7.3.2.2 Effect of flocculant dosage

7.3.2.2.1 Turbidity removal

One of the known major parameters that influence flocculation is the flocculant dosage, as discussed in Section 2.6.2 (Chapter 2). Hence, the effects of Chi-*g*-PAM and CTA-Chi-*g*-PAM flocculant dosages on the removal efficiency of T_i and P_i were investigated. Figure 7.4c represents T_i removal efficiency as a function of flocculant dosage at pH 6.5 for all the flocculants studied herein. Figure 7.4d also shows the zeta potential of the supernatant collected as a function of the flocculant dosage. All the flocculants followed a general trend, where there is a rise in the removal efficiency with increasing flocculant dosage until it reached an optimal value and then decreased upon further addition of the flocculant. This shows that the amount of the flocculant employed can

have a remarkable impact on the outcome of the flocculation process. At initial flocculant dosage of 0.1 mg/L, the removal efficiency (%) were 40.4, 70.1, 86.1, 87.5, 89.1 and 96.8 for Chi-*g*-PAM, CTA-Chi-*g*-PAM-1, CTA-Chi-*g*-PAM-2, CTA-Chi-*g*-PAM-3, CTA-Chi-*g*-PAM-4 and CTA-Chi-*g*-PAM-5, respectively. This suggests that the introduction of CTA on the grafted copolymer to form cationic flocculants led to the improved separation of the liquid-solid colloidal system. Increased CTA DS in the flocculant resulted in the greatest removal efficiency at an initial dosage of 0.1 mg/L. Optimal dosages (in mg/L) with the corresponding removal efficiency in parenthesis are 0.75 (72.7%), 0.5 (81.3). 0.4 (92.7), 0.3 (94.9), 0.3 (98.2) and 0.2 (98.6) for Chi-*g*-PAM, CTA-Chi-*g*-PAM-1, CTA-Chi-*g*-PAM-2, CTA-Chi-*g*-PAM-3, CTA-Chi-*g*-PAM-4 and CTA-Chi-*g*-PAM-5, respectively. From Figure 7.4c, the optimum dosage required for the non-ionic flocculant (Chi-*g*-PAM) is relatively high. However, for the cationic flocculants, the required optimum dosage decreased as the CTA DS increased. This phenomenon occurs because the cationic quaternary ammonium group destroys the electrical double layer of the colloidal particles, which causes them to be destabilized via coagulation and form microflocs. The polymer flocculant components then aided aggregation of the microflocs through polymer bridging and adsorption, resulting in the formation of denser and more compact flocs. According to Figure 7.4d, the ζ-potential of the supernatant increased with the flocculant dosage. However, at the initial dosage (0.1 mg/L), the ζ-potential was negative except for CTA-Chi-*g*-PAM-5, which was near zero due to its high DS of CTA. At the optimal dosage, the ζ-potential was near zero for all the flocculants; however, it became positive beyond the optimal dosage. This confirms that the flocculation process occurs via charge neutralization, where the cationic groups on the flocculant neutralized the anionic surface of the kaolinite particles. At the initial stage (below optimal dosage), there is insufficient flocculant added; hence some of the colloidal particles are not fully neutralized, resulting in a negative ζ-potential and relatively low removal efficiency, as shown in Scheme 7.2. At the optimal dosage, there is an equal ratio of the cations to the colloidal particles; therefore, there is complete neutralization that results in a nearly zero zeta potential and removal efficiency of T_i, as shown in Scheme 7.2. In addition, the quaternary ammonium ion groups resulted in an extended conformation to maximize separation between like-charges along the polymer backbone at the low and optimal dosage, which greatly improved bridging flocculation mechanism that led to excellent T_i removal.[11] In Scheme 7.2, the T_i removal decreased gradually and the ζ-potential became positive when the flocculant dosage was beyond the optimal value. At this point, there is

an overdose of the flocculant and the presence of excess cationic flocculants restabilized the kaolinite colloidal particles due to the overall positive charge of the system and consequently decreasing the flocculation efficacy.

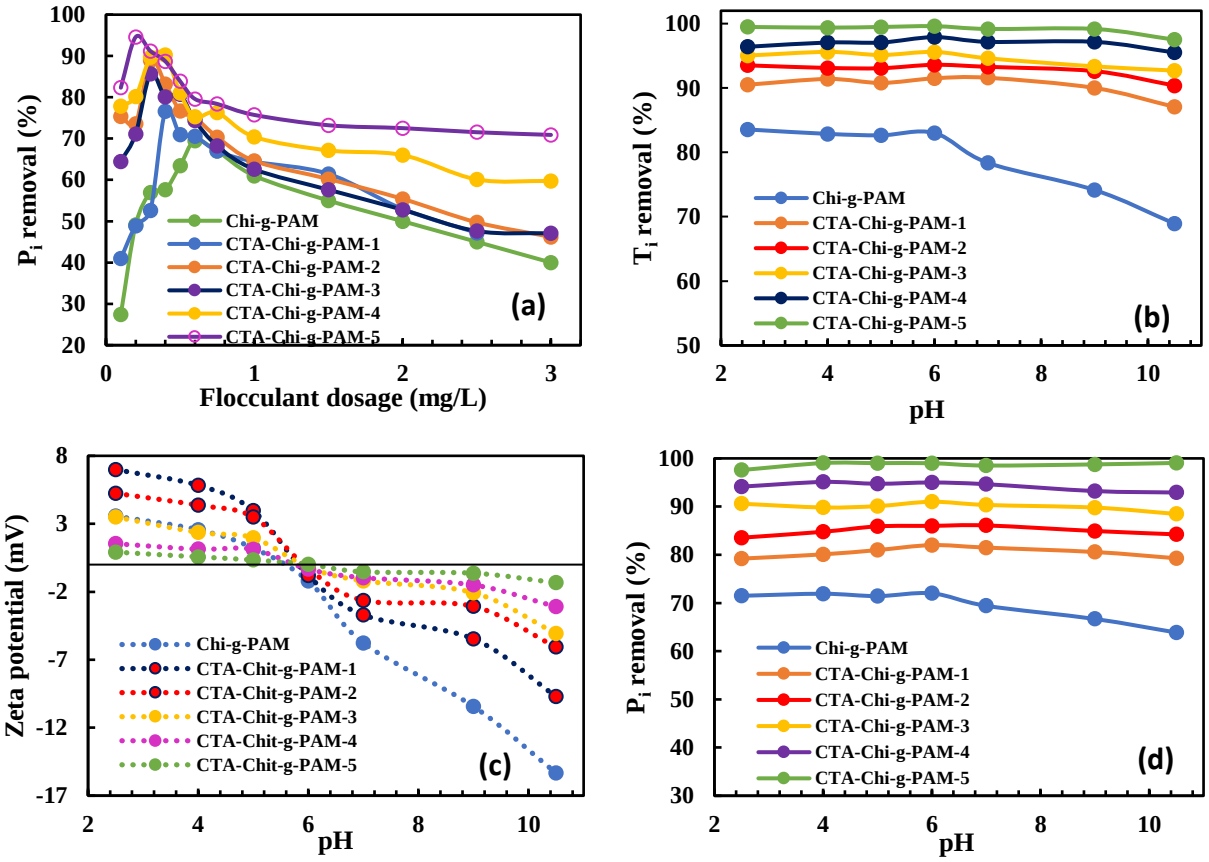

Figure 7.5: (a) Effects of flocculant dosage on phosphate removal. pH effects on (b) turbidity removal, (c) Zeta potential and (d) phosphate.

7.3.2.2.2 Phosphate removal

The removal of phosphate in wastewater often requires the use of metal ion coagulants through precipitation, followed by sedimentation and/or filtration. However, the process is pH dependent, and a high dosage of the coagulant is required, which produces a large sludge volume. Herein, cationic chitosan-based flocculants were used for the efficient removal of phosphate without metal coagulants. Figure 7.5a illustrates P_i removal efficiency as a function of flocculant dosage at pH 6.5 for Chi-*g*-PAM and CTA-Chi-*g*-PAMs. The flocculation process followed a general trend, where an increase in the P_i removal occurs with an increase in the flocculant dosage, and thereafter

decreases steadily with a further increase in the dosage. Chi-*g*-PAM generally showed lower removal relative to the CTA-Chi-*g*-PAM flocculants with an optimal dosage of 0.6 mg/L (70.6%). At pH 6.5, this occurred because Chi-*g*-PAM remained as a non-ionic flocculant since its pH_{pzc} is 6.3. The increased molecular weight of this system assisted in the flocculation of the phosphate through polymer adsorption and bridging mechanisms, as discussed in Sections 2.7.2 and 2.7.3 in Chapter 2. On the other hand, the CTA-Chi-*g*-PAM flocculants had increased P_i removal with reduced optimum dosage as the CTA DS in the copolymer increased from CTA-Chi-*g*-PAM-1 through to CTA-Chi-*g*-PAM-5. At high CTA DS, there are sufficient cationic quaternized ammonium groups, which act as a coagulant to stabilize the phosphate particles via charge neutralization to form microflocs. The polymer flocculant component aggregates the individual microflocs through flocculation via polymer bridging to form stable macroflocs. At low DS of CTA, there are a few cationic species in the system to electrostatically neutralize the phosphate anion species; hence, the flocculation is dominated by polymer bridging and electrostatic patching. The optimal dosage (in mg/L) with the removal efficiency in parentheses is 0.4 (76.6%), 0.3 (85.6%), 0.3 (88.9%), 0.3, (90.3%) and 0.2 (94.6%) for CTA-Chi-*g*-PAM-1 through to CTA-Chi-*g*-PAM-5, respectively. The results obtained before and after the optimum dosage agree with the zeta potential data discussed above, where the ζ-potential of the supernatant increased with increased flocculant dosage. At the optimum dosage, ζ-potential values were near-zero, whereas before and after the optimum dosage, they were negative and positive due to excess phosphate and cationic flocculants, respectively, as shown in Scheme 7.2. The excellent performance of the flocculants in removing P_i with minimal dosage (0.2 mg/L) is related to their solubility in water. A previous study has shown that soluble flocculants that form a homogeneous solution are more effective in removing suspended and dissolved particles.[54] This relates to the greater accessibility of the amine groups for dissolved flocculant since it improves the solvent accessibility and kinetics of the process due to improved ionization and biopolymer hydration.[54] Homogeneous dissolution of species displays rapid kinetics of mixing (mass transfer) over solid flocculant forms.

7.3.2.3 Effect of pH

For ionic flocculants, pH plays an important role in the flocculation process. Figure 7.5b shows the effect of pH variation on the T_i removal, while Figure 7.5c represents the zeta potential curves of the colloidal suspension and flocculant aqueous solution as a function of pH. Previous reports have shown that kaolinite has a negative zeta potential from pH 1-14 due to its anionic surface

charge owing to isomorphous substitution in its crystal structure. According to Figure 7.5b, the flocculants showed positive ζ-potential at ambient pH and the pH_{pzc} or an isoelectronic point (IEP) between 6.13 and 9.8. The flocculants are mostly soluble in an aqueous medium over a wide pH range. From Figure 7.5b, for Chi-*g*-PAM, the T_i removal was steady with an increase in pH until pH 6.0, where it decreased thereafter as pH increased. The IEP of Chi-*g*-PAM is 6.2, which indicates that the amine groups of PAM and chitosan were protonated at $pH < pH_{pzc}$, leading to the formation of a cationic flocculant that was able to neutralize the kaolinite particles electrostatically. On the other hand, at $pH > pH_{pzc}$, the amine groups underwent deprotonation and became negatively charged, resulting in electrostatic repulsion with the colloidal particles. Consequently, a reduced T_i removal efficiency was observed at high pH. For the cationic flocculants, the T_i removal efficiency remained unchanged with an increase in pH and may relate to its increased solubility in water at alkaline conditions. The structure of the polymer flocculant in solution has a significant influence on CF properties of the flocculants. In a previous study, the hydrodynamic radius (R_h) of a flocculant was observed to be pH dependent, where the R_h decreases with increasing pH until it reaches its IEP, followed by an increase thereafter.[55] At pH > IEP, the amine group on the flocculants undergo deprotonation, which partially neutralizes the cationic sites of the polymer. Hence electrostatic charge neutralization effect reduces since the net charge of the system will have negative ζ-potential, where flocculation by bridging effects becomes dominant. Also, the morphology of the polymer chains displayed extended conformation at high pH, which aided the bridging flocculation mechanism. However, at lower pH conditions (pH < IEP), due to the opposite charge of the kaolinite and the cationic flocculant at this pH, a charge neutralization mechanism enhances the performance of the flocculants.[56] In addition, a bridging mechanism occurs due to the extended conformation of the polymer. A higher density of cationic groups (CTA) due to greater DS of CTA in the flocculant led to an increased removal efficiency of the colloidal particles. Even though the T_i removal appears to be pH independent, the ζ-potential data in Figure 7.5c show that the supernatant after the flocculation process is near zero at pH 6.0, whereas the ζ-potential values are negative and positive below and above pH 6.0, respectively. Therefore, pH 6 represents an optimum pH for the effective performance of the flocculants. The positive ζ-potential at pH < 6 supports the charge neutralization mechanism while the negative ζ-potential at pH > 6 is favorable for the polymer bridging mechanism.

Table 7.3: Flocs aggregation and breakage kinetic parameters of the cationic flocculant materials for the removal of turbidity, according to equation (7.6)

	Flocculant					
Parameter	**Chi-*g*-PAM**	**CTA-Chi-*g*-PAM-1**	**CTA-Chi-*g*-PAM-2**	**CTA-Chi-*g*-PAM-3**	**CTA-Chi-*g*-PAM-4**	**CTA-Chi-*g*-PAM-5**
0.1 mg/L: Before optimal dosage						
$k_1 \times 10^{-4}$ (count^{-1} s^{-1})	13 ± 1	32 ± 33	37 ± 4	55 ± 2	67 ± 3	81 ± 3
$k_2 \times 10^{-3}$ (s^{-1})	96 ± 6	52 ± 3	35 ± 4	57 ± 2	58 ± 1	21 ± 1
R. Chi$^2 \times 10^{-4}$	6	22	22	2	4	2
R^2	0.980	0.973	0.975	0.997	0.994	0.997
Optimal dosage (mg/L)						
$k_1 \times 10^{-4}$ (count^{-1} s^{-1})	54 ± 4	58 ± 6	136 ± 5	217 ± 6	277 ± 2	244 ± 1
$k_2 \times 10^{-3}$ (s^{-1})	47 ± 4	31 ± 4	85 ± 2	130 ± 11	49 ± 4	65 ± 2
R. Chi$^2 \times 10^{-4}$	11	18	1	2	6	2
R^2	0.984	0.978	0.998	0.997	0.999	0.996
3.0 mg/L: After optimal dosage						
$k_1 \times 10^{-4}$ (count^{-1} s^{-1})	31 ± 3	34 ± 3	70 ± 3	61 ± 2	71 ± 3	67 ± 1
$k_2 \times 10^{-3}$ (s^{-1})	73 ± 4	111 ± 10	239 ± 13	126 ± 6	229 ± 10	192 ± 5
R. Chi$^2 \times 10^{-4}$	19	13	3	2	2	6
R^2	0.970	0.974	0.993	0.997	0.996	0.998

The flocculation of P_i was shown to be pH dependent, where maximum removal obtained in the alkaline and acidic regions for metal ions and polymer flocculants, respectively. Thus, the initial pH of the wastewater plays an important role in the coagulation-flocculation process. The development of flocculant materials without a metal ion coagulant that is pH independent will be beneficial to wastewater treatment process. Figure 7.5d shows pH dependence of the P_i removal efficacy at the respective optimal flocculant dosage without the addition of metal ion coagulants. According to these results, there is no effect of pH on the flocculation of the phosphate species, as the removal efficiency remained relatively unchanged from pH 2 to 10.5. Except for Chi-*g*-PAM, which continued to decrease steadily beyond pH 6.0. The results suggest that the cationic quaternized flocculants are more effective in the removal of P_i species over a wider pH range. At a particular pH, the P_i removal efficiency increased with an increase in DS of CTA from CTA-Chi-*g*-PAM-1 to CTA-Chi-*g*-PAM-5. As an illustration, at pH 5, the removal (%) is 80.9, 85.8, 94.7 and 99.0 from CTA-Chi-g-PAM-1 through to CTA-Chi-*g*-PAM-5, respectively. At pH > pH_{pzc} of the flocculants, they may deprotonate and become amphoteric; hence the flocculants are not able to associate favorably with phosphate via attractive ion-ion interaction; therefore,

electrostatic interaction is minimized, but the polymer flocculant favors polymer bridging via hydrogen bonding. The opposite occurs when pH < pH_{pzc}, where greater association occurs with the P_i species through ion-ion-interaction via charge neutralization as the cationic content of the flocculants increases. Since there is no variation in the P_i removal for all of the cationic flocculants in both acidic and alkaline media, it can be inferred that the magnitude of the polymer bridging and charge neutralization mechanisms are equal which results in a steady removal over a wide pH range, as evidenced herein.

7.3.2.4 Flocculation kinetics

7.3.2.4.1 Turbidity removal

Flocculation kinetics is complicated since various processes such as polymer-particle mixing, attachment of polymer onto the particle surface, rearrangement of adsorbed polymer chains, collisions of destabilized particles, and breakage of flocs due to shearing occur simultaneously and continuously. Despite the complexity of the process, an understanding of the fundamentals of flocculation kinetics and elucidation of the flocculation mechanism will contribute to further development of effective flocculants.[57–59] Smoluchowski[60] first described flocculation kinetics of colloidal particles through the formulation of classical mathematical expressions. Several modifications have been made to the formulation, which provides a variety of alterations regarding collision efficiency, hydrodynamic interactions, floc breakage and surface chemistry.[10,57–59] Two main processes are accounted for in the formulation, which are floc aggregation and floc breakage, where they are considered to follow second-order and first order kinetics, respectively, as given in equation (7.8).

$$\frac{d\left(N_t \diagup N_0\right)}{dt} = -N_0 k_1 \left(\frac{N_t}{N_0}\right)^2 + k_2 \frac{N_t}{N_0} \tag{7.8}$$

$$\frac{N_t}{N_0} = \frac{k_2 \cdot e^{k_2 \cdot t}}{(k_1 \cdot N_0) \cdot e^{k_2 \cdot t} + k_2 - k_1 (k_1 - N_0)} \tag{7.9}$$

Here, N_0 and N_t are the number concentration of the kaolinite colloidal dispersion at the initial time (t = 0) and at time, t, respectively. k_1 and k_2 are the kinetic rate constants for the floc aggregation and breakage, respectively. Values of k_1 and k_2 can be obtained through nonlinear fitting of the integral equation (7.8), as given in equation (7.9). Using equation (7.9), the particle aggregation

and particle breakage kinetics can be compared. To evaluate the turbidity, the relationship between the number concentration of kaolinite particle and the measured transparency (*%T)* of the water is given according to equation (7.10), where, T_o and T_t are %T of the water before and after the flocculation process. The value of N_o was kept constant at 1000 mg/L throughout.

$$\left(\frac{N_o}{N_t}\right) = \frac{100 - T_o}{100 - T_t} \tag{7.10}$$

Figure 7.6 (top) represents floc aggregation and breakage kinetic curves. The flocculation process for each flocculant was divided into three categories to understand how the flocculant dosage affects the flocculation kinetics: (i) below the optimal dosage (underdosing); (ii) at optimal dosage; and (iii) above the optimal dosage (overdosing). Figure 7.6 (a-c) shows that after the addition of the flocculants, particle aggregation occurred within the first five min and it reached equilibrium at 15 min. Before the optimal dosage, Chi-*g*-PAM showed low values of k_1 ((13 ± 1) x10^{-4} counts^{-1} s^{-1}) and high values of k_2 ((96 ± 6) x10^{-3} counts^{-1} s^{-1}). This indicates that the rate of particle breakage is greater than the particle aggregation, meaning as the flocs are formed, they have a greater tendency to break, which results in the poor T_i removal efficiency, as reported earlier relating to perikinetic flocculation process. This occurs because the use of pH 6.5 is above the pH_{pzc} of Chi-*g*-PAM (pH_{pzc} 6.3), where the flocculant is nearly neutral and its interaction with the kaolinite will be dominated by polymer bridging effects without any charge neutralization effects. For the cationic flocculants, k_1 values increased while the k_2 values decreased from CTA-Chi-*g*-PAM-1 through to CTA-Chi-*g*-PAM-5, as presented in Table 7.3, suggesting that the presence of CTA on the polymer enhanced the formation of stable aggregates that resist breakage upon addition of shear stress. According to Figure 7.6b, at the optimal dosage, the values of k_1 for all the flocculants are greater than below or above the optimal dosages, as reported in Table 7.3. This shows that the flocs formed at the respective optimal dosage of the flocculants are stronger, denser and more compact, and are able to resist breakage, leading to optimal T_i removal at these values. Beyond the optimal dosage, flocculation rate decreases as the particle aggregation rate constant (k_1) becomes smaller and the particle breakage rate constant (k_2) increases. This occurs because a higher flocculant concentration provides coverage of the available sites on each particle. Thus, the bridging mechanism become negligible. Beyond the optimum flocculant dosage, there is an excess positive charge from the cationic quaternary ammonium groups, which then causes restabilization

of the flocs. This effect is due to electrostatic repulsion, which leads to an increase in aggregate breakage constant and a reduction in the flocculation performance at this dosage.

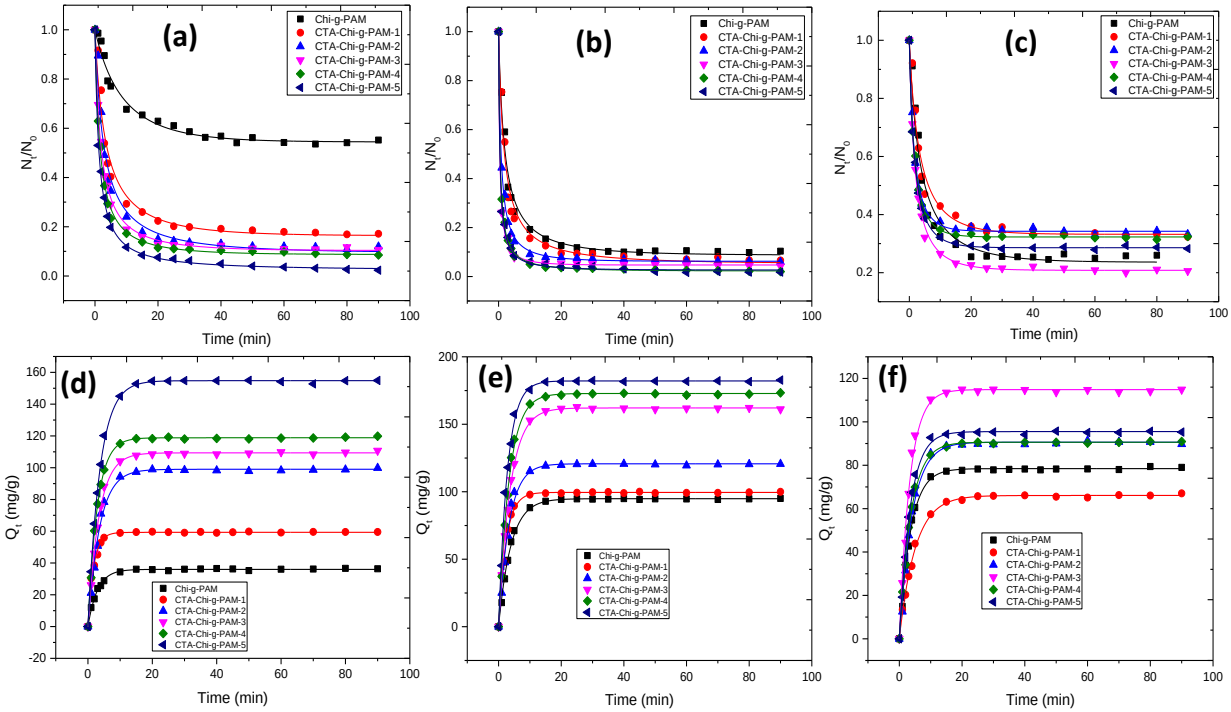

Figure 7.6: Kinetic profiles of flocculation processes for kaolinite suspension (top) and phosphate (bottom) with respect to PFO model (a & d) below the optimum dosage, (b & e) at the optimum dosage and (c & f) beyond the optimum dosage at pH 6.5.

7.3.2.4.2 Phosphate removal

Flocculation kinetics of dissolved substances such as dyes, phosphate, sulphate, etc. have been shown to follow kinetic process that differs from suspended colloidal particles. The kinetic results herein were obtained using a one-pot method, the details of which have been reported elsewhere.[61] The effect of contact time on the flocculation ability of Chi-*g*-PAM and CTA-Chi-*g*-PAM flocculants on the phosphate removal at pH 6.5 and an initial phosphate concentration of 50.0 mg/L is presented in Figure 7.6 (bottom) for the PFO kinetic model. There is a rapid increase in the P_i flocculation within the first 5 min, where it increased steadily up to 15 min to where it reached a dynamic equilibrium, and then remained virtually constant thereafter. The sharp increase within the first min for the flocculation process could be attributed to electrostatic interactions between the phosphate and the cationic flocculants, leading to charge neutralization, since this

effect was less obvious in Chi-*g*-PAM flocculant.[62,63] Prior to reaching the dynamic equilibrium, there is a gradual increase in the flocculation efficacy because of a reduced effective cationic charge on the flocculant surface. The rapid equilibrium process at 5-15 min as reported in Figure 7.6 (d, e & f), indicates that P_i species interact with the outermost surface of the flocculant system.

Table 7.4: Flocculation kinetic parameters for P_i removal at pH 6.5 and initial P_i dosage of 50.0 mg/L according to the PFO model

	Flocculant					
Parameter	**Chi-*g*-PAM**	**CTA-Chi-*g*-PAM-1**	**CTA-Chi-*g*-PAM-2**	**CTA-Chi-*g*-PAM-3**	**CTA-Chi-*g*-PAM-4**	**CTA-Chi-*g*-PAM-5**
PFO: 0.1 mg/L dosage						
Q_e (mg/g)	36 ± 1	59 ± 1	99 ± 1	109 ± 1	119 ± 1	155 ± 1
k_1 x 10^{-3} (min^{-1})	340 ± 9	562 ± 23	274 ± 10	292 ± 6	346 ± 5	273 ± 4
R. χ^2	1	2	7	2	1	3
R^2	0.996	0.991	0.994	0.998	0.999	0.999
PFO: Optimal dosage (mg/L)						
Q_e (mg/g)	95 ± 1	100 ± 1	121 ± 1	162 ± 1	173 ± 1	182 ± 1
k_1 x 10^{-3} (min^{-1})	255 ± 5	415 ± 15	297 ± 12	260 ± 3	267 ± 7	357 ± 10
R. χ^2	2	6	12	1	9	12
R^2	0.998	0.993	0.992	1.000	0.997	0.996
PFO: 3.0 mg/L dosage						
Q_e (mg/g)	78 ± 1	66 ± 1	91 ± 1	115 ± 1	91 ± 1	96 ± 1
k_1 x 10^{-3} (min^{-1})	279 ± 6	169 ± 5	245 ± 9	299 ± 11	272 ±5	289 ± 9
R. χ^2	2	1	6	9	2	4
R^2	0.997	0.997	0.994	0.994	0.998	0.996

The flocculation kinetics of P_i with the cationic flocculant systems was investigated using the pseudo-first-order (PFO) and pseudo-first-order (PSO) kinetic models. The PFO kinetic model assumes that the sorption rate decreases linearly as the adsorption rate increases.[64,65] By comparison, the PSO kinetic model assumes that the rate-limiting step involves interaction between the adsorbent and adsorbate is often applied to describe an adsorption process.[65,66] The PFO and PSO kinetic models are shown in equations (7.11) and (7.12), respectively.

$$q_t = q_e(1-e^{-k_1 t}) \tag{7.11}$$

$$q_t = \frac{k_2 q_e^{\,2} t}{1+k_2 q_e t} \tag{7.12}$$

Here, q_e and q_t are the amount of phosphate adsorbed (mg/g) at dynamic equilibrium and at time *t*. k_1 and k_2 are the rate constants for the PFO and PSO kinetic models, respectively. k_1, k_2 and q_e were estimated using non-linear regression fitting according to equations (7.8) and (7.9).

In Figure 7.6 (bottom), the experimental kinetic results were fitted by the PFO model, whereas fitted results for the PSO model are presented in Figure A9.15 (Appendix A). The results are well-described by PFO in comparison to PSO. The fitting parameters, k_1, k_2, q_e and R^2 obtained from the regression analysis are listed in Table 7.4. The correlation coefficient (R^2) and reduced χ^2 for the PFO model exceeds that of the PSO model for all the flocculants, in accordance with Figure 7.6 (d, e, & f). Also, it is evident that the predicted values of q_e determined by the PFO model agree well with the experimental values relative to the PSO kinetic model. Moreover, the rate constant (k_1) of the PFO model is significantly greater than that of the PSO model rate constant (k_2). The value of k_1 increased as the DS of CTA increases, which is in agreement with the results obtained for the floc aggregation rate constant for the suspended particles. Also, k_1 values are greater at the optimal flocculant dosage relative to dosage values below and above the optimal levels, showing that charge neutralization is the main flocculation mechanism at the optimal dosage. The adsorption of P_i by the flocculant system indicates that the sorption rate decreases linearly as the adsorption rate increases. Similar results were reported for the flocculation of anionic dyes and arsenates by related polysaccharide-based flocculants.[67–70]

7.3.2.5 Adsorption isotherms

Flocculation-adsorption processes can be described through graphical isotherms. Adsorption isotherms provide insight concerning the interaction between adsorbates and adsorbents at the optimal conditions.[71] The Langmuir[72], Freundlich[73] and Sips[74] isotherm models are the most frequently used to describe adsorption during a flocculation process. In this study, the adsorption isotherm models were used to understand the adsorption processes to elucidate the flocculation mechanism. The Langmuir adsorption isotherm model assumes that adsorption occurs at specific homogeneous sites with the adsorbent and is described by equation (7.13). The Freundlich isotherm model, represented by equation (7.14), accounts for multilayer sorption by assuming that the adsorbent has a heterogeneous surface with non-uniform distribution of sorption sites. The Sips isotherm model (equation (7.15)) shares features of the Langmuir and Freundlich isotherms. At low adsorbate concentrations, it converges to a Freundlich isotherm. At high adsorbate concentration (or $n = 1$), the model reduces to a Langmuir isotherm.[75]

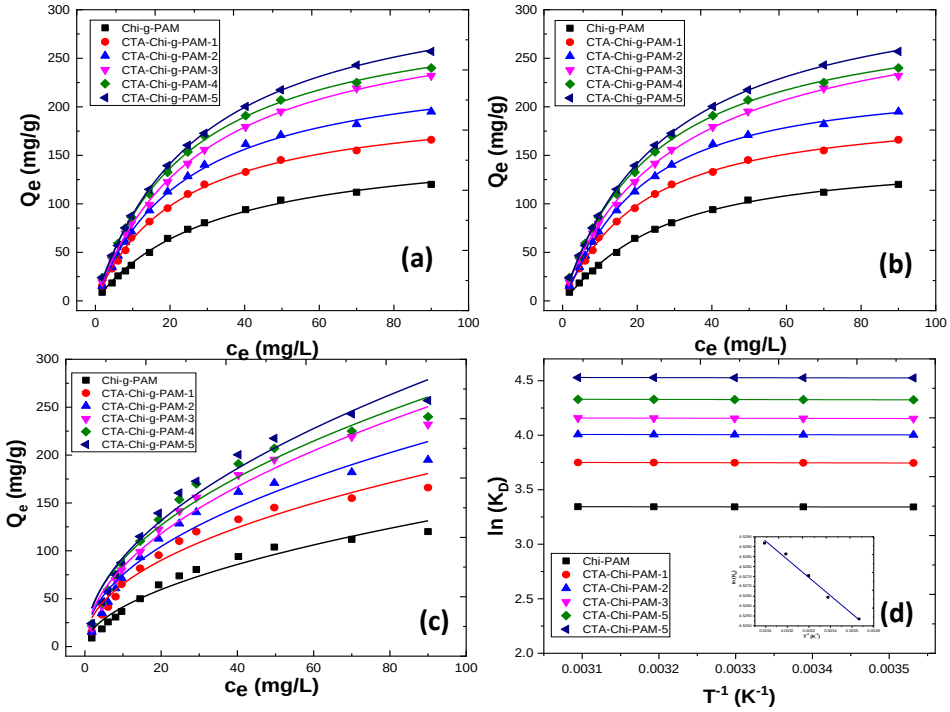

Figure 7.7: Adsorption isotherms of phosphate by CTA-Chi-*g*-PAM flocculants at pH 6.5 according to (a) Langmuir, (b) Sips and (c) Freundlich. Initial phosphate concentration (1.0–50 mg/L). (d) van't Hoff plot of lnK_D vs 1/T for the phosphate adsorption on CTA-Chi-*g*-PAM. Note: K_s is the equilibrium distribution coefficient, as defined in equation (7.12), according to the Sips isotherm model.

$$q_e = \frac{K_l q_m c_e}{1 + K_l c_e} \tag{7.13}$$

$$q_e = K_f c_e^{1/n} \tag{7.14}$$

$$q_e = \frac{K_s q_m c_e^{n_s}}{1 + K_s c_e^{n_s}} \tag{7.15}$$

The variables in the equations are defined herein: q_m (mg·g^{-1}) is the monolayer adsorption of P_i per unit mass of CTA-Chi-*g*-PAM adsorbent, and q_e is the amount of adsorbed P_i (mg·g^{-1}). K_l and K_s (Lg^{-1}) are the equilibrium adsorption constants for Langmuir and Sips isotherms, respectively, which relate to the affinity of the binding sites. K_f is the Freundlich isotherm constant, which relates to the adsorption capacity, where n is a dimensionless constant. The value of n describes the type of adsorption, where it can be classified as unfavorable ($1/n > 1$), favorable ($1/n < 1$), and irreversible ($1/n = 0$).

Figure 7.7 (a-c) is the isotherms for the removal of P_i in the flocculation process by Chi-*g*-PAM and CTA-Chi-*g*-PAM aqueous flocculant systems at a variable concentration (5–50 mg/L). The experimental data were fitted by the Langmuir, Freundlich and Sips isotherm models. The fitting parameters and the correlation coefficients are listed in Table 7.5. The results in Figure 7.7 (a-c) and Table 7.5 show that the removal of P_i by the CTA-Chi-*g*-PAM flocculant materials is well-described by the best-fit according to the Langmuir and Sips models. Favorable adsorption of phosphate is reflected by these models since $R^2 > 0.95$ and the reduced χ^2 is relatively low. In addition, the monolayer adsorption capacity (q_m; mg/g) for P_i at the optimal conditions for Langmuir (former) and Sips (latter) isotherms given in parentheses are (166 ± 4; 148 ± 4), (208 ± 3; 199 ± 5), (251 ± 5; 224 ± 4), (305 ± 4; 318 ± 10), (308 ± 3; 303 ± 8) and (339 ± 3; 336 ± 7) for Chi-*g*-PAM, CTA-Chi-*g*-PAM-1, CTA-Chi-*g*-PAM-2, CTA-Chi-*g*-PAM-3, CTA-Chi-*g*-PAM-4 and CTA-Chi-*g*-PAM-5, respectively. The equilibrium adsorption capacity obtained for Chi-*g*-PAM is lower compare to the quaternized flocculants. This trend is due to the absence of cationic moieties to neutralize the anionic colloid particles efficiently. Also, as the DS of CTA in the cationic flocculant increases, the q_m values increased, as listed in Table 7.5. The values obtained from the Langmuir and Sips models are comparable, where the Langmuir model is considered more reliable due to its relative simplicity and favorable *goodness-of-fit* for the cationic flocculant isotherm systems. Moreover, the exponent term (n_s) is near unity, which implies that the Sips isotherm converges with the Langmuir model when $n_s = 1$. Thus, it can be inferred that the flocculation of orthophosphate by cationic polymeric flocculants follows a homogeneous mechanism based on the charge neutralization reaction between the anionic P_i and the cationic quaternary ammonium groups.[76] In the Freundlich isotherm model, the dimensionless constant, n^{-1} is less than unity, indicating favorable adsorption, but the correlation coefficient was lower than those obtained by the Sips and Langmuir models. The Langmuir (K_l) and Sips (K_s) adsorption constants resided within the same range for all the flocculants, revealing the strong affinity for the phosphates towards the flocculant binding sites. This shows that the flocs formed from the interaction between P_i with CTA-Chi-PAM have stronger stability in solution.[77]

Table 7.5: Langmuir, Sips and Freundlich adsorption isotherm coefficients for the flocculation of phosphate by CTA-Chi-*g*-PAM flocculants at pH 6.5

	Flocculant					
Parameter	**Chi-*g*-PAM**	**CTA-Chi-*g*-PAM-1**	**CTA-Chi-*g*-PAM-2**	**CTA-Chi-*g*-PAM-3**	**CTA-Chi-*g*-PAM-4**	**CTA-Chi-*g*-PAM-5**
Langmuir Isotherm						
Q_m (mg/g)	165 ± 4	208 ± 3	251 ± 5	305± 4	308 ± 3	339 ± 3
K_l x 10^{-3}	31 ± 2	44 ± 2	41 ± 2	36 ± 1	40 ± 1	36 ± 1
R. χ^2	4	4	10	4	5	3
R^2	0.997	0.998	0.997	0.999	0.999	0.999
Sips Isotherm						
Q_m (mg/g)	148 ± 4	199 ± 5	227 ± 4	318 ± 10	303 ± 8	336 ± 7
K_s x 10^{-3}	40 ± 3	49 ± 3	51 ± 2	32 ± 2	41.4 ± 2.4	36.6 ± 2
$\boldsymbol{n_s}$	1.1 ± 0.1	1.1 ± 0.1	1.2 ± 0.1	1.0 ± 0.1	1.0 ± 0.1	1.0 ± 0.1
R. χ^2	2	3	3	4	5	3
R^2	0.999	0.999	0.999	0.999	0.999	1.0
Freundlich Isotherm						
K_f	12 ± 2	23 ± 3	25 ± 4	26 ± 3	30 ± 4	29 ± 4
n	1.9 ± 0.1	2.1 ± 0.2	2.1 ± 0.1	2 ± 0.1	2.1 ± 0.1	2.0 ± 0.1
R. χ^2	58	111	188	129	188	189
R^2	0.962	0.958	0.952	0.975	0.966	0.971

7.3.2.6 Flocculation thermodynamics

The temperature effect on the flocculation of P_i by CTA-Chi-*g*-PAM flocculants was investigated from calculated thermodynamic parameters. The thermodynamic parameters were obtained by performing the flocculation process at different temperatures. The difference in the standard Gibbs free energy (ΔG^o), enthalpy (ΔH^o) and entropy (ΔS^o) was evaluated at equilibrium, according to the equations below.

$$\Delta G^o = -RT \ln K_D \tag{7.16}$$

$$\ln K_D = \frac{\Delta S^o}{R} - \frac{\Delta H^o}{RT} \tag{7.17}$$

Here, R is the universal gas constant (8.314 $J \cdot mol^{-1} \cdot K^{-1}$), T is the temperature in kelvin and K_D is the equilibrium distribution coefficient, which is defined by equation (7.18), which relates to the equilibrium constant obtained from the Langmuir or Sip isotherms.[78]

$$K_D = \frac{q_e}{c_e} \tag{7.18}$$

ΔG^o was calculated at a variable temperature by using equation (7.16). A plot of $\ln K_D$ as a function of T^{-1} resulted in a straight line, in accordance with equation (7.17). The values of ΔH^o and ΔS^o

were obtained from the slope and intercept, respectively (*cf*. Figure 7.7d and Table 7.6). ΔG^o for the P_i adsorption by all the flocculants was negative, indicating the spontaneous nature of the flocculation-adsorption process. For each flocculant, ΔG^o becomes more negative with increasing temperature, which shows that the flocculation of P_i is energetically favorable at all temperatures. The positive values of ΔH^o obtained herein confirm that the flocculation process is endothermic and the product (flocs) is thermodynamically stable. Since ΔH^o is less than 40 kJ/mol and ΔG^o is less than 20 kJ/mol for all the flocculants, it can be deduced that the flocculation process involves physical interaction (physisorption) between the adsorbate (phosphate) and the adsorbent (cationic flocculant materials). The value of ΔS^o is positive for all the studied flocculants, suggesting increased randomness at the liquid-liquid interface during the flocculation-adsorption process, and the values reflect the affinity of the CTA-Chi-*g*-PAM flocculants towards the phosphate. Values of ΔG^o and ΔS^o increased as the DS of CTA increases at each temperature, while the magnitude of ΔH^o remained virtually constant. This implies that the spontaneity of the flocculation process is entropically driven. The thermodynamic results obtained herein are comparable to other previous reports.[78–81]

Table 7.6: Thermodynamic parameters for the phosphate adsorption on CTA-Chi-*g*-PAM flocculants from 10-50 °C

Flocculant	ΔG^o (kJ/mol)					ΔH^o (kJ/mol)	ΔS^o (J/K mol)	R^2	RSS
	283 K	295 K	303 K	313 K	323 K				
Chi-PAM	-7.86	-8.20	-8.43	-8.71	-8.98	15.4 ± 0.7	28.0 ± 1.2	0.993	2.95E-08
CTA-Chi-PAM-1	-8.81	-9.19	-9.45	-9.76	-10.1	26.4 ± 0.6	31.5 ± 0.9	0.999	1.88E-08
CTA-Chi-PAM-2	-9.42	-9.83	-10.1	-10.4	-10.8	20.5 ± 0.6	33.5 ± 0.8	0.998	1.74E-08
CTA-Chi-PAM-3	-9.78	-10.2	-10.5	-10.8	-11.2	27.8 ± 1.3	34.9 ± 1.4	0.993	9.57E-08
CTA-Chi-PAM-5	-10.2	-10.6	-10.9	-11.3	-11.6	27.1 ± 0.9	36.3 ± 1.4	0.996	4.98E-08
CTA-Chi-PAM-5	-10.7	-11.1	-11.4	-11.8	-12.2	22.7 ± 1.4	37.9 ± 0.5	0.989	1.11E-07

7.3.3 Floc properties and characterization

7.3.3.1 FT-IR spectra of flocs

FTIR spectra were obtained for the flocs produced and isolated from the flocculation process. The IR spectra of the cationic polymer flocculants were posited to reveal whether there are any physical or chemical interactions between the flocculants and the kaolinite particles. In Figure 7.8a, the FTIR spectra of kaolinite, CTA-Chi-*g*-PAM-5, flocs and physical mixture of the kaolinite and the flocculant are presented. The results of the other cationic flocculants are identical to that

of CTA-Chi-*g*-PAM-5 presented in Figure A9.16 (Appendix A). It is observed that the spectra of the produced flocs, kaolinite and the physical blend are similar. The samples have comparable IR signatures in their respective spectra. According to Figure (7.8a), the absorption band at 3698 represents the inner surface –OH stretching vibration and those at 1114 cm^{-1}, 910.8 cm^{-1}, 792.7 cm^{-1} are due to the Si-O, Al-OH bending vibrations and Si-O-Si stretching of cristobalite, respectively.[53,82] The results show that the major components of the kaolinite were compounds of Si and O. The presence of these IR bands in the floc spectra, compared to a physical blend between the kaolinite and the flocculants suggest that no chemical reaction occurred in the flocculation process because no new unique spectral signatures were observed. Figure 7.8a(ii) shows expanded IR spectra of the physical blend, kaolinite and the flocs from 1500 cm^{-1} to 3380 cm^{-1}. Comparing the spectra of the flocs to the physical blend, there are bands at 1669 cm^{-1} and 1606 cm^{-1}, which are both absent in the kaolinite spectra. These IR bands are also present in the CTA-Chi-*g*-PAM flocculants, where they represent stretching vibration of $–NH_2$ and stretching of –C=O in the amide of the polyacrylamide component of the cationic flocculants.[45,82] There is an IR band at 1452 cm^{-1}, which was attributed to the methyl group in the quaternary ammonium ion of the polymer flocculant. The presence of these bands in the physical blend and the flocs suggest that the cationic polymer flocculant adsorbed on the surface of the kaolinite particles by electrostatic charge neutralization and polymer bridging. The results herein support the fact that there was physical interaction (physisorption) between the flocculants (adsorbent) and the kaolinite (adsorbate), as suggested by the values of ΔG^o and ΔH^o in the thermodynamic studies reported above.

7.3.3.2 SEM images of flocs

The structural orientation and organization of the flocculants with the kaolinite microparticles were evaluated using SEM imaging analysis. According to the micrographs, significant changes are observed in the morphology of the kaolinite colloidal particles before and after flocculation. In the presence of the flocculants, colloidal particles can associate in three different ways, namely, face-to-face (F-F), face-to-edge (F-E) and edge-to-edge (E-E) interactions, to form a card-house type structure, as discussed in Chapter 2.[12,83] While van der Waals forces and double layer repulsion between like charges or neutral faces lead to F-F and E-E aggregation, E-F association is driven by Coulombic attractive forces between oppositely charged faces. Interactions between kaolinite colloidal particles and polymer flocculants occur due to charge neutralization, polymer bridging, the formation of complex or a combination of these mechanisms.[12,84] Non-ionic and cationic

polymer flocculants lead to polymer bridging and electrostatic charge neutralization, respectively. According to the SEM micrographs shown in Figure 7.8b, Chi-*g*-PAM flocculated flocs had F-F and E-E floc aggregation, while the cationic quaternary ammonium groups of the flocs had F-F, E-E and E-F associations. The SEM images of the flocs obtained from the other flocculants are shown in Figure A9.17 in Appendix A. This suggests that both non-ionic and cationic flocculants are adsorbed onto the faces and edges of the kaolinite particles. However, because of the greater proportion of face vs. edge surface area on the colloidal particles, F-F aggregation is evident in all the flocs. Hence, polymer bridging takes place due to linking of two or more particles to the polymer flocculant.[85] E-F interaction of the colloidal particles was present in the cationic containing flocs via electrostatic charge neutralization due to the presence of the positively charged quaternary ammonium groups of the polymer flocculants. Also, long-range van der Waals attraction and short-range ion-dipole forces led to F-F and E-E association of the particles. For the cationic flocculants, Coulombic attraction is the dominant force resulting in a charge neutralization mechanism. This occurs because the cationic quaternary ammonium ions are attracted to the negatively charged sites along the kaolinite particle surface.

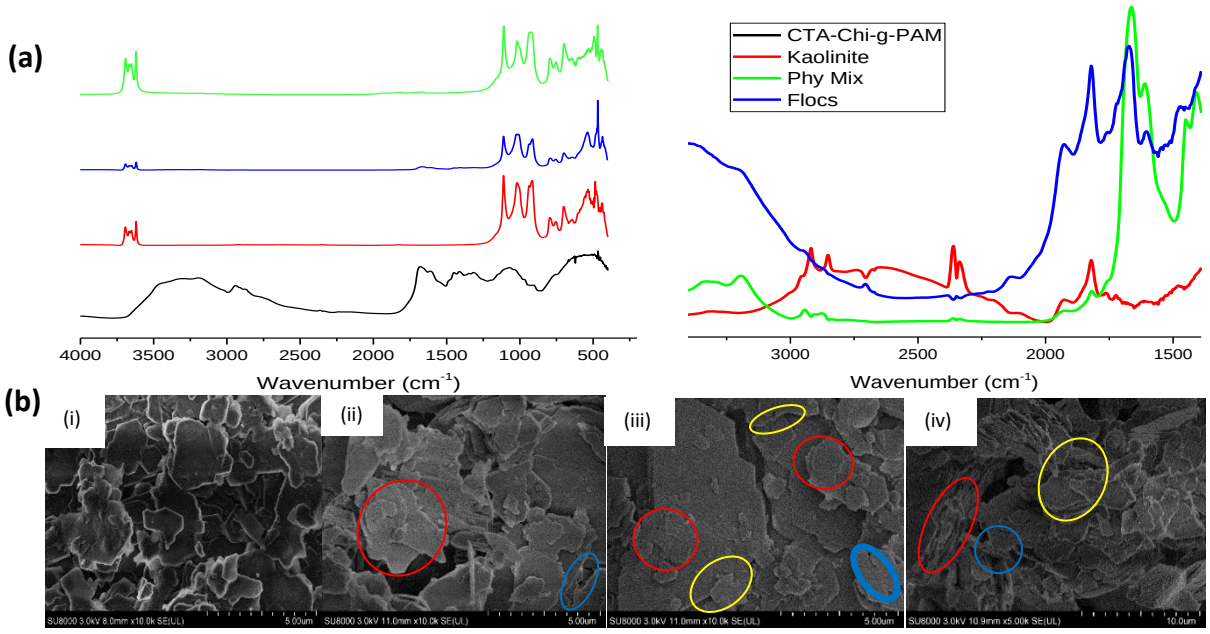

Figure 7.8: (a) FT-IR spectra of CTA-Chi-*g*-PAM, kaolinite, flocculant-kaolinite physical mixture and flocs. (b) SEM images of (i) kaolinite and flocs obtained with (ii) Chi-*g*-PAM, (iii) CTA-Chi-*g*-PAM-1 and (iv) CTA-Chi-*g*-PAM-5. Here, red, yellow and blue circles indicate F-F, E-F and E-E association of the microflocs, respectively.

7.3.3.3 Particle size of flocs

In order to better elucidate the flocculation mechanism, it is important to study the variation in the floc size and size distribution. The median volumetric diameter (d_{50}) was used to denote the floc size in this study. The size distribution and average particle size of the kaolinite colloidal particles in the presence and absence of the cationic flocculants are shown in the Figure 7.9. In the absence of the flocculant the kaolinite dispersion showed a broad size distribution with a particle size of 5.3 μm, which is in agreement with previous reports.[52,86–90] The addition of the flocculant resulted in a narrow particle size distribution that showed significant increase in the average size of the flocs. The particle size of the flocs had maximum value at the optimal flocculant dosages as compared to values obtained before and after the optimum dosage. Also, as the DS of CTA increases, the size of the aggregated flocs increased. For instance, at the optimum dosage, the average aggregate size (in μm) of the flocs flocculated by CTA-Chi-*g*-PAM-1 through to CTA-Chi-*g*-PAM-5 are 96, 105, 152, 264 and 500, respectively. The increased size with the cationic content can be associated with charge neutralization and polymer bridging effects. Regarding charge neutralization, the charged quaternized ammonium group of the flocculant binds with the negative edges of the kaolinite surface and aggregate via electrostatic attraction. This is in agreement with the ζ-potential results, where the addition of the cationic flocculant increased the ζ-potential of the supernatant of the suspension until it reached near-zero at the optimal dosage. As indicated above, for highly charged flocculants, less dosage is required to obtain maximum T_i and P_i removal. This suggests that the amount of flocculant needed to neutralize the particle charge of the kaolinite is inversely related to the charge density, where polymers with high charge density can neutralize the particle surface charge more rapidly than polymers with low charge density. The high molecular weight of the polymer flocculant also increased the size of the flocs via a flocculation bridging mechanism. The high molecular weight of CTA-Chi-*g*-PAM flocculants would result in adequate chain branches and adsorption sites to enhance its bridging ability. As the polymer molecular weight is higher, long-chain polymer conformational rearrangements occur at the particle surface more slowly. Therefore, the addition of the high molecular weight flocculant will lead to an extension of the long polymer chain to the particle surface, which may span over the electrical double layer domains of the approaching particles that cause bridging flocculation to occur. In addition, the cationic flocculants would neutralize the negatively charged particle surface to lose their stability. During the bridging process, the destabilized particles were tightly absorbed

on the CTA-Chi-PAM polymer chain to form large and compact flocs. The average particle size of the flocs is smaller below and above the optimum dosage due to excess of the negative and positive charged particles present after the flocculation process, respectively. Below the optimum dosage, there is limited availability of sufficient cation groups to neutralize the colloidal particle surface charge, resulting in a negatively charged dispersion. This is confirmed by the ζ-potential results and a reduced floc size, along with a lower flocculation performance. On the other hand, beyond the optimum dosage, there is an excess of cation groups to neutralize the negatively charged particles, resulting in a net positive charge, which leads to restabilization of the floc due to charge reversal effects. Hence, there is a reduction in their average size.

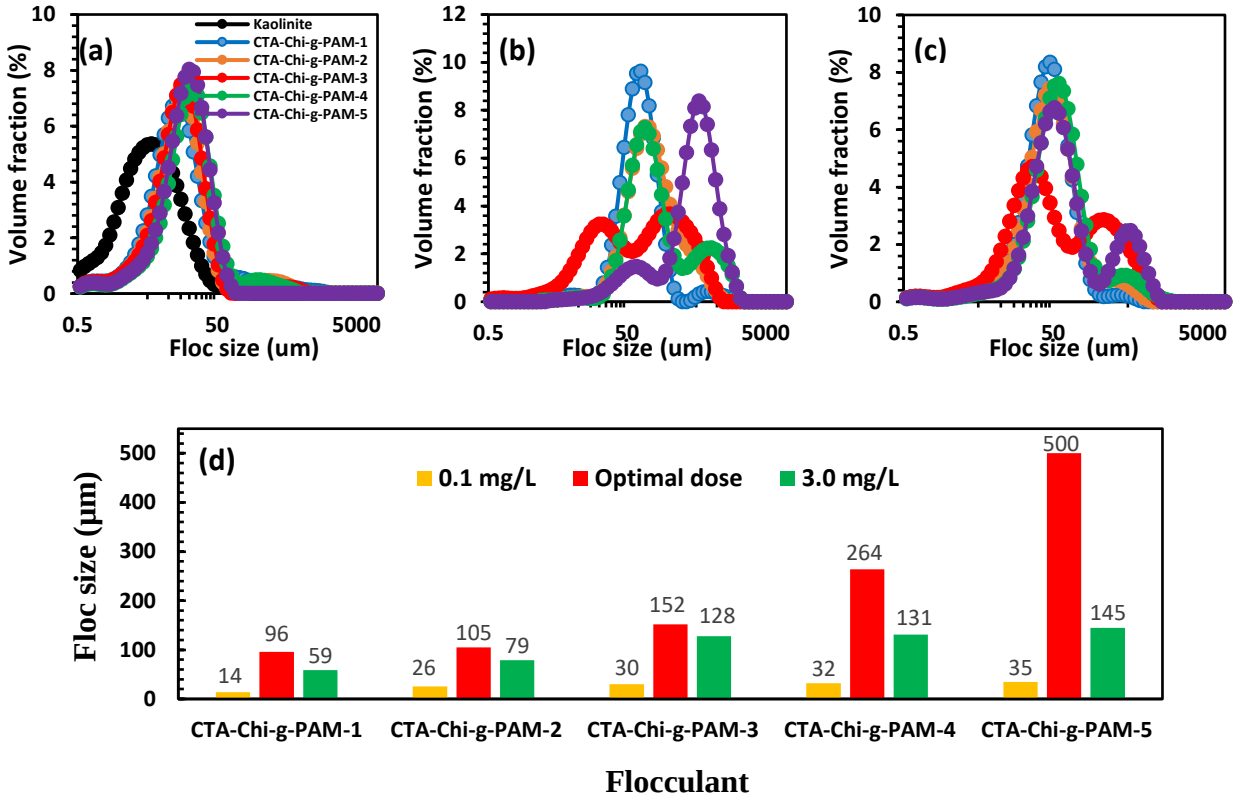

Figure 7.9: Kaolinite floc size distribution (a) below the optimum dosage, (b) at the optimum dosage and (c) beyond the optimum dosage at pH 6.5. (d) Floc size of kaolinite-flocculant particles at different flocculant dosage.

7.4 Conclusion

A copolymer flocculant was synthesized by grafting polyacrylamide (PAM) onto chitosan to obtain Chi-*g*-PAM. The product was then quaternized with CTA to prepare a series of cationic

polymer flocculants (CTA-Chi-*g*-PAM) by varying the weight ratio of the CTA and Chi-*g*-PAM. The structure of CTA-Chi-*g*-PAM was supported by various characterization methods, where the products were found to be soluble in water with positive surface charge at both acidic and alkaline conditions. The effects of temperature, settling time, pH and flocculant dosage on the flocculation properties of the materials were tested on the removal of suspended solids (turbidity) and phosphate. Maximum removal of P_i and T_i was obtained within 5 mins of settling of the flocs and they showed independent trend towards pH, in that, greater and equal removal efficiency was obtained from pH 2 to 10.5. The optimal flocculant dosage ranged from 0.2 to 0.5 mg/L with CTA-Chi-*g*-PAM-5 having the smallest optimal dosage of 0.2 mg/L with 99.0 % (P_i) and 98.6 % (T_i) removal efficiency. Kinetics of the T_i flocculation shows that the rate constant for particle aggregation is greater at the optimal conditions, relative to the rate constant for particle breakage. The P_i removal was well described by PSO kinetic model and Langmuir adsorption isotherm, indicating that the process is physisorption. Thermodynamic study at variable temperatures showed that the flocculation process is endothermic, spontaneous and entropy-driven (due to hydrophobic effects, as discussed in Chapter 2), where the removal efficiency increased steadily with increasing temperature. Stronger, denser and more compact flocs with remarkably increased floc size were formed at the respective optimal dosage of the flocculants. F-F, E-E and E-F microfloc associations were observed without any chemical interaction between the kaolinite and the flocculants. The CF process involved cooperative Coulombic electrostatic charge neutralization mechanism between the cationic ammonium ion group of the flocculant and the anionic species (P_i and kaolinite), followed by polymer bridging due to adsorption of microflocs on the surface of the polymer and formation of an ordered layered structure through a bridging mechanism. This study contributes to the field of sustainable environmental science since a minimal dosage (0.2 mg/L) of the flocculant was deployed without the use of additional metal-ion coagulants for efficient removal of P_i and T_i. As well, a short settling time (5 min), and the process is noted to be pH independent of the initial wastewater conditions. The flocculant reported herein in this research is anticipated to be efficient for the removal of other oxyanions species such as arsenate, nitrate, sulphate and organophosphate, and this direction is the subject of on-going research.

7.5 References

(1) Zhu, H.; Zhang, Y.; Yang, X.; Liu, H.; Shao, L.; Zhang, X.; Yao, J. *J. Hazard. Mater.* **2015**, *296*, 1–8.

(2) Teh, C. Y.; Budiman, P. M.; Shak, K. P. Y.; Wu, T. Y. *Ind. Eng. Chem. Res.* **2016**, *55* (16), 4363–4389.

(3) Lichtfouse, E.; Morin-Crini, N.; Fourmentin, M.; Zemmouri, H.; do Carmo Nascimento, I. O.; Queiroz, L. M.; Tadza, M. Y. M.; Picos-Corrales, L. A.; Pei, H.; Wilson, L. D.; Crini, G. *Environ. Chem. Lett.* **2019**, *17* (4), 1603–1621.

(4) Sharma, B. R.; Dhuldhoya, N. C.; Merchant, U. C. *J. Polym. Environ.* **2006**, *14* (2), 195–202.

(5) Kean, T.; Thanou, M. *Adv. Drug Deliv. Rev.* **2010**, *62* (1), 3–11.

(6) Xu, J.; McCarthy, S. P.; Gross, R. A.; Kaplan, D. L. *Macromolecules* **1996**, *29* (10), 3436–3440.

(7) Renault, F.; Sancey, B.; Badot, P. M.; Crini, G. *Eur. Polym. J.* **2009**, *45* (5), 1337–1348.

(8) Wang, S.; Zhang, L.; Yan, B.; Xu, H.; Liu, Q.; Zeng, H. *J. Phys. Chem. C* **2015**, *119* (13), 7327–7339.

(9) Vajihinejad, V.; Gumfekar, S. P.; Bazoubandi, B.; Rostami Najafabadi, Z.; Soares, J. B. P. *Macromol. Mater. Eng.* **2019**, *304* (2), 1–43.

(10) Ghorai, S.; Sarkar, A.; Panda, A. B.; Pal, S. *Ind. Eng. Chem. Res.* **2013**, *52* (29), 9731–9740.

(11) Lu, Y.; Shang, Y.; Huang, X.; Chen, A.; Yang, Z.; Jiang, Y.; Cai, J.; Gu, W.; Qian, X.; Yang, H.; Cheng, R. *Ind. Eng. Chem. Res.* **2011**, *50* (12), 7141–7149.

(12) Sharma, S.; Lin, C. L.; Miller, J. D. *Miner. Eng.* **2017**, *101*, 20–29.

(13) Liu, J.; Sandaklie-Nikolova, L.; Wang, X.; Miller, J. D. *J. Colloid Interface Sci.* **2014**, *420*, 35–40.

(14) Gupta, V.; Miller, J. D. *J. Colloid Interface Sci.* **2010**, *344* (2), 362–371.

(15) Powers, S. M.; Bruulsema, T. W.; Burt, T. P.; Chan, N. I.; Elser, J. J.; Haygarth, P. M.; Howden, N. J. K.; Jarvie, H. P.; Lyu, Y.; Peterson, H. M.; Sharpley, A. N.; Shen, J.; Worrall, F.; Zhang, F. *Nat. Geosci.* **2016**, *9* (5), 353–356.

(16) Némery, J.; Garnier, J. *Nat. Geosci.* **2016**, *9* (5), 343–344.

(17) Smith, V. H.; Schindler, D. W. *Trends Ecol. Evol.* **2009**, *24* (4), 201–207.

(18) Latifian, M.; Liu, J.; Mattiasson, B. *Environ. Technol.* **2014**, *35* (18), 2289–2295.

(19) Dunets, C. S.; Zheng, Y. *Hortscience* **2015**, *50* (6), 921–926.

(20) Li, Y.; Li, L.; Yasser Farouk, R.; Wang, Y. *Int. J. Environ. Res. Public Health* **2019**, *16* (6), 996.

(21) Liu, X.; Zhang, L. *Powder Technol.* **2015**, *277*, 112–119.

(22) Chung, Y. C.; Li, Y. H.; Chen, C. C. *J. Environ. Sci. Heal. - Part A Toxic/Hazardous Subst. Environ. Eng.* **2005**, *40* (9), 1775–1790.

(23) Turunen, J.; Karppinen, A.; Ihme, R. *SN Appl. Sci.* **2019**, *1* (3), 1–9.

(24) Song, H.; Wu, H.; Li, S. J.; Tian, H.; Li, Y. R.; Wang, J. G. *Molecules* **2018**, *23* (8).

(25) Li, H.; Du, Y.; Wu, X.; Zhan, H. *Colloids Surfaces A Physicochem. Eng. Asp.* **2004**, *242* (1–3), 1–8.

(26) Wang, M.; Feng, L.; Fan, X.; Li, D.; Qu, W.; Jiang, S.; Li, S. *Materials (Basel).* **2018**, *11* (10), 1–20.

(27) Labidi, A.; Salaberria, A. M.; Fernandes, S. C. M.; Labidi, J.; Abderrabba, M. *Materials (Basel).* **2019**, *12* (3).

(28) Chintakunta, R.; Buaron, N.; Kahn, N.; Moriah, A.; Lifshiz, R.; Goldbart, R.; Traitel, T.; Tyler, B.; Brem, H.; Kost, J. *Carbohydr. Polym.* **2016**, *150*, 308–318.

(29) Pennetta De Oliveira, L.; Gumfekar, S. P.; Lopes Motta, F.; Soares, J. B. P. *Energy and Fuels* **2018**, *32* (4), 5271–5278.

(30) Labidi, A.; Salaberria, A. M.; Fernandes, S. C. M.; Labidi, J.; Abderrabba, M. *Materials (Basel).* **2019**, *12* (3), 4–5.

(31) Liu, Z.; Huang, M.; Li, A.; Yang, H. *Water Res.* **2017**, *119*, 57–66.

(32) Cai, J.; Xu, D.; Dong, Z.; Yu, X.; Yang, Y.; Banks, S. W.; Bridgwater, A. V. *Renew. Sustain. Energy Rev.* **2018**, *82*, 2705–2715.

(33) Wang, S.; Li, Y.; Li, Z. *Ind. Eng. Chem. Res.* **2020**, *59*, 6855–6866.

(34) Moussout, H.; Ahla, H.; Aazza, M.; Bourakhouadar, M. *Polym. Degrad. Stab.* **2016**, *130*, 1–9.

(35) Sun, J. Y.; Zhao, X.; Illeperuma, W. R. K.; Chaudhuri, O.; Oh, K. H.; Mooney, D. J.; Vlassak, J. J.; Suo, Z. *Nature* **2012**, *489* (7414), 133–136.

(36) Yuan, N.; Xu, L.; Wang, H.; Fu, Y.; Zhang, Z.; Liu, L.; Wang, C.; Zhao, J.; Rong, J. *ACS Appl. Mater. Interfaces* **2016**, *8* (49), 34034–34044.

(37) Yuan, B.; Shang, Y.; Lu, Y.; Qin, Z.; Jiang, Y.; Chen, A.; Qian, X.; Wang, G.; Yang, H.; Cheng, R. *J. Appl. Polym. Sci.* **2010**, *117* (I), 1876–1882.

(38) Xu, L.; Che, L.; Zheng, J.; Huang, G.; Wu, X.; Chen, P.; Zhang, L.; Hu, Q. *RSC Adv.* **2014**, *4* (63), 33269–33278.

(39) Li, H.; Zhao, J.; Bai, Y.; Song, C.; Yu, Y. *Adv. Sustain. Syst.* **2019**, *1900029*, 1900029.

(40) Yang, Z.; Yang, H.; Jiang, Z.; Cai, T.; Li, H.; Li, H.; Li, A.; Cheng, R. *J. Hazard. Mater.* **2013**, *254–255* (1), 36–45.

(41) Dong, C.; Chen, W.; Liu, C. *Bioresour. Technol.* **2014**, *170*, 239–247.

(42) Zhang, H.; Neau, S. H. *Biomaterials* **2001**, *22* (12), 1653–1658.

(43) Wu, Y.; Zheng, Y.; Yang, W.; Wang, C.; Hu, J.; Fu, S. *Carbohydr. Polym.* **2005**, *59* (2), 165–171.

(44) Fan, J.; Chen, Q.; Li, J.; Wang, D.; Zheng, R.; Gu, Q.; Zhang, Y. *J. Polym. Environ.* **2019**, *27* (2), 275–285.

(45) Lü, T.; Luo, C.; Qi, D.; Zhang, D.; Zhao, H. *React. Funct. Polym.* **2019**, *139*, 133–141.

(46) Pei, Y.; Zhao, L.; Du, G.; Li, N.; Xu, K.; Yang, H. *Petroleum* **2016**, *2* (4), 399–407.

(47) Sun, Y.; Ren, M.; Zhu, C.; Xu, Y.; Zheng, H.; Xiao, X.; Wu, H.; Xia, T.; You, Z. *Ind. Eng. Chem. Res.* **2016**, *55* (38), 10025–10035.

(48) Ma, J.; Fu, K.; Shi, J.; Sun, Y.; Zhang, X.; Ding, L. *Carbohydr. Polym.* **2016**, *151*, 565–575.

(49) Ma, J.; Zhou, G.; Chu, L.; Liu, Y.; Liu, C.; Luo, S.; Wei, Y. *ACS Sustain. Chem. Eng.* **2017**, *5* (1), 843–851.

(50) Yang, R.; Li, H.; Huang, M.; Yang, H.; Li, A. *Water Res.* **2016**, *95* (2015), 59–89.

(51) Jiang, M. qin; Wang, Q. ping; Jin, X. ying; Chen, Z. liang. *J. Hazard. Mater.* **2009**, *170* (1), 332–339.

(52) Djibrine, B. Z.; Zheng, H.; Wang, M.; Liu, S.; Tang, X.; Khan, S.; Jimenéz, A. N.; Feng, L. *Int. J. Polym. Sci.* **2018**, *2018*.

(53) Teh, C. Y.; Wu, T. Y.; Juan, J. C. *Ecol. Eng.* **2014**, *71*, 509–519.

(54) Guibal, E.; Van Vooren, M.; Dempsey, B. A.; Roussy, J. *Sep. Sci. Technol.* **2006**, *41* (11), 2487–2514.

(55) Momeni, M. M.; Kahforoushan, D.; Abbasi, F.; Ghanbarian, S. *J. Environ. Manage.* **2018**, *211*, 347–355.

(56) Yang, Z.; Degorce-Dumas, J. R.; Yang, H.; Guibal, E.; Li, A.; Cheng, R. *Environ. Sci. Technol.* **2014**, *48* (12), 6867–6873.

(57) Rahn-Chique, K.; Puertas, A. M.; Romero-Cano, M. S.; Rojas, C.; Urbina-Villalba, G. *Adv. Colloid Interface Sci.* **2012**, *178*, 1–20.

(58) Yang, Z.; Yang, H.; Jiang, Z.; Huang, X.; Li, H.; Li, A.; Cheng, R. *Colloids Surfaces A Physicochem. Eng. Asp.* **2013**, *423*, 11–19.

(59) Smoczyński, L.; Mróz, P.; Wardzynska, R.; Załeska-Chróst, B.; Dłuzyńska, K. *Chem. Eng. J.* **2009**, *152* (1), 146–150.

(60) Smoluchowski, M. von. *Z. Phys. Chem.* **1917**, *92*, 129–168.

(61) Xue, C.; Wilson, L. D. *Carbohydr. Polym.* **2016**, *135*, 180–186.

(62) Rezende, R.; Bártolo, P.; Mendes, A.; Filho, R. *eight Int. Conf. Chem. Process Eng.* **2007**, *11*, 509–514.

(63) Simpson, N. E.; Stabler, C. L.; Simpson, C. P.; Sambanis, A.; Constantinidis, I. *Biomaterials* **2004**, *25* (13), 2603–2610.

(64) Lagergren, S. *K. Sven. Vetensk. Sakademiens Handl.* **1898**, *24* (1–39), 2474–2479.

(65) Zhen, Y.; Ning, Z.; Shaopeng, Z.; Yayi, D.; Xuntong, Z.; Jiachun, S.; Weiben, Y.; Yuping, W.; Jianqiang, C. *ACS Appl. Mater. Interfaces* **2015**, *7* (44), 24446–24457.

(66) Ho, Y. S.; McKay, G. *Process Biochem.* **1999**, *34* (5), 451–465.

(67) Singh, R. P.; Pal, S.; Rana, V. K.; Ghorai, S. *Carbohydr. Polym.* **2013**, *91* (1), 294–299.

(68) Guibal, E.; Roussy, J. *React. Funct. Polym.* **2007**, *67* (1), 33–42.

(69) Lin, Q.; Qian, S.; Li, C.; Pan, H.; Wu, Z.; Liu, G. *Carbohydr. Polym.* **2012**, *90* (1), 275–283.

(70) Kwok, K. C. M.; Koong, L. F.; Chen, G.; McKay, G. *J. Colloid Interface Sci.* **2014**, *416*, 1–10.

(71) Kono, H.; Kusumoto, R. *J. Water Process Eng.* **2015**, *7*, 83–93.

(72) Langmuir, I. *J. Am. Chem. Soc.* **1916**, *252*, 2221–2295.

(73) Freundlich, H. M. F. . *Z. Phys. Chem.* **1909**, *57*, 385–470.

(74) Sips, R. *J. Chem. Phys.* **1948**, *18* (5), 490–495.

(75) Ho, Y. S.; Porter, J. F.; Mckay, G. *Water, Air, Soil Pollut.* **2002**, *141* (1–4), 1–33.

(76) Crini, G. *Dye. Pigment.* **2008**, *77* (2), 415–426.

(77) Chen, M.; Huo, C.; Li, Y.; Wang, J. *ACS Sustain. Chem. Eng.* **2016**, *4* (3), 1296–1302.

(78) Karunanayake, A. G.; Navarathna, C. M.; Gunatilake, S. R.; Crowley, M.; Anderson, R.; Mohan, D.; Perez, F.; Pittman, C. U.; Mlsna, T. *ACS Appl. Nano Mater.* **2019**, *2* (6), 3467–3479.

(79) Xie, F.; Dai, Z.; Zhu, Y.; Li, G.; Li, H.; He, Z.; Geng, S.; Wu, F. *Colloids Surfaces A Physicochem. Eng. Asp.* **2019**, *562*, 16–25.

(80) Hena, S.; Atikah, S.; Ahmad, H. *Int. J. Eng. Sci.* **2015**, *4* (1), 51–62.

(81) Lin, J.; He, S.; Wang, X.; Zhang, H.; Zhan, Y. *Colloids Surfaces A Physicochem. Eng. Asp.* **2019**, *561*, 301–314.

(82) Ma, J.; Fu, X.; Xia, W.; Fu, K.; Liao, Y. *Processes* **2019**, *7* (2), 108–122.

(83) Olphen, H. Van. *An introduction to clay colloid chemistry, for clay technologists, geologists, and soil scientists.*; 2nd, Ed.; Wiley: New York, USA, 1977.

(84) Dwari, R. K.; Mishra, B. K. *Int. J. Min. Sci. Technol.* **2019**, *29* (5), 745–755.

(85) Zhang, W.; Cao, Q.; Xu, G.; Wang, D. *ACS Sustain. Chem. Eng.* **2018**, *6* (8), 11087–11096.

(86) Aktas, T. S.; Fujibayashi, M.; Maruo, C.; Nomura, M.; Nishimura, O. *Desalin. Water Treat.*

2013, *51* (22–24), 4729–4735.

(87) Hasan, A.; Fatehi, P. *Sci. Rep.* **2019**, *9* (1), 1–12.

(88) Peng, S.; Jiang, G.; Li, X.; Yang, L.; Liu, F.; He, Y. *J. Pet. Sci. Eng.* **2018**, *162*, 55–62.

(89) Wang, S.; Konduri, M. K. R.; Hou, Q.; Fatehi, P. *RSC Adv.* **2016**, *6* (46), 40258–40269.

(90) Xu, Y.; Chen, T.; Cui, F.; Shi, W. *Chem. Eng. J.* **2016**, *287*, 225–232.

CHAPTER 8

8 Discussion, Concluding Remarks and Proposed Work

8.1 Integrated discussion of manuscript chapters

This section provides an overview of the findings of the thesis research and outlines how the objectives were addressed by the respective studies listed in the manuscript chapters (Chapters 3-7). As outlined in Chapter 1, the overall aim of the thesis research relates to the development and application of a sustainable coagulation-flocculation system that has improved water treatment performance toward oxyanion (where the focus is directed to phosphate, P_i) and colloidal particles (finely dispersed kaolinite particles, turbidity, T_i) removal from aqueous medium over conventional CF systems currently available. Generally, coagulation-flocculation (CF) processes require the use of mineral salts (e.g., alum, ferric chloride, ferric sulphate, etc.) as coagulants and synthetic polymers (e.g., polyacrylate, polystyrene sulphonate, polyethylene oxide, etc.) as flocculants. However, due to the several disadvantages associated with these materials, especially regarding health and environmental concerns, as discussed in Section 2.5.1, there is an impetus to eliminate them in the wastewater treatment process. Hence, this thesis was focused on strategies to develop single-component CF materials that possess dual function properties akin to that of conventional binary and ternary systems, from biopolymers with more exceptional performance toward wastewater treatment and able to overcome the disadvantages accompanied with inorganic salt and synthetic polymers. The overall objective of the thesis was further divided into three categories (themes), as illustrated in Figure 8.1:

i. Flocculation efficacy of combined biopolymer-metal salt system towards dissolved phosphate removal in wastewater in single-component, binary and ternary CF systems.
ii. Synthesis, characterization and flocculation properties of high molecular weight chitosan-based amphoteric flocculant for P_i and T_i removal in a single-component and binary systems.
iii. Synthesis, characterization and flocculation performance and floc properties of high molecular weight cationic chitosan-based flocculants.

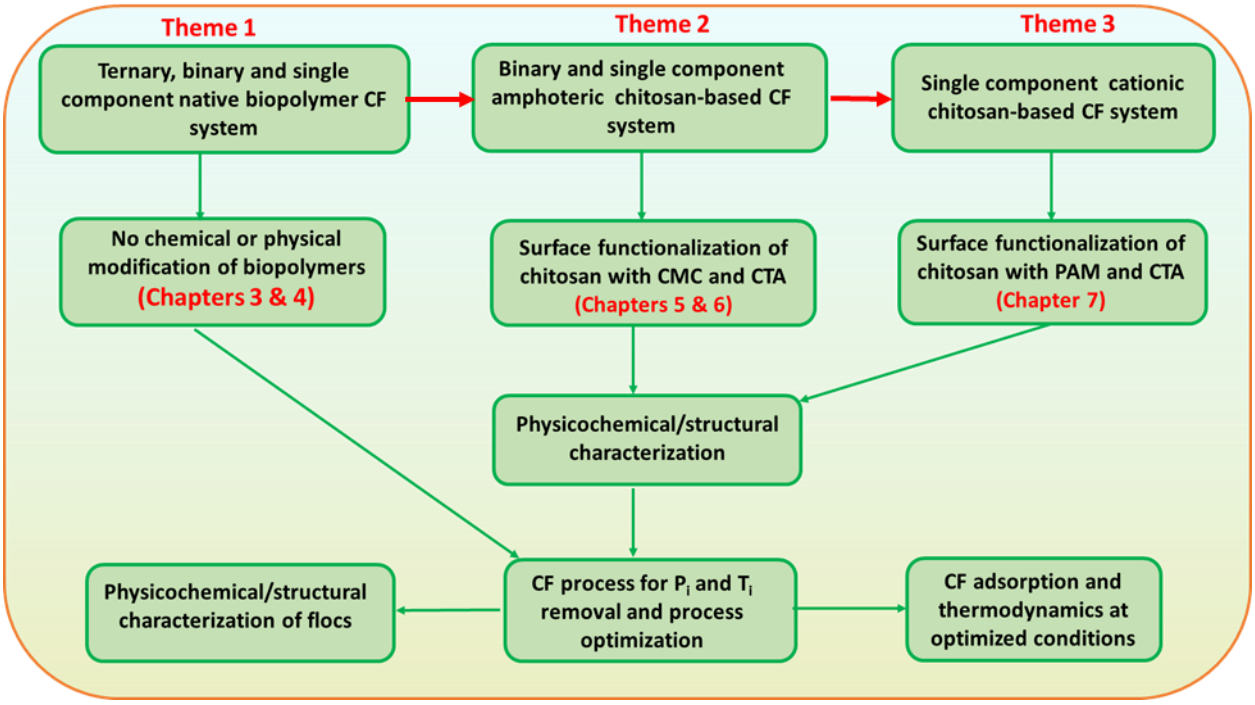

Figure 8.1: Organization of the Ph.D. thesis objectives into three research themes in this study.

The selected biopolymers in this thesis research are chitosan and alginate (cationic versus anionic biopolymers, respectively), which are known to have several advantages for wastewater treatment due to their physicochemical properties. Chitosan has several amine (-NH_2) and hydroxyl (-OH) groups on its surface.[1] In an acidic medium, the active amine groups in its structure can be protonated, resulting in the formation of cationic polyelectrolyte.[2] The presence of the cationic charge on the polymer leads to a strong electrostatic attraction between chitosan and anionic contaminants such as phosphate, nitrate and anionic organic dyes such as Reactive black 5.[2–4] However, it undergoes deprotonation to become negatively charged in an alkaline environment, making it useful for chelating metal ions at variable pH conditions. Characteristic properties of chitosan are influenced by its molecular weight, degree of deacetylation (DD), crystallinity and solubility in water.[5] Alginate, on the other hand, is anionic and possesses a negative surface charge.[6] Among all polysaccharides, it is the only one that naturally maintains two carboxyl groups in each constituent unit with several -OH groups, and has several applications due to its physicochemical properties (*cf* Section 2.9.2.2).[6,7] Unlike chitosan, which has been explored as a functional material, especially in wastewater treatment, alginate is now gaining attention. The recent interest in the use of alginate for water treatment is due to the following

advantageous features it shares with chitosan. Both alginate and chitosan are cost-effective and possess no adverse health effects for handling or an additive to drinking water. In addition, they have improved sludge dewatering characteristics and are effective flocculants to increase the size and weight of flocs. Moreover, a small dosage of these materials is required in a CF process and does not significantly alter the solution pH. These biopolymers are also biodegradable and biocompatible.[8,9]

Since the CF process is directed toward the removal of suspended particles, it is hypothesized that the CF process can also be effectively employed for the removal of dissolved substances such as phosphate using a biopolymer-metal salt system in Chapters 3 and 4. Several reports have shown that chitosan or alginate combined with metal ion coagulants such as alum or $FeCl_3$ is effective for removing suspended solids, dyes, and turbidity in wastewater via CF or by a conventional adsorption process. Prior to the commencement of this PhD research, no study was reported on the use of alginate, chitosan and $FeCl_3$/alum in an aqueous medium for the removal of dissolved species such as phosphate. Hence, chitosan, alginate and oat hull biomass were studied as the biopolymer flocculants, and $FeCl_3$ or alum were used as the coagulants in this study. In Chapter 1, various single and multicomponent systems were compared, single (alum, chitosan, alginate, oat hull), (ii) binary (alum + chitosan, alum + alginate or alum + oat hull), and (iii) ternary (alum + alginate + chitosan) coagulant−flocculant systems, to evaluate the P_i removal properties and the role of synergistic effects. The role of pH, component dosages, and P_i concentration on the coagulation−flocculation efficacy was evaluated. For the single-component system, it was noted that chitosan had greater phosphate removal efficiency relative to alum and alginate, with each material having an optimal dosage. Below, the optimum dosage, the CF process was controlled by charge neutralization and polymer bridging effects. However, a charge reversal effect occurs when an excess of cationic species is present in the solution. The excess positive charge stabilizes the neutral P_i containing aggregates and the macroflocs undergo repulsive interactions, resulting in a progressive decrease in the P_i removal efficiency. Similar results were reported by Roussy et al.[10] as well as Huang and Chen[11]. The low removal efficiency of the alginate was related to its anionic nature. Since P_i is also negatively charged, it resulted in electrostatic repulsions in solution and stabilization of unbound P_i. However, the biopolymer nature of the alginate favored the removal of P_i by a bridging mechanism, especially when used in combination with cationic polyelectrolytes such as chitosan. Greater P_i removal efficiency occurred for the ternary system over the binary and

single-component systems, where the flocculant dosage decreased significantly from the single-component system to the ternary system. In the ternary system, the presence of chitosan and alginate as flocculants underwent self-assembly to form a network-like structure, which led to the formation of macroflocs via adsorption and polymer bridging after alum coagulated the dissolved P_i to form microflocs. There was an optimal dosage of alum (30 mg/L), while alginate and chitosan were 15 mg/L. P_i removal was 85 ± 0.8, 98 ± 1.2% for alum and 98 ± 0.8% for the ternary systems containing a varied dosage of alum, chitosan and alginate, respectively. P_i removal for the alum−alginate−chitosan ternary system was pH dependent, where the CF process was more effective under acidic conditions, and these results show agreement with other reports.[12–14] At a given pH, the P_i removal had a strong dependence on the relative chitosan dosage due to its cationic nature. The amine groups of chitosan are deprotonated at pH > 6.5; hence, chitosan is unable to associate favorably with phosphate via attractive ion-ion interactions. However, at acidic conditions, attractive ion-ion interactions occur owing to the association of chitosan/phosphate (cation/anion) complexes. Excess chitosan cation species in solution may result in colloidal stabilization at lower pH values. P_i removal was independent of the initial P_i concentration except at lower levels, [P_i] < 10 mg/L. This occurred because at low phosphate concentration (< 10 mg/L), there is competition from the formation of hydroxides, which prevents the occurrence of aluminium-to-phosphate ratio necessary for aluminium phosphate precipitation. Additionally, the alum−refined oat hull binary system was 99% effective for P_i removal, especially when [P_i] = 25 mg/L, with greater removal over the use of oat hulls alone. The removal mechanism for the flocculation of P_i with the oat hulls may relate to the enhanced polymer bridging and/or adsorption processes, as illustrated in Scheme 3.1 (Chapter 3), along with synergistic effects. Polymer bridging involved the nucleation of micro- to macro-flocs due to the coagulation of alum upon the addition of oat hulls.

Since the alginate-alum binary system showed lower CF efficiency towards the removal of P_i in an aqueous medium, an optimal condition was necessary to ensure the effective application of this system. In Chapter 4, a CF optimization study was conducted on a $FeCl_3$-alginate binary system for the removal of orthophosphate using the Box-Behnken experimental design (BBD) and response surface methodology (RSM). The BBD method is an efficient and widely used approach in experimental design.[15] The RSM is a collection of statistical and mathematical methods which are useful for developing, improving, and optimizing multi-parameter processes.[16–18] RSM is

aimed at the factorial design for determining the optimal operational conditions for a given system to meet regulatory requirements.[19] Herein, the BBD was used to evaluate the effects and interactions of four independent variables: pH, $FeCl_3$ dose, alginate dose, and settling time. The RSM analysis showed that the experimental data followed a quadratic polynomial model with optimum conditions at pH 4.6, [$FeCl_3$] = 12.5 mg/L, [alginate] = 7.0 mg/L and a 37-minute settling time. Optimum conditions led to a P_i removal of 99.6% according to the RSM optimization, in good agreement with experimental removal (99.7 ± 0.7%), at an initial phosphate concentration of 10.0 mg/L. The three-dimensional (3D) response surface plots and 2D contour plots showed that there was an interactive relationship between the independent variables (CF factors) and the response function (P_i removal). This was due to the elliptical contour plots and the obvious peak in the 3D plots of the response surfaces that indicate the optimal conditions were located exactly within the design boundary. The results reveal there are significant interactive effects on the response variable between $FeCl_3$ and alginate dosage, $FeCl_3$ dosage and pH, $FeCl_3$ dosage and settling time, alginate dosage and settling time, pH and settling time, as well as alginate dosage and pH. Electrostatic charge neutralization and ion-binding adsorption mechanisms were found to control the flocculation process. At the optimized condition, Fe(III) precipitates phosphate in an aqueous medium according to equation (8.1) through electrostatic charge neutralization. The flocculation process is controlled by an ion-binding adsorption mechanism that occurs at hydroxyl polar functional groups on alginate or charged sites on the polymer backbone. Adsorption of P_i onto alginate occurs when there is sufficient ferric ions present since Fe(III) can act as a bridge between alginate and P_i. In the absence of Fe(III), limited flocculation occurs even at high ionic strength, as observed in Chapter 3.

$$FeCl_3 + PO_4^{3-} \rightarrow FePO_4 \downarrow + 3Cl^- \tag{8.1}$$

The results from Chapters 3 and 4 revealed that the biopolymers, especially chitosan, can be combined with metal ion coagulants for the removal of phosphate in a ternary system. However, the process is pH dependent, and high dosage of the coagulant and flocculants are often required. Hence, there is a need to optimize these conditions through the development of new flocculant materials. In turn, this led to the second theme of this thesis (*cf.* Chapters 5 and 6), where it was hypothesized that increasing the molecular weight and altering the surface charge of the flocculant will enhance the CF conditions. Hence, Chapter 5 was aimed at developing a high molecular weight amphoteric chitosan-based flocculant for enhanced removal of P_i and turbidity (T_i). In this

study, turbidity represents the presence of finely dispersed colloids in the P_i-contaminated wastewater, which is common to most industrial, municipal and agricultural wastewater. Turbidity was achieved by the dispersion of fine clay minerals (kaolinite) in the synthetic P_i-contaminated wastewater. Herein, a high molecular weight amphoteric flocculant (CMC-CTA) was prepared from chitosan by grafting 3-chloro-2-hydroxypropyl trimethylammonium chloride (CTA) onto carboxymethyl chitosan (CMC). The CMC was initially prepared via etherification reaction between chitosan and monochloroacetic acid. The structures of CMC-CTA and CMC were confirmed by various characterization methods such as spectroscopy (^{1}H-NMR, ^{13}C-NMR, FTIR), potentiometric determination of the degree of substitution, TGA, and titrimetric estimation of the point-of-zero charge (isoelectric point, IEP). The modification of chitosan via etherification and grafting yielded a modified biopolymer flocculant with tunable structural and physicochemical properties. This finding was in agreement with previous studies of synthetically modified biopolymers with increased molecular weight and pH-dependent surface functionality.[20,21] At acidic and neutral pH conditions, the flocculants had positive surface charge due to the presence of the grafted quaternary ammonium ion and pronation of the carboxylate in the carboxymethyl group. However, the surface charge of the polymer flocculant was negative due to the presence of the carboxymethyl group.

The flocculation properties of the polymer flocculants were tested for the dual removal of T_i and P_i in an aqueous environment (in the presence or absence of $FeCl_3$) in binary and single-component systems, respectively. At a fixed $FeCl_3$ dosage, the effects of flocculant dosage, pH and settling time were evaluated. The binary system (flocculant + $FeCl_3$) was more effective for the flocculation process compared to the single-component system. Generally, the removal efficiency for P_i and T_i followed a similar trend, where a rise and fall in the CF performance occur as the factors under consideration increase beyond their optimal values. This trend follows an electrostatic charge neutralization mechanism since more cation species are present in the turbid water that undergo charge neutralization with the negatively charged colloidal particles as the flocculant dosage increases beyond the optimum value. The similarity in the trend between P_i and T_i is due to their surface charge. Estimates of the ζ-potential by Yang et al.[20] reveal that kaolinite is negatively charged at alkaline and acidic pH and P_i species that are dominant under these conditions are HPO_4^{2-} and $H_2PO_4^-$. The P_i and T_i removal efficiency of CMC-CTA with $FeCl_3$ in the binary system was greater in comparison to chitosan or CMC combine with Fe(III) in a binary

system. The presence of CTA and the carboxymethyl (CM) species on the chitosan backbone resulted in a size increase of the CMC-CTA flocculant and its hydrodynamic volume (V_{hyd}), in accordance with its intrinsic viscosity. The greater V_{hyd} of the biopolymer relates to its greater flocculation efficiency, following the flocculation model by Brostow et al.[22] T_i removal (%) and optimal dosage (mg/L) was determined as follows for the binary system in parentheses: CMC-CTA (95.8%; 5), CHI (88.8%; 7.0) and CMC (68.8%; 9.0). The corresponding P_i removal and dosage (mg/L) are listed in parentheses: (93.4%; 10), (90.6%; 10), and (67.4%; 5). The presence of the metal coagulant led to a decrease in the optimum dosage of the polymer flocculant to achieve high P_i and T_i removal efficiency. This demonstrates that Fe(III)-CMC-CTA flocculant system was able to reduce the optimum flocculant dosage to 5.0 mg/L, and the process was more effective in acidic to neutral pH conditions.

The flocculation properties of the Fe(III)-CMC-CTA binary flocculant system was further investigated in Chapter 6 through optimization studies to obtain its optimized conditions to further evaluate and understand the flocculation mechanism via adsorption kinetic and isotherm models and equilibrium thermodynamic studies. The Box-Behnken response surface methodology was employed to evaluate the relationship between the flocculation process responses (P_i and T_i removal) with the most important variables ($FeCl_3$ dosage, CMC-CTA dosage, pH and settling time) and analyze the optimal conditions to maximize P_i and T_i removal (%). The effect of individual independent variables on the response functions was evaluated using the main effect plots. These plots provide a preliminary conclusion about the effects of the flocculation and independent variables on P_i and T_i removal efficiency. Flocculant dosage, $FeCl_3$ and pH had a significant effect on the P_i and T_i removal whereas, the settling time appeared to have an independent effect on the P_i and T_i removal (%) since an increase in the settling time of the flocs did not significantly affect their removal efficiency. Interactive effects between any two independent variables had a remarkable effect on the response factors, as demonstrated in Figures 6.6 & 6.7. The elliptical contour plots in Figure A9.5 (*cf.* Appendix A) show significant interactive effects on P_i removal (%) between any two variables. In addition, the obvious peak in the response surfaces for the P_i and T_i removal (%) confirms that the optimal conditions were exactly located inside the design boundary. The RSM analysis showed that the experimental data followed a quadratic polynomial model with optimal conditions at [CMC-CTA] = 3.0 mg/L, [$FeCl_3$] = 10.0 mg/L, pH 6.8, and a 28 minute settling time.

According to the use of RSM optimization, optimal conditions led to a P_i and T_i removal of 96.4% and 96.7%, respectively, in good agreement with experimental results with an initial phosphate concentration of 30.0 mg P_i/L. Analysis of the flocculation kinetics showed that P_i and T_i followed PFO and PSO kinetics, respectively. This shows that the P_i species are adsorbed by the Fe(III)-CMC-CTA flocculant system, where the rate decreases linearly as the adsorption rate increases. Similar results were reported for the flocculation of phosphate (Chapters 4 and 5), arsenate and anionic dyes with polysaccharide-based flocculants.[23–25] On the other hand, the analysis of kinetic parameters indicates the rate-limiting-step for flocculation involves interaction between the Fe(III)-CMC-CTA flocculant system and the anionic colloidal kaolinite, where it followed a chemisorption-like process, where the flocculation process is considered to be irreversible. Adsorption isotherms of the flocculation of P_i were well described by the Langmuir model, which shows that there is a strong binding affinity between P_i with Fe(III)-CMC-CTA to form stable flocs which are large and dense in solution. The CF process is characterized by electrostatic charge neutralization, polymer bridging and polymer adsorption mechanisms. This demonstrates that the CMC-CTA flocculant led to a reduction in the optimum flocculant dosage, and the process was more effective from acidic to neutral pH conditions. In addition, the settling time for CMC-CTA was shorter (28 min) relative to that of chitosan (37 min). The significant improvement in the optimized conditions of the CF process relates to the use of high molecular weight CMC-CTA flocculant. As well, its cationic nature at acidic and neutral conditions (pH < 7) arises due to the protonation of the amine and carboxylate groups on the modified chitosan flocculant at these pH conditions.

Despite the major improvement in the CF conditions, the amphoteric flocculant was less effective at alkaline pH conditions and $FeCl_3$ was needed as a metal ion coagulant (at a minimal dosage, 10 mg/L). In order to improve the flocculation performance of the biopolymers at all pH conditions and to eliminate the use of metal ion coagulants, a series of high molecular weight cationic flocculants were prepared from chitosan in Chapter 7, which relate to theme 3 (*cf.* Figure 8.1). In the synthesis of the cationic flocculants, a non-toxic CTA was quaternized onto the chitosan-grafted-polyacrylamide (Chi-*g*-PAM) backbone. The amount of Chi-*g*-PAM was kept constant, while varying the amount of CTA for each synthetic experiment, in order to prepare a series of CTA- Chi-*g*-PAM flocculant samples with various degrees of substitution of CTA. The various mass ratios of Chi-*g*-PAM to CTA were denoted as CTA-Chi-*g*-PAM-1, CTA-Chi-*g*-

PAM-2, CTA-Chi- *g*-PAM-3, CTA-Chi-*g*-PAM-4, CTA-Chi-*g*-PAM-5 in ascending order of CTA mass. The physicochemical, textural, morphological and electrical properties of the polymer flocculants were studied by spectroscopy, microscopy, thermal and potentiometric methods. The results obtained from the characterization studies affirmed the synthesis of the cationic flocculants. In the ^{1}H-NMR spectra (Figure 7.1a), the appearance of new peaks at 1.55 ppm and 2.11 ppm, as well as 3.13 ppm, confirmed the presence of PAM[26,27] and CTA[27,28] on the chitosan backbone. The presence of these installed groups onto chitosan was further confirmed by the new NMR signatures at 173.9 ppm (PAM)[29,30] and 54.8 ppm (CTA)[28–30] per the ^{13}C-NMR spectra (Figure 7.1b). Moreover, the properties of the flocs were characterized by various methods (laser particle size analyzer, FTIR spectroscopy, SEM, and zeta potential).

The functional properties of the flocculants were studied for the removal of orthophosphate (P_i) and turbidity (T_i), where the effects of initial pH, settling time, flocculant dosage and temperature were studied in a single-component system. Greater P_i and T_i removal were obtained within the first 5.0 min of floc sedimentation, and the results were independent of pH variation, where greater removal efficiency was observed at all pH conditions. The optimal dosage ranged from 0.2 mg/L to 0.5 mg/L, where CTA-Chi-*g*-PAM-5 with the greatest degree of substitution of CTA, had the lowest optimal dosage (0.2 mg/L), along with very efficient P_i (99.0 %) and T_i (98.6 %) removal. The significantly improved CF conditions in the single-component system are associated with the increased molecular weight and the cationic nature of the polymer flocculant at both acidic and alkaline conditions along with enhanced solubility at all conditions. The structure of the polymer flocculant in solution has a significant influence on their performance. In a previous study, it was reported that the hydrodynamic radius (R_h) of a chitosan-based flocculant is pH dependent, where R_h decreases with increasing pH until it reaches its IEP and then increases thereafter.[31] At pH > IEP, the amine group of the flocculants undergoes deprotonation. Hence, the electrostatic charge neutralization effect reduces, and the bridging flocculation effect dominates due to the extended morphology of the polymer chains. However, at pH < IEP, due to the opposite charge of the kaolinite or P_i and the cationic flocculant at this pH, charge neutralization mechanism enhances the performance of the flocculants.[32] The novelty of this polymer flocculant lies in its ability to function simultaneously as a coagulant and a flocculant for P_i and T_i removal in a single-component system. This phenomenon occurs because the cationic quaternary ammonium group destabilizes the electrical double layer of the colloidal particles, which results in coagulation and

formation of microflocs. The polymer flocculant components aggregate the microflocs through polymer bridging and adsorption mechanisms that result in the formation of denser and compact flocs.

The T_i flocculation kinetics showed that the flocs formed at the optimal dosage had a greater rate of aggregation relative to breakage due to higher particle collision rate, resulting in the formation of harder, denser and compact flocs that are able to resist breakage. However, the P_i flocculation kinetics followed pseudo-second-order kinetics, as observed in previous chapters. The adsorption profile of the P_i during flocculation is well described by the Langmuir model, where the process was endothermic and spontaneous according to the values of the standard change of the Gibbs free energy (ΔG^o) at equilibrium. The maximum floc size (500 µm) was obtained at the optimum dosage of CTA-Chi-*g*-PAM-5, and the flocs were formed mainly via Coulombic electrostatic edge-to-face (E-F) attraction between the cationic CTA-Chi-*g*-PAM flocculant and the negatively charged kaolinite dispersed particles. Other minor associations that occurred are face-to-face (F-F) and edge-to-edge (E-E) interaction via electrostatic repulsive and van der Waals attractive forces between faces or edges with the same charge surface. The flocculation process was governed by electrostatic charge neutralization and polymer bridging mechanisms. The results show that the cationic polymer materials possess both coagulant and flocculant properties and are able to effectively remove colloidal suspended particles and dissolved substances in wastewater with an improved, optimized condition relative to that of CMC-CTA and chitosan. Due to the remarkably improved optimized conditions of the CTA-Chi-PAM flocculants, they are likely to be useful for the removal of organophosphate (*p*-nitrophenyl phosphate, PNPP) anions and sulphate ions in aqueous media.

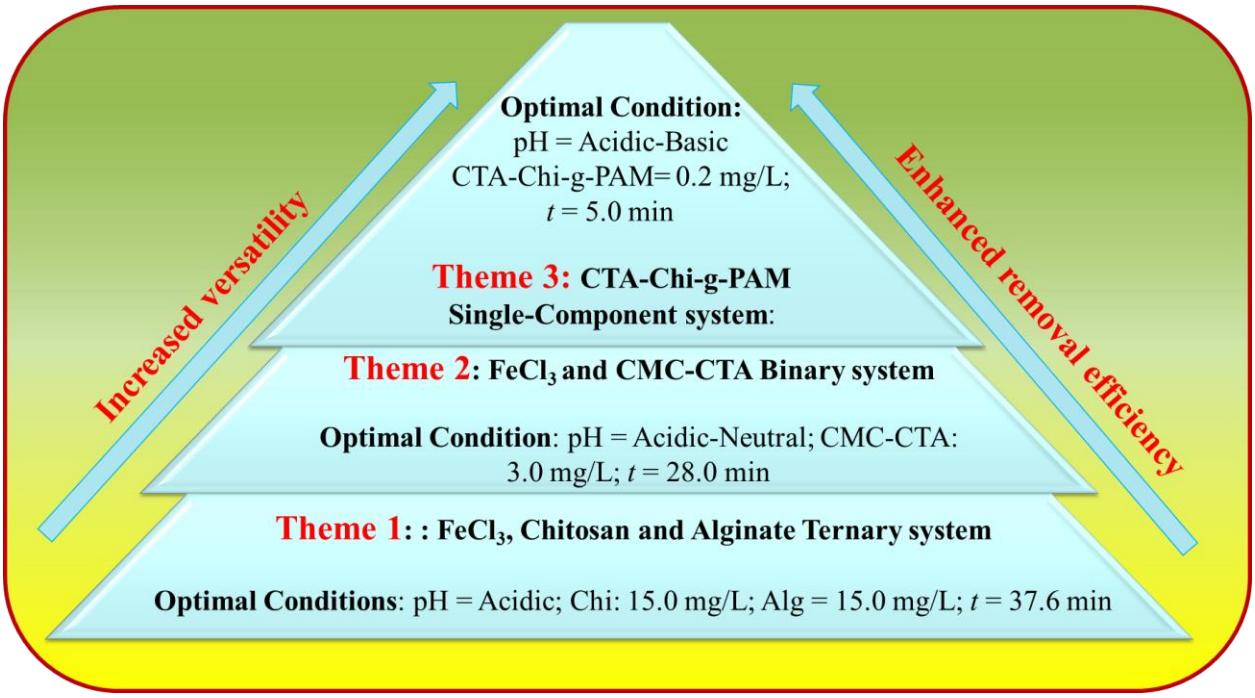

Figure 8.2: Sequential progression from Theme 1-3 depicting the achievement of the overall thesis objectives.

8.2 Conclusion

In summary, the overall objective of this PhD thesis research focused on the development of biopolymer flocculant materials from natural polymers for the removal of phosphate and colloidal particles (turbidity, T_i) from aqueous medium. Flocculation properties of natural biopolymers such as chitosan and alginate and modified derivatives of chitosan with and without inorganic mineral salt coagulants were studied for the removal of P_i and T_i in synthetic wastewater. The CF experiment was carried out using a jar test and one-pot experimental design when it was necessary to monitor the kinetics *in situ* for the process. This research provided many unique results that relate to new knowledge of biopolymer materials and their application in wastewater treatment. The materials design approach to achieve this overall objective of biopolymer flocculants is divided into three strategies described by Themes 1-3, as discussed in Chapter 1 and the concluding results are illustrated in Figure 8.2.

Theme 1 was further described in Chapters 3 and 4 that address hypotheses 2, 4, 5, and 6. Theme 1 relates to study of the flocculation properties for selected biopolymers with metal ion

coagulants for the removal of dissolved orthophosphate in a ternary system through CF optimization study, as shown in Figure 8.2. In Chapter 3, CF of P_i using alum in conjunction with biopolymers (chitosan and alginate), along with oat hull biomass, are reported in single-component, binary and ternary systems. The efficiency of the P_i removal relates to the dosage of the coagulant-flocculant system, where an optimum dosage was achieved for each system. Variable alum dosing in the alum-chitosan-alginate ternary system revealed an optimum alum dosage of 30 mg/L when the initial P_i level was 10-11 mg/L. P_i removal was more effective for the ternary system relative to the binary and single-component systems. The binary system (alum/alginate or alum/chitosan) had a lower P_i removal (80% and 88%) relative to the ternary system (98%). The presence of flocculants and the smaller value of alum to phosphate molar ratios (Table 3.3) indicate that the P_i removal depends on pH, with an optimum value at pH 6–7, in agreement with a process that occurs by charge neutralization and polymer-bridging. The initial level of P_i was relatively independent of the P_i removal efficacy. Among the polymer flocculants used, chitosan was superior over alginate for P_i flocculation. The poorer performance of alginate relates to its negative surface charge, due to the carboxylate groups on its surface, as discussed in Chapter 3. Refined and unrefined oat hulls aided the flocculation process by further removal of dissolved P_i. Variable P_i removal occurs for the refined (99%) and unrefined (93%) oat hulls at an initial P_i dosage of 25 mg/L in the binary system. The availability and abundance of oat hull biomass reveal its utility for wastewater treatment, as evidenced by its lower material cost and enhanced pollutant removal when used in conjunction with conventional flocculation-coagulation processes.

Due to the poor flocculation performance of alginate, it was further studied to obtain an optimum condition for the removal of P_i in a binary system with $FeCl_3$. Hence, in Chapter 4, the optimization of the CF process for P_i removal in aqueous medium was studied using a jar test system. The response surface methodology (RSM) using the Box-Behnken design (BBD) method was studied to optimize the conditions for maximum P_i removal. The $FeCl_3$ and alginate dosage, along with pH and settling time, were determined as significant factors to yield optimal P_i removal. The predicted quadratic polynomial model by the RSM method was evaluated to estimate the P_i removal over the range of experimental variables. Optimal conditions for the CF process occurred at pH 4.6, $FeCl_3$ (12.5 mg/L), alginate dosage (7.3 mg/L) and settling time (37 min), where the P_i removal was 99.7 ± 0.7%. This study shows good agreement between experimental results and the

RSM predictions, and further illustrates that RSM can be used to model and optimize CF processes for phosphate removal. The results for the optimized conditions indicate that P_i removal occurs via a charge neutralization, along with ion-binding adsorption of P_i by the Fe(III)-alginate flocculant system. Greater P_i removal occurred at acidic relative to alkaline pH conditions. The variable P_i removal relates to the electrostatic interaction between orthophosphate anion species and the flocculant system. Kinetic adsorption profiles show uptake within 37 min, where the experimental results are well-described by the pseudo-first-order kinetic model and Langmuir isotherm model at equilibrium conditions. Electrostatic charge neutralization and ion-binding adsorption mechanisms were demonstrated to govern the flocculation process. The results of this study will contribute to the further development of advanced water treatment processes for the controlled removal of other waterborne oxyanion species. Therefore, by considering other properties of alginate and chitosan such as sorption and chelation of metal ions, biocompatibility, biodegradability, non-toxic nature and antimicrobial activity, the use of such biopolymers can enhance P_i and other complex types of waterborne contaminant removal.

The results related to the second theme was outlined in Chapters 5 and 6 which address hypotheses 1 to 6 of the thesis research. Theme 2 relates to the synthesis, characterization and flocculation properties of high molecular weight chitosan-based amphoteric flocculant for P_i and T_i removal in a single-component and binary systems. In chapter 5, an amphoteric flocculant (CMC-CTA) was prepared from chitosan by grafting 3-chloro-2-hydroxypropyl trimethylammonium chloride (CTA) onto carboxymethyl chitosan (CMC), where the CMC precursor was originally prepared via etherification reaction chitosan and monochloroacetic acid. The physicochemical properties and the structure of CMC-CTA were supported by various characterization methods such as spectroscopic (^{1}H- and ^{13}C-NMR, FT-IR), TGA and point-of-zero-charge analysis. The introduction of the CTA and monochloroacetic acid groups onto the chitosan backbone served to increase its molecular weight and to enhance its surface charge properties at acidic and alkaline conditions for effective flocculation activity. The dual removal of T_i and P_i by flocculation was studied using CMC-CTA, chitosan (CHI) and CMC, with and without $FeCl_3$ coagulant in binary and single-component systems. The removal efficiency of P_i and T_i using CMC-CTA, Chi and CMC flocculants with $FeCl_3$ in the binary system was much greater than in the absence of Fe(III) in the single-component system. CMC-CTA showed greater flocculation over chitosan and CMC at all pH conditions, especially at the optimal pH, where the T_i (99.2%)

and P_i (97.8%) removal was favored. Flocculation processes are governed by charge neutralization, followed by polymer bridging and adsorption processes. The flocculation kinetics for P_i and T_i removal are well-described by the pseudo-first-order (PFO) and pseudo-second-order (PSO) models. The rate limiting step for turbidity removal involve interactions between the flocculant and the kaolinite species in agreement with a chemisorption-like process. In contrast, P_i removal was reported to follow a physisorption-based process.

The traditional CF process with multi-parameter effects that involve changing one factor at a time, while keeping the other independent variables fixed. This approach often requires many experiments, which may be time-consuming that yield a low optimization efficiency. To address this problem, the design of experiment (DOE) was used to study the effect of independent variables (CF factors) and their responses whilst using a minimum number of experiments, as outlined in Chapter 6. A preliminary study in Chapter 5, indicated that important variables which affect T_i and P_i, removal include $FeCl_3$ dosage, CMC-CTA dosage, pH and settling time. Herein, a jar test system was used to investigate the optimization of the CF system for P_i and T_i removal in aqueous media. The BBD-RSM was used to design the order of the experimental runs and to statistically analyze the experimental data in order to optimize the conditions for maximum P_i and T_i removal. By employing the BBD, guided by RSM, a combination of CMC-CTA dosage, $FeCl_3$ dosage, pH and settling time was shown to have considerable effect on removal of the selected response functions. The predicted quadratic polynomial models by the RSM method were used to estimate the P_i and T_i removal over the range of experimental design. Optimal conditions for the CF process occurred at pH 4.1, $FeCl_3$ (10.4 mg/L), CMC-CTA dosage (3.1 mg/L) and settling time (21.9 min) for P_i removal, and pH 9.4, $FeCl_3$ (10.2 mg/L), CMC-CTA dosage (1.0 mg/L) and settling time (30.8 min) for T_i removal with a high removal efficiency for P_i (98.4%) and T_i (99.8%). The compromised optimal conditions calculated from the regression equation were as follows: CMC-CTA dosage (3.0 mg/L), $FeCl_3$ dosage (10.1 mg/L), pH 6.8 and settling time of 28.0 min. The corresponding removal was 96.4% and 96.7%, for P_i and T_i. The validation results show good agreement between experimental results and the RSM predictions; further illustrating that RSM can enable modeling and optimization of the CF process for P_i and T_i removal required for demanding water treatment applications. A study of the flocculation and adsorption properties for P_i and T_i removal at equilibrium and optimized conditions revealed that modified biopolymer (CMC-CTA) systems had tunable adsorption properties. Evidence of such synthetic modification

and tunability of the physicochemical properties were further confirmed by the improved sorption capacities toward P_i of the CMC-CTA flocculant relative to that of CMC, chitosan and alginate. The thermodynamic study showed that the flocculation process for P_i removal by the modified polymer material was spontaneous and followed a physisorption process and was driven by entropy effects (positive ΔS^o). The Fe(III)-CMC-CTA flocculant system affords the use of acidic and neutral conditions for effective removal of T_i and P_i, where this study is anticipated to catalyzed future research and expand the scope of wastewater treatment using non-conventional conditions.

The studies reported in chapter 7 is based on the third thesis objective (Theme 3) that accounts for hypotheses 1, 2, 3 and 6 introduced in Chapter 1. Herein, a copolymer flocculant was synthesized by grafting polyacrylamide (PAM) onto chitosan to obtain Chi-*g*-PAM. The product was then quaternized with CTA to prepare a series of cationic polymer flocculants (CTA-Chi-*g*-PAM) by varying the weight ratio of the CTA and Chi-*g*-PAM. The structure, physicochemical, thermal and electrical properties of the CTA-Chi-*g*-PAM flocculants were supported by various characterization methods and were also found to be water soluble with positive surface charge at both acidic and alkaline conditions. The morphological and electrical properties of the new flocculant materials showed that they had tunable flocculation characteristics. The effects of temperature, settling time, pH and flocculant dosage on the flocculation properties of the materials were tested on the removal of kaolinite colloidal dispersion (turbidity) and phosphate. The maximum removal of P_i and T_i occurred within 5 min of settling of the flocs that was independent of pH, where greater and equal removal efficiency was shown between pH 2 to 10.5. A minimal optimal flocculant dosage (0.2 mg/L) was noted for CTA-Chi-*g*-PAM-5 with 99.0 % (P_i) and 98.6 % (T_i) removal efficiency.

Kinetics of the T_i flocculation process shows that the rate constant for particle aggregation is greater at the optimal conditions, relative to the rate constant for particle breakage, suggesting that there was a greater tendency for floc formation. The P_i removal was well-described by the PSO kinetic model and Langmuir adsorption isotherm at equilibrium, indicating that the process is physisorption in nature. An equilibrium thermodynamic study at variable temperatures showed that the flocculation process is endothermic, spontaneous and entropy-driven, where the removal efficiency increased steadily with a temperature increase. Harder, denser and more compact flocs with greater floc size were formed at the respective optimal dosage of the flocculants, where F-F,

E-E and E-F microfloc associations were observed without any chemical interaction between the kaolinite and the flocculants. The CF process involved cooperative Columbic electrostatic charge neutralization between the cationic ammonium ion group of the flocculant and the anionic species (P_i and kaolinite), followed by polymer bridging due to adsorption of microflocs on the surface of the polymer and forming an ordered layered structure through a bridging mechanism. This study contributes to the field of sustainable environmental science in that minimal dosage (0.2 mg/L) of the flocculant without the addition of metal ion coagulants is required for efficient removal of P_i and T_i with a short settling time (5 min), and the process is independent of pH of the initial wastewater. The flocculant obtained herein in this report is anticipated to be efficient for the removal of other oxyanions species such as arsenate, nitrate, sulphate and organophosphate, which are on-going projects in our research group.

In summary, in this Ph.D. thesis research, the CF properties of novel native and modified biopolymers toward the removal of P_i and T_i was studied by characterizing the structural and flocculation properties. These results are strongly supported by the physicochemical properties related to flocculation (solubility, surface charge, removal efficiency and isotherm effects) and structural characterization. The results obtained herein provide the support that polysaccharide materials such as alginate, chitosan and oat hull biomass have enormous potential for effective removal of dissolved and colloidal species in wastewater when combined with an inorganic metal ion coagulant in a multicomponent system. However, the flocculation potential of these materials is limited by several factors, such as being ineffective at neutral and alkaline pH, requiring large coagulant and flocculant dosage that results in the production of a large amount of sludge which may cause secondary pollution effects. In addition, the resultant flocs formed are not stable upon exposure to shear stress. These limitations were addressed through the combined effects of synthetic modification. Greater flocculation properties resulted when chitosan was modified through etherification and grafting to increase its molecular weight and alter its surface charge at different pH conditions in a binary system. Additionally, grafting and quaternization of chitosan produced a single-component stable cationic flocculant with outstanding flocculation properties, which had greater P_i and T_i removal efficiency at all pH conditions, the formation of sizable and stable flocs which sedimented within 5 min of settling, and required minimal flocculant dosage without the addition of any inorganic coagulant.

The studies reported herein provide a greater understanding of the structure-property relationship for polymer-based flocculation phenomena. Studies that report the structure-property relationship of orthophosphate-biopolymer systems are limited in the literature due to the complexity associated with the coagulation-flocculation of dissolved species. The results reported in this thesis will add to the design of biopolymer-based flocculant materials with superior and tunable physicochemical properties, especially for applications involving CF processes such as liquid-liquid and solid-liquid chemical separations and environmental remediation of waterborne contaminants.

8.3 Future work

In this thesis, the flocculation properties of biopolymers and their modified derivatives were studied for the removal of dissolved species and suspended colloidal particles in a modeled wastewater system. The chemical modification of the biopolymers focused mainly on chitosan, and the results showed significant improvement of the flocculation conditions and the removal efficiency in a single-component system. However, alginate, in its natural form, showed poor flocculation performance in a single component-system but showed greater removal efficiency when combined with $FeCl_3$ and/or chitosan in binary and ternary systems. The poor performance of the alginate in removing anionic species in the wastewater is due to the negative surface charge because of the presence of carboxylate groups on its structure. Hence, it was hypothesized that the chemical modification of alginate with cationic groups to alter its surface charge can enhance its flocculation activity in a single-component system. Several modifications of alginate have focused on increasing its molecular weight and chelating properties for the removal of trace metal ions in wastewater, but none has been reported on the removal of anionic species.[8,9,33,34,34–38]

A commonly used cationic polymer material that is used to modify the surface charge of polyelectrolytes is poly(acrylamide-acryloxyethyl trimethyl ammonium chloride), denoted as P(AM-DAC). P(AM-DAC) is a water-soluble polymer that shows high flocculation efficiency in water treatment. Grafting of P(AM-DAC) onto the backbone of natural polymers produces cationic flocculants with tunable structure, physicochemical and flocculation properties. P(AM-DAC) have recently been grafted onto chitosan for kaolinite and algae wastewater treatment, and the flocculation efficiency and the floc properties were significantly improved when compared with pristine chitosan and commercially available flocculant materials.[39–42] Alginate has several

hydroxyl groups, similar to chitosan, making it susceptible for chemical modification through grafting. Therefore, the grafting of alginate with cationic P(AM-DAC) will lead to the formation of a cationic alginate-based flocculant system. The grafting of alginate using microwave radiation or ultrasonication can specifically excite only the polar bonds in the backbone, resulting in their cleavage and creation of free radical sites.[43] Microwave-based grafting can be enabled by combining microwave radiation and chemical-free radical initiation. This approach was shown to be effective in the modification of alginate, where polymethylmethacrylate (PMMA) and N,N′-dimethylacrylamide were separately grafted onto sodium alginate, combining microwave radiation and ceric ammonium nitrate or azobisizobutyronitrile (AIBN) initiators, respectively.[44,45]

The physicochemical, structural, morphological and electrical properties of the cationic alginate-based flocculant can be characterized using spectroscopic, thermal analyses, SEM imaging, zeta potential and point-of-zero-charge measurements. Flocculation properties can be tested for the removal of dissolved orthophosphate and dispersed kaolinite particles are compared with that of the native alginate biopolymer. In a recent study similar to the proposed research herein, Tian et al. introduced a cationic group on sodium alginate backbone to form an amphoteric alginate-based flocculant.[8,9] The amphoteric flocculant material was prepared by adding the cationic groups of $–N^{+}(CH_3)_3$ of 3-chloro-2-hydroxypropyltrimethyl ammonium chloride (CTA) onto sodium alginate under alkaline conditions. The prepared amphoteric flocculants displayed excellent flocculation efficiency for removing humic acid when combined with an inorganic coagulant. However, their flocculation properties were not studied for the removal of dissolved species such as phosphate. Additionally, the CF process required the use of inorganic coagulants, which could be problematic in wastewater remediation. Hence, by changing the cationic group and introducing polyacrylamide to the alginate structure and varying the concentration of the cationic group, a robust cationic flocculant can be prepared, which will be useful for removing phosphate and other anionic species in wastewater.

In addition to the chemical modification of alginate, other biopolymers and biomass materials such as starch, cellulose, guar gum, xanthan gum, flaxseed gum and oat hulls can be explored to evaluate their flocculation potentials. These materials are naturally abundant, and they have been proven to be relevant as functional materials for wastewater treatment. These materials may offer cost-effective and sustainable flocculant materials with suitable flocculation activity, especially toward the removal of dissolved species in wastewater. Several reports have been made on the use

of these materials for the flocculation of TSS, COD, turbidity in industrial, municipal and agricultural effluents in their native and chemically modified forms.[46–56] This shows that such materials have high flocculation potential; however, these systems are yet to be applied for the removal of dissolved species such as phosphate and sulphate. Hence, they can be used for the removal of phosphate in further studies. Synthetic modification of these materials will tune their hydration, hydrophilic/hydrophobic, morphological, textural and flocculation properties. Recently, the grafting of methacryloxyethyltrimethyl ammonium chloride (DMC) and acrylic acid (AA) onto microcrystalline cellulose (MCC) in NaOH/urea homogeneous system showed to be effective in the removal of wastewater turbidity.[46] The modification of cellulose increased its solubility in aqueous media by destroying its highly-ordered intermolecular hydrogen bond network and highly crystalline structure. Moreover, the modification of several other polysaccharides have shown that they could be effectively used for separation of liquid-solid and liquid-liquid wastewater effluents.[46–56] Some of these modification methods could be employed and modified when and where necessary to tune their functional properties for the simultaneous removal of dissolved and colloidal species in wastewater.

Properties of the flocs formed during the coagulation-flocculation process may provide useful information on the flocculation mechanism and its efficacy. In this research, the flocs obtained from the flocculation process between CTA-Chi-*g*-PAM and kaolinite colloidal particles can be characterized by several techniques. The nature of the floc relates to the components of the flocculant that contribute to their formation and the types of interactions (physical or chemical) that occur. Hence, further characterization of the flocs could lead to an improved understanding of the mechanism of the floc formation process. Additionally, the preparation of the flocs after the flocculation process for characterization is critical since it could alter their physical and chemical properties. In the thesis research reported herein, the flocs were obtained by oven drying at 45 ^{o}C after the CF process were completed prior to their characterization. Therefore, a comparative drying process such as freeze-drying can be used to evaluate differences in the physicochemical properties of the flocs. A recent study by Zhoa et al.[57] revealed that kaolinite flocs obtained from coagulation with $AlCl_3$ and PACl showed different physicochemical and structural properties when oven-dried and freeze-dried, where freeze-drying gave improved floc properties, such as greater density, lower pore volume and resistance to breakage upon exposure to shear stress. Hence, it is expected that freeze-drying of the bioflocculant-based flocs will improve the floc

properties because it may be a less destructive drying process over oven drying, since the latter involves more rapid removal of residual solvent than freeze drying. In addition to the techniques employed in this study for the characterisation of the flocs, other techniques that could provide useful information on the properties of the flocs are X-ray photoelectron spectrometry (XPS), powder X-ray diffraction (pXRD), dynamic light scattering (DLS) and X-ray absorption spectroscopy (XAS). The surface composition of flocs can be identified by XPS, while pXRD will provide information on the morphology of the flocs formed versus the original kaolinite structure. DLS, XAS may reveal the mode of binding within the flocs.

The study reported herein was achieved using model orthophosphate and kaolinite systems in Millipore water. This was carried out to minimize the contribution of secondary or competing ionic species on the flocculation process and focus mainly on the targeted contaminants since these competing ionic species are known to affect the uptake of contaminants, structure of the biopolymers, floc properties and the flocculation mechanism. Hence the flocculation performance can be further tested on the modeled wastewater system in the presence of other competing ionizable salts such as NaCl, Na_2SO_4, $NaNO_3$, etc. Also, the application of the flocculants in this work is not intended to be restricted to the model systems. Therefore, additional studies can be carried out with real environmental wastewater samples from different natural, industrial, agricultural and municipal sources. Such samples may contain other contaminants apart from phosphate and colloidal particles to affirm the *proof-of-concept* of the coagulation-flocculation treatment process using these biopolymer-based flocculants. In doing this, phosphate and turbidity removal efficiency, equilibrium adsorption and kinetics, as well as floc properties of the environmental and simulated wastewater samples, can be compared. These comparative investigations would provide an understanding of the role of the competitive and/or secondary ions, whether they favor or impede the flocculation process for removing phosphate and turbidity by these modified flocculants. The outcome of this study will contribute to the development of new biopolymer-based flocculants for selective and combined uptake of different species in liquid-liquid or liquid-solid contaminated wastewater systems.

8.4 References

(1) Lichtfouse, E.; Morin-Crini, N.; Fourmentin, M.; Zemmouri, H.; do Carmo Nascimento, I. O.; Queiroz, L. M.; Tadza, M. Y. M.; Picos-Corrales, L. A.; Pei, H.; Wilson, L. D.; Crini,

G. *Environ. Chem. Lett.* **2019**, *17* (4), 1603–1621.

(2) Yang, R.; Li, H.; Huang, M.; Yang, H.; Li, A. *Water Res.* **2016**, *95*, 59–89.

(3) George, A.; Sanjay, M. R.; Sriusk, R.; Parameswaranpillai, J.; Siengchin, S. *Int. J. Biol. Macromol.* **2020**, *154*, 329–338.

(4) Liu, Y.; Zheng, H.; Sun, Y.; Ren, J.; Zheng, X. *J. Clean. Prod.* **2020**, *249*, 119350.

(5) Rinaudo, M. *Prog. Polym. Sci.* **2006**, *31* (7), 603–632.

(6) Salehizadeh, H.; Yan, N.; Farnood, R. *Biotechnol. Adv.* **2018**, *36* (1), 92–119.

(7) Yang, J. S.; Xie, Y. J.; He, W. *Carbohydr. Polym.* **2011**, *84* (1), 33–39.

(8) Tian, Z.; Zhang, L.; Sang, X.; Shi, G.; Ni, C. *J. Phys. Chem. Solids* **2020**, *141*, 109408.

(9) Tian, Z.; Zhang, L.; Ni, C. *Environ. Sci. Pollut. Res.* **2019**, *26* (31), 32397–32406.

(10) Roussy, J.; Van Vooren, M.; Guibal, E. *J. Dispers. Sci. Technol.* **2005**, *25* (5), 663–677.

(11) Huang, C.; Chen, Y. *J. Chem. Technol. Biotechnol.* **1996**, *66* (3), 227–232.

(12) Kurita, K. *Mar. Biotechnol.* **2006**, *8*, 203–226.

(13) Mohammed, S. A. M.; Shanshool, H. A. *Iraqi J. Chem. Pet. Eng.* **2009**, *10* (2), 35–42.

(14) Banu, R. J.; Do, K. U.; Yeom, I. T. *Int. J. Environ. Sci. Technol.* **2007**, *5* (1), 93–98.

(15) Ferreira, S. L. C.; Bruns, R. E.; Ferreira, H. S.; Matos, G. D.; David, J. M.; Brandão, G. C.; da Silva, E. G. P.; Portugal, L. A.; dos Reis, P. S.; Souza, A. S.; dos Santos, W. N. L. *Anal. Chim. Acta* **2007**, *597* (2), 179–186.

(16) Aslan, N.; Cebeci, Y. *Fuel* **2007**, *86*, 90–97.

(17) Aslani, H.; Nabizadeh, R.; Nasseri, S.; Mesdaghinia, A.; Alimohammadi, M.; Mahvi, A. H.; Rastkari, N.; Nazmara, S. *Desalin. Water Treat.* **2016**, *3994*, 1–12.

(18) Bezerra, M. A.; Santelli, R. E.; Oliveira, E. P.; Villar, L. S.; Escaleira, L. A. *Talanta* **2008**, *76* (5), 965–977.

(19) Montgomery, D. C. *Design and analysis of experiments*, 9th ed.; Wiley: Hoboken, New Jersey, 2017.

(20) Yang, Z.; Shang, Y.; Huang, X.; Chen, Y.; Lu, Y.; Chen, A.; Jiang, Y.; Gu, W.; Qian, X.; Yang, H.; Cheng, R. *J. Environ. Sci. (China)* **2012**, *24* (8), 1378–1385.

(21) Yang, Z.; Shang, Y.; Lu, Y.; Chen, Y.; Huang, X.; Chen, A.; Jiang, Y.; Gu, W.; Qian, X.; Yang, H.; Cheng, R. *Chem. Eng. J.* **2011**, *172*, 287–295.

(22) Brostow, W.; Pal, S.; Singh, R. P. *Mater. Lett.* **2007**, *61*, 4381–4384.

(23) Kwok, K. C. M.; Koong, L. F.; Chen, G.; McKay, G. *J. Colloid Interface Sci.* **2014**, *416*, 1–10.

(24) Lin, Q.; Qian, S.; Li, C.; Pan, H.; Wu, Z.; Liu, G. *Carbohydr. Polym.* **2012**, *90* (1), 275–

283.

(25) Singh, R. P.; Pal, S.; Rana, V. K.; Ghorai, S. *Carbohydr. Polym.* **2013**, *91* (1), 294–299.

(26) Wang, M.; Feng, L.; Fan, X.; Li, D.; Qu, W.; Jiang, S.; Li, S. *Materials (Basel).* **2018**, *11* (10), 1–20.

(27) Song, H.; Wu, H.; Li, S. J.; Tian, H.; Li, Y. R.; Wang, J. G. *Molecules* **2018**, *23* (8).

(28) Lu, Y.; Shang, Y.; Huang, X.; Chen, A.; Yang, Z.; Jiang, Y.; Cai, J.; Gu, W.; Qian, X.; Yang, H.; Cheng, R. *Ind. Eng. Chem. Res.* **2011**, *50* (12), 7141–7149.

(29) Labidi, A.; Salaberria, A. M.; Fernandes, S. C. M.; Labidi, J.; Abderrabba, M. *Materials (Basel).* **2019**, *12* (3).

(30) Chintakunta, R.; Buaron, N.; Kahn, N.; Moriah, A.; Lifshiz, R.; Goldbart, R.; Traitel, T.; Tyler, B.; Brem, H.; Kost, J. *Carbohydr. Polym.* **2016**, *150*, 308–318.

(31) Momeni, M. M.; Kahforoushan, D.; Abbasi, F.; Ghanbarian, S. *J. Environ. Manage.* **2018**, *211*, 347–355.

(32) Yang, Z.; Degorce-Dumas, J. R.; Yang, H.; Guibal, E.; Li, A.; Cheng, R. *Environ. Sci. Technol.* **2014**, *48* (12), 6867–6873.

(33) Tripathy, T.; Kolya, H.; Jana, S. *J. Polym. Environ.* **2018**, *26* (3), 926–937.

(34) Tian, Z.; Zhang, L.; Shi, G.; Sang, X.; Ni, C. *J. Appl. Polym. Sci.* **2018**, *135* (31), 1–7.

(35) Da Feira, J. M. C.; Klein, J. M.; De Camargo Forte, M. M. *Polimeros* **2018**, *28* (2), 139–146.

(36) Tian, Z.; Zhang, L.; Ni, C. *Russ. J. Appl. Chem.* **2017**, *90* (4), 641–647.

(37) Yang, N.; Wang, R.; Rao, P.; Yan, L.; Zhang, W.; Wang, J.; Chai, F. *Crystals* **2019**, *9* (5).

(38) Benettayeb, A.; Guibal, E.; Morsli, A.; Kessas, R. *Chem. Eng. J.* **2017**, *316*, 704–714.

(39) Chen, L.; Sun, Y.; Sun, W.; Shah, K. J.; Xu, Y.; Zheng, H. *Sep. Purif. Technol.* **2019**, *210*, 10–19.

(40) Djibrine, B. Z.; Zheng, H.; Wang, M.; Liu, S.; Tang, X.; Khan, S.; Jimenéz, A. N.; Feng, L. *Int. J. Polym. Sci.* **2018**, *2018*.

(41) Wei, H.; Gao, B.; Ren, J.; Li, A.; Yang, H. *Water Res.* **2018**, *143* (2015), 608–631.

(42) Sun, Y.; Zhu, C.; Xu, Y.; Zheng, H.; Xiao, X.; Zhu, G.; Ren, M. **2016**, *44071*, 1–12.

(43) Vajihinejad, V.; Gumfekar, S. P.; Bazoubandi, B.; Rostami Najafabadi, Z.; Soares, J. B. P. *Macromol. Mater. Eng.* **2019**, *304* (2), 1–43.

(44) Rani, P.; Mishra, S.; Sen, G. *Carbohydr. Polym.* **2013**, *91* (2), 686–692.

(45) Akin, A.; Işiklan, N. *Int. J. Biol. Macromol.* **2016**, *82*, 530–540.

(46) Wang, Z.; Huang, W.; Yang, G.; Liu, Y.; Liu, S. *Carbohydr. Polym.* **2019**, *215*, 179–188.

(47) Hasan, A.; Fatehi, P. *Sci. Rep.* **2019**, *9* (1), 1–12.

(48) Zeng, D.; Hu, D.; Cheng, J. *J. Environ. Prot. (Irvine,. Calif).* **2011**, *02* (10), 1370–1374.

(49) Dwari, R. K.; Mishra, B. K. *Int. J. Min. Sci. Technol.* **2019**, *29* (5), 745–755.

(50) Ghorai, S.; Sarkar, A.; Panda, A. B.; Pal, S. *Ind. Eng. Chem. Res.* **2013**, *52* (29), 9731–9740.

(51) Guo, K.; Gao, B.; Wang, W.; Yue, Q.; Xu, X. *Chemosphere* **2019**, *215*, 214–226.

(52) Jain, V.; Tammishetti, V.; Joshi, K.; Kumar, D.; Pradip; Rai, B. *Miner. Eng.* **2017**, *109*, 144–152.

(53) Jiang, J.; Zhu, J.; Zhang, Q.; Zhan, X.; Chen, F. *Langmuir* **2019**, *35* (37), 11959–11967.

(54) Levy, N.; Garti, N.; Magdassi, S. *Colloids Surfaces A Physicochem. Eng. Asp.* **1995**, *97* (2), 91–99.

(55) Patra, A. S.; Patra, P.; Chowdhury, S.; Mukherjee, A. K.; Pal, S. *Colloids Surfaces A Physicochem. Eng. Asp.* **2020**, *586*, 1–6.

(56) Sand, A.; Kwark, Y. J. *Fibers Polym.* **2017**, *18* (4), 675–681.

(57) Zhao, H.; Hu, C.; Zhang, D.; Liu, H.; Qu, J. *PLoS One* **2016**, *11* (1), 1–17.

9 Appendices

9.1 Appendix A: Supplementary information

9.1.1 Appendix A (Chapter 2)

9.1.1.1 Chemical analysis of phosphorus

The need to reduce phosphorus levels in wastewater requires robust analytical methods with low detection limit, high sensitivity, precision and accuracy. The colorimetric technique is the standard method for determining phosphorus levels in water. Colorimetric method involves the formation of a colored phosphate-complex solution in which the intensity of the color is proportion to the concentration of the phosphate ion in the solution in accordance with the Beer-Lambert law is given by equation (A9.1)[1]

$$A = cl\varepsilon \tag{A9.1}$$

Here, A is the absorbance of the colored complex solution, measured at 420 nm, c (mol/L) is the molar concertation of the solution, l (cm) is the path length of the cell (sample holder) and ε is the molar absorptivity coefficient. This method has several advantages such as being easy to automate, less expensive, easy to operate, not requiring specialized equipment and able to measure the speciation of phosphate.[2] The use of colorimetry for determining phosphorus levels in aqueous medium dates back to early works of Riley and Murphy[1], John ad Bright[3] and Dickman and Bray[4]. In this method, orthophosphate reacts with ammonium molybdate in an acidic medium to form a heteropolyacid, 12-phosphomolybdic acid, according to the reaction equation (A9.2).[2]

$$PO_4^{3-} + 12MoO_4^{2-} + 27H^+ \rightarrow H_3PO_4(MoO_3)_{12} + 12H_2O \tag{A9.2}$$

$$H_3PO_4(MoO_3)_{12} \rightarrow H_7PO_4(MoO_3)_4(MoO_3)_8 \tag{A9.3}$$

The product is then reduced to phosphomolybdenum blue complex in which Mo(VI) is reduced to Mo(V) using ascorbic acid with potassium antimony tartrate as a catalyst, as shown in equation (A9.3). Also, the reaction of 12-phosphomolybdic acid with ammonium vanadate reagent produces a yellow complex (vanadomolybdophosphoric acid) solution which does not require any further reduction and the absorbance of the solution can be measured at 400 – 470 nm. The colorimetric method for measuring phosphorus levels is only appropriate with orthophosphate because the ammonium molybdate reagent reacts with the orthophosphate in an acidic environment.[2] Hence, to measure the phosphorus levels of other forms such as polyphosphate, condensed phosphate or

organic phosphate, requires conversion to orthophosphate prior to analysis. To achieve this, digestion processes were employed, where the phosphorus-based materials are heated at acidic conditions to convert them to orthophosphate for colorimetric analysis. Complete digestion leads to the determination of total phosphorus (TP), which includes all forms of phosphate. In this thesis, since the focus is on orthophoto removal from wastewater, no further digestion of the water samples was required.

Other techniques for analyzing phosphorus levels in an aqueous medium are inductively coupled plasma optical emission spectroscopy (ICP-OES)[5–11] and ion chromatography (IC)[6]. In ICP technique, molecules are broken down into individual elements after heating the molecules at high temperatures (~320 ^{o}C) and the elements are measured by spectroscopy.[12] This technique is more expensive relative to colorimetry. Additionally, it is unable to analyze phosphate speciation unless coupled with other speciation techniques. However, it is time efficient since it does not require separate digestion and detection methods. Detection limits for colorimetry and ICP-OES for TP determination are reported to be in the range of 5-10 µg/L[13] and 1-20 µg/L[14], respectively.

9.1.1.2 Jar test

The coagulation-flocculation process depends on several factors; hence, an appropriate technique is needed to optimize these factors. For instance, overdosing of coagulant or flocculant may produce fluffy or fragile flocs. Similarly, underdosing will lead to inadequate contaminant removal with small or no flocs and poor settling phenomena. Hence, in order to optimize the CF condition to obtain maximum removal efficiency, the jar test apparatus has been employed. The jar test is an effective method used to simulate coagulation, flocculation and sedimentation at a full-scale treatment plant.[15–17] It has been employed as a standard tool to optimize the factors that affect the CF process in the wastewater treatment industry.[18] The application of the jar test aids in the selection of coagulant and flocculant types and dosages, optimum pH, mixing speed (velocity gradient), mixing time and the sequence of the addition of the coagulant and flocculant.[19] The jar test is a bench-scale apparatus that consists of six identical plexiglass jars (which could be square or circular shape) and a mixing device with standard mixer paddles which are compute program-controlled, as shown in Figure A9.1. The six jars contain same volume and concentration of feeds and are charged simultaneously with different doses of a potential coagulant or flocculant and are stirred at the same speed simultaneously at the same time.[20] The use square jars have several

advantages over the circular counterparts:[18] (i) the square configuration reduces the rotation of the treated water during mixing, (ii) it reduces the change in the temperature of the water during the CF process due to the thick wall and low heat conductivity of the square plexiglass, (iii) water samples are more quickly and easily sampled from the sampling tap, and (iv) square jars provide the greatest velocity gradient at a given impeller speed.

During CF process using the jar test apparatus, three stages are required in the process, which are coagulation, flocculation and sedimentation, and they correspond to the basic processes of dispersing the coagulant or flocculant onto particle surface, gently sweeping the colloidal particles together to form large flocs, and allowing the flocs to settle, respectively.[20] In the coagulation, stage an appropriate coagulant is added to the wastewater sample in the jars and they are stirred rapidly at 100 to 700 rpm for 0.5 - 5 min. This stage represents the destabilization of the colloidal particles through EDL depression to form microflocs. In the flocculation stage, a polymer flocculant or coagulant aid is added to the wastewater followed by slow mixing at 10 - 50 rpm for 10 - 60 min. This process aids the aggregation of the microflocs to form larger flocs (macroflocs). The size of the flocs formed at this stage mostly depends on the type of polymer flocculant (cationic, anionic or non-ionic), dosage, velocity gradient, and mixing time. The last stage is the sedimentation process, where the macroflocs are allowed to settle over time. Large flocs have greater settling properties than smaller flocs. The three stages occur sequentially and are based on the large-scale plants of rapid mixing, coagulation-flocculation and settling basins. An aliquot of the wastewater sample is withdrawn at the end of the settling process for further analytical analysis. Despite the widespread application of the jar test, it is time consuming to obtain optimum conditions for such a multi-parameter process. Hence, in this thesis research, a statistical tool (Box-Behnken design of experiment and response surface methodology) was employed to efficiently optimize the CF conditions with a reduced number of experiments.

Figure A9.1: Convention jar test apparatus for the coagulation-flocculation process. Images of wastewater (a) before and (b) after the CF process using biopolymer-based flocculant.

Table A9.1: Comparison of the removal of phosphate (P_i) and turbidity (T_i) in water and wastewater using different coagulant-flocculant systems

Water source	Conta-minant	Coagulant/ flocculant	Optimum dosage (mg/L)	Optimum pH	Efficiency (%)	Reference
Conventional inorganic coagulants						
SW	P_i	Alum and $CaCl_2$	80 and 60	6	85	Mohammed & Shanshool[21]
MW	P_i	PACl	6.35	N/A	94.6 & 96.6	Chen & Luan[22]
AW	P_i	Alum & $FeCl_3$	90	7.14	89 & 93	Ebeling et al.[23]
IW	P_i	Alum	10	5.7-5.9	98	Banu et al.[24]
IW	P_i	$FeCl_2$	25	8	98.5	An et al.[25]
IW	P_i	Alum & $FeCl_3$	13	N/A	80.4	Kim et al.[26]
IW	T_i	PACl	40	7	93.13	Kadhum et al.[27]
IW	T_i	$AlCl_3$, PACl & $CuSO_4$	8.0, 5.0 & 5.0	5, 4 & 6	92, 74 & 78	Kumar et al., 2011
IW	TDS & Ti	PACl	25	7	74.09 & 93.47	Migo et al.[28]
IW	SS	$FeSO_4$, $FeCl_3$, & Alum	500, 500, 250	9	24,28 & 70,	Gupta & Gupta[29]
IW	TSS	Alum, $FeCl_3$ & $FeSO_4$	2	9.5	90, 88 & 28	Ghaly et al.[30]
IW	TSS	PACl	60	4	80	Smita et al.[31]
IW	TDS & Ti	$FeSO_4$ & Alum	200 & 100	4.5	99 70	Tassoula et at.[32]
MW	Pi	Alum & $FeCl_3$	5 & 7.5	6.5 and 7.0	50 & 90	Ahmad et al.[33]
AW	TSS & P_i	Alum	50	7.4	99, 98	Lofrano et al.[34]

+Table A9.1 continued

Water source	Chemical species	Coagulant/ flocculant	Optimum dosage (mg/L)	Optimum pH	Efficiency (%)	Reference
Conventional inorganic coagulants						
IW	P_i	Chitosan and Alginate	10, 20	N/A	80	Latifian et al.[35]
SW	P_i	Chitosan*	N/A	7.5−7.9	60	Fierro et al.[36]
SW	P_i	Chitosan*	N/A	4	30	Filipkowska et al.[37]
MW	P_i	Chitosan, Starch & Guar gum*	60, 24, 24	9.5	89, 86, 82	Dunets & Zheng[38]
SW	P_i	Chitosan + PACl	67.9; 20.05	7.5	99.4	Li et al.[39]
SW	P_i	zirconiumion modified chitosan*	50	4	60.6	Liu and Zhang [8]
AW	P_i	HMW Chitosan*	12	7.2	99.1	Chung et al.[40]
MW	P_i	Chitosan*	10	7	98	Turunen et al.[41]
IW	T_i	$FeCl_3$ + Chitosan	80; 50	6	75	Rodrigues et al.[42]
IW	T_i	PACl + Chitosan	0.3–0.4; 7.0	7.7	85	Renault et al.[43]
IW	T_i	$AlCl_3$ + Chitosan	13.5; 5.0	7	80	Hu et al.[44] 2013
SW	T_i	Chitosan	2	7.5	95	Divakaran et al.[45]
SW	P_i	Fly ash and bottom ash*	3.4 & 9.1	8	97	Barbosa et al.[46]
SW	P_i	Fly ash and bottom ash*	34.5 & 46.6	8	90	Barbosa et al.[46]
SW	P_i	$La(OH)_3$ modified pine needles	0.7	3	65	Wang et al.[47]
SW	P_i	Wheat straw biochars*	6	< 7.0	88	Li et al.[48]
SW	P_i	Sugarcane bagasse*	16	N/A	11	Hena et al.[49]

+Table A9.1 continued

Water source	Chemical species	Coagulant / flocculant	Optimum dosage (mg/L)	Optimum pH	Efficiency (%)	Reference
Conventional inorganic coagulants						
SW	T_i	$Al_2(SO_4)_3$ + Alginate	4.5; 1.0	6.1-8.0	73.8	Wu et al.[50]
SW	Congo red dye	$CaCl_2$ + Alginate	6000; 60	4	96	Vijayaraghavan et al.[51]
SW	Sulphur black dye	$CaCl_2$ + Alginate	6001; 30	4	98.2	Vijayaraghavan et al.[52]
SW	T_i	$FeCl_3$ + Alginate	12.0; 2.0	4	55.7	Zhao et al.[53]

Note:

SW: Synthetic wastewater; IW: Industrial wastewater; AW: Agricultural wastewater; MW: Municipal wastewater

* Phosphate removal was achieved by adsorption process.

9.1.2 Appendix A (Chapter 3)

Table A9.2: Removal of P_i in wastewater using optimized coagulation-flocculation condition at different pH and levels of phosphate. Alum dosage was kept at 30 mg/L. Initial P_i concentration is 10.0 mg/L

Initial pH of P_i soln.	**Final pH of P_i soln.**	**Initial [P_i] (mg/L)**	**Final [P_i] (mg/L)**	**% P_i removal**
		Initial [P_i] = 6.5 mg/L		
2.45	2.48	5.7	1.43	75.0
4.33	4.32	6.28	1.15	81.7
5.53	5.51	7.5	1.06	85.8
7.03	7.01	6.58	0.82	87.5
8.55	8.52	5.6	0.89	84.2
10.3	10	7.15	1.58	77.8
		Initial [P_i]= 10.6 mg/L		
2.18	2.21	10.6	1.79	83.2
3.23	3.22	10.5	1.19	88.7
4	4.05	10.7	0.56	94.8
6.15	6.2	10.6	0.2	98.2
7.02	7.05	10.6	0.19	98.2
8.32	8.29	10.6	0.67	93.7
9.63	9.59	10.6	1.18	88.8
		Initial [P_i] = 16.5 mg/L		
2.55	2.58	16	2.163	86.5
4.36	4.37	17.1	0.406	97.6
5.57	5.51	16.9	0.174	99
7.01	7.01	16.3	0.264	98.4
8.53	8.52	16.7	1.517	90.9
10.22	10.23	16.3	1.653	89.88
		Initial [P_i] = 20.4 mg/L		
2.45	2.48	22.4	1.46	93.5
4.33	4.32	14.2	0.37	97.4
5.53	5.51	21.4	0.41	98.1
7.03	7.01	20.9	0.55	97.3
8.55	8.52	21.7	1.02	95.3
10.3	10	21.5	0.12	99.5

Table A9.2 Continued

Initial pH of P_i soln.	Final pH of PO_4 soln.	Initial [P_i] (mg/L)	Final [P_i] (mg/L)	% $P_{i\ removal}$
		Initial [P_i] = 36.1 mg/L		
2.26	2.32	35.2	3.82	89.1
4.43	4.42	35.1	2.04	94.2
5.66	5.64	35.5	1.46	95.9
7.02	7.04	35.5	2.35	93.4
8.74	8.78	35.6	2.04	94.3
10.1	10.2	39.88	1.17	97.1
		Initial [Pi] = 41.2 mg/L		
2.34	2.33	40.7	3.81	90.6
4.33	4.37	41	2.06	95
5.53	5.51	41.1	0.9	97.8
7.04	7.06	41.2	0.93	97.8
8.54	8.56	42	2.32	94.5
10.3	10.3	40.8	2.75	93.3
		Initial [Pi] = 56.4 mg/L		
2.22	2.28	53.8	3.82	92.9
4.43	4.46	57.1	1.59	97.2
5.62	5.64	56.4	1.55	97.3
7.02	7.05	57	1.13	98
8.45	8.43	57.2	2.04	96.4
10.2	10.1	56.7	2.23	96.1

Table A9.3: Removal of P_i in wastewater using optimized condition at varying chitosan and alginate dosage. Alum dosage was kept at 30 mg/L. Initial P_i concentration is 10.0 mg/L

Flocculant dosage/ mg/L	Initial pH	Final pH	Initial [P_i] / mg/L	Final [P_i] / mg/L	P_i removal
			Chitosan		
0.00	5.45	5.85	22.2	11.2	49.8
2.00	5.55	5.89	22.0	7.85	64.3
4.99	5.54	5.79	21.5	7.27	66.2
7.99	5.65	5.79	21.7	5.16	76.2
10.0	5.58	5.84	21.2	3.45	83.7
19.9	5.56	5.83	21.9	4.10	81.3
29.8	5.54	5.58	20.8	3.44	83.5
39.6	5.61	5.87	21.6	2.52	88.3
49.4	5.62	5.87	22.3	2.86	87.2
59.2	5.59	5.85	21.8	3.13	85.6
68.9	5.62	5.89	22.7	3.26	85.6
78.6	5.64	5.87	23.3	3.60	84.5
			Alginate		
0.00	5.45	5.85	23.5	11.8	49.9
1.95	5.55	5.89	22.9	7.13	68.8
5.00	5.54	5.79	22.9	6.75	70.5
7.48	5.65	5.79	22.0	6.19	71.9
9.96	5.58	5.84	22.1	5.01	77.4
19.8	5.56	5.83	22.1	4.33	80.4
29.7	5.54	5.58	22.9	4.73	79.4
39.4	5.61	5.87	21.7	4.82	77.8
49.0	5.62	5.87	21.8	4.66	78.6
58.6	5.59	5.85	22.1	4.35	80.3
68.1	5.62	5.89	21.9	4.94	77.4
77.6	5.64	5.87	22.1	6.27	71.7

Table A9.4: Removal of P_i (%) of using optimized conditions of alum-refined oat hull binary system. Alum dosage was kept at 30 mg/L

Initial pH	Final pH	Oat Hull Concentration / mg/L	Initial [P_i] / mg/L	Final [P_i] / mg/L	P_i removal
		Refined oat hull; initial [Pi] = 25.0 mg/L			
5.35	5.38	0	26.7	17.1	34.0
5.32	5.35	930.9	26.8	4.78	82.2
5.33	5.32	1097	25.6	3.82	85.1
5.35	5.33	1258	26.0	2.25	91.3
5.36	5.38	1412	24.4	0.87	96.4
5.32	5.37	1562	23.8	1.77	92.5
5.34	5.33	1707	24.3	1.04	95.7
5.31	5.37	1847	26.5	0.08	99.7
5.36	5.36	2021	24.7	0.04	99.8
5.35	5.36	2155	24.2	0.41	98.3
5.41	5.38	2284	24.3	0.48	98.0
5.42	5.39	2379	23.3	0.27	98.8
5.43	5.35	2500	24.0	0.65	97.3
		Refined oat hull; initial [Pi] = 11.5 mg/L			
6.87	6.86	0	11.8	5.02	57.4
6.85	6.86	931	11.5	2.52	78.2
6.88	6.86	1097	11.4	2.53	77.9
6.86	6.86	1258	10.9	2.3	78.9
6.88	6.86	1412	10.9	1.45	86.6
6.85	6.86	1562	11.6	1.19	89.7
6.86	6.86	1707	12.2	1.16	90.5
6.87	6.86	1847	12.3	1.09	91.2
6.86	6.86	2021	12.5	1.62	87.1
6.84	6.86	2155	11.8	1.62	86.4
6.83	6.86	2284	12.2	1.75	85.7
6.82	6.86	2379	12.7	1.91	84.9

Table A9.5: Removal of P_i (%) of using optimized conditions of alum-unrefined oat hull binary system. Alum dosage was kept at 30 mg/L

Initial pH	Final pH	Oat Hull Concentration / mg/L	Initial [P_i] / mg/L	Final [P_i] / mg/L	P_i removed
		Unrefined oat hull; initial [P_i] = 25.5 mg/L			
5.01	5.03	0	26.7	17.1	36.0
5.03	5.06	959.6	26.6	8.36	68.6
5.03	5.03	1131	26.2	6.54	75.0
5.05	5.60	1296	26.3	3.45	86.9
5.11	5.01	1456	26.9	3.21	88.0
5.10	5.05	1610	26.4	1.78	93.2
5.11	5.06	1759	25.7	1.64	93.6
5.06	5.07	1903	26.0	3.5	86.6
5.08	50.4	2096	25.7	2.08	91.9
5.12	5.08	2234	27.0	1.98	92.7
5.03	5.09	2369	27.4	2.32	91.5
5.04	5.04	2388	27.2	2.43	91.1
5.09	5.08	2509	26.7	2.41	91.0
		Unrefined oat hull; initial [P_i] = 11.5 mg/L			
6.58	6.55	**0**	11.8	5.02	57.4
6.52	6.57	921.6	12.4	3.86	68.8
6.25	6.58	1086	11.8	3.68	68.8
6.48	6.52	1245	12.0	3.49	71.0
6.44	6.49	1398	11.7	2.18	81.5
6.45	6.54	1546	11.9	1.83	84.7
6.43	6.48	1672	11.9	2.53	78.7
6.47	6.51	1809	12.1	2.09	82.8
6.29	6.50	1942	11.8	1.85	84.4
6.54	6.51	2128	11.8	1.54	86.9
6.43	6.52	2256	11.9	1.28	89.2
6.55	6.51	2379	12.3	1.44	88.3

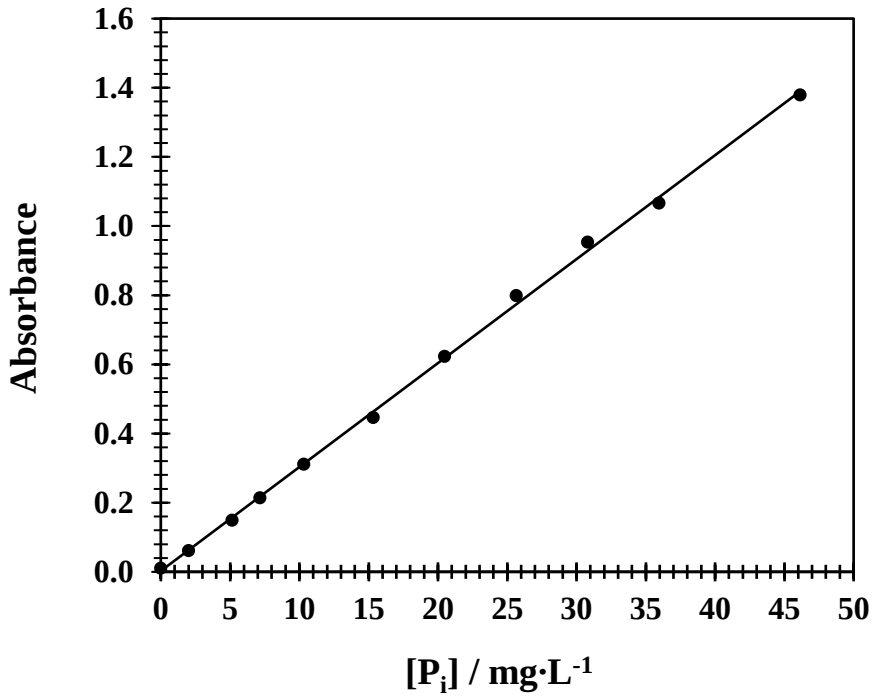

Figure A9.2: Calibration curve of phosphate at 420 nm using vanadate-molybdate colorimetry. $R^2 = 0.998$.

9.1.3 Appendix A (Chapter 4)

Table A9.6: The Box-Behnken experimental design matrix of four variables along with the related experimental and calculated response

Test	pH (*x*)	Alginate dose (*z*) (mg/L)	Settling time (*m*) (min)	$FeCl_3$ dose (*n*) (mg/L)	$P_{i,removal}$ Expt. (%)	$P_{i,removal}$ Calc. (%)
1	2	0.50	35	12.5	87.6 ± 0.2	88.3
2	10	0.50	35	12.5	46.9 ± 0.2	46.1
3	2	15.0	35	12.5	79.2 ± 0.5	79.9
4	10	15.0	35	12.5	58.5 ± 1.0	57.8
5	6	7.75	10	10.0	85.3 ± 0.5	85.5
6	6	7.75	60	10.0	85.0 ± 0.3	85.1
7	6	7.75	10	15.0	82.1 ± 1.0	81.9
8	6	7.75	60	15.0	87.7 ± 1.0	87.4
9	2	7.75	35	10.0	82.6 ± 0.4	80.9
10	10	7.75	35	10.0	55.5 ± 0.9	55.2
11	2	7.75	35	15.0	87.5 ± 0.9	86.8
12	10	7.75	35	15.0	47.2 ± 0.8	48.0
13	6	0.50	10	12.5	84.7 ± 0.5	82.6
14	6	15.0	10	12.5	85.0 ± 0.9	85.4
15	6	0.50	60	12.5	87.6 ± 1.2	86.3
16	6	15.0	60	12.5	85.7 ± 0.8	86.8
17	2	7.75	10	12.5	79.8 ± 0.8	80.5
18	10	7.75	10	12.5	48.0 ± 0.9	48.8
19	2	7.75	60	12.5	83.2 ± 0.5	83.5
20	10	7.75	60	12.5	50.6 ± 0.9	50.8
21	6	0.50	35	10.0	85.1 ± 0.6	87.2
22	6	15.0	35	10.0	88.1 ± 0.8	87.6
23	6	0.50	35	15.0	83.8 ± 0.3	85.3
24	6	15.0	35	15.0	89.4 ± 0.7	88.3
25	6	7.75	35	12.5	98.4 ± 0.9	97.7
26	6	7.75	35	12.5	97.1 ± 0.7	97.7
27	6	7.75	35	12.5	97.6 ± 0.7	97.7

Table A9.7: Comparison of the removal of phosphate in water and wastewater using different coagulant-flocculant systems

Water Source	Flocculant	Optimum dosage (mg/L)	Optimum pH	Efficiency (%)	Reference
Synthetic wastewater	Fe(III)-alginate	10	4.7	99.7±0.7	This thesis**
Synthetic wastewater	Alginate	25	5.7−7.0	38	This thesis*
Synthetic wastewater	Alum/alginate	30/59	5.7−7.0	80	This thesis*
Synthetic wastewater	Ferric chloride	80	7.2	82	Yang et al.[54]
Struvite	Chitosan and Alginate	10, 20	N/A	80	Latifian et al.[35]
Synthetic wastewater	Chitosan	N/A	7.5−7.9	60	Fierro et al.[36]
Synthetic wastewater	Chitosan	N/A	4	30	Filipkowska et al.[37]
Synthetic wastewater	Polydiallyldimethyl-ammonium chloride	0.5	8	59	Chen & Luan[22]
Municipal wastewater	Chitosan Starch Guar gum	60 24 24	9.5	89 86 82	Dunets & Zheng[38]
Synthetic wastewater	Alum and $CaCl_2$	80, 60	6	85	Mohammed & Shanshool[21]
Aquaculture effluent discharge	Alum and $FeCl_3$	90	7.1	89, 93	Ebeling et al.[23]
Secondary effluent wastewater	Alum	10	5.7−5.9	92	Banu et al.[24]
Activated sludge effluent discharge	$FeCl_2$	13	N/A	80	An et al.[25]

Note: This thesis* and This thesis** are results from Chapters 3 and 4, respectively.

9.1.4 Appendix A (Chapter 6)

9.1.4.1 Box-Behnken experimental design

The traditional method of coagulation-flocculation involves changing one factor at a time and requires many experiments, which may be time-consuming, often leading to low optimization efficiency. To address this problem, the design of experiment (DOE) was used to study the effect of variables and their responses using a minimum number of experiments. RSM is a collection of statistical and mathematical methods that are useful for developing, improving, and optimizing processes.[55–57] The selection of an adequate experimental design is a key consideration for experimental optimization. The BBD method was employed to obtain the optimum T_i and $P_{i,}$ removal. The BBD is an independent, rotatable quadratic design with no embedded factorial or fractional factorial points where the variable combinations are at the mid-points of the edges of the variable space and at the center.[58] The BBD requires fewer treatment combinations than the central composite design, and is less expensive to perform, especially in cases with three or four factors. BBD allows efficient estimation of the first- and second-order coefficients and does not have axial points. Thus, it is certain that all design points fall within a safe operating zone. The BBD approach ensures that not all factors are set at their high levels at the same time. This affords identification of significant effects of interaction for batch studies.[58–61] Preliminary experiments from Chapter 5 indicate that important variables affecting T_i and $P_{i,}$ removal include ferric chloride dosage, CMC-CTA dosage, pH and settling time. The variables were evaluated to optimize T_i and $P_{i,}$ removal. $FeCl_3$ dosage varied between 5 mg/L and 15 mg/L, CMC-CTA dosage (1 mg/L to 5 mg/L), pH (2 to 12), and settling time (10 to 60 min). In Table 6.1, the experimental design had four variables (*A*, *B. C* and *D*), each at three levels, coded as -1, 0 and +1, for low, middle and high values, respectively. Twenty-nine experiments were carried out according to the statistical matrices developed by the RSM, in order to account for variability of the independent variables on T_i and $P_{i,}$ removal. The experimental data was fit using a non-linear regression method with a second order polynomial to identify significant coefficient terms. The application of RSM provides an empirical relationship between the response function and the independent variables. The quadratic response model is based on all linear terms, square terms, and linear interaction terms, according to equation (A9.4).[62]

$$Y = b_\circ + \sum b_i x_i + \sum b_{ii} x_{ii}^{\,2} + \sum b_{ij} x_{ij} \qquad \text{(A9.4)}$$

Here, Y is the predicted response (T_i or P_i, removal efficiency) b_o is the model constant, b_i is the linear coefficient, b_{ii} is the quadratic effect of the input factor x_{ii}, b_{ij} is the linear interaction effect between the input factors x_i and x_j.

The response function coefficients were determined by regression using the experimental data and the Quantum LX Sigmazone DOE regression program. The response functions for turbidity and phosphate removal (%) were approximated by the standard quadratic polynomial equation in equation (4), which describes the regression model of the system, including the interaction terms.[62]

$$Y = b_0 + b_1A + b_2B + b_3C + b_4D + b_{11}A^2 + b_{12}AB + b_{13}AC + b_{14}AD + b_{22}B^2 + b_{23}BC + b_{23}BD + b_{33}C^2 + b_{34}CD + b_{33}D^2 \quad \text{(A9.5)}$$

Here, Y is the predicted response, T_i or P_i removal (%); A, B, C and D are the coded levels of the independent variables: CMC-CTA dose (mg/L), $FeCl_3$ (mg/L) dose, pH and settling time (min), respectively. The regression coefficient, b_0 denotes the intercept term; b_1, b_2, b_3 and b_4 represent the linear coefficients; b_{12}, b_{13}, b_{14}, b_{23}, b_{24}, b_{34} represent the interaction coefficients and b_{11}, b_{22}, b_{33} and b_{44} denote the quadratic coefficients. Analysis of variance (ANOVA) was employed to perform diagnostic tests on the adequacy of the proposed model. The ANOVA test estimates the suitability of the response functions and the significance of the effects for the independent variables.

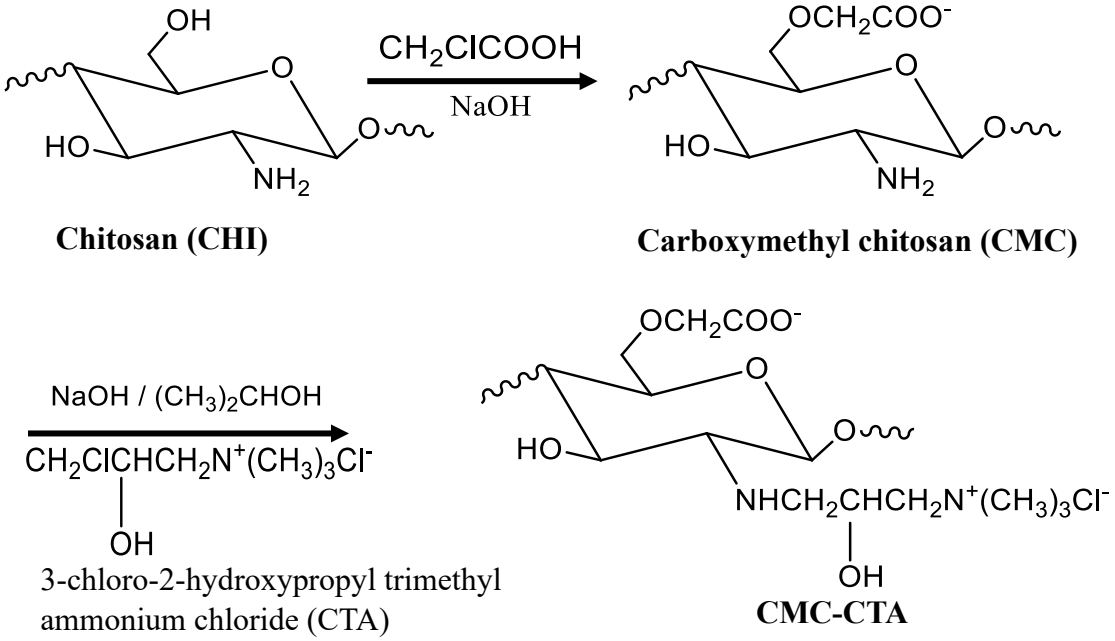

Scheme A9.1: Synthetic route of carboxymethyl chitosan (CMC) and 3-chloro-2-hydroxypropyl trimethylammonium chloride grafted onto CMC (CTA-CMC).

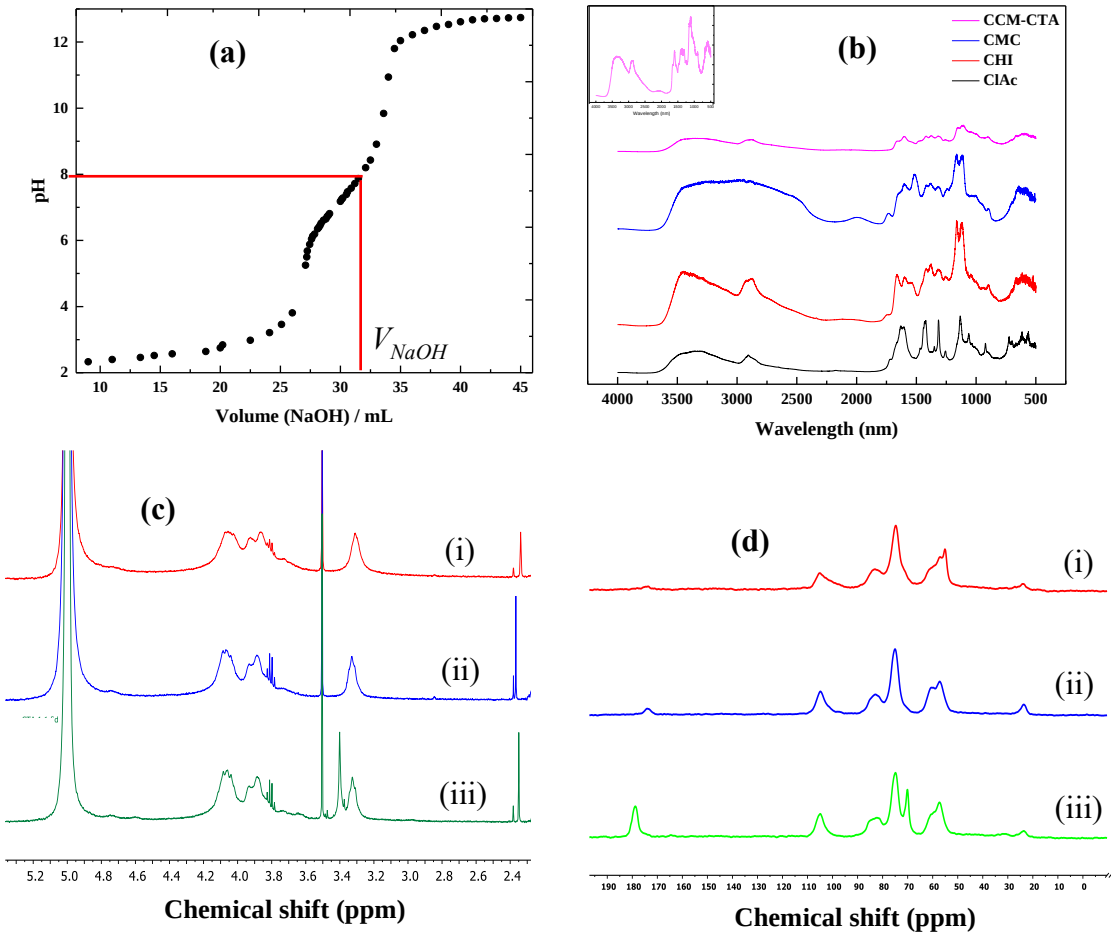

Figure A9.3: (a) Titration curve for estimation of the DS for CMC, where V_{NaOH} denotes the titrant volume of NaOH at the equivalent point (b) FT-IR spectra of chloroacetic acid (ClAc), Chitosan (CHI), CMC and CMC-CTA. The insert is an IR spectrum of CMC-CTA. (c) ^{1}H-NMR spectra of chitosan (i), carboxymethyl chitosan, CMC (ii) and CMC-CTA (iii). (d) ^{13}C-NMR of chitosan (i), carboxymethyl chitosan, CMC (ii) and CMC-CTA (iii).

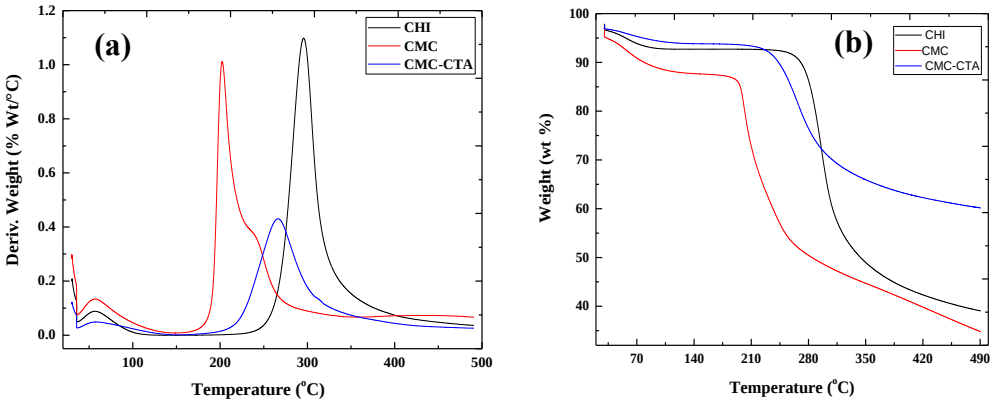

Figure A9.4: TGA profile of chitosan, carboxymethyl chitosan (CMC) and CMC-CTA: (a) First derivative of weight loss with temperature against temperature, and (b) weight loss with temperature. (c) PZC of CMC-CTA. The insert illustrates the PZC determination for CMC.

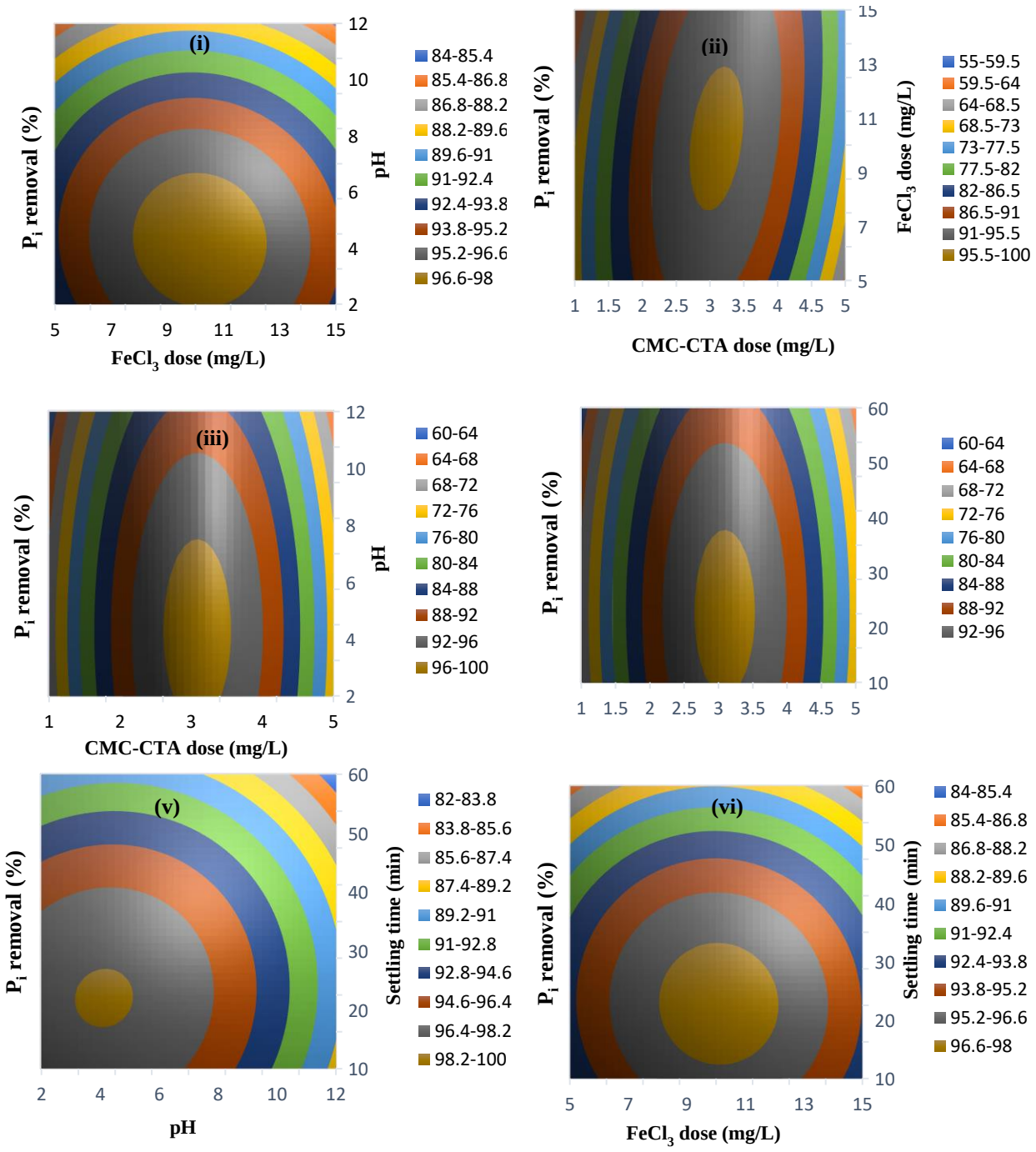

Figure A9.5: Two-dimensional Box-Behnken contour plots of phosphate removal efficiency as a function of (i) pH and $FeCl_3$; (ii) CMC-CTA dose and $FeCl_3$ dose; (iii) CMC-CTA dose and pH; (iv) CMC-CTA dose and setting time; (v) pH and settling time; and (vi) $FeCl_3$ dosage and settling time.

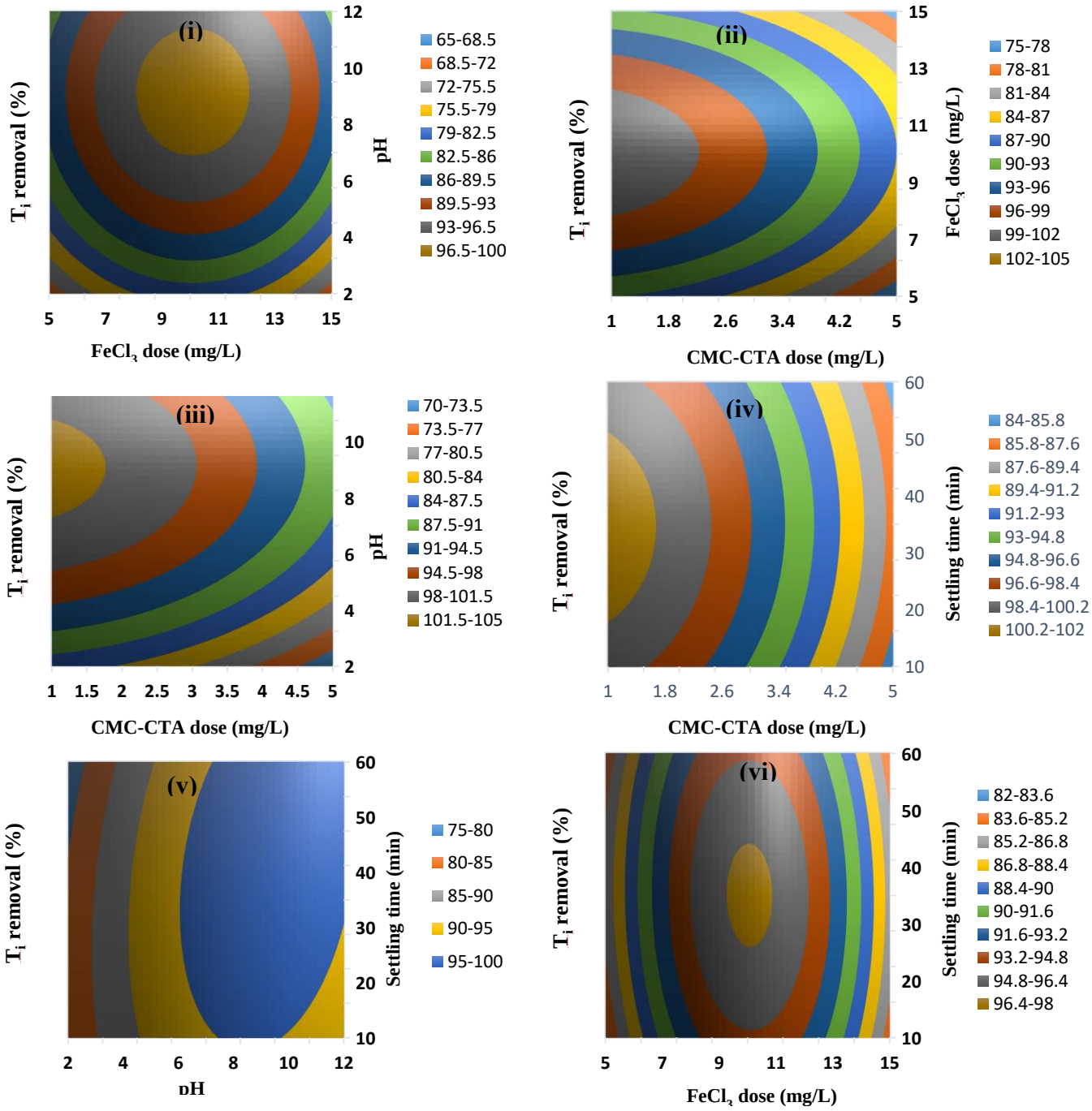

Figure A9.6: Two-dimensional Box-Behnken contour plots of T_i removal efficiency as a function of (i) pH and $FeCl_3$; (ii) CMC-CTA dose and $FeCl_3$ dose; (iii) CMC-CTA dose and pH; (iv CMC-CTA dose and setting time.

Table A9.8: Comparison of the removal of phosphate in water and wastewater using different coagulant-flocculant systems.

Water Source	Flocculant	Optimum Dosage (mg/L)	Optimum pH	Efficiency (%)	Reference
Synthetic wastewater	Fe(III)-CMC-CTA	10, 3.0	6.5	96.4	This work
Synthetic wastewater	Chitosan	20	6.2 - 7.0	78 ± 0.1	This thesis*
Synthetic wastewater	Chitosan + Alum	49	5.8 - 7.0	88 ± 0.8	This thesis*
Struvite	Chitosan and Alginate	10, 20	N/A	80	Latifian et al.[35]
Synthetic wastewater	Chitosan	N/A	7.5 - 7.9	60	Fierro et al.[36]
Synthetic wastewater	Chitosan	N/A	4	30	Filipkowska et al.[37]
Municipal wastewater	Chitosan	60	9.5	89	Dunets and Zheng [38]
Synthetic wastewater	Chitosan + PAC	67.9; 20.05	7.5	99.4	Li et al.[39]
Synthetic wastewater	zirconiumion modified chitosan	50	4	60.6	Liu and Zhang [8]
Agricultural wastewater	HMW Chitosan	12	7.2	99.1	Chung et al.[40]
Municipal wastewater	Chitosan	10	7	98	Turunen et al.[41]
Synthetic wastewater	Chitosan	7	4	59.5	This thesis**
Synthetic wastewater	CMC-CTA	5	6.5	70.5	This thesis**
Synthetic wastewater	CMC	8	6.5	29.8	This thesis**

+Table A9.9 Continued

Water Source	Flocculant	Optimum dosage (mg/L)	Optimum pH	Efficiency (%)	Reference
Synthetic wastewater	$FeCl_3$ + chitosan	7.5 + 7	6.5	88.8	This thesis**
Synthetic wastewater	$FeCl_3$ + CMC	7.5 + 9	6.5	68.8	This thesis**
Synthetic wastewater	$CaCl_2$ + CS-*g*-PAD	6	10	98.8	Sun et al.[63]
Secondary effluent	Chitosan	5.5	5	80	Rojsitthisak et al.[64]
Activated sludge effluent discharge	Ferrous chloride	13	N/A	80	An et al.[25]
Synthetic wastewater	Ferric chloride	80	7.2	82	Yang et al.[65]
Secondary effluent wastewater	Alum	10	5.7−5.9	92	Banu et al.[24]
Synthetic wastewater	Polydiallyldimethyl-ammonium chloride	0.5	8	59	Chen and Luan[22]

Note: This thesis* and This thesis** are results from Chapters 3 and 4, respectively.

9.1.5 Appendix A (Chapter 7)

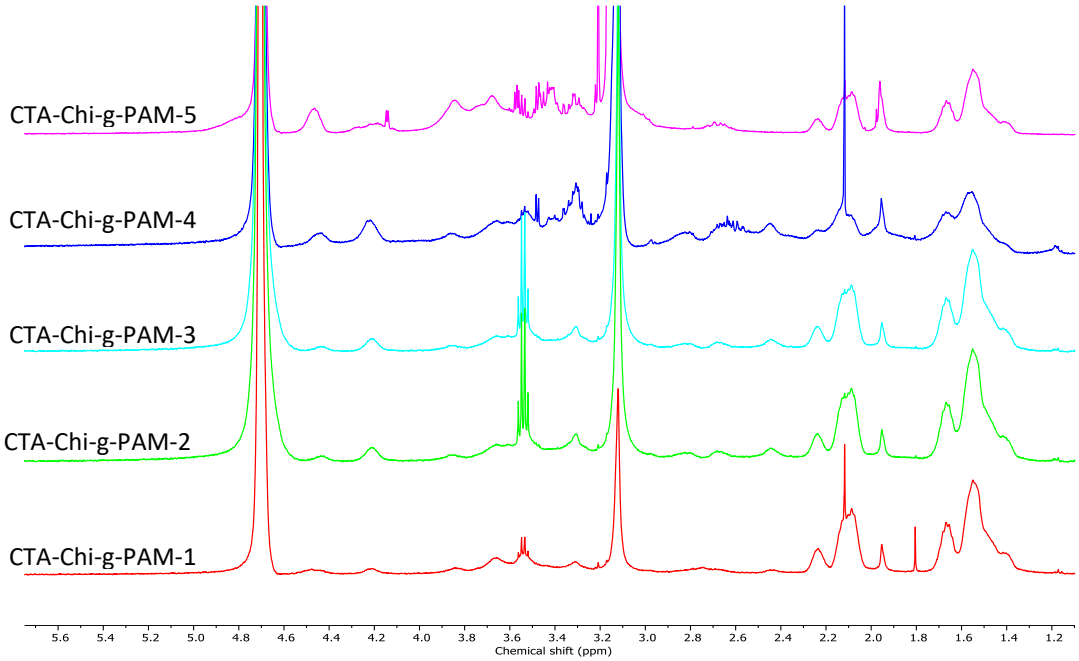

Figure A9.7: ^{1}H-NMR of cationic flocculants with varying degrees of CTA DS.

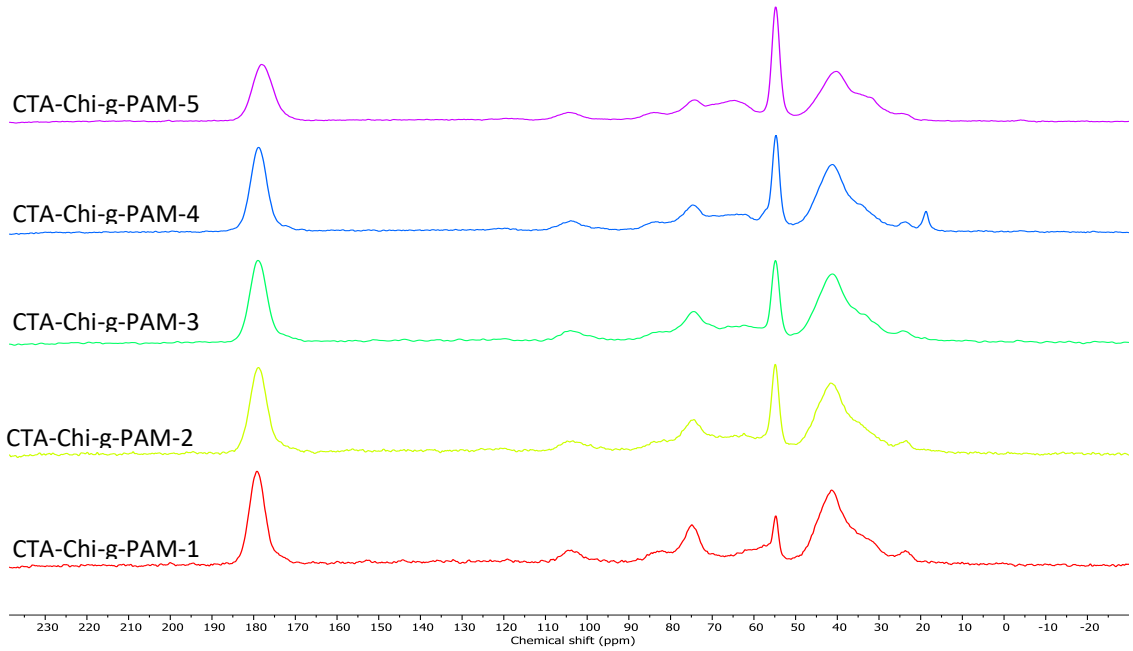

Figure A9.8: ^{13}C-NMR of cationic flocculants with varying degrees of CTA DS.

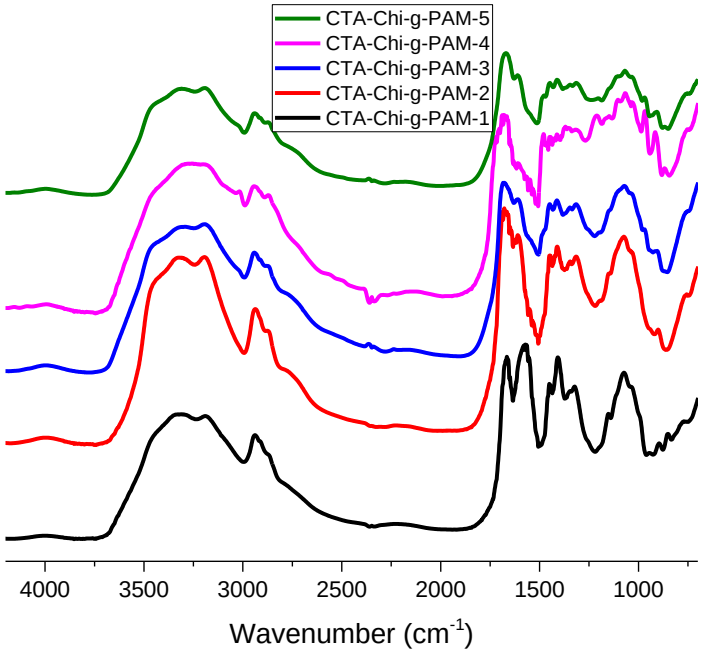

Figure A9.9: FT-IR of cationic flocculants with varying degrees of CTA DS.

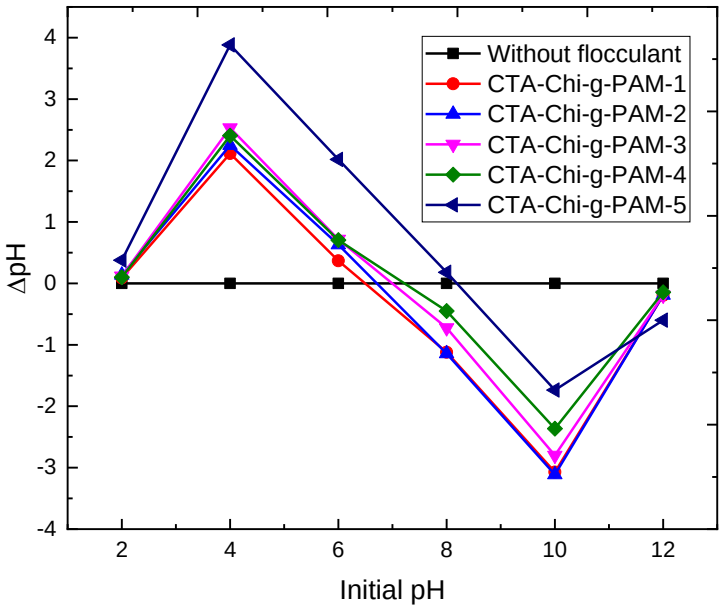

Figure A9.10: Point-of-zero-charge (pH_{pzc}) of cationic flocculants with varying degrees of CTA DS.

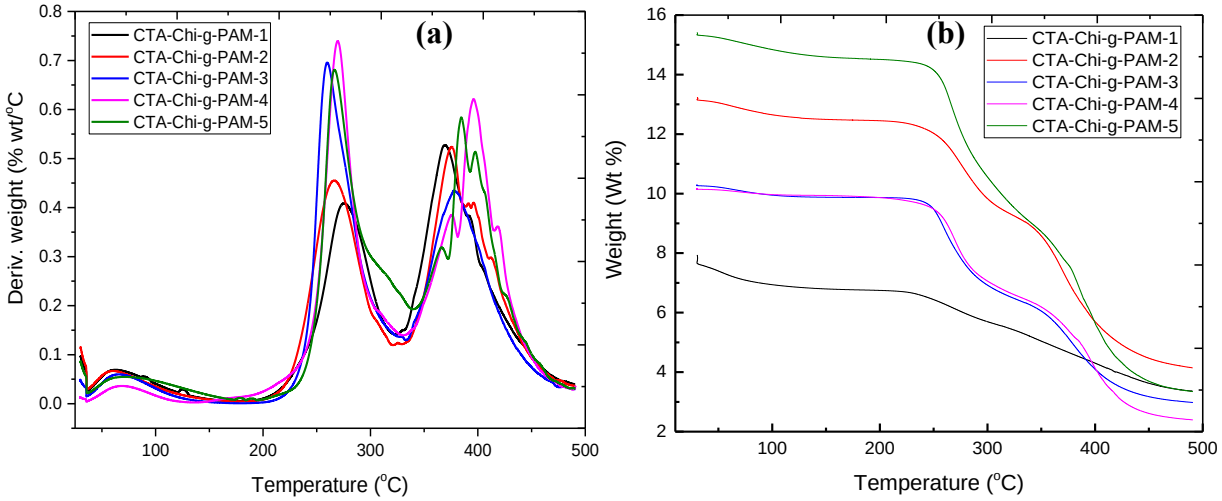

Figure A9.11: First derivative weight loss (a) and weight loss (b) of cationic flocculants with varying degrees of CTA DS as a function of temperature.

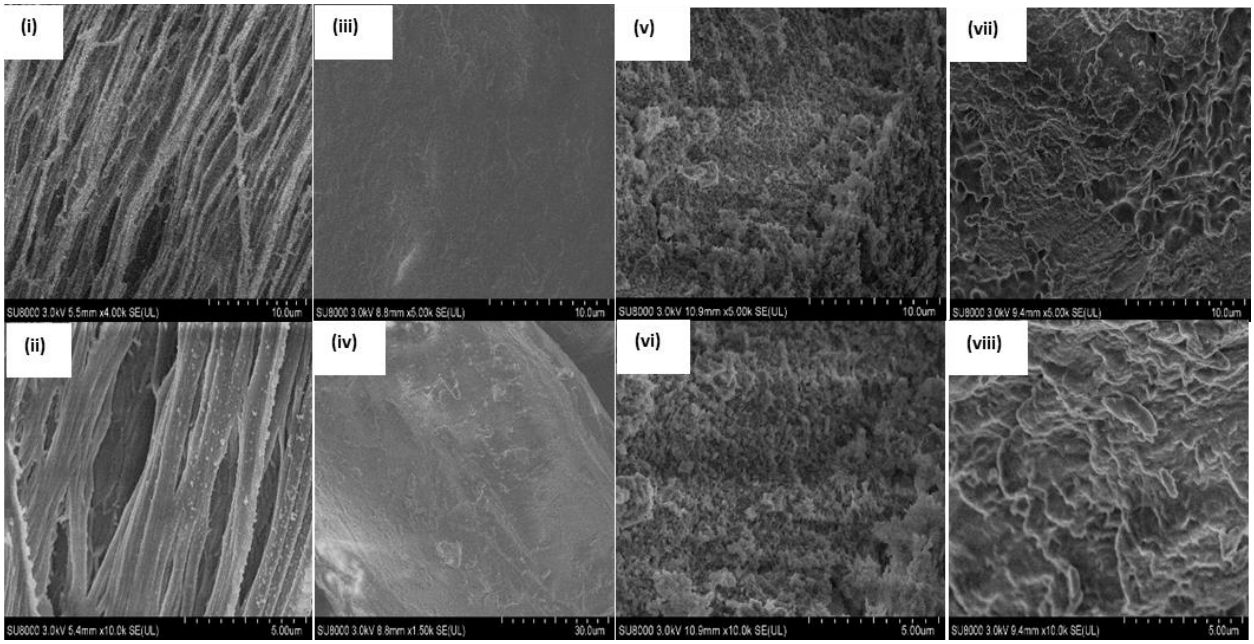

Figure A9.12: SEM micrographs of acrylamide (i & ii), chitosan (iii & iv), Chi-*g*-PAM (v & vi) and CTA-Chi-*g*-PAM (vii & viii). Magnification: top = 5K and bottom = 10K.

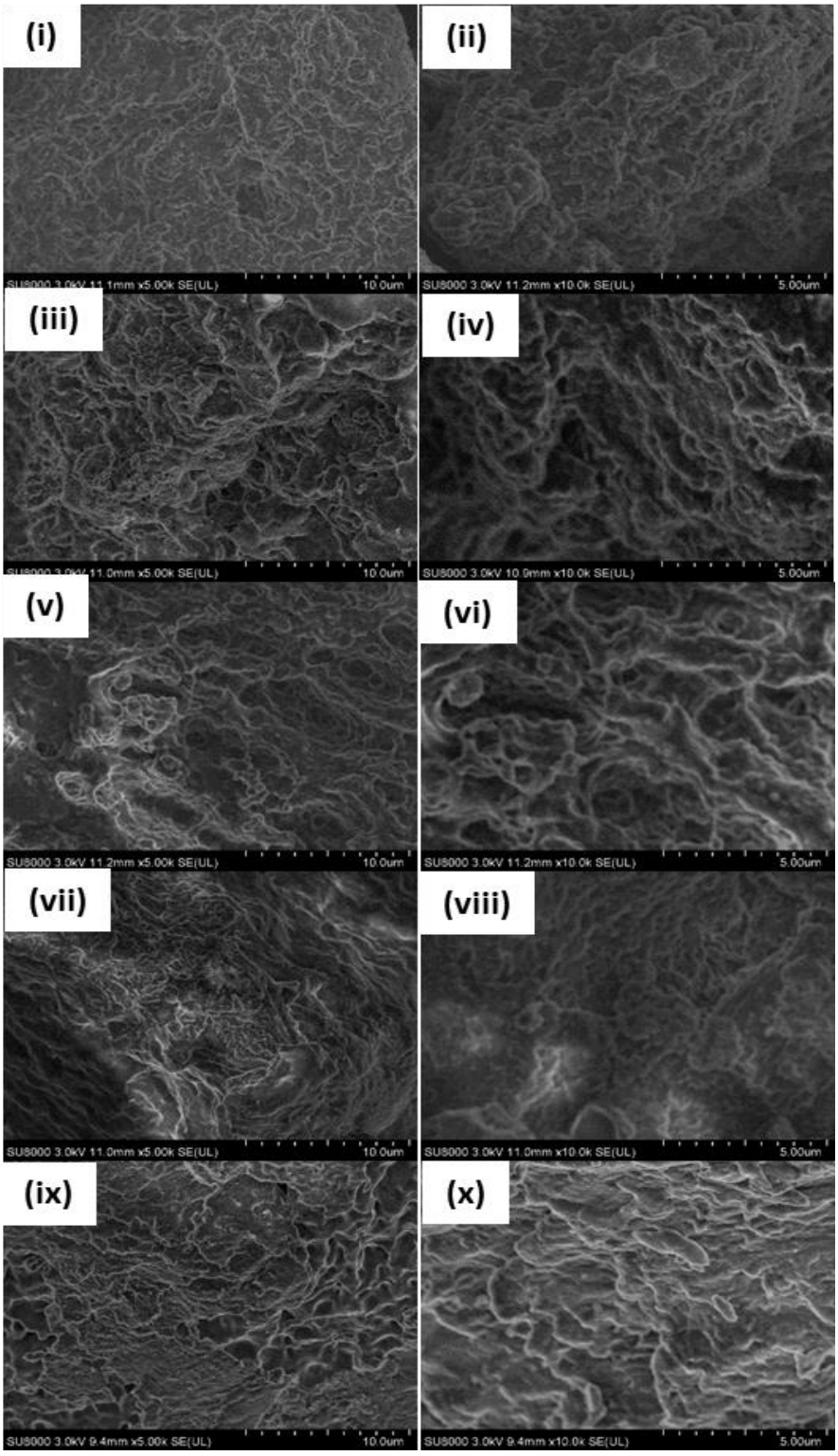

Figure A9.13: SEM micrographs of cationic flocculants: (i & ii) CTA-Chi-*g*-PAM-1; (iii & iv) CTA-Chi-*g*-PAM-2 (v & vi) CTA-Chi-*g*-PAM-3; (vii & viii) CTA-Chi-*g*-PAM-4;. (ix & x) CTA-Chi-*g*-PAM-5. Magnification: left = 5K and right = 10K**.**

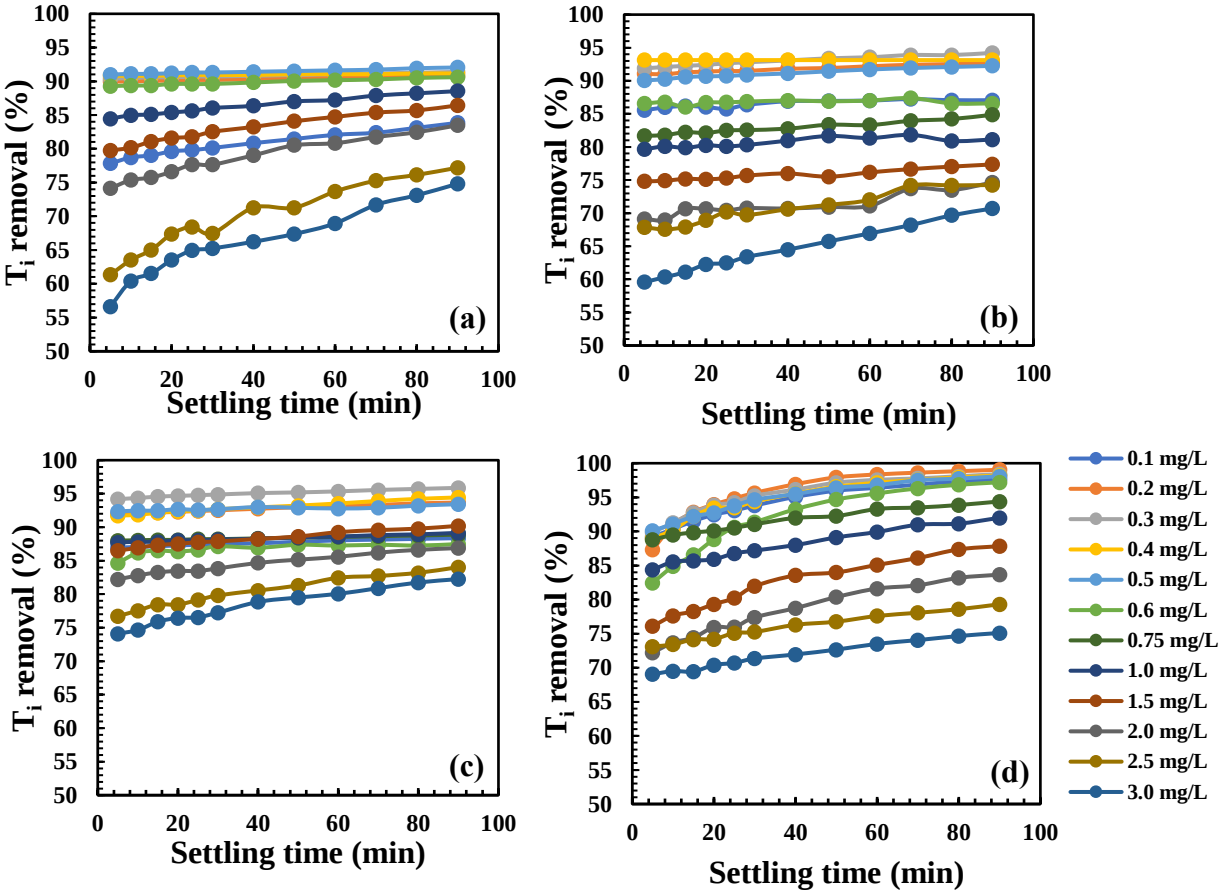

Figure A9.14: Effects of settling time on the removal turbidity with (a) CTA-Chi-*g*-PAM-1 (b) CTA-Chi-*g*-PAM-2, (c) CTA-Chi-*g*-PAM-3 and (d) CTA-Chi-*g*-PAM-5.

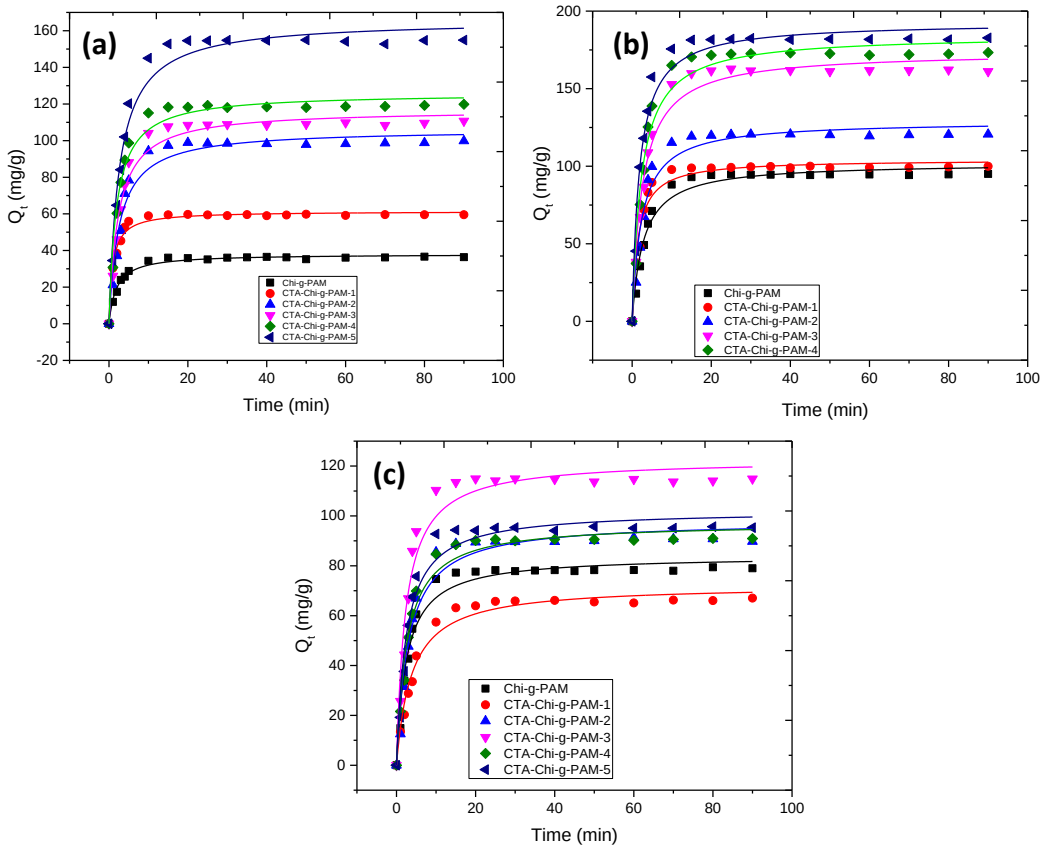

Figure A9.15: Kinetic curves of flocculation processes for phosphate removal with respect to PSO model at (a) below the optimum dosage, (b) at the optimum dosage and (c) beyond the optimum dosage at pH 6.5.

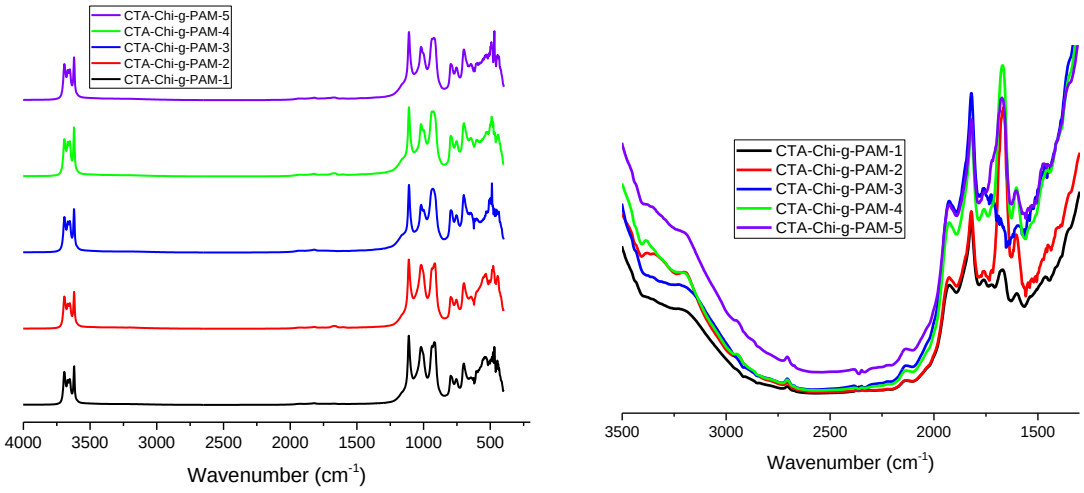

Figure A9.16: FT-IR spectra of kaolinite-cationic flocculants flocs with varying degrees of CTA DS.

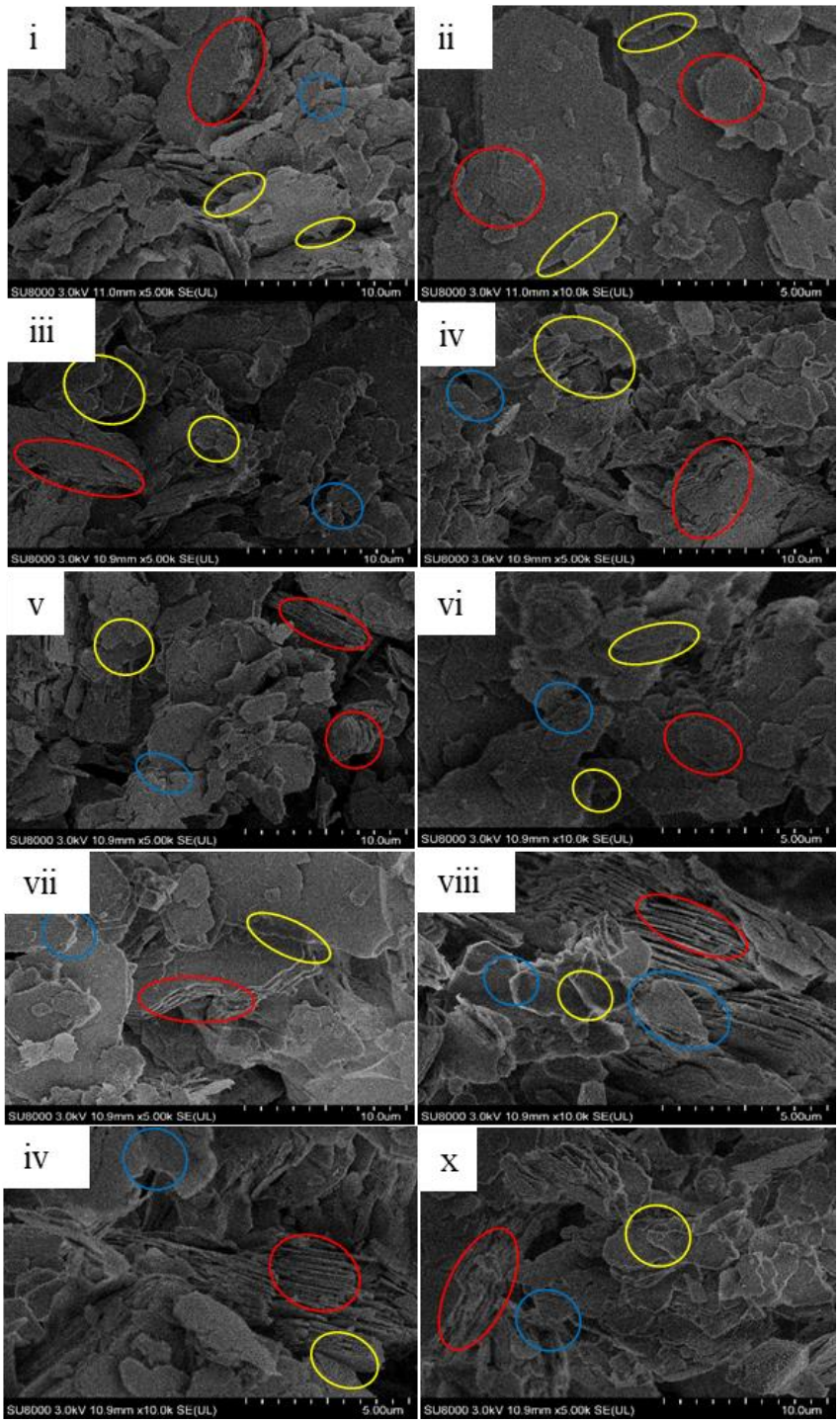

Figure A9.17: SEM images of kaolinite flocs obtained with (i & ii) CTA-Chi-*g*-PAM-1, (iii & iv) CTA-Chi-*g*-PAM-2, (v & vi) CTA-Chi-*g*-PAM-3, (viii & viii) CTA-Chi-*g*-PAM-4 and (ix & x) CTA-Chi-*g*-PAM-5 (ii) CTA-Chi-*g*-PAM-1 and (iv) CTA-Chi-*g*-PAM-5. Here, red, yellow and blue circles indicate F-F, E-F and E-E association of the microflocs, respectively. Magnification: left = 5K and right = 10K**.**

A7.3 References

(1) Murphy, J.; Riley, J. P. *Anal. Chim. Acta* **1962**, *27*, 31–36.

(2) Smith, D. S. *Phosphorus Analysis in Wastewater : Best Practices*; The Water Environment Research Foundation: Alexandria, VA, 2015.

(3) John, B.; Bright, H. A. *Natl. Bur. Stand.* **1941**, *26* (1938), 405–413.

(4) Dickman, S. R.; Bray, R. H. *Ind. Eng. Chem.* **1940**, *12* (11), 665–668.

(5) Sun, Y.; Zhou, S.; Sun, W.; Zhu, S.; Zheng, H. *Sep. Purif. Technol.* **2020**, *241*, 116737.

(6) Cieślik, B.; Konieczka, P. *J. Clean. Prod.* **2017**, *142*, 1728–1740.

(7) Huang, Y.; Yang, J. K.; Keller, A. A. *ACS Sustain. Chem. Eng.* **2014**, *2* (5), 1128–1138.

(8) Liu, X.; Zhang, L. *Powder Technol.* **2015**, *277*, 112–119.

(9) Chakraborty, T.; Gabriel, M.; Amiri, A. S.; Santoro, D.; Walton, J.; Smith, S.; Ray, M. B.; Nakhla, G. **2017**, 12302–12309.

(10) Chakraborty, T.; Balusani, D.; Smith, S.; Santoro, D.; Walton, J.; Nakhla, G.; Ray, M. B. *Sep. Purif. Technol.* **2020**, *231*, 115894.

(11) Gray, H. E.; Powell, T.; Choi, S.; Smith, D. S.; Parker, W. J. *Water Res.* **2020**, 115968.

(12) Ateeq, F. Chemical Removal of Total Phosphorus from Wastewater to Low Levels and Its Analysis, MSc. Thesis, Laurier University, 2016.

(13) Jarvie, H. P.; Withers, P. J. A.; Neal, C. *Hydrol. Earth Syst. Sci.* **2002**, *6* (1), 113–132.

(14) Maryutina, T. A.; Muntau, H. *Pure Appl. Chem.* **1999**, *71* (11), 2161–2176.

(15) Siah, C.; Robinson, J.; Fong, M. *Process Saf. Environ. Prot.* **2014**, *92* (6), 489–508.

(16) Szpak, J. P.; Woods, D. R.; Bouchard, K. *Water Qual. Res. J. Canada* **1996**, *31* (1), 51–64.

(17) Farrow, J. B.; Swift, J. D. *Int. J. Miner. Process.* **1996**, *46*, 263–275.

(18) Ebeling, J. M.; Sibrell, P. L.; Ogden, S. R. *Agric. Eng.* **2003**, *29*, 23–42.

(19) Amirtharajah, A. A.; Mills, K. M.; Journal, S.; Water, A.; Association, W.; Amirtharajah, A.; Mills, K. M. *J. Am. Water Work. Assoc.* **1982**, *74* (4), 210–216.

(20) Tripathy, T.; De, B. R. *J. Phys. Sci.* **2006**, *10*, 93–127.

(21) Mohammed, S. A. M.; Shanshool, H. A. *Iraqi J. Chem. Pet. Eng.* **2009**, *10* (2), 35–42.

(22) Chen, J.; Luan, Z. *Fresenius Environ. Bull.* **2010**, *19* (10), 2200–2204.

(23) Ebeling, J. M.; Sibrell, P. L.; Ogden, S. R.; Summerfelt, S. T. *Aquac. Eng.* **2003**, *29* (1–2), 23–42.

(24) Banu, R. J.; Do, K. U.; Yeom, I. T. *Int. J. Environ. Sci. Technol.* **2007**, *5* (1), 93–98.

(25) An, J.-S.; Back, Y.-J.; Kim, K.-C.; Cha, R.; Jeong, T.-Y.; Chung, H.-K. *Environ. Technol.* **2014**, *35* (13–16), 1668–1675.

(26) Kim, W. K.; Sung, Y. K.; Yoo, H. S.; Kim, J. T. *J. Ind. Eng. Chem.* **2015**, *21*, 269–277.

(27) Shabeeb, K. M.; Abdulbari, H. A.; Resources, N.; Abbas, A. A.; Education, F. T. *Al-Qadisiya J. Eng. Sci.* **2011**, *4* (4), 546–555.

(28) Migo, V. P.; Matsumura, M.; Del Rosario, E. J.; Kataoka, H. *J. Ferment. Bioeng.* **1993**, *75* (6), 438–442.

(29) Gupta, S. K.; Gupta, S. K.; Hung, Y. *Waste Treat. Process Ind.* **2006**, 167–233.

(30) Ghaly, A.; Snow, A.; Faber, B. *Can. Biosyst. Eng.* **2006**, *48*, 13–22.

(31) Borchate, S. S.; Kulkarni, G. S.; Kore, S. V; Kore, V. S. *Int. J. Eng. Sci. Technol.* **2012**, *4* (05), 1944–1948.

(32) Tassoula, E.; Diamadopoulos, E.; Vlachos, C. *Glob. NEST J.* **2007**, *9* (2), 166–173.

(33) Ahmad, A. L.; Sumathi, S.; Hameed, B. H. *Chem. Eng. J.* **2006**, *118* (1–2), 99–105.

(34) Lofrano, G.; Belgiorno, V.; Gallo, M.; Raimo, A. *Glob. NEST J.* **2006**, *8* (2), 151–158.

(35) Latifian, M.; Liu, J.; Mattiasson, B. *Environ. Technol.* **2014**, *35* (18), 2289–2295.

(36) Fierro, S.; del Pilar Sánchez-Saavedra, M.; Copalcúa, C. *Bioresour. Technol.* **2008**, *99* (5), 1274–1279.

(37) Filipkowska, U.; Jóźwiak, T.; Szymczyk, P. *Prog. Chem. Appl. Chitin its Deriv.* **2014**, *19* (1), 5–14.

(38) Dunets, C. S.; Zheng, Y. *Hortscience* **2015**, *50* (6), 921–926.

(39) Li, Y.; Li, L.; Yasser Farouk, R.; Wang, Y. *Int. J. Environ. Res. Public Health* **2019**, *16* (6), 996.

(40) Chung, Y. C.; Li, Y. H.; Chen, C. C. *J. Environ. Sci. Heal. - Part A Toxic/Hazardous Subst. Environ. Eng.* **2005**, *40* (9), 1775–1790.

(41) Turunen, J.; Karppinen, A.; Ihme, R. *SN Appl. Sci.* **2019**, *1* (3), 1–9.

(42) Rodrigues, A. C.; Boroski, M.; Shimada, N. S.; Garcia, J. C.; Nozaki, J.; Hioka, N. *J. Photochem. Photobiol. A Chem.* **2008**, *194* (1), 1–10.

(43) Renault, F.; Sancey, B.; Charles, J.; Morin-Crini, N.; Badot, P. M.; Winterton, P.; Crini, G. *Chem. Eng. J.* **2009**, *155* (3), 775–783.

(44) Hu, C. Y.; Lo, S. L.; Chang, C. L.; Chen, F. L.; Wu, Y. De; Ma, J. L. *Sep. Purif. Technol.* **2013**, *104*, 322–326.

(45) Divakaran, R.; Sivasankara Pillai, V. N. *Water Res.* **2001**, *35* (16), 3904–3908.

(46) Barbosa, R.; Lapa, N.; Lopes, H.; Morujo, A.; Mendes, B. *Water Sci. Technol.* **2013**, *68* (9),

2019–2027.

(47) Wang, X.; Liu, Z.; Liu, J.; Huo, M.; Huo, H. *PLoS One* **2015**, *10* (12), 1–16.

(48) Li, J.; Lv, G.; Bai, W.; Liu, Q.; Zhang, Y.; Song, J. *Desalin. Water Treat.* **2016**, *57*, 4681–4693.

(49) Hena, S.; Atikah, S.; Ahmad, H. *Int. J. Eng. Sci.* **2015**, *4* (1), 51–62.

(50) Wu, C.; Wang, Y.; Gao, B.; Zhao, Y.; Yue, Q. *Sep. Purif. Technol.* **2012**, *95*, 180–187.

(51) Vijayaraghavan, G.; Shanthakumar, S. *Desalin. Water Treat.* **2015**, *3994*, 1–9.

(52) Vijayaraghavan, G.; Shanthakumar, S. *Environ. Prog. Sustain. Energy* **2015**, *34* (5), 1427–1434.

(53) Zhao, Y. X.; Wang, Y.; Gao, B. Y.; Shon, H. K.; Kim, J.-H.; Yue, Q. Y. *Desalination* **2012**, *299*, 79–88.

(54) Yang, K.; Li, Z.; Zhang, H.; Qian, J.; Chen, G. *Environ. Technol.* **2010**, *31* (6), 601–609.

(55) Aslan, N.; Cebeci, Y. *Fuel* **2007**, *86*, 90–97.

(56) Aslani, H.; Nabizadeh, R.; Nasseri, S.; Mesdaghinia, A.; Alimohammadi, M.; Mahvi, A. H.; Rastkari, N.; Nazmara, S. *Desalin. Water Treat.* **2016**, *3994*, 1–12.

(57) Bezerra, M. A.; Santelli, R. E.; Oliveira, E. P.; Villar, L. S.; Escaleira, L. A. *Talanta* **2008**, *76* (5), 965–977.

(58) Usharani, K.; Lakshmanaperumalsamy, P. *J. Microbiol. Biotechnol. Food Sci.* **2016**, *05* (06), 534–547.

(59) Usharani, K.; Muthukumar, M. *Int. J. Environ. Sci. Technol.* **2013**, *10* (3), 591–606.

(60) Rakić, T.; Kasagić-Vujanović, I.; Jovanović, M.; Jančić-Stojanović, B.; Ivanović, D. *Anal. Lett.* **2014**, *47* (8), 1334–1347.

(61) Zolgharnein, J.; Shahmoradi, A.; Ghasemi, J. B. *J. Chemom.* **2013**, *27*, 12–20.

(62) Jain, M.; Garg, V. K.; Kadirvelu, K. *Bioresour. Technol.* **2011**, *102* (2), 600–605.

(63) Sun, Y.; Ren, M.; Zhu, C.; Xu, Y.; Zheng, H.; Xiao, X.; Wu, H.; Xia, T.; You, Z. *Ind. Eng. Chem. Res.* **2016**, *55* (38), 10025–10035.

(64) Rojsitthisak, P.; Burut-Archanai, S.; Pothipongsa, A.; Powtongsook, S. *Water Environ. J.* **2017**, *31* (4), 598–602.

(65) Yang, K.; Li, Z.; Zhang, H.; Qian, J.; Chen, G. *Environ. Technol.* **2010**, *31* (6), 601–609.

(66) Song, H.; Wu, H.; Li, S. J.; Tian, H.; Li, Y. R.; Wang, J. G. *Molecules* **2018**, *23* (8).

(67) Singh, J.; Mishra, N. S.; Uma; Banerjee, S.; Sharma, Y. C. *BioResources* **2011**, *6* (3), 2732–2743.

(68) Chang, C.; Stone, A. K.; Green, R.; Nickerson, M. T. *Food Chem.* **2019**, *277*, 84–95.

(69) Smoluchowski, M. von. *Z. Phys. Chem.* **1917**, *92*, 129–168.

9.2 Appendix B: Copyright Permissions

Biopolymer Flocculants and Oat Hull Biomass To Aid the Removal of Orthophosphate in Wastewater Treatment

Author:
Henry K. Agbovi, Lee D. Wilson, Lope G. Tabil
Publication:
Industrial & Engineering Chemistry Research
Publisher:
American Chemical Society
Date:
Jan 1, 2017

PERMISSION/LICENSE IS GRANTED FOR YOUR ORDER AT NO CHARGE

This type of permission/license, instead of the standard Terms & Conditions, is sent to you because no fee is being charged for your order. Please note the following:

- Permission is granted for your request in both print and electronic formats, and translations.
- If figures and/or tables were requested, they may be adapted or used in part.
- Please print this page for your records and send a copy of it to your publisher/graduate school.
- Appropriate credit for the requested material should be given as follows: "Reprinted (adapted) with permission from (COMPLETE REFERENCE CITATION). Copyright (YEAR) American Chemical Society." Insert appropriate information in place of the capitalized words.
- One-time permission is granted only for the use specified in your request. No additional uses are granted (such as derivative works or other editions). For any other uses, please submit a new request.

Flocculation Optimization of Orthophosphate with FeCl3 and Alginate Using the Box–Behnken Response Surface Methodology

Author:
Henry K. Agbovi, Lee D. Wilson

Publication:
Industrial & Engineering Chemistry Research
Publisher:
American Chemical Society
Date:
Mar 1, 2017

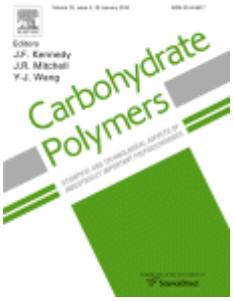

Design of amphoteric chitosan flocculants for phosphate and turbidity removal in wastewater

Author:
Henry K. Agbovi, Lee D. Wilson

Publication:
Carbohydrate Polymers
Publisher:
Elsevier
Date:
1 June 2018

Permission request

PUBLISHING - General Info <publishing@csiro.au>
Fri 2020-05-22 12:49 AM

To: Agbovi, Henry

Dear Henry,

Thank you for your request.

You do not need permission from CSIRO Publishing to reuse your own material in further work.

The 'Licence to Publish' form that you signed when you submitted the paper gave us a licence to publish your paper. An extract from the Licence to Publish is copied below.

> *In addition to the Author's moral rights in respect of the Work, the Author retains the right to:*
>
> - *Use copies of the work for non-commercial purposes within his/her institution subject to the usual copyright licencing agency arrangements*
> - *Use the work for further research and presentations at meetings and conferences*
> - *Use the illustrations (line art, photographs, figures, plates) and research data in his/her own future works*
> - *Share print or digital copies of his/her work with colleagues for personal use or study*
> - *Include the work in part or in full in a thesis provided it is not published for commercial gain*
> - *Place his/her pre-publication version of the work on a pre-print server*
> - *Place his/her pre-publication version of the work on a personal website or institutional repository on condition that there is a link to the definitive version on the **CSIRO** PUBLISHING website.*

Further details about article sharing can be found on the journal website at the link http://www.publish.csiro.au/journals/forauthors

Best regards

Claire Gibson
Rights & Special Sales
CSIRO Publishing
claire.gibson@csiro.au | +61 3 9545 2444 | www.publish.csiro.au
Private Bag 10, Clayton South, VIC 316